ANNUAL PROGRESS REPORT ON THE HYDROTHERMAL INJECTION PROGRAM, FY 1983

PHASE 1 DATA ANALYSIS

PHYSICAL FRACTURE FLOW ANALYSIS
LABORATORY FRACTURE FLOW TESTING
INTEGRATED FIELD ANALYSES

GEOSCIENCES STAFF

D.W. Allman
W.F. Downs
L.C. Hull
K.N. Koslow
R.M. Large
R.E. McAtee
J.D. Miller
B.F. Russell
P.A. Skiba

September, 1983

FOREWORD

The results of the physical fracture flow analysis, laboratory fracture flow testing, and the integrated field analyses are presented in this appendix. Sections 1 and 2 provide a summary of the tests conducted and the experimental data obtained during the test sequence. Section 3 constitutes the work performed in support of the physical fracture flow analysis. This section includes the analysis and interpretation of pressure, tracer mixing, and heat transfer data. Section 4, Numerical Modeling, represents this year's activity directed at the integration of the field analysis. The acquired simulator presented in this section will be used next year to help integrate the data and results presented in this progress report. Section 5, Physical Modeling, presents the laboratory fracture flow testing activities conducted to assist in the interpretation of the data obtained during the Raft River injection/backflow test sequence.

ANNUAL PROGRESS REPORT ON THE HYDROTHERMAL INJECTION PROGRAM, FY 1983

APPENDIX A

PHYSICAL FRACTURE FLOW ANALYSIS
LABORATORY FRACTURE FLOW TESTING
INTEGRATED FIELD ANALYSES

CONTENTS

FIGURES

TABLES

ANNUAL PROGRESS REPORT ON THE HYDROTHERMAL INJECTION PROGRAM, FY 1983

1. INTRODUCTION

1.1 Background

In mid-summer, 1982, the Department of Energy funded a hydrothermal injection program to investigate new methods for characterizing geothermal reservoirs. Because of time and resource constraints, the test site had to meet the following criteria:

1. The reservoir had to be fracture dominated
2. The site had to be immediately available
3. A monitoring system for physical and chemical parameters had to have been in place.

Due to the late spring termination of the 5-MW demonstration power plant, the Raft River KGRA met all of these requirements. An additional advantage to this site was the large differences in the geochemistries of the various wells that make up the producing well field.

Raft River geothermal production Well 5 (RRGP-5) was chosen as the test well. RRGP-5 was drilled during the summer of 1978.[1] At about 1373 m (4505 ft), the well started producing large amounts of high temperature fluid--6.3 x 10^{-2} m^3 1/sec (1000 gpm) at 135°C (275°F). A few days later at a depth of 1497 m (4911 ft), the drill stem twisted off. In order to reduce the danger to the drilling personnel during the fishing operation, approximately 178,000 kg (198 tons) of salt were pumped into the well as a heavy brine in order to kill the artesian flow. Once the drill stem had been recovered, the bore was cemented shut to a depth of 1121 m (3735 ft). A second leg was then drilled starting at 1052 m (3450 ft) and

bottoming out at 1501 m (4925 ft). This second leg (B) never intersected the high flow fracture zone that was found in leg A. After several months of testing, the decision was made to try to stimulate the well by hydrofracturing.[2] A 61-m (200-ft) section of the well was isolated between 1397 m (4583 ft) and 1458 m (4784 ft). This section of the well was chosen because it was devoid of large natural fracture zones. The hydrofracture treatment injected 1211 m^3 (320,000 gal) of fluid and 195,000 kg (215 tons) of propant sand into the well. The nominal injection rate was 0.13 m^3/s (2100 gal/min). This treatment was designed to create a massive, planar, vertical fracture. The pressure response during stimulation is plotted in Figure 1.[3] There seems to have been three periods of decline in pressure. After injecting approximately 110 m^3 (29,400 gal), there is a gentle pressure decrease with increasing injection. This is interpreted as indicating the dilation of an existing fracture set. There is a rapid pressure decrease probably associated with the opening of a new fracture or fracture system. This system expanded to a volume of a little over 300 m^3 (83,200 gal) with little increase in pressure. This period is followed by a rather rapid pressure increase over the next 250 m^3 (66,050 gal) as the newly-formed fracture set expanded succeeded by a continual pressure decrease due to the intersection of the man-made fracture with a natural fracture system.

At the conclusion of the hydrofracture treatment, the well was cleaned by artesian flow and during pump testing. Analysis of the return of injected material indicated about 46% recovery. An acoustic televiewer log was run after the cleanup was completed. A vertical fracture 43 m (140 ft) long and 1.5 cm (0.6 m) wide was observed. This fracture is oriented northeast-southwest. Pumping tests conducted after the stimulation procedure indicate that the hydrofracture driven from the B leg of RRGP-5 did not intersect the high production fracture system found in leg A. The artesian flow rates were much lower and the pressure drawdown was much more rapid.

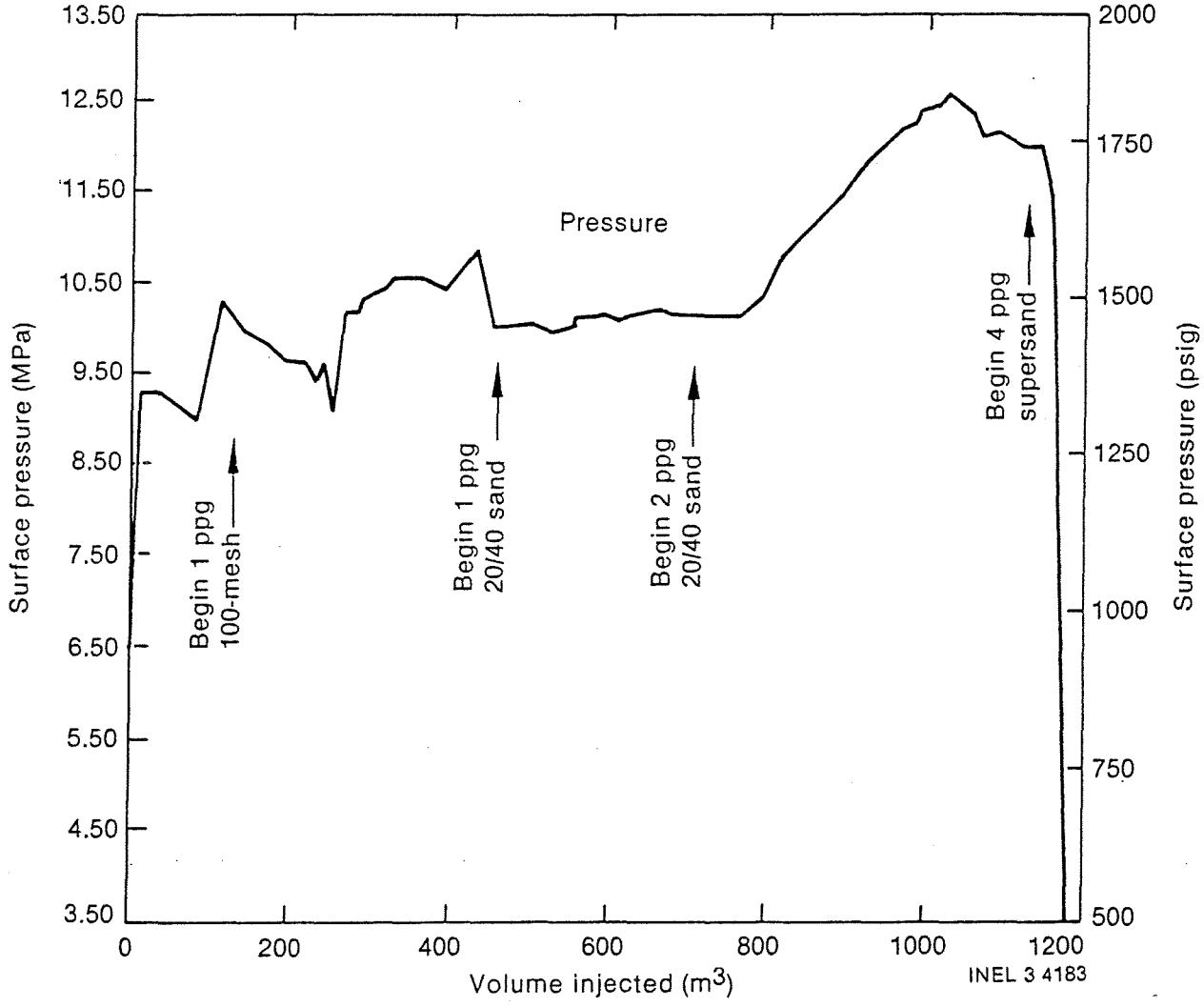

Figure 1. Pressure history of RRGP-5 hydrofracture experiment.

The first pumping test was performed on 10/10/80. Duration of this pumping was approximately 1290 min including 125 min when the pump was shut down. An average pumping rate was 4.0×10^{-2} m^3/sec (640 gpm) with some high up to 4.2×10^{-2} m^3/sec (660 gpm) and low of 3.8×10^{-2} m^3/sec (600 gpm).

The drawdown data for the early time is missing, first measurement point was 8 min after pump start-up. The plot of bubbler readings indicates rapid initial drawdown and no further pressure decline. Bubbler pressure readings stabilized at approximately 428-430 psig level. Recovery data are equally poor. The highest pressure value recorded was 570 psi which occurred 6 min after the pump shut down. Bubbler was not purged prior to this reading. Maximum drawdown during this pumping was approximately 148 psi, indicating specific capacity of 2.7×10^{-4} m^3/sec (4.3 gpm/psi). The reservoir parameters cannot be evaluated from the test data.

A second pumping test was conducted on March 12-14, 1981. The duration of this test was approximately 5540 min. A pumping rate of 4.4×10^{-2} m^3/s (700 gpm) was maintained for 3900 min; after 3900 min, the pumping rate was reduced to 4.1×10^{-2} m^3/sec (655 gpm) because of the deterioration of the pump condition due to abrasion by the sand produced. Temperature reached 128°C (262°F) after 40 min of pumping and was relatively steady until the termination of flow. A rapid pressure decline was observed in the first 30 min of pumping. Bubbler pressure declined to below 240 psi at about 180 min of pumping and fluctuated between 230 and 240 psi until the rate change at 3900 min. The well recovered to 566 psi level in about 5 min. Maximum drawdown during this pumping was at 338 psi indicating specific capacity of 1.3×10^{-4} m^3 sec/psi (2.07 gpm/psi).

The results obtained from the pumping tests indicate high well losses and high reservoir transmissivity near the wellbore. High well losses may be due to limited fluid entry through the hydrofracture which results in the turbulent flow conditions.

In summary, the drilling, stimulation and test history of RRGP-5 indicated that it was indeed in a fracture dominated reservoir. In addition, the Raft River Facility was immediately available and a monitoring system was in place.

Table 1 presents a series of selected physical and chemical data for the wells in the Raft River field. The deeper exploration and production wells--designated RRGE and RRGP--represent a spectrum of chemistries. The low conductivity wells--1, 2, and 5--lie in a NE-SW line along the NW edge of the valley (Figure 2). The higher conductivity well, RRGP-3, is located across the valley to the SE, and RRGP-4 is located near the center of the valley and represents an intermediate composition. By choosing RRGP-3 as the supply well and using RRGP-5 as the test well significant concentration differences were present and the injectant fluid acted as its own primary tracer.

1.2 Description of Tests

The test descriptions compiled in this section will not include a listing of all of the chemical and physical data collected during these tests. A separate report has been issued which lists all of the data that were collected and which of those data were included in the data base stored as files in the INEL computer: R. M. Large, Hydrothermal Injection Program Phase I Test Data, EGG-PBS-015-83, July 1983.

1.2.1 Baseline Data

Before the initiation of any of the injection-backflow tests, a series of data sets was collected on both the test wells and selected monitor wells. These baseline data are listed in Table 2.

As indicated in the data set title, the objective of collecting these data was to provide a reference data base for comparison with the results of the tests.

TABLE 1. SELECTED PHYSICAL AND CHEMICAL DATA FROM THE RAFT RIVER KGRA WELLS.

Well	Well depth (m)	Casing[a] depth (m)	Temperature (°C)	Specific conductivity (μs)	pH	Chemical Concentrations (mg/L)					
						Ca^{2+}	Na^{+}	K^{+}	HCO_3^{-}	Cl^{-}	SiO_2
Geothermal											
RRGE-1	1521	1105	141	2 800	7.3	48	456	33	39	746	138
RRGE-2	1994	1289	144	2 500	7.1	42	441	38	41	708	131
RRGP-3	1789	1293	149	8 000	6.6	200	1256	101	32	2433	151
RRGP-4	1654	1054	142	4 050	6.7	51	512	39	30	869	145
RRGP-5	1497	1398	135	2 700	7.5	38	427	28	50	666	140
RRGI-6	1176	509	71	10 800	7.2	171	2200	32	73	3640	94
RRGI-7	1185	623	78	12 000	—	350	2200	—	32	4000	83

INEL 3 4177

a. Depth to bottom of casing or to first perforations.

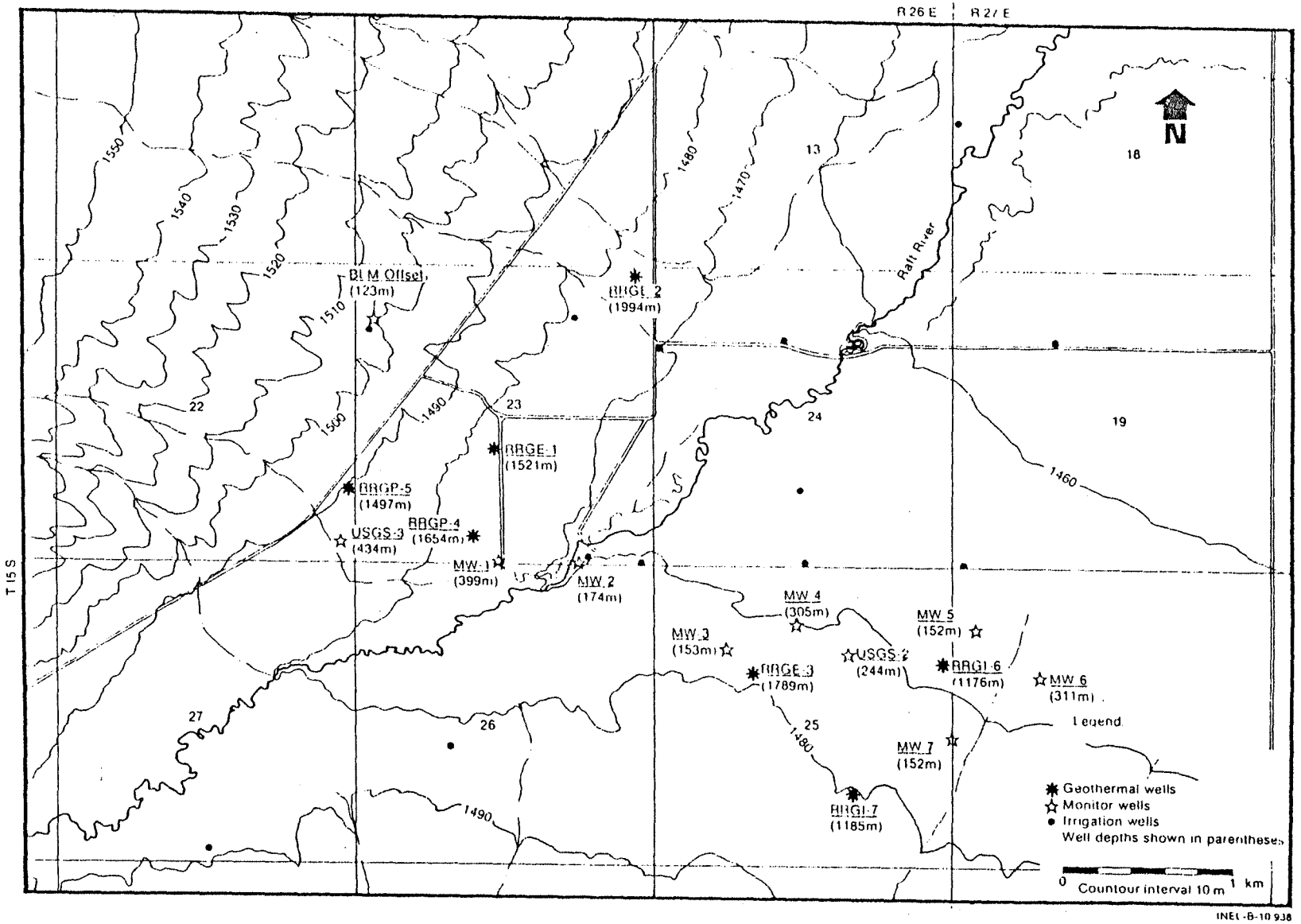

Figure 2. Raft River wells field locations.

TABLE 2. BASELINE DATA COLLECTED

Well	Data Sets (Number of Logs)
Test Wells:	
RRGE-1	a. Downhole Temperature Logs (2) 1. Flow rate: 0.0 m^3/sec (0 gpm) 2. Flow rate: 1.9 x 10^{-2} m^3/sec (300 gpm) b. Spinner Flowmeter Log (1) 1. Flow rate: (300 gpm) c. Downhole Conductivity/Temperature Logs (2) 1. Flow rate: 0.0 m^3/sec (0 gpm) 2. Flow rate: 1.9 x 10^{-2} m^3/sec (300 gpm) d. Wellhead Pressure
RRGP-5	a. Downhole Caliper Log (1) 1. Open hole portion of the well b. Spinner Flowmeter Logs (2) 1. Flow rate: 0.0 m^3/sec (0 gpm) 2. Flow rate: 9.4 x 10^{-3}/sec (149 gpm) c. Downhole Temperature Logs (3) 1. Flow rate: 0.0 m^3/sec (0 gpm) 2. Flow rate: 9.5 x 10^{-3} m^3/sec (150 gpm) d. Downhole Conductivity/Temperature Logs (2) 1. Flow rate: 0.0 m^3/sec (0 gpm) 2. Flow rate: 9.5 x 10^{-3} m^3/sec (150 gpm) e. Chemical Samples 1. Field sampling and measurements 2. Laboratory analyses
Monitor Wells:	
RRGP-4	a. Downhole Temperature (1) 1. Flow rate: 0.0 m^3/sec (0 gpm) b. Wellhead Pressure

TABLE 2. (Continued)

Well	Data Sets (Number of Logs)
BLM Offset	a. Downhole Conductivity/Temperature Log (1) 1. Flow rate: 0.0 m^3/sec (0 gpm)
	b. Downhole Temperature (1) 1. Flow rate: 0.0 m^3/sec (0 gpm)
	c. Wellhead water level
RRMW-1	a. Downhole Temperature (2) 1. Flow rate: 6.3×10^{-4} m^3/sec (10 gpm) 2. Logged in and out
	b. Caliper log (1)
	c. Wellhead Pressure
RRMW-2	a. Downhole Temperature (2) 1. Flowrate: 3.8×10^{-4} m^3/sec (6 gpm) 2. Logged in and out
Pitwell 5	a. Wellhead Water Level

1.2.2 Test 2A-1

Test 2A-1 was an operational system check-out test. The supply and injection system had been modified to accommodate the injection tests and it was necessary to familiarize all of the operations personnel with these modifications. The first half of the test consisted of injecting fluid from RRGP-2 into RRGP-5. The chemistries of these two wells are very similar (Table 1) and caused no perturbation of the reservoir during the training of operations personnel. During shutdown of the first injection, the transite piping near RRGP-2 developed a leak and had to be isolated from the rest of the supply system. The second portion of the system checkout used fluid from the regular supply well RRGP-3. This portion of Test 2A-1 was designed to checkout the tracer injection system as well as to test the downhole conductivity/temperature probe. Calculation of the cased bore volume indicated that it should take a little over 2 h to replace the fluid in the bore and to reach the formation with an injection rate of 9.5×10^{-3} m^3 sec (150 gpm). Both halves of Test 2A-1 had total injection times of about 1 h. This kept the entire volume of injected fluid within the cased bore and did not contaminate the formation.

During the second portion of Test 2A-1, a tracer cocktail was injected into the well. The final concentrations of the injected fluid were:

I^- (NaI)	22.0 mg/kg
Br^- (NaBr)	22.0 mg/kg
Mg^{2+} ($MgCl_2$)	22.0 mg/kg
B^{3+} (Borax)	10.9 mg/kg

Solution samples were collected during injection and backflow, and analyses showed very little change in concentration. The recoveries were 96-99% for Mg^{2+}, B^{3+} and I^-. Several difficulties were encountered in trying to analyze for the tracers in the field. The halide ions, Br^- and I^-, were detected by selective ion electrodes (SIE). These electrodes proved to be sensitive to the high concentrations of chloride ion, Cl^-, that is naturally occurring in the geothermal brines (Table 1). The Cl^- ion will

attach itself to the I^- site on the SIE cause a spurious reading. This problem is even more pronounced with the Br^- SIE because the atomic radii are more nearly the same between Br^- and $Cl^=$m-1.32 A and 0.97 A, respectively. The iodide analyses made in the field were always checked by reanalysis of the samples in the laboratory. The laboratory analyses were conducted using a standard additions method which lessens the effects of interfering ions. Unfortunately, even this analytical modification was not sufficient to provide reasonable results for bromide ion, Br^-. Some Br^- analyses were conducted by ion chromatography; but this technique was so time consuming and expensive that Br^- was used as a tracer only when previous experiments caused significant contamination of the other tracer species.

At the onset of planning of the injection-backflow tests, the scientists involved decided that they could make maximum use of the contrast in the well chemistries if they had a down hole solution resistivity probe. Comprobe Corporation, Ft. Worth, TX, contracted to fabricate a probe which would measure temperature and solution conductivity down hole. The probe was calibrated in standard conductivity solutions at 25°C. The first high temperature, down hole test of the instrument was during the second portion of Test 2A-1. The probe was set at a depth of 61 m (200 ft) in RRGP-5. Calculation of the well bore volume and solution arrival time indicated that the probe should sense an increase in conductivity in 10.1 min. This estimate was off by less than 10 sec. The instrument performed at 80°C for over 2 h. It was noted, however, that the response of the sensing unit to a change in solution conductivity of 5300 µmho/cm was considerably less at 80°C than at 25°C. This is opposite to the actual change in conductivity that would be expected. We were unable to calibrate this change in response; so, the downhole conductivity data was only qualitative. In spite of this limitation, the downhole conductivity probe was extremely valuable in that it indicated the exact time that the injected fluid entered the formation and the amount of mixing of the native and injected fluids that occurred in the well bore.

1.2.3 Test 2A-2

Test 2A-2 was the first injection-backflow test conducted at Raft River. Geothermal fluid from RRGP-3 was injected into the reservoir at RRGP-5 at a rate of 9.2×10^{-3} m^3/sec (146 gpm) for a total of approximately 2 h. The injectant fluid was innocluated with a 200 mg/kg iodide (I^-) tracer as NaI. There was no appreciable quiescent time between injection and backflow. The well was backflowed at a rate of 9.7×10^{-3} m^3/sec (154 gpm) for 10.37 h. This rate reduced to 1.9×10^{-3} m^3/sec (30 gpm) for the next 10.05 h at which time the final chemical samples were taken and the test was terminated.

The downhole conductivity/temperature probe was set at a depth of 1389 m (4557 ft) which was 1.5 m (5 ft) from the bottom of the casing. The probe registered a sharp change in conductivity 2 h and 6 min after the start of injection. This increase continued and reached 90% of full deflection within 7 min. The lower most section of casing has an inside diameter of 0.0178 m (7 in.). The mixing zone between the injected and native fluids was 154 m (506 ft) long by the time it reached the bottom of the casing. The injectant fluids were on the order of 92°C during injection and the formation temperature was 134°C at the initiation of the test. This caused a cooling of the well bore and the formation during injection. This cooling caused a decrease in the probe response to the fluid conductivity. This decrease very closely follows the temperature change so we are confident that the readings are a reflection of probe response and not an actual conductivity change. About 4 min after the initiation of backflow, the downhole conductivity started a long slow decrease toward the background valve.

Solution samples were collected at 15-min intervals for tracer (I^-) analysis. Each hour a larger solution sample was collected which was immediately analyzed for pH, conductivity and alkalinity. This sample was later analyzed for major and minor components.

1.2.4 Test 2C

Test 2C, the intermediate term injection-backflow test, had an injection time of 46.5 h. Once again, the quiescent time was the few min necessary to realign the valves and was followed by approximately 110 h of backflow. The injection rate was 9.2×10^{-3} m^3/sec (146 gpm) and the backflow rate was 9.7×10^{-3} m^3/sec. The reason for this difference was the presence of the liquid sampling port between the orifice plate which measured flow and the injection well. The sampling line circulated from the port, through the chemistry trailer and into the RRGP-5 holding pond at a flow rate of 0.35×10^{-3} m^3/sec (4 gpm). This loss was compensated for in the last few test series so that the injection and backflow rates were the same.

The tracer selected for Test 2C was magnesium ion, Mg^{2+}, injected as magnesium chloride. The tracer was injected continously over the entire 48 h of injection time. The chemical used was an industrial grade $MgCl_2$ that had been purchased for treatment of the cooling water for the 5 MW demonstration power plant. When this chemical was mixed with the RRGP-3 fluids, a very fine grained, dark grey precipitate formed. In the early stages of injection--at about 4 h--this precipitate clogged the tracer line filters. A filter cleaning schedule was initiated and there was only one significant interruption of tracer injection for the remainder of the test--after 32 h of injection. The addition of $MgCl_2$ to the injectant fluid provides two moles of chloride ion, Cl^-, for each mole of magnesium, Mg^{2+}. The addition of these ionic species increased the conductivity of the injection fluid.

The downhole conductivity/temperature probe was set near the bottom of the casing to monitor the arrival of the higher conductivity injection fluids. As soon as the solution interface had passed the probe, a series of downhole traverses were made of the open bore. The solution interface very quickly moved down through the upper portion of the bore and then its progress decelerated and became very slow in the lower part.

The solution sampling schedule was modified from that of Test 2A-2 because of the much longer injection and backflow times. Table 3 summarizes the sampling interval for the tracer samples collected during Test 2C. Total chemistry samples were collected approximately every fourth tracer sample. A total of 97 tracer samples and 21 total chemistry samples were collected during this test.

1.2.5 Test 2D

Test 2D was conducted after the Test 4 series and immediately before the final test, Test 5. This was the longest term injection-backflow experiment in the series. Fluid from RRGP-3 was injected into the aquifer at RRGP-5 at a rate of 9.5×10^{-3} m^3/sec (150 gpm) for a total of 96.5 h. There was no appreciable quiescent time between injection and backflow, and backflow continued for a total of 231.5 h at a rate of 9.5×10^{-3} m^3/sec (150 gpm).

During all of the previous injection-backflow tests, the tracers were continuously added to the injection fluid for as long as fluid was entering the reservoir. Tracers in Test 2D, however, were injected as high concentration slugs. The first slug had a volume of 1.14 m^3 (300 gal) and contained 3500 mg/kg I^- as NaI and 70 mg/kg of fluorescein. This slug was added in less than 12 min at the initiation of injection. Twenty-four h later another 1.14 m^3 (300 gal) slug was injected which contained 3800 mg/kg B^{3+} as borax ($Na_2B_4O_7 \cdot 10\ H_2O$) and 55 mg/kg fluorescein. Forty-eight h into the test a 1.14 m^3 (300 gal) slug containing 80 mg/kg fluorescein was added to the injectant. The final tracer injected into the formation during this test was a 280 mg/kg solution of Mg^{2+} as $MgCl_2$ during the final 3.6 h.

Unfortunately, there was a large interference between the chemistry of the geothermal fluids and the organic dye fluorescein. We used both spectrometric and fluorometric analytical techniques and the data always showed a great amount of scatter. This scatter was not evident in the chemical tracer data. For this reason, no attempt was made to interpret the measured fluorescein concentrations.

TABLE 3. SAMPLING INTERVALS FOR TEST 2C

Test Interval (h)	Tracer Sampling Interval (h)
0.0 - 17.5	1.0
18.0 - 40.0	4.0
40.0 - 48.5	0.50
48.5 - 56.0	0.25
56.0 - 57.5	0.50
57.5 - 73.5	1.0
73.5 - 101.5	4.0
101.5 - 149.5	8.0

This long term injection-backflow test explored a larger volume of the reservoir than had been looked at previously. By continuously injecting Mg^{2+} into the formation for the last 3.6 h before backflow, a comparison can be made between these data and those collected during Test 2C. A second objective of this test was to compare the dispersion of conservative tracer slugs that had been injected at different times. The final objective was to use the extended backflow time to clean up the reservoir in preparation for a well-to-well breakthrough experiment, Test 5, during which a UURI geophysical team was going to try to measure the extent of fluid movement.

1.2.6 Test 4 Series

The first two injection-backflow tests conducted at the Raft River KGRA showed that within a very few min of the initiation of backflow, the downhole conductivity and tracer concentration started to decrease. This led the investigators to the conclusion that either we were injecting a relatively small amount of fluid into a very large, open reservoir which caused an immediate dilution or that there was a natural hydrologic flow through the reservoir that swept the injected fluids asymmetrically away from the well and that added native fluid immediately upon the initiation of backflow. In order to test this second hypothesis, the Test 4 series experiments were designed to inject a small amount of fluid into the formation and to try to trace its movement as a function of time. Conductivity data from the previous tests indicated that at 9.5×10^{-3} m^3/sec (150 gpm) backflow, there were only 4 to 7 min of flow before dilution became evident. The test specifications stipulated a short term, 20 min, injection of fluid into the formation, a variable length quiescent time and backflow until background conditions were reestablished. This technique allowed for a very small amount of fluid--11.4 m^3 (3000 gal)--to be placed in the immediate vicinity of the well and the movement of this mass away from the well could be monitored as a function of arrival time during backflow. Table 4 is a list of the test times for the Test 4 series.

TABLE 4. SUMMARY OF TEST 4 SERIES

Test	Injection (h)	Quiescence (h)	Backflow (h)
4A	0.3	27.5	8.0
4B	0.3	2.2	10.5
4C	0.3	12	8.5
4D	0.3	50	48.5

Iodide ion, I^-, as sodium iodide was used as a tracer for Test 4A. A 20-min injection period was followed by 27.5-h quiescent time and 8.0 h of backflow. The injection and backflow rates were 9.2 x 10^{-3} m^3/sec (146 gpm) and 9.7 x 10^3 m^{-3}/sec (154 gpm), respectively. At the conclusion of the test, it was discovered that about 24.9 m^3 (6580 gal) of injected fluid had not been recovered from the well, RRGP-5. A check of the system and the operating procedure indicated that due to a known leakage through the master valve of RRGP-5, a tight downstream valve was used to control flow. At the time of initiation of the quiescent period, the downstream valve was closed but the chemistry sampling line which was located between the well head and the control valve was left open. This allowed the leakage of 0.25 x 10^{-3} m^3/sec (4 gpm) and accounted for an estimated total loss of 25.0 m^3 (6600 gal) of injected fluid. This estimate fits very well with the measured recovery of fluid for Test 4A.

The second experiment in the series, 4B, had fluorescein as a secondary tracer. Injection into the formation was for 20 min followed by a 2.2-h quiescent period and a 10.5-h backflow. The injection and backflow rates were the same as in the previous experiment, 9.2 10^{-3} m^3/sec respectively. During the quiescent period, the downhole conductivity/temperature probe was used to run a series of traverses from the casing to the bottom of the hole. These indicated that there was no detectable flow up the casing or within the bore.

Fluorescein is a long chain organic dye which is detectable at very low concentrations by fluorimetry. In addition to the analytical problems mentioned earlier, fluorescein adsorbs on many surfaces including metal oxides and silicate minerals. This adsorption precludes fluorescein from being a conservative tracer. The recoveries of tracer and injectant fluid from Test 4B were 78% and 94%, respectively.

Iodide ion, I^-, as NaI was used as the secondary tracer in experiment 4C. The injection and backflow rates were the same as in Tests 4A and 4B. A 12 h quiescent period was preceeded by a 20-min injection into the formation and succeeded by an 8.5-h backflow. Once again,

vertical profiles of the well were taken with the temperature/conductivity probe in order to monitor any leakage or movement of fluid during the quiescent period. During backflow, 83% of the iodide and injected fluid were recovered. The I^- concentration and conductivity curves generated during backflow are, within analytical error, the same curve.

Because of time constraints imposed by the abandoning of DOE's Raft River site, there was time for only one additional Test 4 series experiment, 4D. The quiescent time was set at 50 h. Geothermal fluids from RRGP-3 were innoculated with fluorescein and bromide ion, Br^- as NaBr, and injected into the formation for 30 min at a rate of 9.5×10^{-3} m^3/sec. Backflow continued for 48.5 h at a similar rate which allowed recovery of 81% of the florescein and 78% of the injected fluid.

1.2.7 Test 5

Injection Test 5 was the only attempt to establish communication between two different wells at Raft River. During the RRGP-5 stimulation experiment, a pressure increase was noted at RRGE-1.[3] This indication of communication between the two wells sponsored Test 5. An additional objective was to provide an extended injection period test for University of Utah Research Institute geophysists to attempt to trace the movement or extent of movement of injected fluid. Two surface geophysical techniques were used. The self potential method measures the electrokinetic effects generated at the interface between the moving injected fluid and the fluid contained in the matrix. The second geophysical technique used was electrical resistivity. This effort was an attempt to measure the interface between the higher conductivity injected RRGP-3 fluids and the lower conductivity RRGP-5 fluids. Baseline data were collected before the initiation of any of the tests and these data were compared with those collected during Test 5.

Because well-to-well breakthrough was the ultimate goal of Test 5, a 18.9×10^{-3} m^3 (800 gal) high concentration tracer cocktail was injected into the stream at the initiation of injection. The composition of this cocktail is listed in Table 5.

TABLE 5. COMPOSITION OF TEST 5 TRACER COCKTAIL

Tracer Specie	Tracer Compound	Tracer Concentration (mg/kg)
I^-	NaI	21,800
Br^-	NaBr	20,000
Fluorescein	Fluorescein	5,150
Rhodamine B	Rhodamine B	380

The injection flow rate was 9.5×10^{-3} m^3/sec (150 gpm) into RRGP-5 and in order to expedite flow between the wells, RRGE-1 was flowed

at 18.9 x 10^{-3} m^3/sec (300 gpm). A portion of the flow from RRGE-1 passed through a cooling coil to an on-line fluorimeter for fluorescein. Full scale deflection for the fluorimeter was set at 20 µg/kg. In addition to the on-line monitoring of both fluorescein and conductivity, solution samples were collected from RRGE-1 every 6 h during injection. Injection continued for 376 h. During the last 48 h of injection, the UURI geophysical team conducted their self-potential survey. The injection was followed by an 80-h quiescent period during which the resistivity survey was conducted. As soon as this last geophysical survey was completed, a 120-h backflow was initiated. During backflow, a flow rate of 9.5 x 10^{-3} m^3/sec (150 gpm) was maintained. Tracer samples were collected from the backflowing RRGP-5 fluid at 1-h intervals for the first 36 h, every 2 h for the next 12 h, and at 4-h intervals for the remainder of the test.

At the conclusion of the test a series of pressure pulse tests was conducted. RRGP-5 was flowed until the pressure and flow stabilized and then the well was shut in. The annulus pressure was monitored as a function of time until steady state conditions were reached in the well. The time of pressure recovery as a function of flow rate provides insight into the physical characteristics of the reservoir. These tests were run at 3.2 x 10^{-3} m^3/sec (50 gpm) intervals between 4.7 x 10^{-3} m^3/sec (75 gpm) and 17.4 x 10^{-3} m^3/sec (276 gpm). Attempts to sustain flows of 18.9 x 10^{-3} m^3/sec (300 gpm) and 20.5 x 10^{-3} m^3/sec (325 gpm) caused an inflation of the sand column in the bottom of the bore and gave spurious results.

The attempt to establish breakthrough from RRGP-5 to RRGE-1 was unsuccessful. Neither the higher conductivity nor any of the tracers showed up in flow from RRGE-1. There seemed to be a slight increase in the I^- concentration about 10 days after the start of injection; but, the higher concentration was very near the limit of detection and showed a large amount of scatter. This increase in I^- was not accompanied by increases in any of the other injected tracer concentrations. When backflow was initiated from RRGP-5, the tracers which had been injected some 20 days previously appeared immediately in very low concentrations.

There was a continual increase in tracer concentration over the five days of backflow but the data showed a great deal of scatter and only gross trends can be distinguished.

2. EXPERIMENTAL DATA

2.1 Physical Data

The primary objective of the test sequence was to acquire experimental data necessary to develop an improved technique for characterizing the fracture dominated Raft River geothermal reservoir. The test sequence employed to obtain this objective has been labeled "injection-backflow."

The existing Raft River Injection and supply system was modified in order to utilize RRGP-5 as the test well. Figure 3 represents a schematic diagram of the RRGP-5 well schematic used for supply and disposal of geothermal fluids. As depicted in the figure, the injection supply water from RRGE-3 could be passed into the pond at RRGP-5 through spargers or directly to the suction side of the injection pump. The injection pump was also used as a method of disposal for backflow of warm-up flow fluids which had collected in the RRGP-5 pond. RRGP-5 fluids could also flow directly to RRGI-7 for reinjection.

2.1.1 Instrumentation

Wellhead and downhole instrumentation were used in support of the test sequence. The wellhead instrumentation included temperature indicators, two orifice plates and automatic flow controller values, and a pressure transducer. The downhole instrumentation employed include a temperature probe, an x-y caliper, a temperature/conductivity probe, and a spinner tool. Combined, these instruments provide much of the data necessary to determine reservoir characteristics such as transmissivity, permeability, and storativity.

Temperature measurements at the wellhead were obtained to determine the temperature of the fluid being injected from RRGE-3 and produced from RRGP-5. The wellhead temperature measurements combined with downhole temperature can be used to develop an understanding of the heat transfer within the wellbore and allow for correction of wellhead pressure measurements due to thermal effects. A mercury thermometer was used to

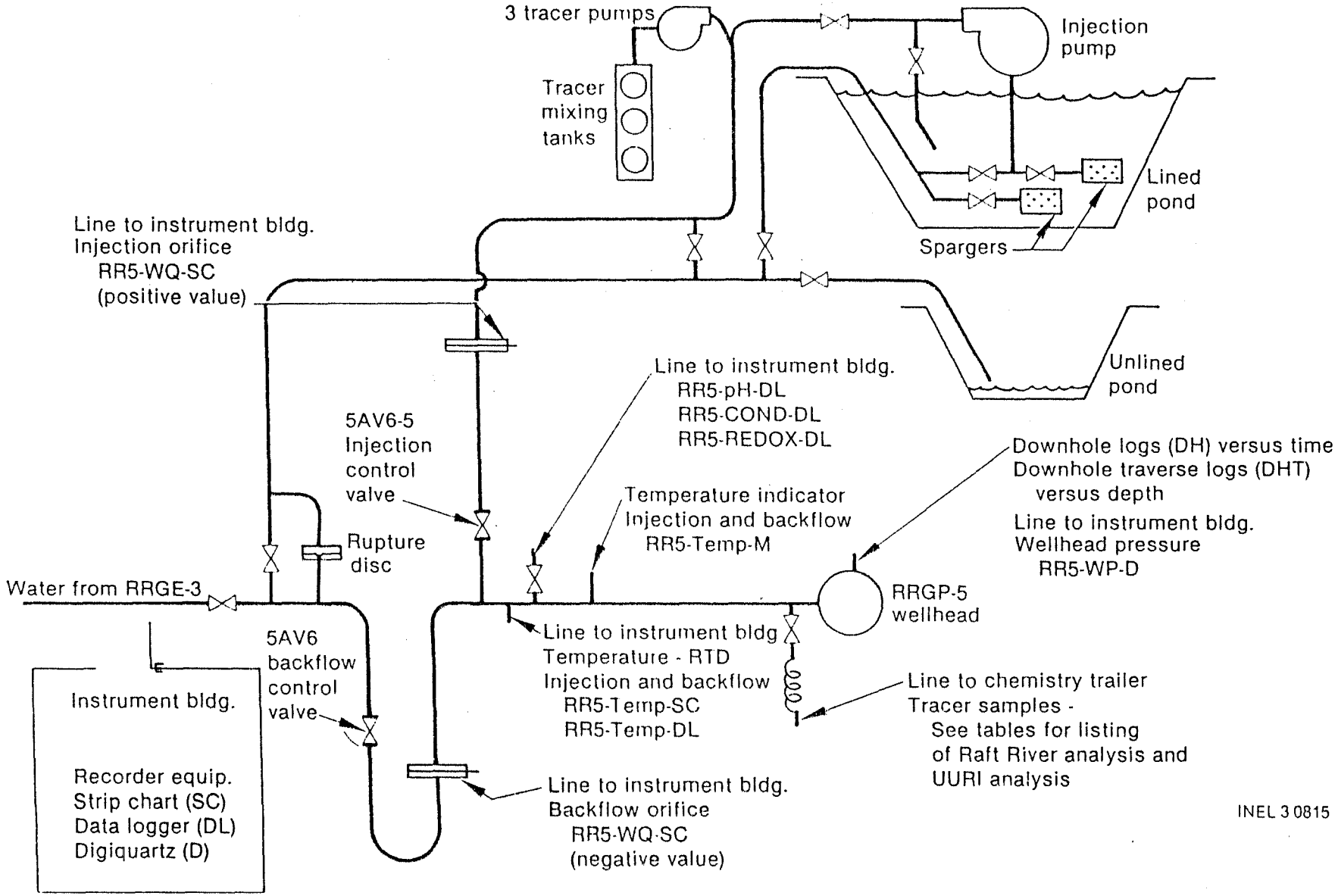

Raft River RRGP-5 Well Flow Schematic
Figure 3

obtain manual readings and a platinum resistance temperature detector (RTD) connected to a data logger was used for recording data on a continuous basis.

The rate of flow (Q) was measured during the injection and backflow portions of the test sequence. A constant Q of 9.5×10^{-3} m^3/sec (150 gpm) was achieved by using an automatic flow controller valve capable of maintaining a constant flow, plus or minus 5%. Strip chart recorders were connected to the orifice plate and provide a continuous record of the flow data.

The wellhead pressure measurements were collected using a pressure transducer, pressure computer, and data logger. These measurements provide the primary basis for determining the reservoir characteristics including transmissivity, storativity, and permeability. Continuous records were maintained prior to, during, and after completion of the individual tests.

A logging truck was required in order to perform the downhole logging operations. These operations were not always successful but, in general, provided valuable information to complement the data set obtained with the surface instruments. All logging data were recorded on strip charts to provide a continuous record.

A downhole temperature probe was used to obtain a wellbore temperature profile and provide the data necessary to allow for correction of wellhead pressure measurements resulting from thermal effects in the wellbore. In addition, the temperature logs assisted the reservoir engineer in delineating the production/injection zones adjacent to the wellbore.

The cased and open borehole of RRGP-5 was characterized by using an x-y three-arm caliper. Specifically, the caliper was used to determine the dimensions of the open borehole and in an attempt to delineate fractures in the formation. Data from the caliper was required in order to adequately evaluate downhole flow data obtained with the spinner tool.

A custom-built downhole temperature/conductivity probe was fabricated to aid in determining the movement of the high conductivity RRGE-3 fluids within the RRGP-5 wellbore and to measure fluid conductivity at depth during the injection-backflow portion of the test sequence. Although the tool was never successfully calibrated at temperature and pressure, its ability to measure relative changes in temperature and conductivity proved worthwhile. This tool was used extensively for all tests in the program and provided significant insight to the movement of high conductivity fluid in/through RRGP-5.

A spinner tool was used to measure flow velocities within the cased and open portions of RRGP-5. Data from the caliper tool was required to interpret the results of the spinner survey. The spinner tool assisted in determining the zone, where tracer fluid entered and exited the formation. Data from the spinner tool have proved valuable for the development of a conceptual model of the reservoir.

2.1.2 Analytical Data

The physical data compiled during the test sequence have been catalogued, digitized, and entered into the Idaho National Engineering Laboratory's CYBER system as the Hydrothermal Injection Program Data Base.[4] The data base include all physical, chemical and dye tracer analyses, and the major and minor elemental chemistries.

2.2 Chemical Data

This section will deal only with the collection of samples and analyses of species that were conducted on site at the time the experiments were in progress. Samples for major chemical specie and stable isotope analyses were collected by University of Utah Research Institute and presumably those procedures will be covered in the UURI annual progress report.

2.2.1 Analytical Methods

Because of the great potential for change in some of the chemical characteristics, once samples have been removed from the flow stream, several analyses had to be conducted in the field immediately after collection. With most geothermal fluids these changes are due to either the evolution of gaseous species from the solution samples or to the precipitation of mineral phases. The following measurements were made immediately after collection of a sample:

1. pH
2. Conductivity
3. Alkalinity
4. Tracer concentration.

The tracer concentrations were usually stable but were determined immediately and were used for control of the experiments.

pH was determined using a standard combination glass electrode and a digital readout pH meter. Conductivity was measured using a small volume conductance cell and a digital readout meter. Alkalinity was determined by titration with 0.1589 N sulfuric acid H_2SO_4, to a brom cresol green-methyl red indicator end point. Various methods were used to analyze for the tracer concentrations. Iodide, I^-, was done by selective ion electrode; boron, B^{3+}, and fluorescein by UV-VIS spectrophotometry and magnesium, Mg^{2+}, by atomic absorption spectrophotometry. Details of the selective ion electrode and UV-VIS spectrophotometric procedures are contained in Appendix A.

In addition to the conductivity measurements on solution samples, similar measurements were continuously recorded either downhole or in the

chemistry trailer. These data were recorded on strip charts as a function of time. The sample conductivities were then used as calibration points.

2.2.2 Sample Collection and Preparation

A solution sampling line was connected to the injection backflow line very near the well head. This line ran from the well over to the chemical trailer and then into the disposal pond at RRGP-5. A 6.35-mm (1/4-in.) O.D. tubing coil was connected to the sample line. This coil was immersed in a continuously flowing cold water stream to ensure a single phase fluid for sampling. Liquid samples were collected in clean polyethylene bottles. The pH, conductivity, and alkalinity were measured within 10 min of sample collection. The meters used for pH and conductivity were temperature compensated. A portion of the sample was then used for tracer analysis in accordance with the procedures described in Appendix A.

2.2.3 Analytical Data

The data collected during these experiments have been entered into the Idaho National Engineering Laboratory's CYBER System as the Hydrothermal Injection Program Data Base.[4] The data include all physical, chemical and dye tracer analyses and the major and minor elemental chemistries.

3. INTERPRETATION AND RESULTS

The interpretation of the data sets presented in this section resulted in the formulation of a conceptual model for the reservoir in the vicinity of RRGP-5. Figure 4 portrays the conceptual model in the plane of the hydrofracture. This model will be used to assist in the integration of all data into the numerical simulation presented in Section 4.

3.1 Borehole Geophysical Logs

3.1.1 RRGP-5 Logs

3.1.1.1 Production/Receiving Intervals

With the extensive well completion problems and hydraulic fracturing, numerous well logs have been run on RRGP-5A, RRGP-5B, and RRGP-5BF, where the A and B indicate the first and second legs while the F designates the leg has been fractured. Figure 4A depicts the construction characteristics of RRGP-5BF. The 1030 sacks of cement spotted in RRGP-5A have probably plugged a considerable portion of the A leg with cement and with sand which was added to the cement.[1] The decreased well productivity of RRGP-5B as compared to RRGP-5A suggests that the injected cement plug probably accounts for the reduced productivity of RRGP-5B. A spinner log run on RRGP-5A (Figure 5), when combined with a caliper log (Figure 6), indicates two major producing zones, the major one being between 1379 and 1381 m (4523 and 4532 ft) below land surface. The second major production zone is between 1364 and 1367 m (4476 and 4486 ft) below land surface. The spinner log thus indicate two major producing zones. The caliper log and the lithology log also indicate changes near the upper producing zone. The caliper log shows a decrease in borehole diameter from 1362 to 1363 m (4468 to 4471 ft) below land surface. A change in borehole diameter is commonly associated with lithology changes. The driller's log (Figure 7) for RRGP-5A indicates the drilling rate on the left strip chart, while on the right side, the lithology and the mud pit inflow and outflow temperatures are indicated.[7] At 1367 m (4484 ft) [1367 m (4500 ft) below the kelly

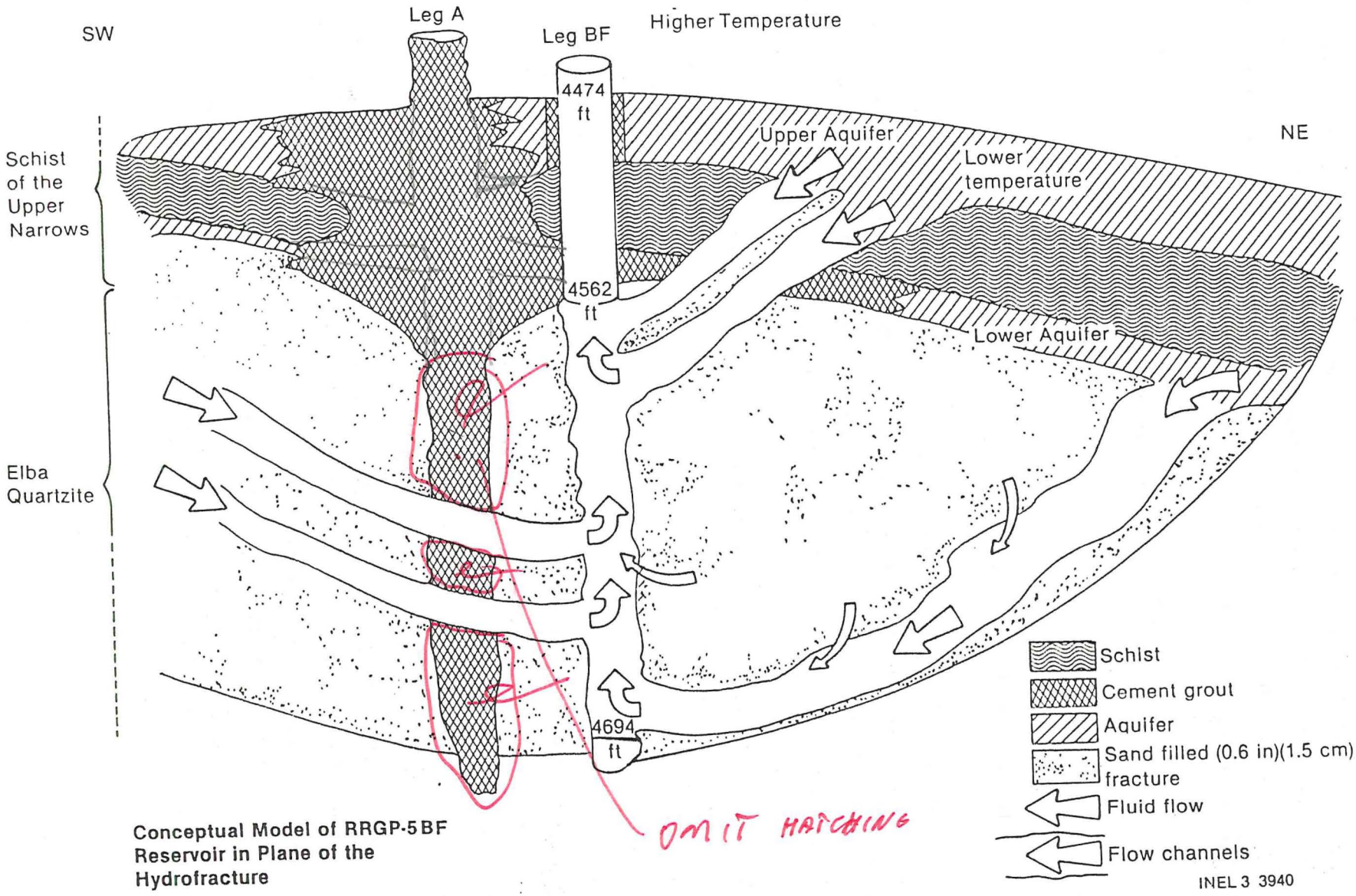

Conceptual Model of RRGP-5BF Reservoir in Plane of the Hydrofracture

Conceptual model of RRGP-5BF reservoir in plane of the hydrofracture.

ROCKY MOUNTAIN GEO—ENGINEERING COMPANY

Grand Junction, Colorado

					FROM	TO
COMPANY	EG&G IDAHO INC.	LOCATION	NESW SEC 22 TWP15S R26E	DEPTH LOGGED	70'	4911'
WELL	RRGP #5	COUNTY	CASSIA	DATE LOGGED	5/10/78	6/22/78
FIELD	RAFT RIVER	STATE	IDAHO			
ELEVATION	G.L. 4988' K.B. 5004'	DRILLING FLUID	MUD & WATER	ENGINEERS	BLAIK COPELAND	

SHALE · SANDSTONE · SILTSTONE · TUFF · SCHIST · QUARTZ · QUARTZ MONZONITE · CONGLOMERATE · RYOLITE

CORE NO. · DST NO. · DEVIATION

NB - NEW BIT
NR - NO RETURNS
CO - CIRCULATE OUT
NS - NO SAMPLE
TG - TRIP GAS

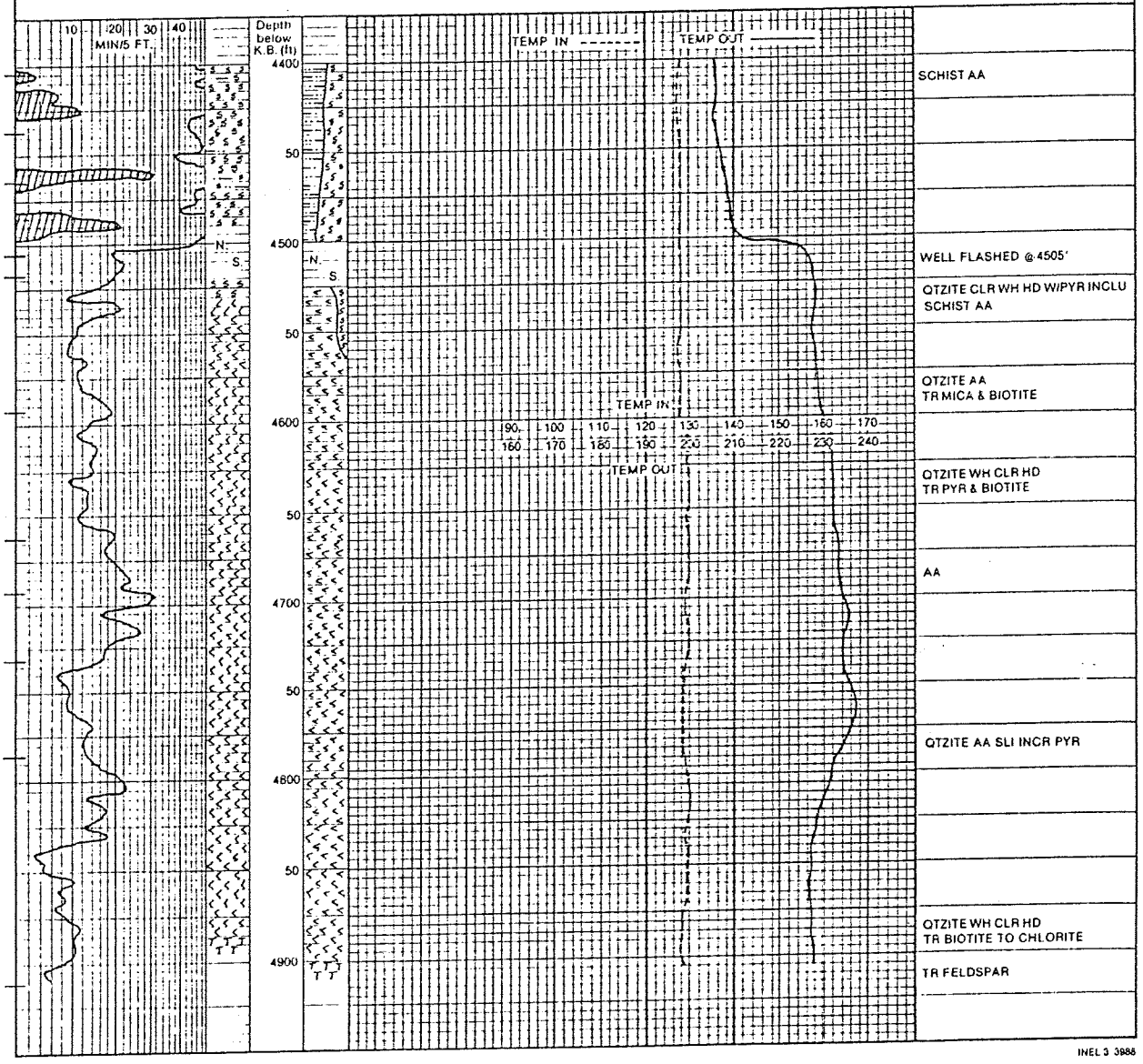

INEL 3 3988

Driller's log from 4400 to 4911 ft. for RRGP-5A.

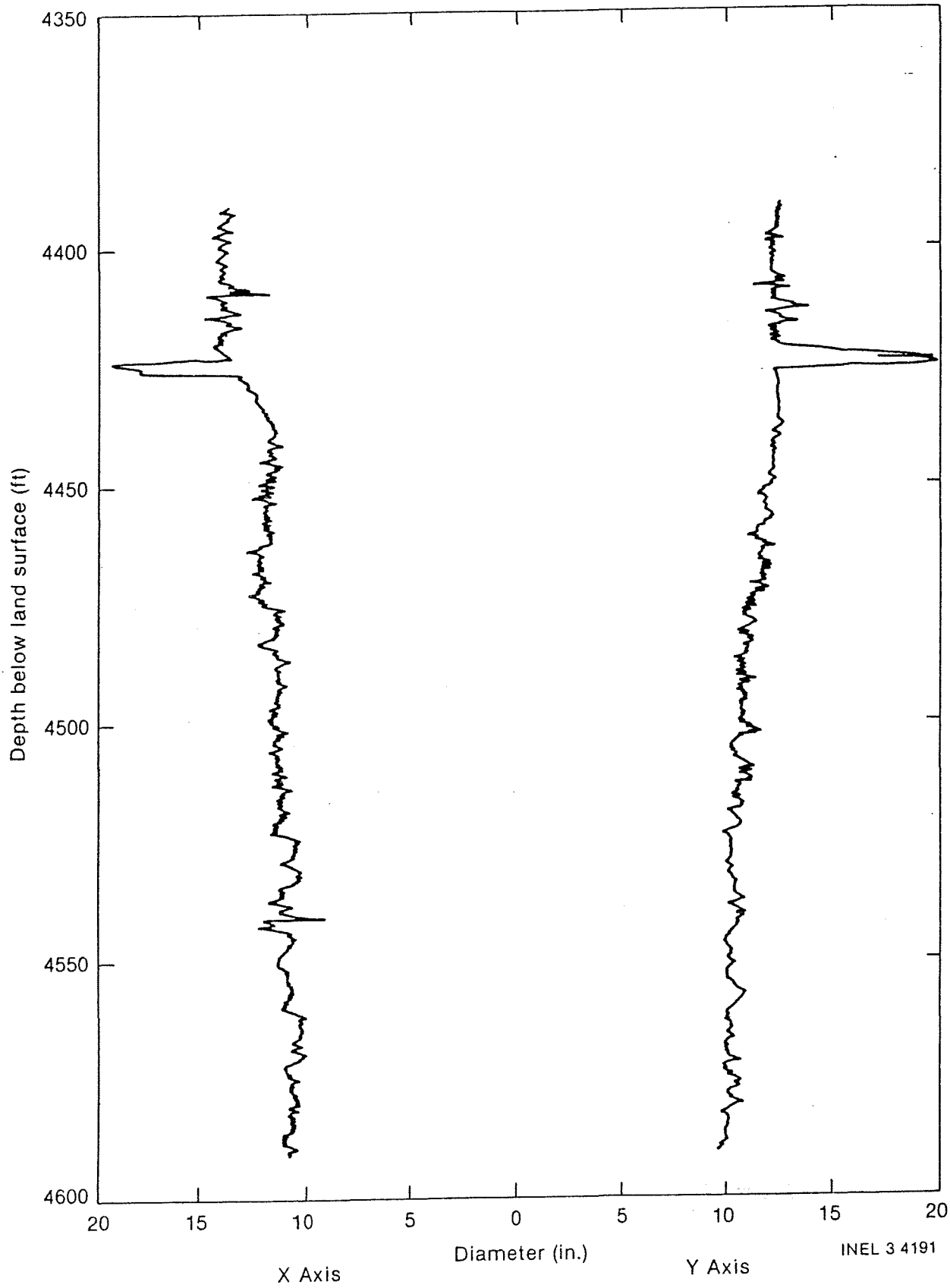

Caliper log on 07-06-78 for RRGP-5A in production zones.

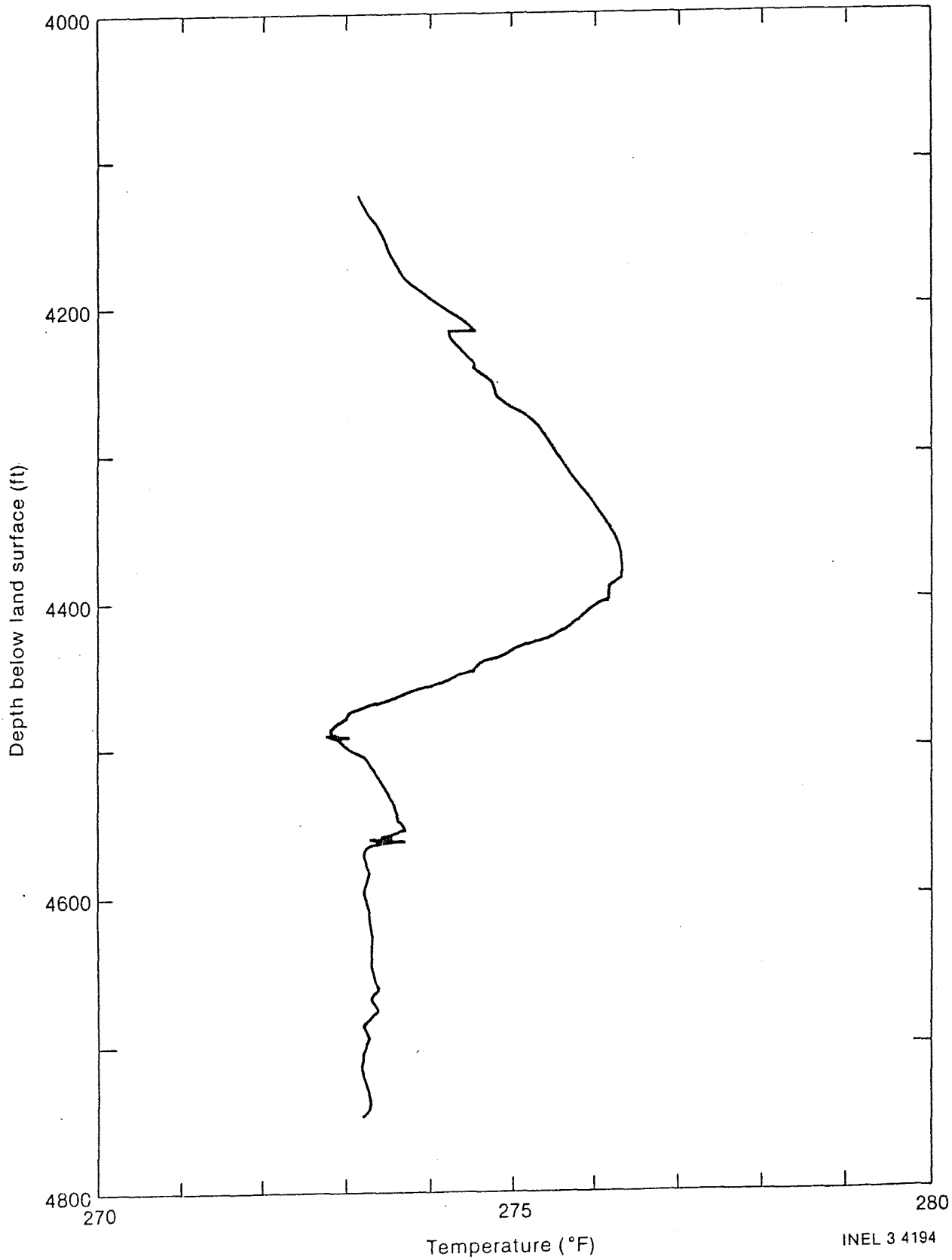

Temperature log on 08-25-82 for RRGP-5BF.

bushing (KB) which is 4.3 m (14 ft) above land surface] the lithology, changes from a schist to a quartzite and the drilling fluid returns are at a higher temperature. The well also is reported to have flowed in excess of 6.3 x $10^{-2}m^3$/sec (1000 gpm)[1] at a depth of 1369 m (4491 ft) [1373 m (4505 ft) below KB]. Acoustic televiewer logs of the USGS[8] indicate near vertical or steeply dipping fractures between 1362 and 1379 m (4470 and 4523 ft). These fractures are probably associated with glide block faulting, thrust faulting, normal faulting, and/or lystric faulting.[9] All of these data indicate a major producing zone is in the vicinity of 1364 to 1370 m (4475 to 4495 ft) below land surface. This production zone is in the Schist of the Upper Narrows which extends from 1335 to 1387 m (4380 to 4550 ft) in depth.[10]

Downhole geophysical logging was conducted in RRGP-5 BF, before and during the injection-backflow tests. The main purpose of logging was to determine the location of production zones within the open hole interval and to monitor undetected fluid movement into and out of the production zones. The logs included: X-Y caliper log, borehole spinner, fluid temperature, and fluid resistivity temperature logs for the well shut-in and under injection and backflowing conditions. Downhole samples for water quality analyses were obtained using a Kuster downhole sampler.

A temperature log was run on 08-25-82 with the section of the log from 1250 m to 1446 m (4100 ft to indicated touch down at 4745), depicted in Figure 8. A marked thermal reversal resulted in elevated temperatures above and below the interval from 1364 m to 1370 m (4475 to 4494 ft) even though the well is cased in thes section. The well was shut-in for several months prior to running this log. This thermal reversal occurs in a production zone encountered in RRGP-5A. It would appear that the grouting of the 17.8-cm (7-in.) liner did not succeed in plugging off this aquifer. The major aquifer between 1379 m and 1381 m (4523 and 4532 ft) in RRGP-5A, however, does appear to be cemented. The suppressed temperature results are due to active flow of ground water in this fracture zone. It is likely that this aquifer is the aquifer which results in little additional drawdown/buildup after approximately 5 min of discharge/injection. This is

a highly productive aquifer which is probably the major hydrologic source/sink affecting the injection-backflow test pressure responses addressed elsewhere in this report. This aquifer is further presumed to have significantly affected the dispersion of chemical tracers and the open borehole thermal anomalies observed during the injection-backflow tests.

A caliper log was run on 09-16-82 (Figure 9). The log indicates the bottom of the 7-in. liner to be at a depth 1394 m (4572 ft). The USGS acoustic televiewer log[3] indicates a liner bottom at 1390 m (4562 ft). The different reported depths for the liner bottom is presumably due to a depth error for one or both of the logging truck depth indicators. All logs had the indicated depths corrected to indicate a liner bottom at 1390 m (4562 ft) in order that all the EG&G and USGS logs, and presumably the commercial logs have the same pertinent hydrogeologic features at equal depths. The EG&G logs' indicated depths have been multiplied by 0.98416 to correct for an instrument factor minus an individual log correction factor. Most logs indicate borehole bottom at 1447 m (4748 ft) below land surface. These data indicate there is 57 m (186 ft) of open borehole with 163 ft of sand in the borehole bottom. Due to differences in indicated depths for the liner bottom, EG&G logs have been adjusted to correspond with USGS logs.

Information from the X-Y caliper log relates to the borehole, casing and liner diameters, wall roughness, and eccentricity of the borehole cross section. The X-Y caliper log conducted on 09-16-82 (Figure 9) indicates borehole diameters ranging from 17.8 to 25.4 cm (7 to 10 in.) between 1394 and 1422 m (4572 and 4665 ft). From 1422 to 1447 m (4665 to 4747 ft), the borehole diameters are over 22.9 cm (9 in.). The borehole wall is much rougher or rugose above 1422 m (4665 ft) than below. A cavity 50.8 cm (20 in.) or more in diameter occurs over a very short section at 1418 m (4653 ft) with a borehole radius of only 5.5 in. for one set of caliper arms 0.6 m (2 ft) below this zone. This enlargement is generally indicative of a fractured zone. A smooth, slightly enlarged hole below 1419 m (4657 ft) probably indicates more uniform drilling characteristics for the quartizite than for the overlying schist (Figure 7). Another

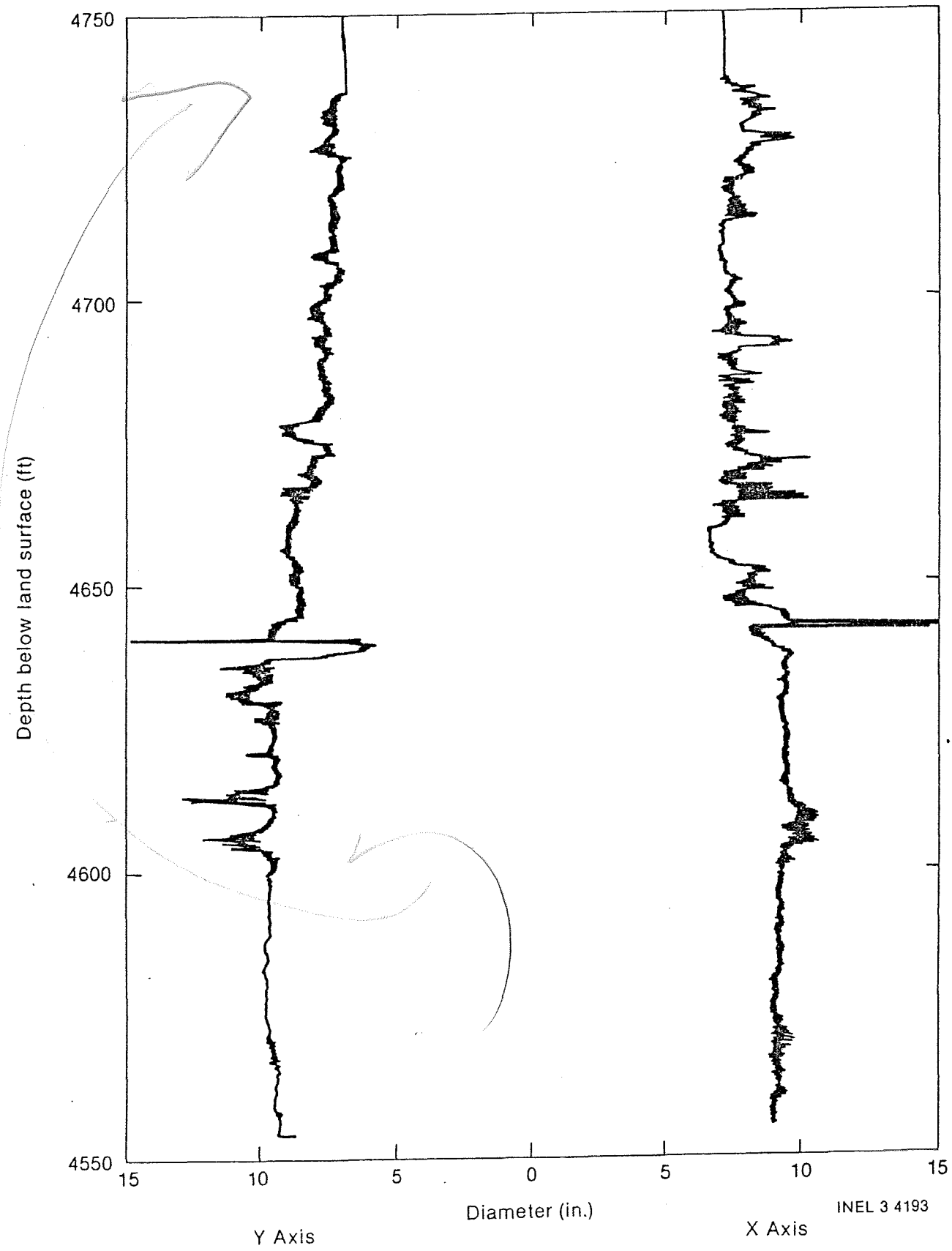

Caliper log on 09-16-82 for RRGP-5BF.

fractured zone indicated by increased borehole cross sectional area has a top at 1427 m (4683 ft) and is approximately 1.8 m (6 ft) thick. It is difficult to define specific production zones based on the caliper log alone, but when combined with other logs the caliper log provides valuable information on aquifer locations.

Fullbore spinner logs when combined with the caliper log of 09-16-82, the temperature log of 10-25-82, and the USGS acoustic televiewer descriptions[3] provide a basis for delineating the production/receiving zones in the open borehole section of RRGP-5BF. Initial spinner logs run prior to 10-20-82 did not yield good data because of defective bearings in the tool. Subsequent spinner logs run on 10-20-82 and 11-29-82 had a properly functioning spinner tool. The cross sectional areas of the borehole were calculated at selected depths where the borehole radii were apparently uniform over a vertical span of a few feet. The logging speed for the spinner tool was held constant during each borehole traverse. The count rates at various positions in the wellbore were calculated as percentages of the apparent differences between the rates in the 17.8-cm (7-in.) liner and the "dead" borehole below 1433 cm (4700 ft). These percentages in velocity were multiplied by the ratio of the cross sectional area at various depths to the cross sectional area in the 17.8-cm (7-in.) liner. The results for the 10-20-82 injection phase of Test 2D and the 11-29-82 backflow phase of Test 5 are plotted in Figure 10. The rugosity of the borehole wall, the nonuniform cross sectional velocity profile in the borehole and the uncentralized spinner (although centralizers were used), in addition to a possible temporally dependent flow rate profile probably accounts for much of the scatter of the percentage of flow. A positive, precise delineation of the producing/receiving zones is not possible using the spinner logs alone.

The temperature log which began at 17:30 on 10-25-82 while backflowing the well provides information for assisting in interpreting the spinner logs (Figure 11). Injection for Test 2D began at 13:30 on 10-18-82 with backflow beginning at 15:55 on 10-22-82. Abrupt temperature changes are indicative of water entering the wellbore at a temperature significantly

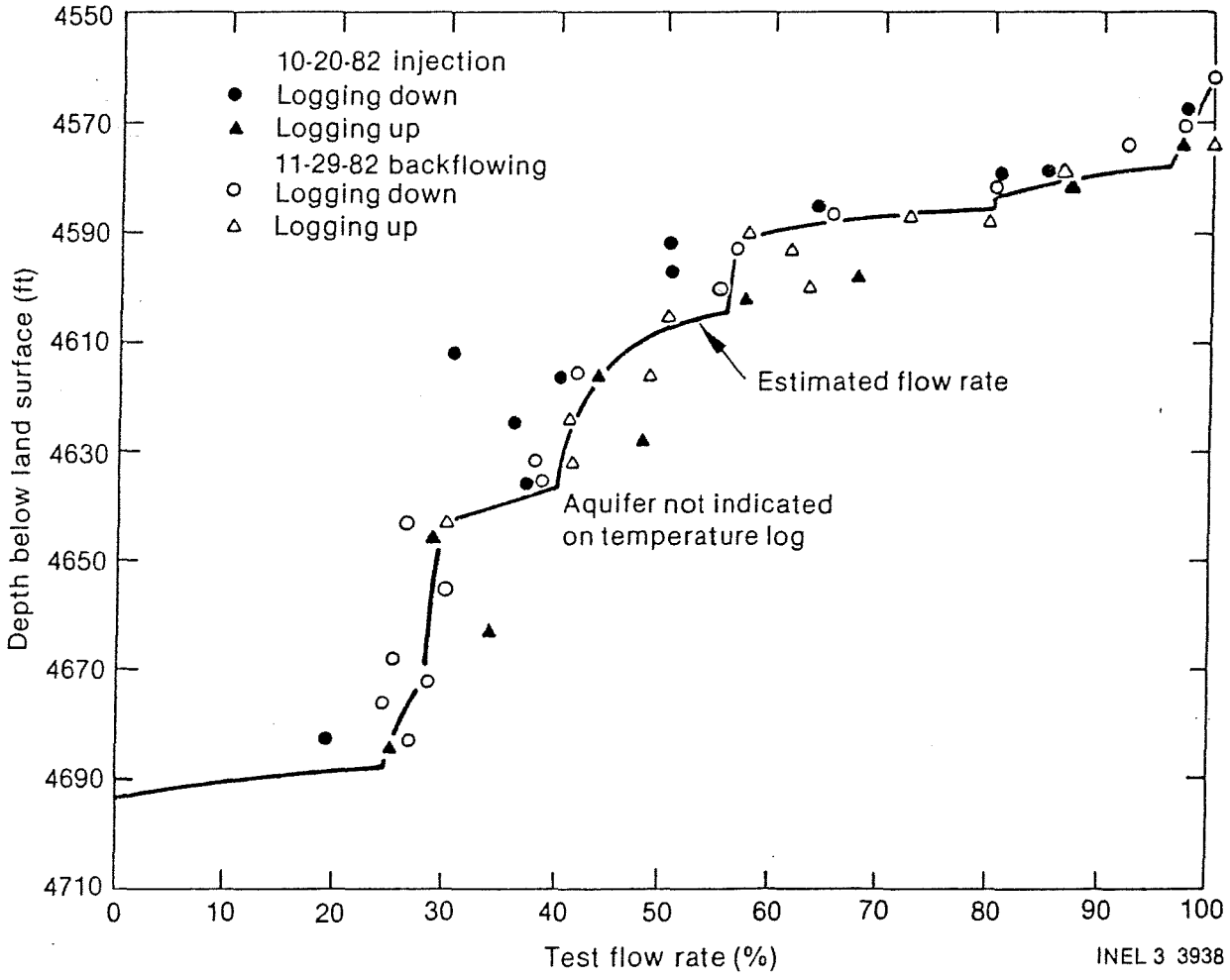

Production/receiving zones discharge/uptake as a percentage of flow rate for RRGP-5BF.

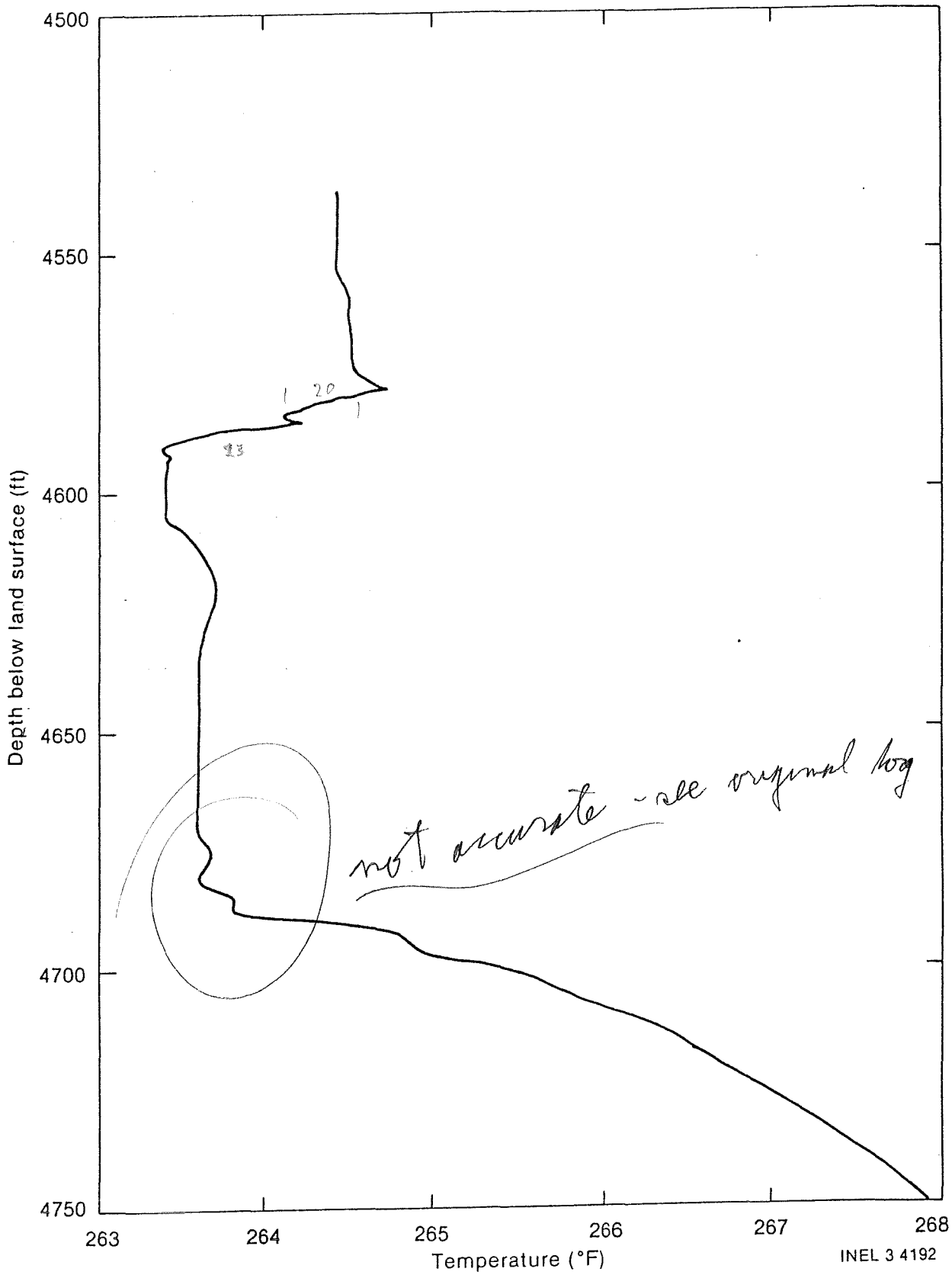

Temperature log in open borehole while backflowing RRGP-5BF during Test 2D on 10-25-82.

different than that of the upward flowing fluid below the inflow zone. Several sequential temperature logs would be needed to understand the significance of the temperature reversals which are probably indicative of exceptionally well developed channels or pipes where the sand has been washed from the fracture. This would result in very high inflow rates with possibly incomplete mixing of the in-flowing fluid within the wellbore at the pipe entrance. Complete mixing may require several feet of flow within the wellbore. These potential pipes defined by elevated temperature spikes, occur at depths of 1396, 1398, and 1428 m (4580, 4586, and 4686 ft) according to the temperature log. Apparently less well developed elevated temperature inflows occur between 1396 and 1398 m (4580 and 4585 ft), between 1398 and 1399 m (4586 and 4591 ft), and between 1427 and 1429 m (4682 and 4687 ft). The zone from 1396 to 1399 m (4580 to 4591 ft) could consist of two well developed pipes discharging into a portion of the fracture which is more enlarged near the wellbore due to erosion of sand. Thus, the thermal effects could extend above and below the actual (pipe entrance). Apparent cold water inflows occur between 1404 and 1408 m (4605 and 4618 ft), between 1423 and 1425 m (4669 and 4676 ft), between 1427 and 1429 m (4682 and 4687 ft) and between 1429 and 1431 m (4689 and 4694 ft). The first and last indicated cold zones are quite distinctive with the other two zones being somewhat more subdued in their thermal effects. An aquifer indicated by the spinner logs and not by the temperature log is at a depth of 1414 m (4640 ft). There is probably a negligible difference in the temperature between the fluid in the aquifer and the fluid rising in the borehole immediately below this producing zone; thus there is no change in wellbore fluid temperature. The combination of spinner and temperature logs appears to permit delineation of the flow rate inflow/outflow from the various aquifers within 10% of the total flow or $\pm 9.5 \times 10^{-4} m^3/sec$ (15 gpm) for these tests.

3.1.1.2 Specific Conductivity-Temperature Probe. Significant data inaccuracies occurred with both the specific conductance and temperature data collected with the specific conductance-temperature well logging probe. The principal problem was that the steel armor on the logging cable was used as a ground for the temperature and specific conductance sensors.

The apparent values for specific conductance/temperature depended on at least the following:

a) the length of cable in the wellbore

b) the temperature of the fluid in the wellbore

c) the specific conductance of the fluid in the wellbore

d) the effects of corrosion deposits on the specific conductance sensors

e) the casing size distribution within the well

f) the degree of centralization of the cable and the probe in the wellbore.

These basic deficiencies resulted in data that are of qualitative value only. A cursory interpretation of the specific conductance data from as quantitative a view point as possible will be attempted, but no interpretation will be attempted for the temperature data of this report.

A typical response of the downhole specific conductance probe occurred during Test 4B. Figure 12 is a graph of the indicated temperature and specific conductance for Test 4B on 10-07-82 versus time. Injection at 146 gpm began at 13:00 on 10-7-82. The tracer injection pump was turned on at 13:01 and was turned off at 14:31, one hour prior to ceasing injection at 15:31. During injection the downhole specific conductance sensor was thus initially exposed to fluid that had remained in the wellbore from backflow during Test 4A. A traverse of the open borehole was run immediately prior to 14:00. From 14:00 to 14:55, the indicated specific conductance increased, although the temperature corrected specific conductance of the backflow fluid from Test 4A was essentially constant. The temperature was expected to decline as the colder water from the upper portion of the borehole was displaced downward. The declining temperature

should have resulted in a decreasing specific conductance rather than the increasing values observed between 14:00 and 14:55. Therefore, it was presumed that the colder, higher specific conductivity fluid being injected into the wellhead which displaced the residual lower specific conductivity RRGP-5BF fluid resulted in a better ground connection between the logging cable armor and the well casing liner. Thus there was an indicated increase in specific conductance while it was actually decreasing. This erroneous temporal data trend resulted because of probe construction.

The slug of injected RRGE-3 water with tracer resulted in a significant increase in the indicated specific conductance beginning at 14:55 which essentially stabilized from 15:00 until the end of injection. These step-like perturbations can be used to quantify to some extent the erroneous indicated downhole specific conductance data. For the 4A Test, the well was backflowed until the specific conductance reached 2600 µmhos/cm at 25°C. Table 6 contains selected specific conductance data collected at the wellhead and downhole for the step-like perturbations observed during the injection phases of the injection-backflow tests. The temporal trend in Figure 12 that developed in the period prior to arrival of the RRGE-3 fluid with tracer appeared to be present for the initial 15 min following the arrival of RRGE-3 fluid with tracer at the downhole sensor. The trend that developed prior to the arrival of the RRGE-3 fluid with tracer was projected into the period following the arrival of the RRGE-3 fluid with tracer which in this case was 2975 µmhos/cm at 15:12 (Figure 12, Table 6). The specific conductance-temperature probe indicated a specific conductance of 5150 mhos/cm at 15:12 (Figure 12, Table 6). Thus, the wellhead specific conductance changed from 2600 to 7400 µmhos/cm which was an increase of 4800 µmhos/cm while the downhole sensor changed from 2975 to 5150 µmhos/cm, a change of only 2175 µmhos/cm. The actual specific conductance change downhole should be greater than that at the wellhead due to the elevated temperature, which is not the case. These apparent errors in the specific conductance data collected downhole limit the utility of the raw data.

TABLE 6. SPECIFIC CONDUCTANCE DATA AT WELLHEAD AND DOWNHOLE FOR STEP-LIKE PERTURBATIONS OBSERVED DURING INJECTION

Test No.	Date	Wellhead Background or Reference Specific Conductance µmhos/cm	Peak Wellhead Specific Conductance µmosh/cm	Mean Wellhead Specific Conductance µmhos/cm	Time For Peak Downhole Specific Conductance	Peak Specific Conductance Temp. Probe Indication µmhos/cm	Projected Pre-peak Downhole Specific Conductance Indication µmhos/cm	Change In Wellhead Specific Conductance µmnos/cm	Change In Downhole Specific Conductance µmnos/cm	Wellhead Specific Conductance Change Per Downhole Probe Chart Division µmhos/cm Chart Div.
2A2	9-15-82	2270	3960	3115	11:11	11600	8750	1690	2850	119
2C	9-16-82	2400	7700	5050	12:00	6300	1800	5300	4500	236
4B	9-7-82	2600	7400	5000	15:12	5150	2975	4800	2175	441
1C	10-08-82	2400	7300	4850	20:08	5100	2500	4900	2600	377
2D	10-18-82	2500	7400	4950	15:31	8800	6000	4900	2800	350
		7400	10050	8725	15:42	9400	8900	2650	500	1060
	10-19-82	8600	16400	12500	15:44	10000	9125	7800	875	1784

1. Five chart divisions/1000 µmho/cm.

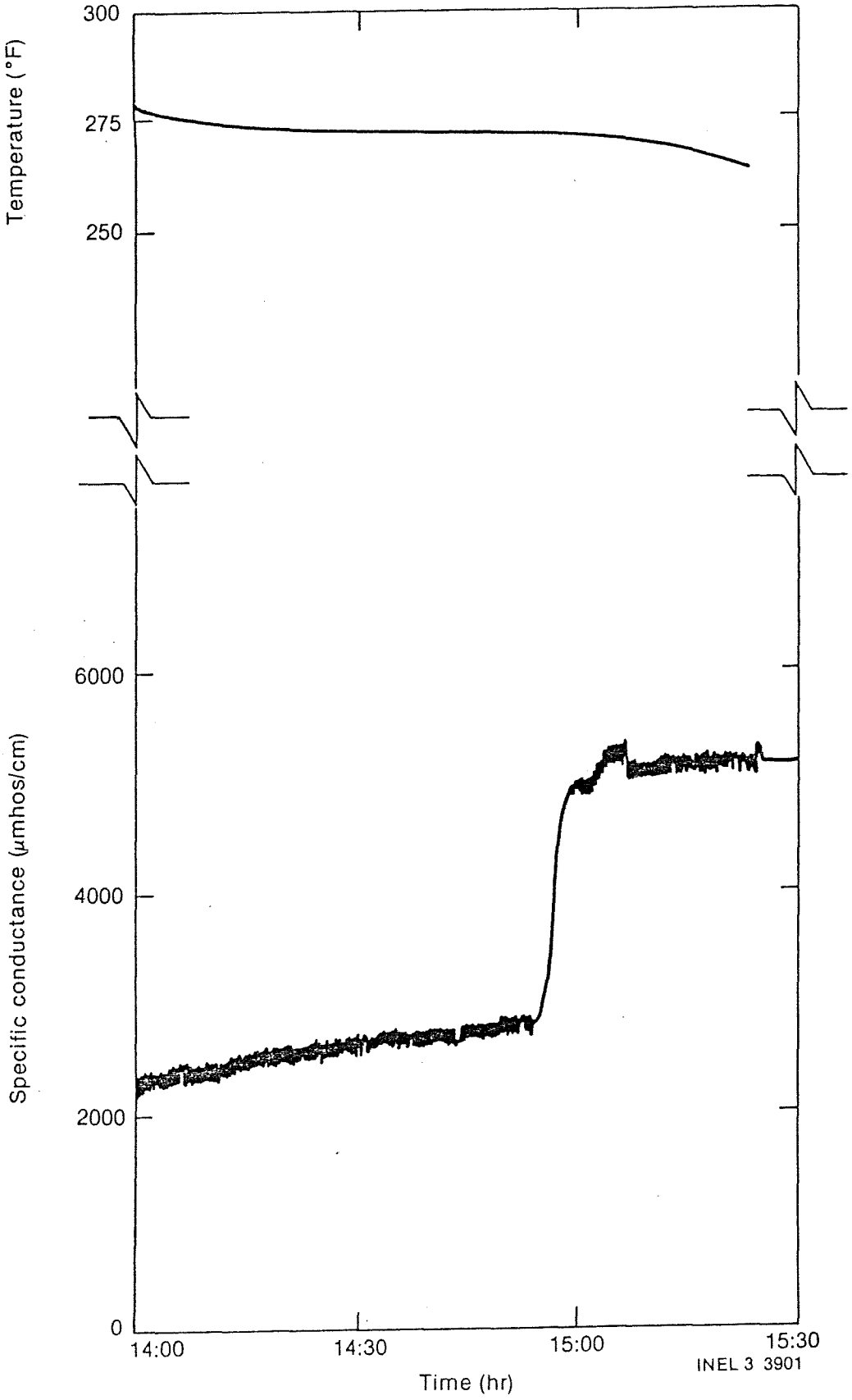

Figure 12. Indicated temperature and specific conductance at a depth of 4514 ft. for Test 4B on 10-07-82 versus time.

The downhole specific conductance data may provide some useful qualitative information on the specific conductance changes in the open borehole during both injection and backflow phases. The specific conductance indicated by the downhole sensor can be recalibrated during injection using the wellhead data collected 1.83 h earlier and during backflow and by using the wellhead data collected 1.82 h after the time for which downhole calibration is desired. Thus, using the wellhead specific conductance data, the data collected using the downhole probe can be corrected for drift in the absolute values indicated.

The next problem is to determine the specific conductance changes in the open borehole that can be attributed to each chart division on the downhole log strip chart (Figure 12). As calibrated on the land surface in solutions having specific conductances of approximately 2000 and 20,000 μmhos/cm, each chart division indicates 200 μmhos/cm. This wellhead calibration was used to indicate the numeric values for the specific conductance-temperature probe data listed in Table 6 and to provide the y axis scale in Figure 12. Thus, for Test 4B, a change of 2175 μmhos/cm downhole (Table 6) is 10.88 chart divisions in Figure 12 on the y axis. Since the actual change in the specific conductance at the wellhead was 4800 μmhos/cm, each chart division is indicative of 4800/(2175/200) = 441 μmhos/cm (Table 6). This downhole specific conductance value per chart division on the logging truck strip chart is plotted in Figure 13 versus wellhead specific conductance. The range of the wellhead specific conductance values that resulted due to the step-like increase due to injection of RRGE-3 fluid into RRGP-5BF are plotted as are means for the interval. These step-like increases in downhole specific conductance that resulted when RRGE-3 fluid was injected into RRGP-5BF indicates that for a change in wellhead specific conductance from 2600 to 7400 μmhos/cm, the downhole specific conductance change per chart division averaged 441 μmhos/cm rather than the 200 μmhos/cm for which the probe was calibrated at the land surface using solutions of different specific conductances and temperatures.

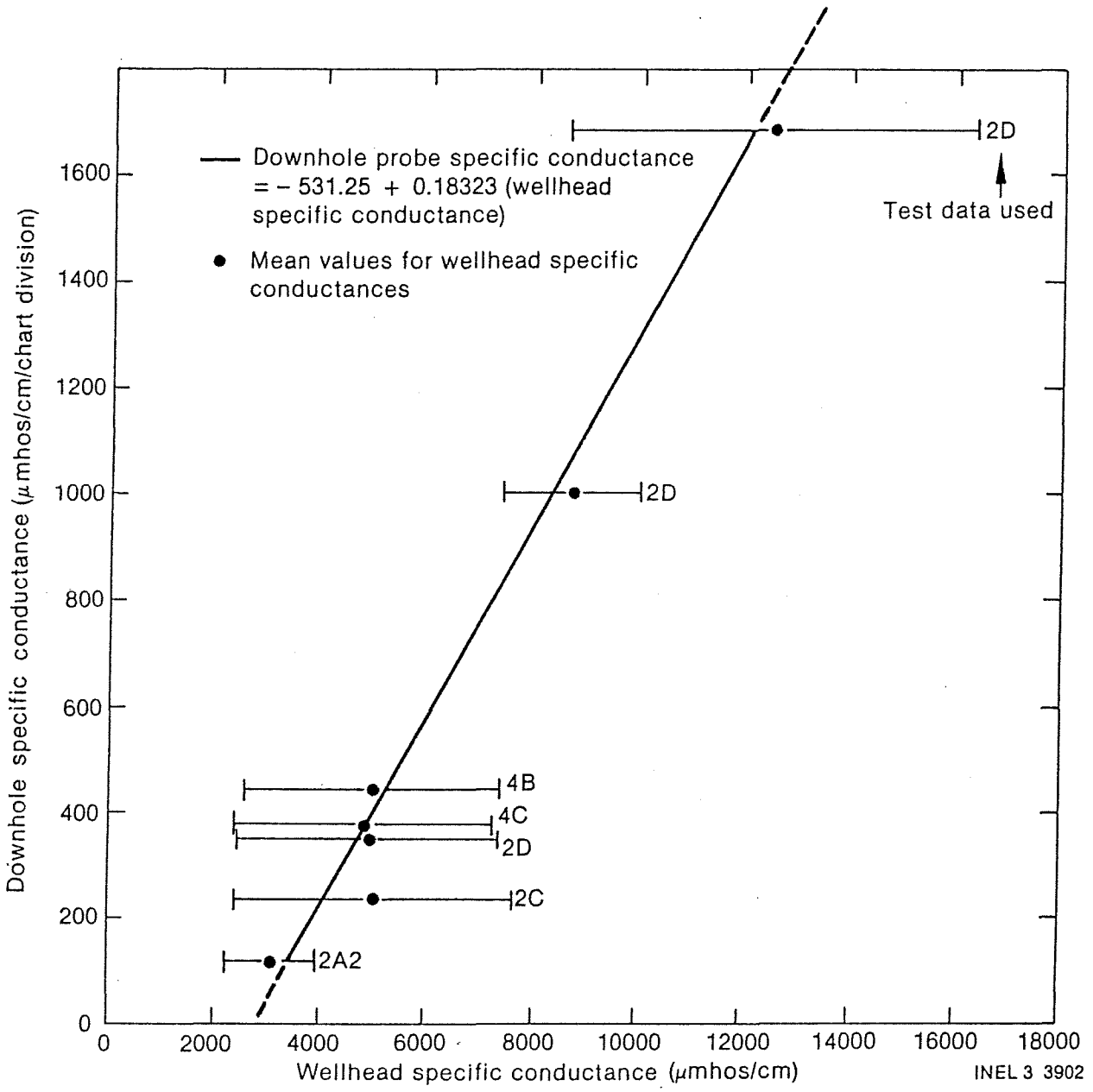

Figure 13. Injection borehole specific conductance changes per logging chart division versus wellhead specific conductances 2 hours prior to downhole data.

The step-like perturbations that resulted due to the injection of RRGE-3 fluid ± tracers into RRGP-5BF fluid as well as the pulses that resulted due to the injection of tracers into RRGE-3 fluid at various times long after injection had been initiated were used for all other injection test data to estimate the relationship between the change in specific conductance per chart division on the strip chart and the wellhead specific conductance. The pertinent data are listed in Table 6 and plotted in Figure 13. The linear regression through the means suggests that each chart division can represent changes in specific conductance ranging from near 200 to 1600 μmhos/cm for actual wellhead specific conductances ranging from 4000 to 12,000 μmhos/cm respectively. These results and the questionable accuracy of the data for mean specific conductances less than 5000 μmhos/cm dictate a prudent approach to quantifying the specific conductance profiles in the open borehole during backflow based on the step-like perturbations in specific conductance that resulted during injection.

3.1.2 RRGE-1 Borehole Temperature Logs

Two temperature logs have sufficient resolution and were run at appropriate times to be considered for analysis. These logs were run on 09-17-82 and 09-21-82 (Figure 14). The pertinent operations log for RRGE-1 is contained in Table 7. Basicially, the well discharge began on 09-15-82 and was increased in a step-like manner to 285 gpm approximately 1 h prior to the beginning of logging the open borehole. Following logging, the flow rate was decreased to 18 gpm until approximately 8 h prior to logging on 09-21-82 when the well was shutin.

The temperature logs indicate there are several producing zones. A major inflow of water which is cooler than that flowing up the borehole from below results in a step-like temperature decline between 4266 and 4276 ft on 09-17-82. This aquifer also results in a change of the thermal gradient in the wellbore on 09-21-82 presumably because the fluids from aquifers below are flowing up the borehole and into this aquifer when the well is shutin because this is a ground-water discharge area with

TABLE 7. RRGE-1 OPERATIONS LOG 09-01-82 TO 09-21-82

Date	Time	Event
09-01		Shutin
09-09		Open-closed
09-15	15:58	Flow to experiments
09-16	08:13	Flow increased to 84 gpm
	09:53	Shutin
	19:19	Begin warm-up flow 136 gpm
09-17	08:03	Flow increased to 150 gpm
	11:48	Flow increased to 285 gpm
	13:00	Logged for temperature
	18:01	Flow decreased to 18 gpm
09-21	07:48	Shutin
	15:30	Logged for temperature

were to occur from RRGP-5BF, it would likely occur in one of the aquifers within the Schist of the Upper Narrows. The upper aquifers in the Schist of the Upper Narrows appear to have a complex microthermal regimen which depends to some degree on the wellhead discharge rate.

Another thermally definable aquifer system exists in the lower section of the Schist of the Upper Narrows between depths of 1425 and 1437 m (4675 and 4714 ft). Two distinct aquifers appear to be present, an upper one which discharges cooler water than the lower one which is between 1430 and 1437 m (4691 and 4714 ft). Since these aquifers presumably discharge fluid into the wellbore even with the wellhead shutin, the thermal differences are not necessarily dependent on the wellhead discharge rate as it is suspected that only a low flow originates from below 1437 m (4714 ft) when the wellhead is shutin or discharging. This wellbore flow system is suggested by the similarity of the temperature logs with the wellhead shutin or discharging. The quality of fluid contributed by these aquifers is not known, as their existence is based only on the temperature logs.

Another aquifer 6 m (20 ft) thick exists between depths of (1492 and 1498 m (4896 and 4916 ft). The temperature increase from the top to the bottom of the borehole fluid in this aquifer section is between 0.03 and 0.16°C (0.12 and 0.20°F). The quantity of water yielded by this aquifer is probably low. This aquifer is the lowest aquifer readily distinguishable on the temperature log.

The temperatures logged at the touchdown or the bottom of the open borehole are less than those originally reported. The borehole originally had a measured borehole depth of 1521 m (4990 ft) and a maximum downhole temperature of 144°C (292°F) according to the drillers log, and 146°C (295°F) according to the USGS.[11] The measured depth of the well is now 1514 m (4966 ft) indicating that 7 m (23 ft) of the borehole has been filled in. This 7 m (23 ft) of fill probably has not significantly affected the maximum borehole temperature. The maximum temperature logged with the well flowing is now 142°C (287.4°F). These data suggest the downhole maximum temperature has probably decreased between 3 and 5°C (5

and 8°F) due to fluid withdrawals since well completion in 1975. Whether these apparent temperature declines are real or due to differences between logging equipment is not known, but wellhead temperature data also suggest a slight decline in temperature. Flow system changes due to geothermal fluid withdrawals and the construction of the wells has undoubtedly affected the thermal and water quality regimen near RRGE-1, with the apparent bottomhole temperature decline probably being a manifestation of the resource exploitation.

3.2 Well-Head Pressure-Temperature Responses

3.2.1 Injection-Backflow Tests

3.2.1.1 Introduction. The injection-backflow testing of the RRGP-5BF was designed primarily to define tracer recovery characteristics as they depend on a specific parameter of the well, the reservoir, and the test procedure used. Pressure response monitoring was an integral part of the test. The set tests combined injection and backflow periods, thus creating a unique opportunity to monitor pressure build-up and fall-off phases as well as pressure decline and recovery phases. Fortunately, an essentially constant head boundary stabilized the wellhead pressure response within 5 min. Shutin periods between tests need only be 5 min or more to permit each test to be treated as a separate experiment with no lingering pressure effects from preceding tests. This shutin period of 5 min or more was met or exceeded in all experiments, and injection or backflow continued for more than 5 min. This rapid stabilization of wellhead pressures simplifies data analysis.

The pressure response data collected during the September-November testing are presented on a test by test basis. There are some general responses characteristic of these tests.

The first is a short period of transient pressure conditions. The wellhead pressure stabilizes after two to four minutes from the beginning of a change in the flow rate. This early time transient pressure period is

characterized by rapid pressure changes. Water hammer effects and flow rate adjustments have significant effects on the pressure response during this period.

The second factor affecting wellhead pressure response is a temporally dependent temperature for the injection and backflow fluids. The semilogarithmic plots of the wellhead pressure and temperature versus time clearly demonstrate pressure responses related to the fluid temperature changes. The injected fluid temperature was, in most cases, approximately 107°C (225°F) while background bottom hole temperature in the RRGP-5 BF is 134°C (273°F). The wellhead temperature while flowing at 9.5 x 10^{-3} m^3/sec (150 gpm) is 125°C (257°F). The temperature differences between the injected fluid, the wellbore fluid, and formation fluid resulted in continual wellbore fluid temperature changes during the injection and backflow phases. The cooling of the wellbore fluid from 125°C (257°F) to 107°C (225°F) over the total depth of 1390 m (4562 ft) reduces wellhead pressures by over 32 psi. Precise correction of wellhead pressure data to a constant wellbore thermal profile is impossible since the exact temperature distribution within the wellbore at all times is not known. In addition, the fluid viscosity changes as the reservoir temperature changes, and that also effects the reservoir induced wellbore pressure response. The fracture widths in the reservoir may also be affected by reservoir temperature changes. This last phenomenon is not well recognized or understood. Because of these factors affecting wellhead pressures, the wellhead pressure response data collected at RRGP-5BF during the injection-backflow testing has limited value for reservoir evaluation.

3.2.1.2 General Pressure-Temperature Responses in RRGP-5BF. Pressure responses to the tests conducted during the injection-backflow experiments are generally consistent from test to test. The following is a test by test summary of the pressure and temperature responses at the wellhead during the injection-backflow testing. The first test, 2A-1, was conducted mainly to check the tracer injection mechanical setup as well as to check operational procedures for the injection-backflow testing.

3.2.1.2.1 Test 2A-2--Test 2A-2, which was conducted on 09-15-82, was the first test where a tracer was injected into the reservoir. Injection at 9.2 x 10^{-3} m^3/sec (146 gpm) was maintained for 242 min. The injected fluid temperature at the wellhead was nonisothermal, increasing from below 93°C (200°F) at the beginning of injection to 104°C (220°F) at the end of injection. Figure 15 is a plot of wellhead pressure and wellhead temperature versus the logarithm of time since injection began. The wellhead pressure buildup response is significantly affected by the fluid density changes within the wellbore. During the first 3-min of injection, the wellhead pressure buildup reached a maximum of 149.7 psia. Problems with the flow rate valve occurred early in the test. The cold water injection results in suppressed wellhead pressures due to a borehole fluid density increase. Between 3 min and 200 min, the pressure decreased, reaching minimum of 102.5 psia. Between 200-min and the end of the test at 242 min, the pressure was steady at 102.5 psia. Correcting the wellhead pressure for the injection of fluid at a temperature of 104°C (220°F) to a temperature of 129°C (265°F) would result in a relatively steady wellhead pressure of 150 psia.

During the first 2 min of quiescent time following wellhead shutin, the wellhead pressure declined to 82.2 psia. A pressure plot is not available since an accurate shutin time is not known. Between 2 min and the end of the quiescent phase at 20.5 min, the wellhead pressure was building up slightly due to an increasing temperature of the wellbore fluid. At the end of the quiescent phase, the wellhead pressure was 84.0 psia.

During the first 2.5 min of backflow, the wellhead pressure decreased rapidly to 62.0 psia (Figure 16). The pressure started to increase after 3.5 min, reaching 110.5 psia at the end of the test. This wellhead pressure increase was caused by a wellbore fluid temperature increase. The temperature recorded at the wellhead increased from below 93°C (200°F) at the beginning of backflow to 124°C (255°F) at the end of the 612 min of the backflow. The wellhead pressure recovered to a maximum pressure of 134.6 psia within less than 20 min after the well was shutin for the

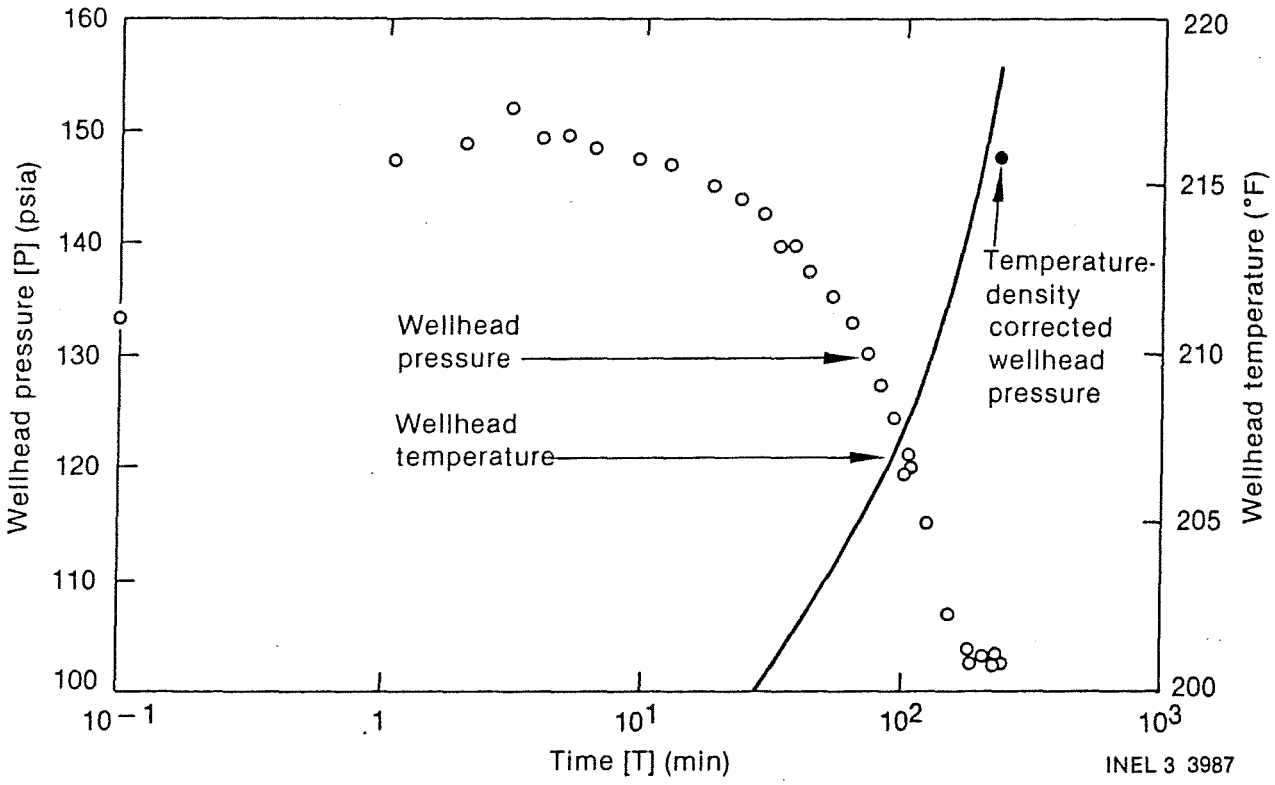

Figure 15. Test 2A-2 injection wellhead pressure and temperature for RRGP-5BF versus log time.

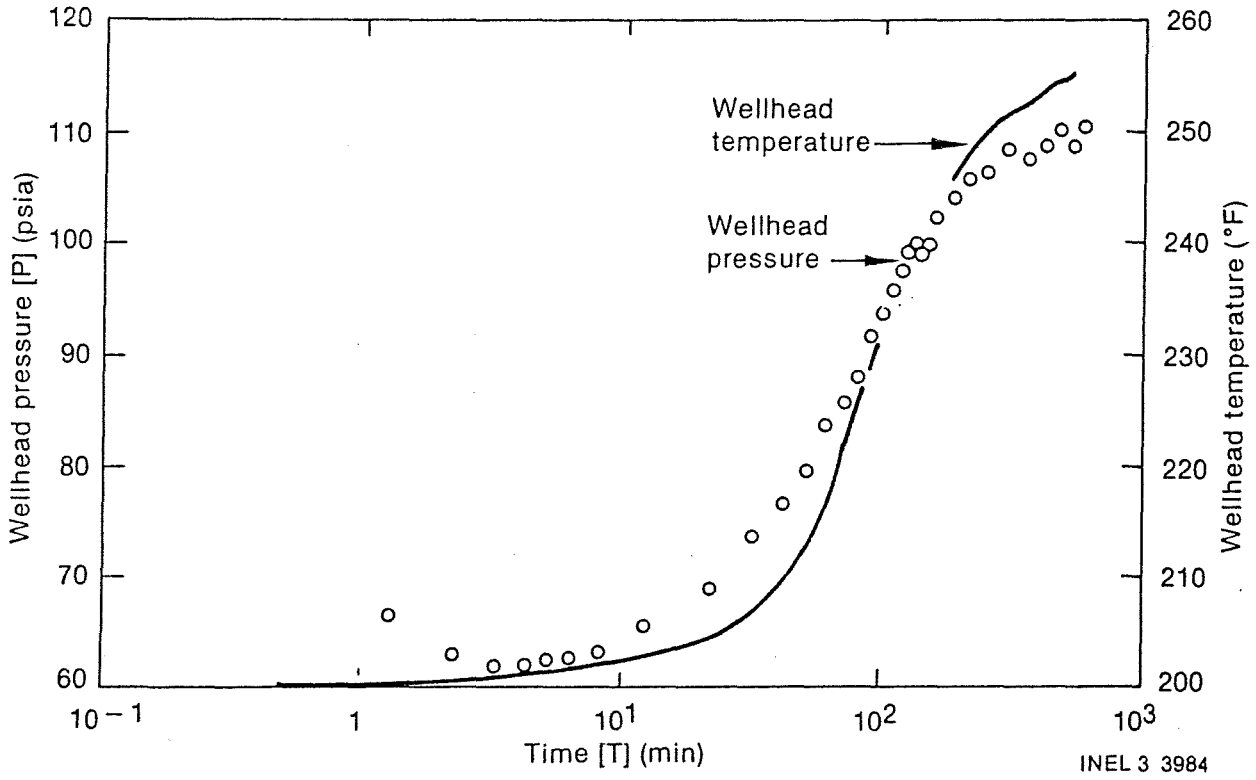

Figure 16. Test 2A-2 backflow wellhead pressure and temperature for RRGP-5BF versus log time.

backflow quiescence phase. A pressure recovery plot is not available for the backflow quiescence period.

3.2.1.2.2 Test 2C--Test 2C was conducted between 09-21-82 and 09-27-82. The injection phase had a duration of 2910 min. A maximum wellhead pressure of 132.7 psia was recorded 7 min into the test (this was the first pressure reading recorded) (Figure 17), and is suspected of not being the peak pressure resulting from injection. Between 7 and 12 min after beginning injection, the wellhead pressure was relatively steady. After 12 min the pressure decreased, reaching a low of 106.5 psia at 130 min. The pressure decrease is correlated with a cooling of the wellbore fluid column since over 120 min of injection was required to replace the total volume of the wellbore. The wellhead had been shutin for 5 days which permitted significant cooling of the wellbore fluid and of the geologic materials and fluid in the vicinity of the wellbore. Between 130 and 320 min of injection the pressure increased from 106.5 psia to 116.5 psia. The pressure remained relatively steady between 320 min and the end of injection when the pressure was 116.8 psia. The injected fluid temperature was relatively steady at 107°C (225°F) during the entire test 2C injection period.

The quiescent period between injection and backflow was short; it took less than 5 min to change from injection to backflow. Since approximately 30 sec was required for shutin, a pressure plot has not been constructed. During the quiescence, the pressure declined to 96.5 psia (a total decline of approximately 20 psi).

The backflow started with an immediate pressure decline of approximately 10 psi (Figure 18). Between 0.2 and 2.2 min, the pressure data formed a straight line on a semilogarithmic plot with a Q/s_{10} value of $8.1 \times 10^{-4} m^3$/sec/psi/log cycle (12.8 gpm/psi/log cycle) where Q is the discharge rate in gpm and s_{10} is the slope of the data on a semilogarithmic plot of pressure versus time. This value is related to the hydraulic conditions near the wellbore, primarily the open channels in the fracture. Between 4.0 and 22 min of backflow, the pressure was relatively

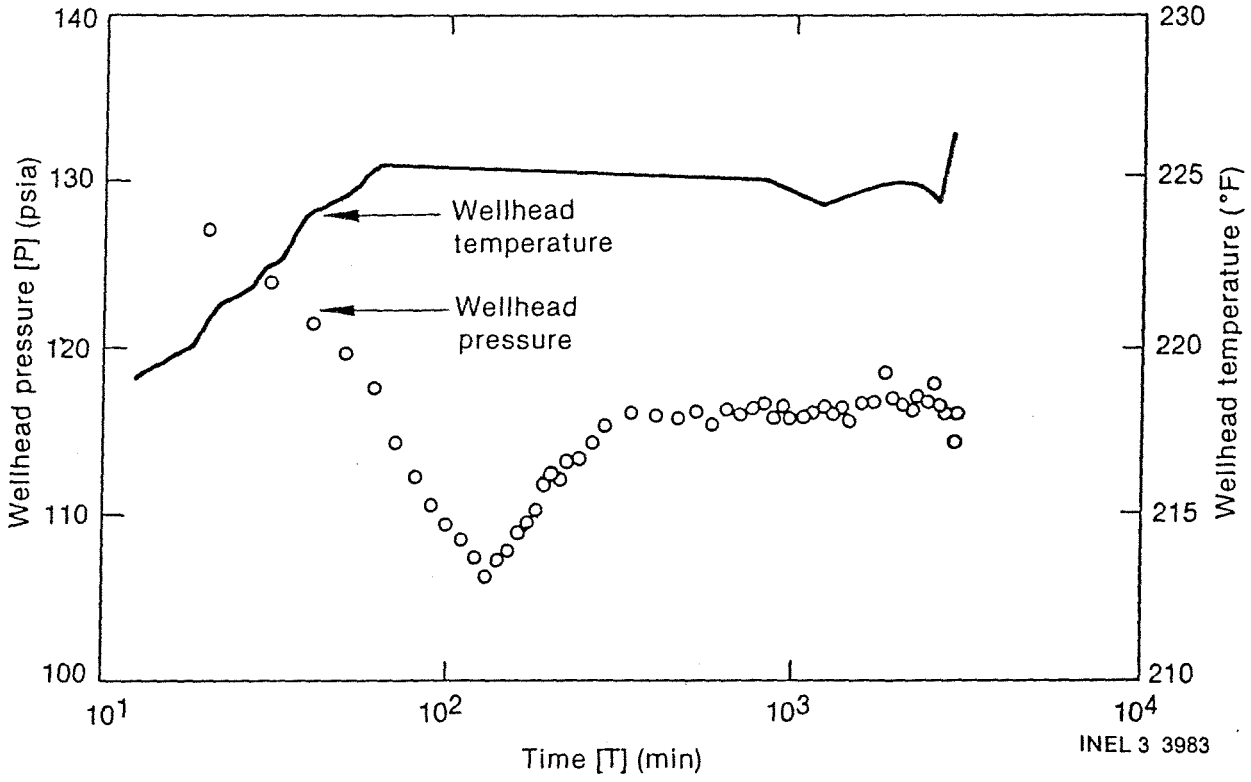

Test 2C injection wellhead pressure and temperature for RRGP-5BF versus log time.

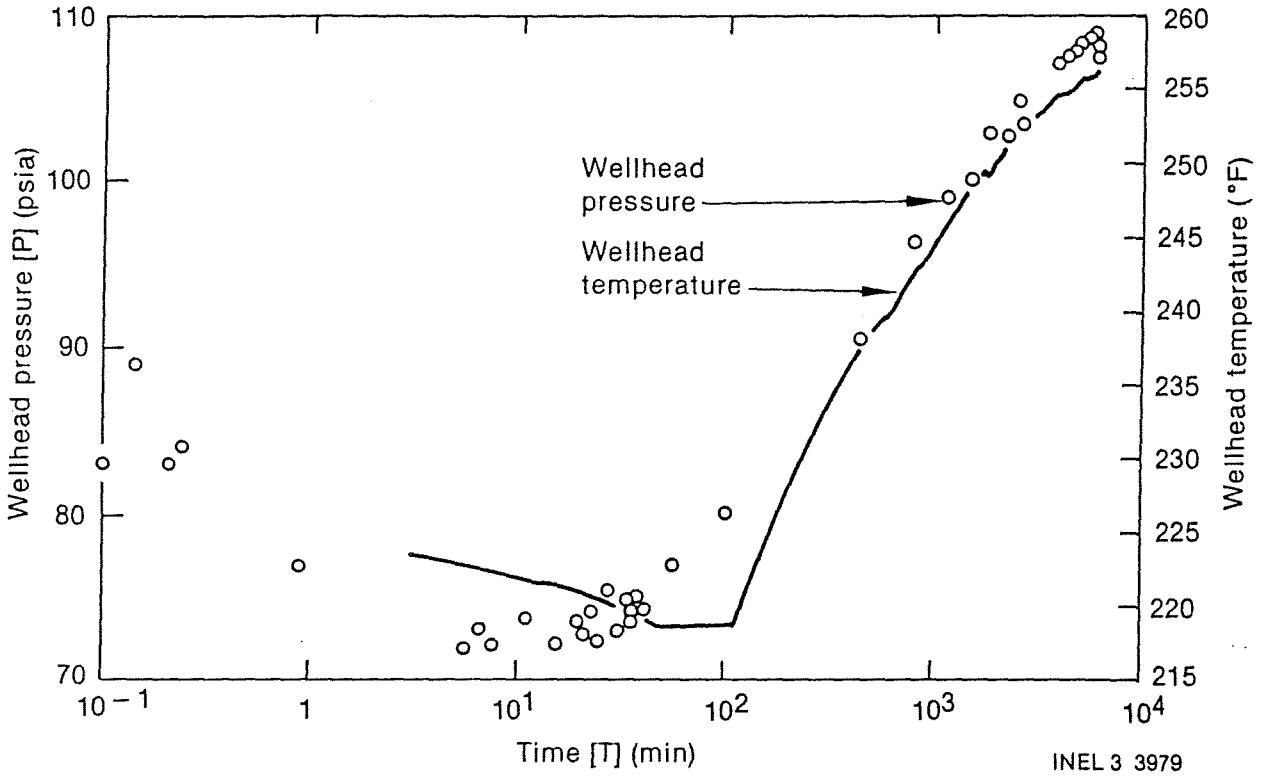

Figure 18. Test 2C backflow wellhead pressure and temperature for RRGP-5BF versus log time.

steady at 72 psia. Between 22 and 60 min the pressure increased from 73 psia to 76 psia; this increase was nonlinear and irregular. After 60 min, the pressure increased, reaching 109 psia at 6000 min. This pressure buildup resulted due to the temperature increase of the fluid in the wellbore. The fluid temperature increased from 103°C (218°F) at 90 min to 124°C (256°F) at the termination of flow at 6400 min.

After the well was shutin, the wellhead pressure recovered to 131.7-psia level in less than 10 min.

3.2.1.2.3 Test 2D--Test 2D was conducted between 10-18-82 and 10-31-82. The injection phase at Test 2D had a duration of 5890 min (Figure 19). The maximum wellhead pressure of 150.5 psia was reached within 2 min of injection. The wellhead pressure was relatively steady between 2 and 6 min and started to decrease after 6 min of injection. At 290 min, the pressure reached 118.5 psia and remained near this valve until the injection ended. The temperature of the injected fluid was approximately 103°-104°C (218°-219°F) from 25 to 300 min. The temperature gradually increased to 106°C (223°F) at the end of injection.

The quiescent period between injection and backflow was less than 9-min duration. Pressure fall-off (Figure 20) was rapid and short. The pressure stabilized at 97.5 psia 2 min after the well was shutin. Total pressure fall-off was of approximately 19.8 psi.

The backflow phase of the test continued for 14,000 min. Pressure drawdown was observed for 5 min (Figure 21). Approximately 1.7 min were required to establish flow at a constant 9.5×10^{-3} m^3/sec (150 gpm). The maximum drawdown was 23.0 psi. Between 5 and 15 min of flow, the pressure remained approximately 74 psia. Between 15 min and the end of flow, the pressure increased, reaching a maximum of approximately 111.8 psia. Density corrected wellhead pressures plotted in Figure 21 suggest steady state conditions were reached early in the test.

Recovery of the wellhead pressure following shutin was very rapid (Figure 22). The wellhead pressure recovered to 135.3 psia within 5 min of

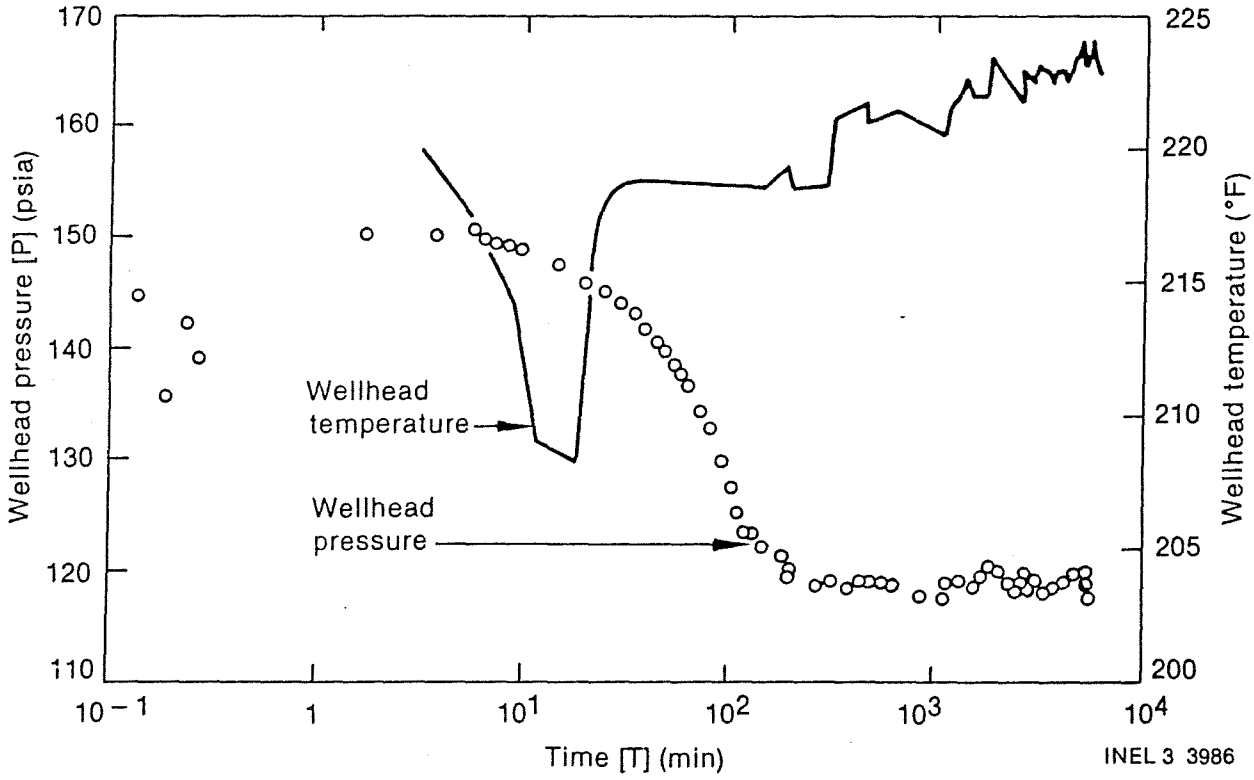

Figure 19. Test 2D injection wellhead pressure and temperature for RRGP-5BF versus log time.

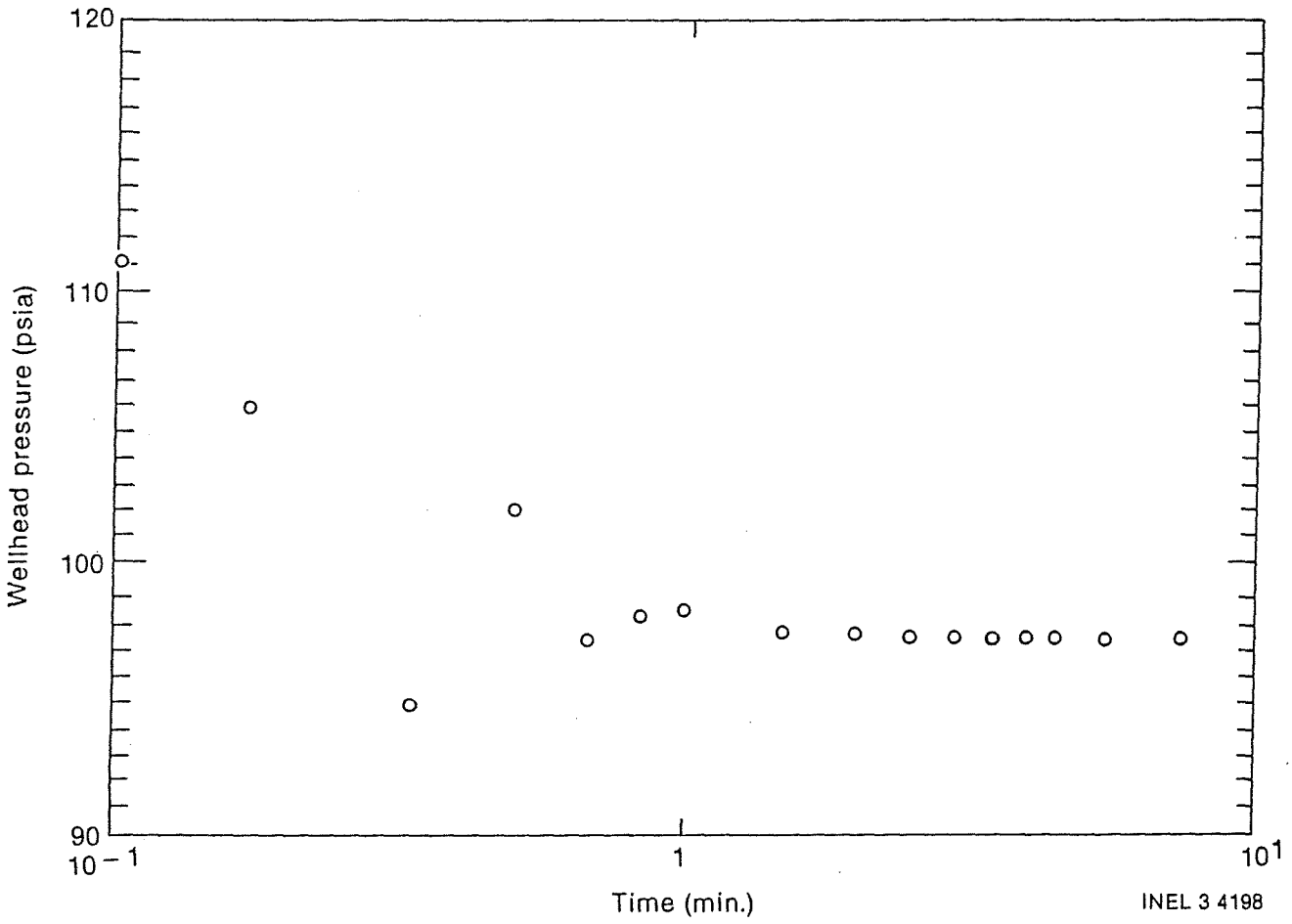

Figure 20. Test 2D injection quiescence wellhead pressure for RRGP-5BF versus log time.

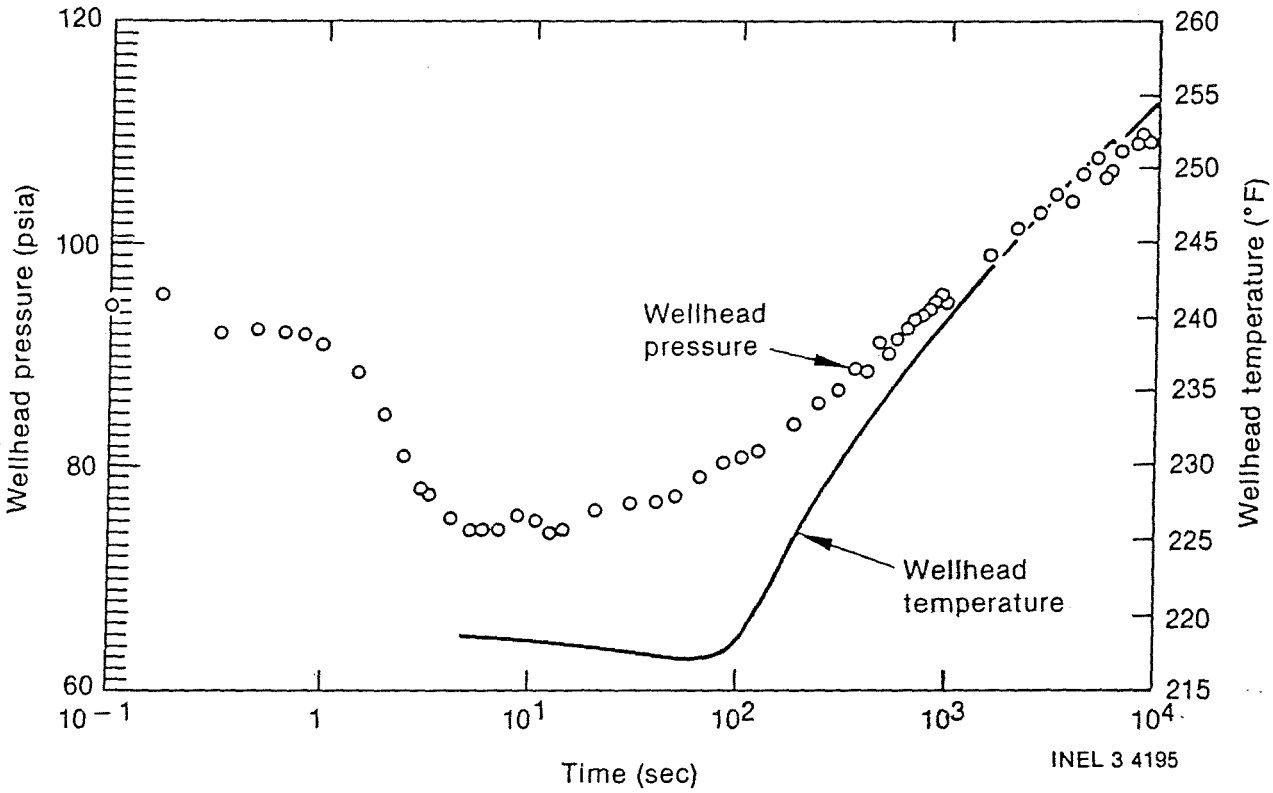

Figure 21. Test 2D backflow wellhead pressure and temperature for RRGP-5BF versus log time.

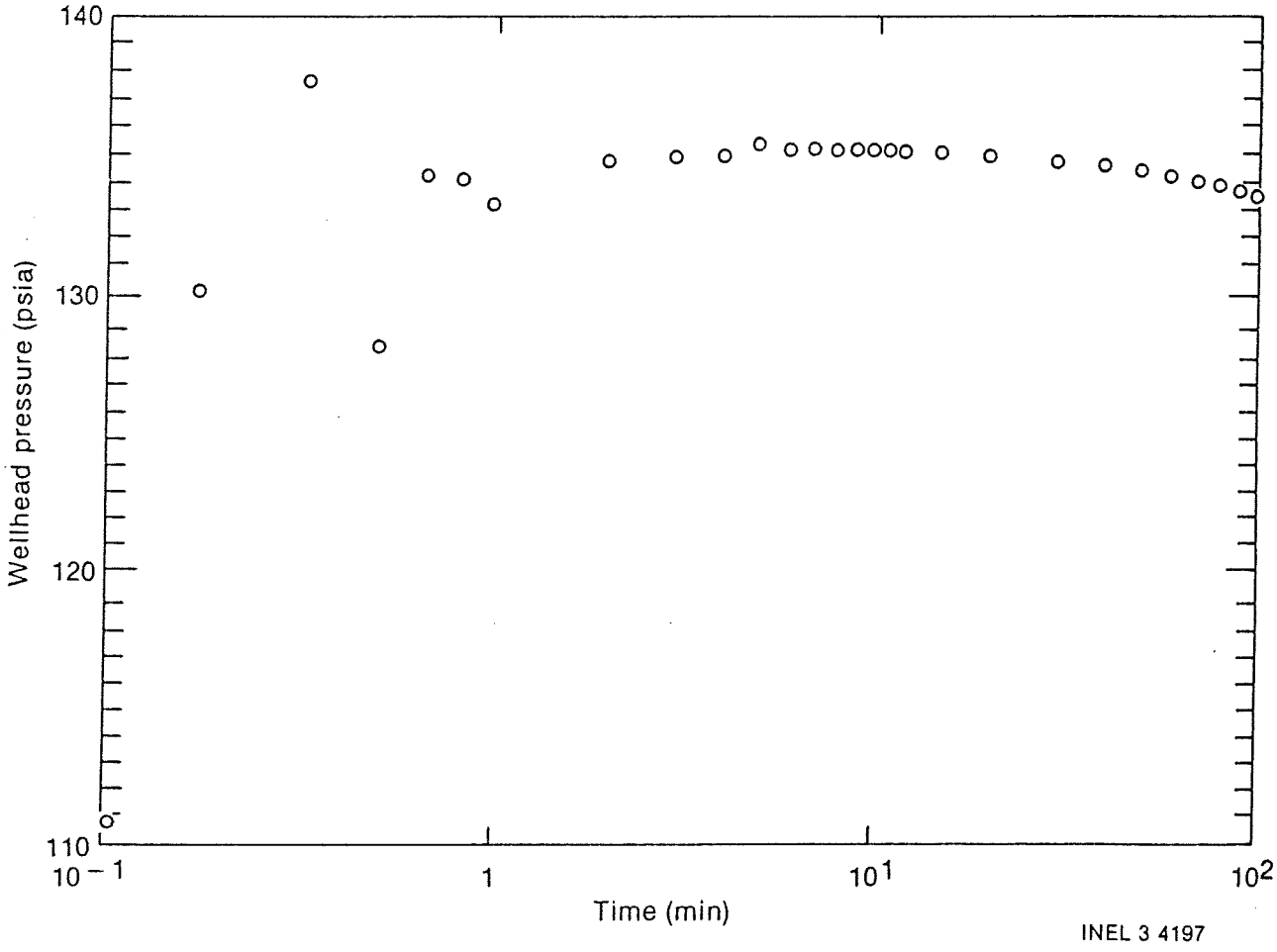

Figure 22. Test 2D backflow quiescence wellhead pressure for RRGP-5BF versus log time.

shutin with a gradual decline in pressure beginning after 10 min due to the gradual temperature decline in the wellbore fluid temperature.

3.2.1.2.4 Test 4A--Test 4A was conducted between 09-30-82 and 10-02-82. It was the first test of the series with a long duration quiescent time relative to the duration of injection. Injection continued for 143 min, which provided approximately 23 min for the injection of tracers into the receiving aquifers. During the first 10 min of the test, the injection rate was unstable, due to a malfunction of the instrument measuring the flow rate (Figure 23). After the injection rate was adjusted to 9.5×10^{-3} m^3/sec (150 gpm), the wellhead pressure decreased rapidly to values below 149 psia, reaching a minimum of 118.5 psia at the end of injection.

The well was shutin for 1653 min between injection and backflow. Pressure fall-off (Figure 24) was observed for less than 1.5 min reaching minimum of 94.3 psia. A sudden pressure surge from 94.8 to 100.4 psia, which was recorded 5.3 min after well was shutin, was probably the result of the closing of a previously leaking valve. The wellhead pressure declined to 96.4 psia in the next 10 sec but continuously increased until it stabilized at 113.9 psia. This increasing pressure resulted due to heating-up of the wellbore fluid during the quiescent phase because of a small leak (estimated at $9.5 \times 10^{-4} m^3$/sec (15 gpm).

The backflow phase had duration of 960 min (Figure 25). Wellhead pressure drawdown observed for the first 3 min of flow reached a minimum of 89.3 psia. Between 3 and 7 min the pressure did not change. The wellhead pressure increased between 7 and 180 min. Between 180 min and the end of the backflow, the pressure remained at approximately 109 psia.

The wellhead pressure recovered to 134.7 psia, 3.5 min after the well was shutin (Figure 26). A slow wellhead pressure decline occurred due to a decrease in wellbore fluid temperature.

3.2.1.2.5 Test 4B--Test 4B was conducted between 10-07-82 and 10-08-82. The injection continued for 141 min (Figure 27). The wellhead

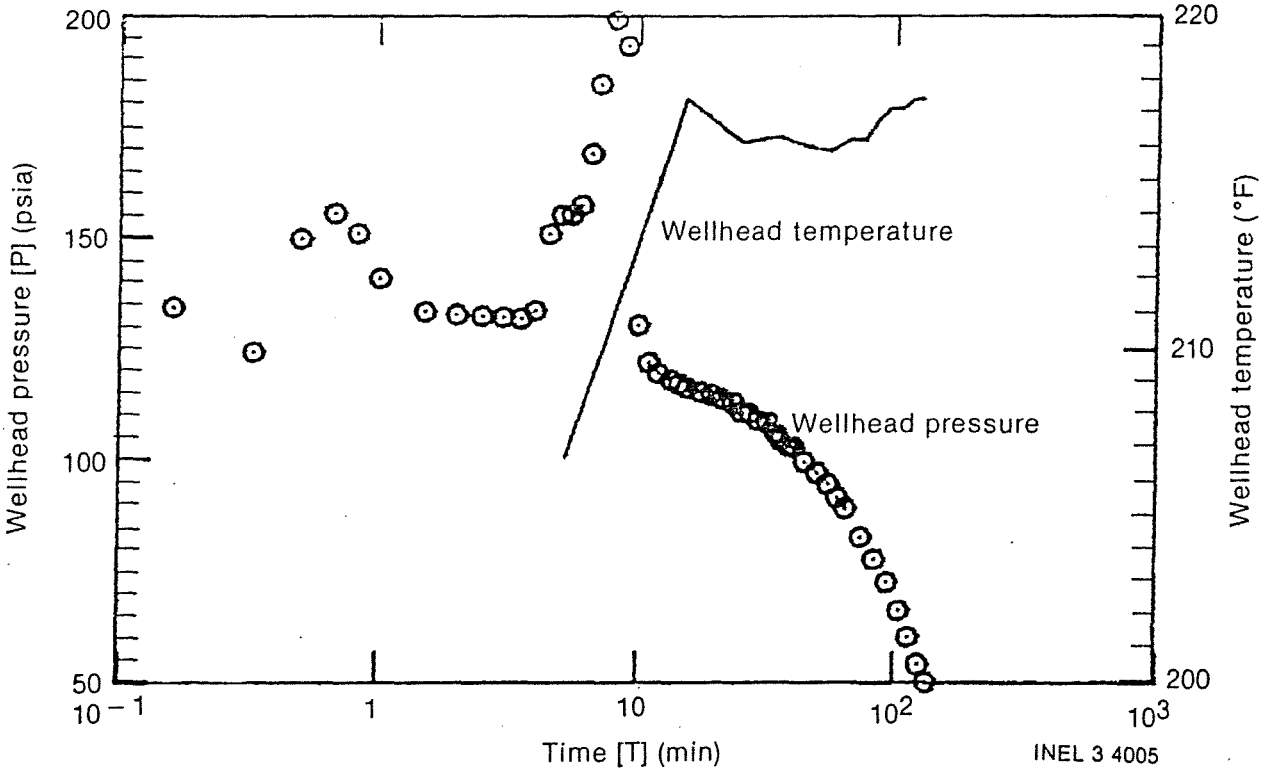

Figure 23. Test 4A injection wellhead pressure and temperature for RRGP-5BF versus log time.

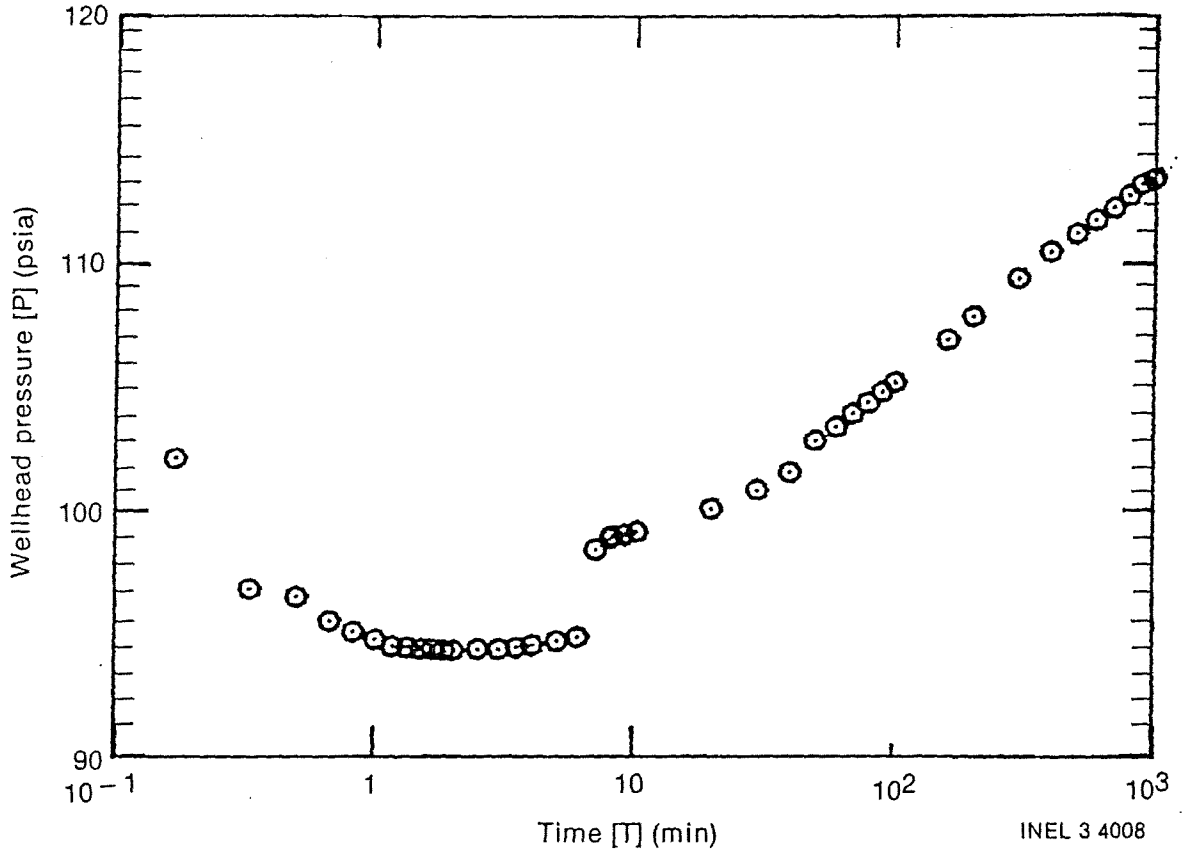

Figure 24. Test 4A injection quiescence wellhead pressure for RRGP-5BF versus log time.

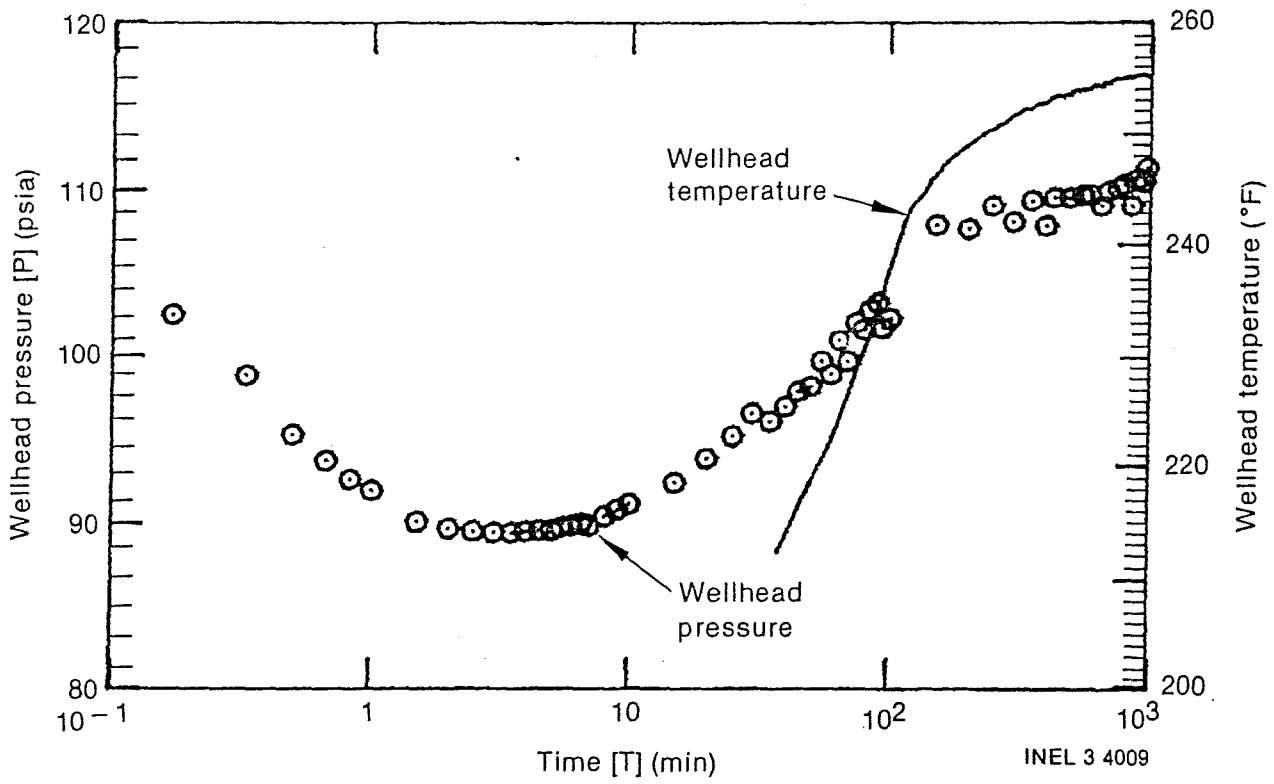

Figure 25. Test 4A backflow wellhead pressure and temperature for RRGP-5BF versus log time.

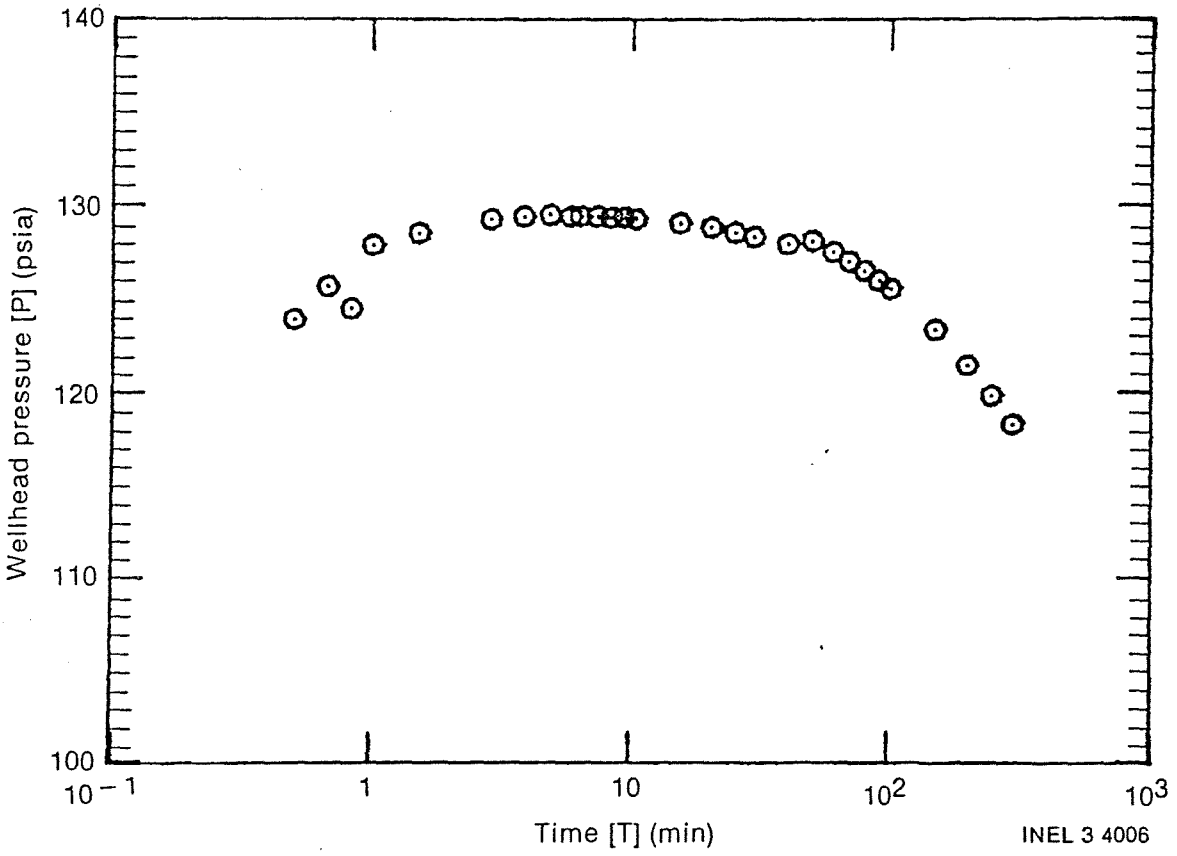

Figure 26. Test 4A backflow wellhead quiescence wellhead pressure for RRGP-5BF versus log time.

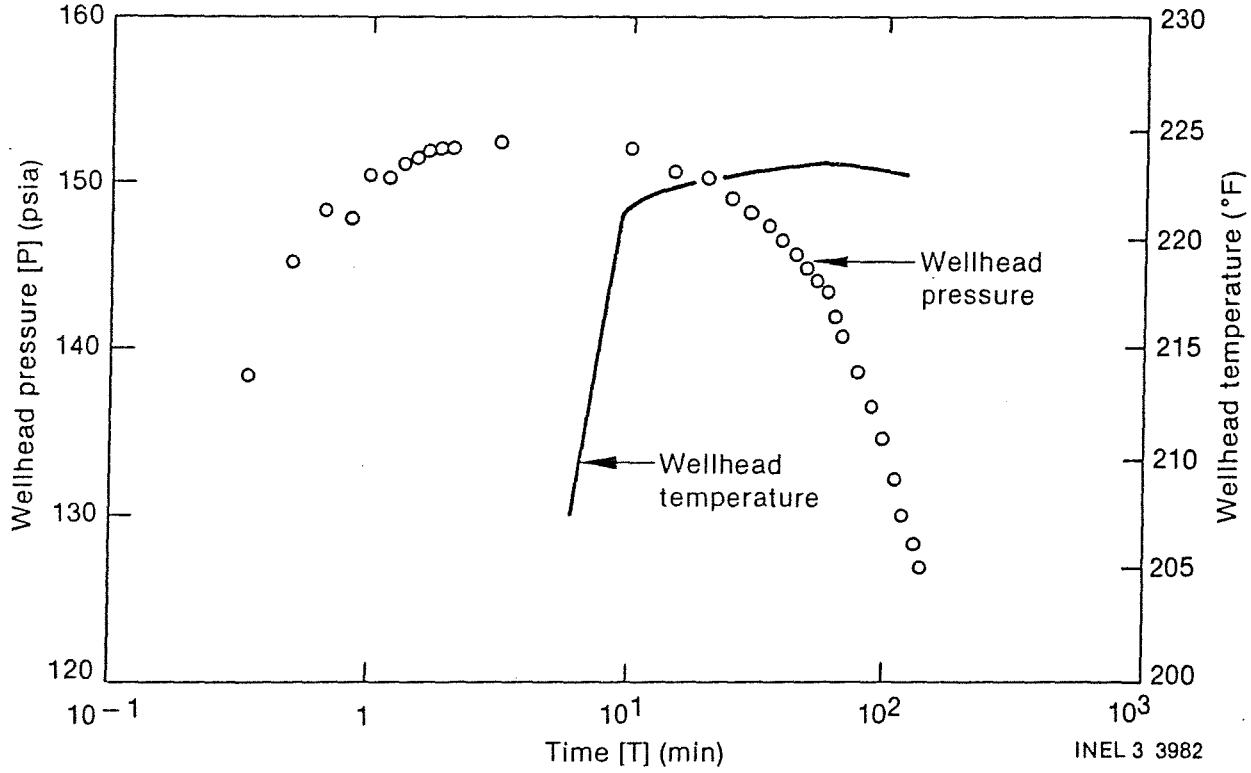

Figure 27. Test 4B injection wellhead pressure and temperature for RRGP-5BF versus log time.

pressure reached a maximum of 152.2 psia in 1.5 min from a preinjection pressure of 134.1 psia. Between 1.5 and 12 min the pressure remained steady. Between 12 min and the end of injection, the pressure decreased reaching a minimum of 126.6 psia. The injected fluid temperature was relatively constant at 106°C (223°F).

The quiescent phase between injection and backflow was 130 min (Figure 28). The wellhead pressure fall-off was rapid, with a minimum pressure of 105.8 psia being reached in 2 min. The steady-state pressure falloff was 20.8 psi. From 2 min until the end of quiescence, the wellhead pressure was increasing indicating an increasing wellbore fluid temperature. The wellhead pressure at the end of quiescence was 111.0 psia.

The backflow phase of Test 4B had duration of 900 min (Figure 29). The pressure declined to 88.6 psia after 3 min of backflow. The maximum pressure drawdown was 22.4 psi. The pressure remained steady between 3 and 11 min. Between 11 and 200 min the pressure increased to 110.5 psia. The wellhead pressure then gradually increased to 111.6 psia at the end of the test. The wellhead temperature for the first 30 min increased from 103°C to 104°C (217°F to 219°F). Between 30 and 200 min the temperature increased from 104°C to 122°C (219 to 251°F). Between 200 and 500 min the temperature increased to 124°C (256°F). After 500 min temperature was steady at 124°C (256°F).

After the well was shutin, the wellhead pressure recovered to 135.5 psia in approximately 10 min. Since data were collected on 10-min intervals, a buildup pressure plot has not been constructed. Total recovery was 23.9 psi.

3.2.1.2.6 Test 4C--Test 4C was conducted on 10-08-82 and 10-09-82. The duration of the injection phase was 140 min. The wellhead pressure response was similar to the previous tests responses (Figure 30). A precise time for the beginning of injection is not known for this test. The maximum wellhead pressure of 150.5 psia was reached in 2.5 min. After 4 min of injection, the wellhead pressure started to decline, reaching

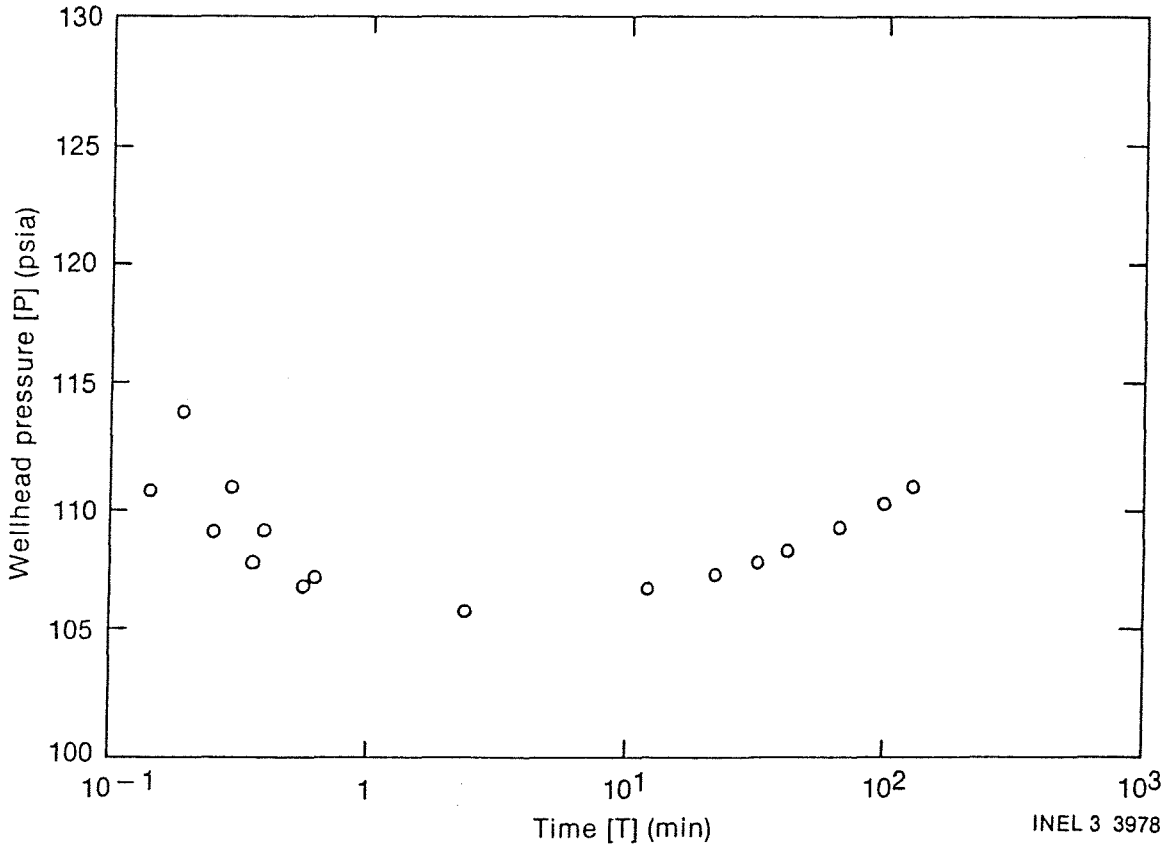

Figure 28. Test 4B injection quiescence wellhead pressure for RRGP-5BF versus log time.

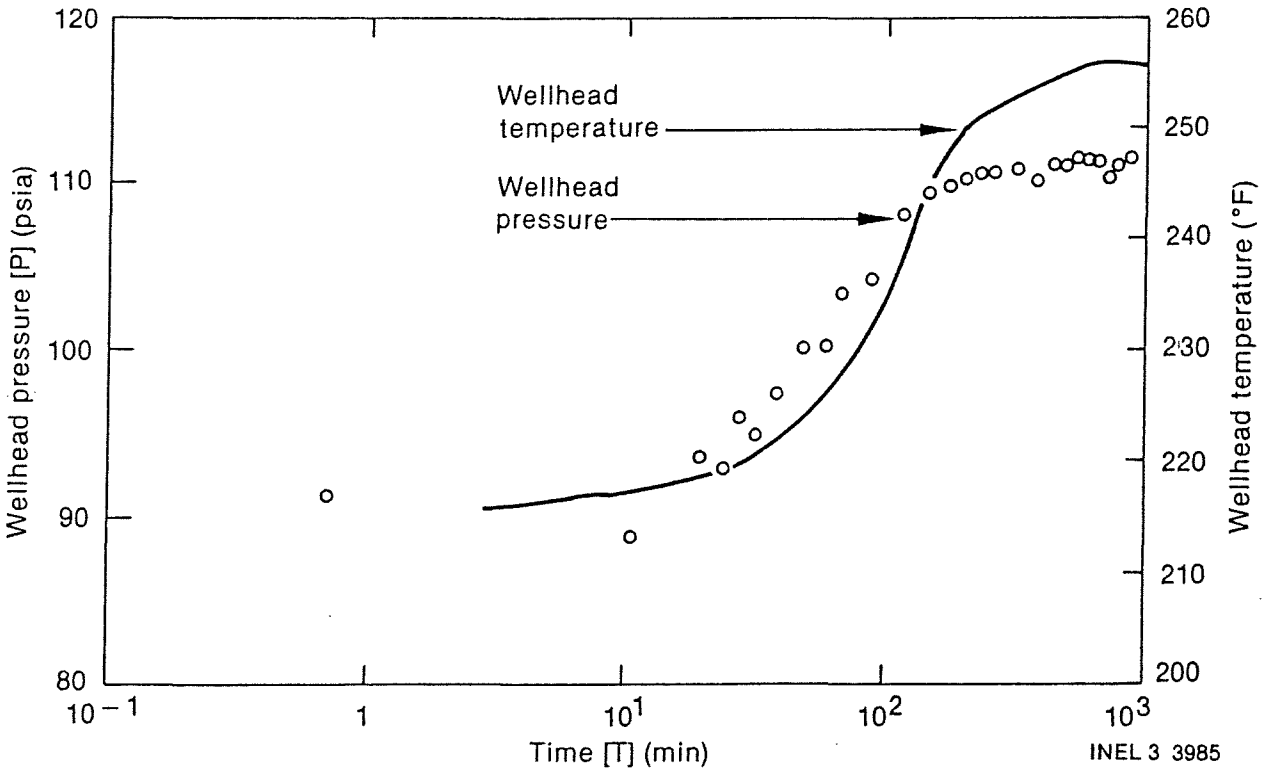

Figure 29. Test 4B backflow wellhead pressure and temperature for RRGP-5BF versus log time.

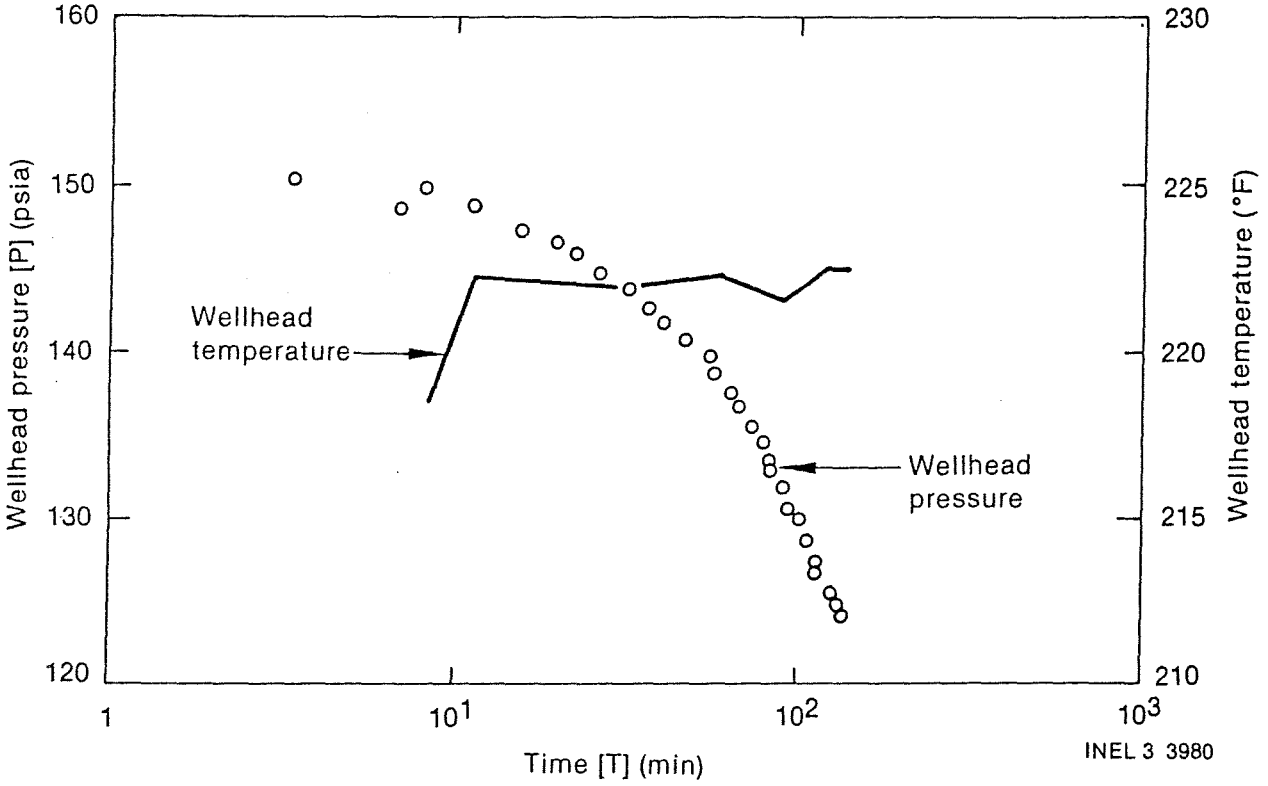

Figure 30. Test 4C injection wellhead pressure and temperature for RRGP-5BF versus log time.

124.0 psia at the end of injection. The injected fluid temperature was relatively steady at 106°C (222°F).

The well was shutin for 720 min between injection and backflow (Figure 31). In less than 2 min of quiescence, the wellhead the pressure decreased by 20.3 psi, reaching 103.7 psia. After 2 min the pressure started to increase, reaching 112.7 psia at the end of the quiescent phase.

Backflow for Test 4C was for 520 min (Figure 32). The minimum pressure of 91.9 psia was reached 2 min after flow started. Between 2 and 6.5 min the pressure was steady. After 6.5 min, the pressure started to increase reaching 110 psia at 200 min. At the end of flow, the pressure had a maximum value of 111.6 psia. The temperature increased from 970°C (207°F) at 10 min to 124°C (255.5°F) at the end of backflow.

Sparse pressure data were collected for backflow quiescence. The maximum recorded pressure of 135.0 psia occurred approximately 16 min after the well was shutin.

3.2.1.2.7 Test 4D. Test 4D was the last of the Test 4 series. Test 4D was conducted from 10-13-82 to 10-18-82. Injection continued for 144 min (Figure 33). The wellhead pressure reached a maximum of 144.0 psia 2.5 min after injection started. Between 2.5 and 6 min, the pressure was steady at 144 psia. The pressure declined after 6 min, reaching a wellhead pressure of 118.5 psia at the end of the injection phase.

The well was shutin for 2973 min between injection and backflow (Figure 34). The pressure decreased to 96.8 psia 3 min after shutin. The pressure increased for the remainder of the quiescence period reaching 114.8 psia at the end of quiescence.

Backflow for Test 4D was conducted for approximately 3660 min (Figure 35). Pressure drawdown was observed for 2.7 min with a minimum wellhead pressure of 93.5 psia. Between 2.7 and 9 min, the pressure fluctuated irregularly from 92.4 to 95.2 psia. After 9 min, the pressure

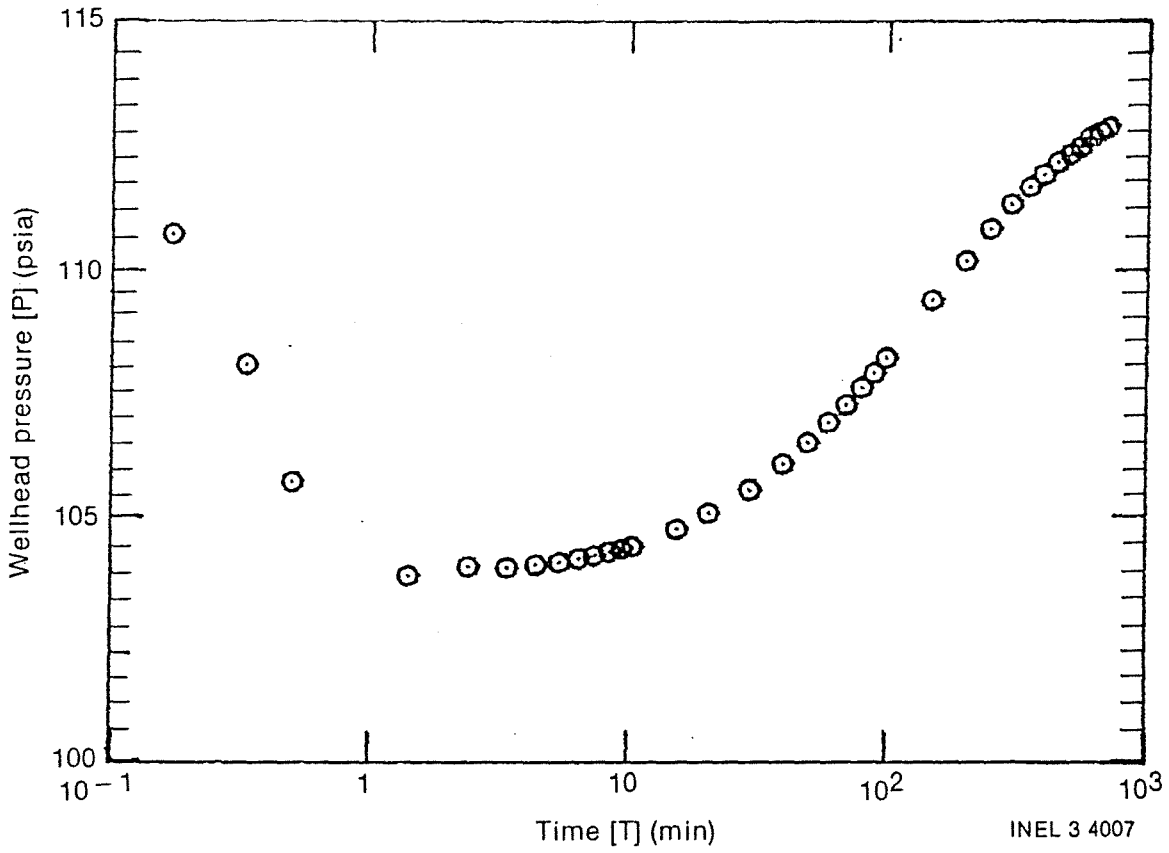

Figure 31. Test 4C injection quiescence wellhead pressure for RRGP-5BF versus log time.

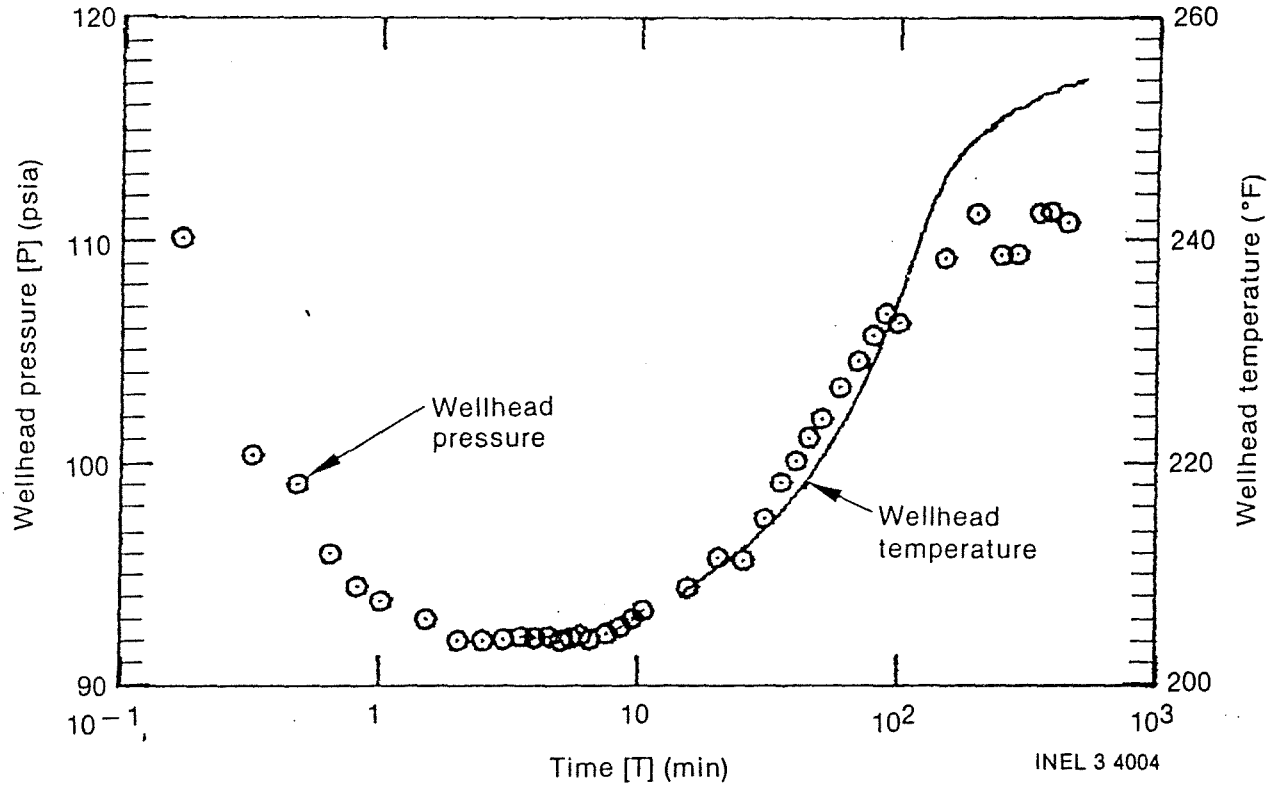

Figure 32. Test 4C backflow wellhead pressure and temperature for RRGP-5BF versus log time.

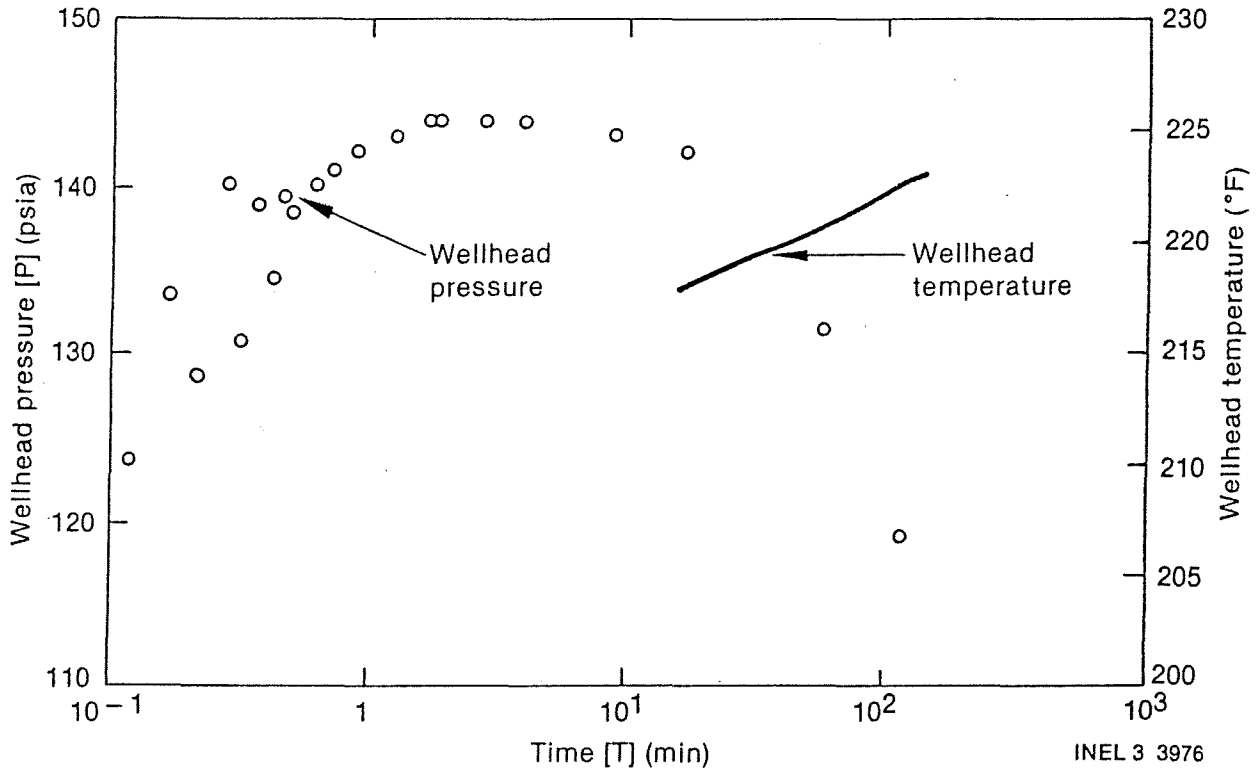

Figure 33. Test 4D injection wellhead pressure and temperature for RRGP-5BF versus log time.

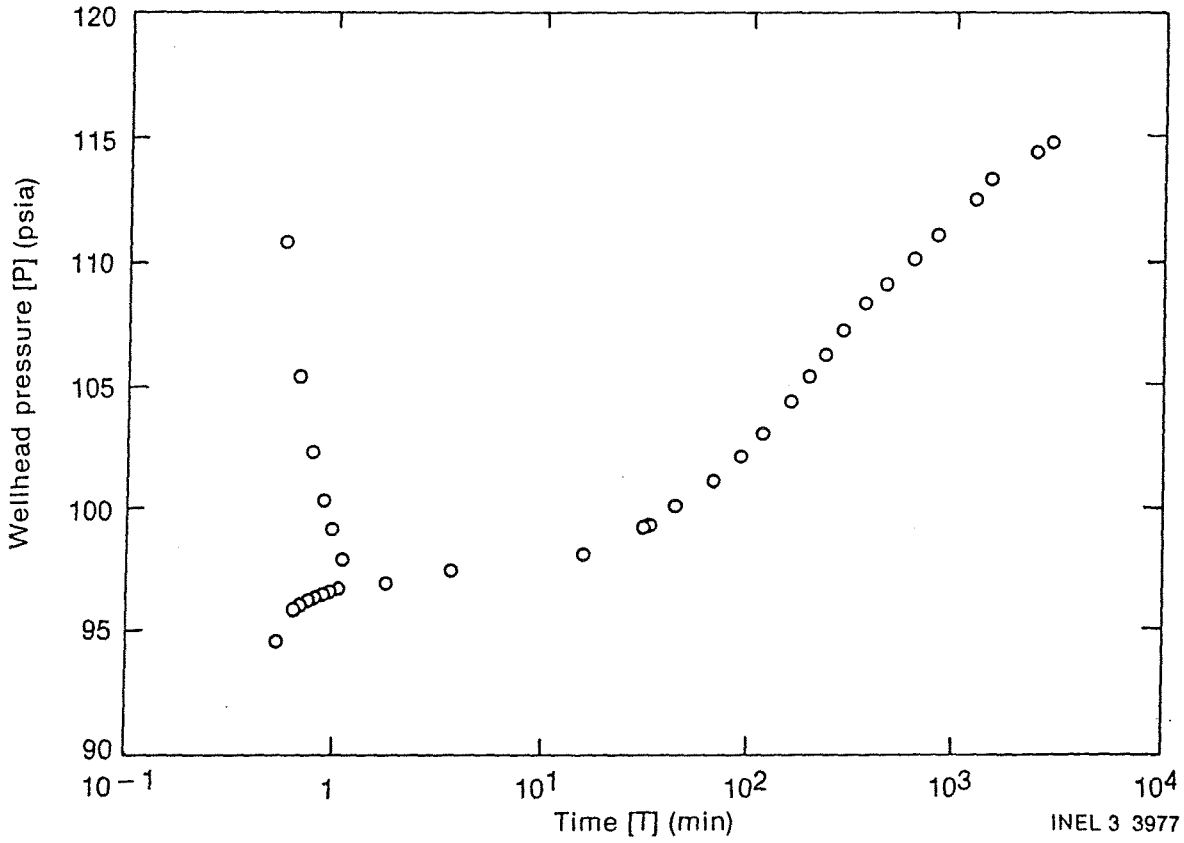

Figure 34. Test 4D injection quiescence wellhead pressure for RRGP-5BF versus log time.

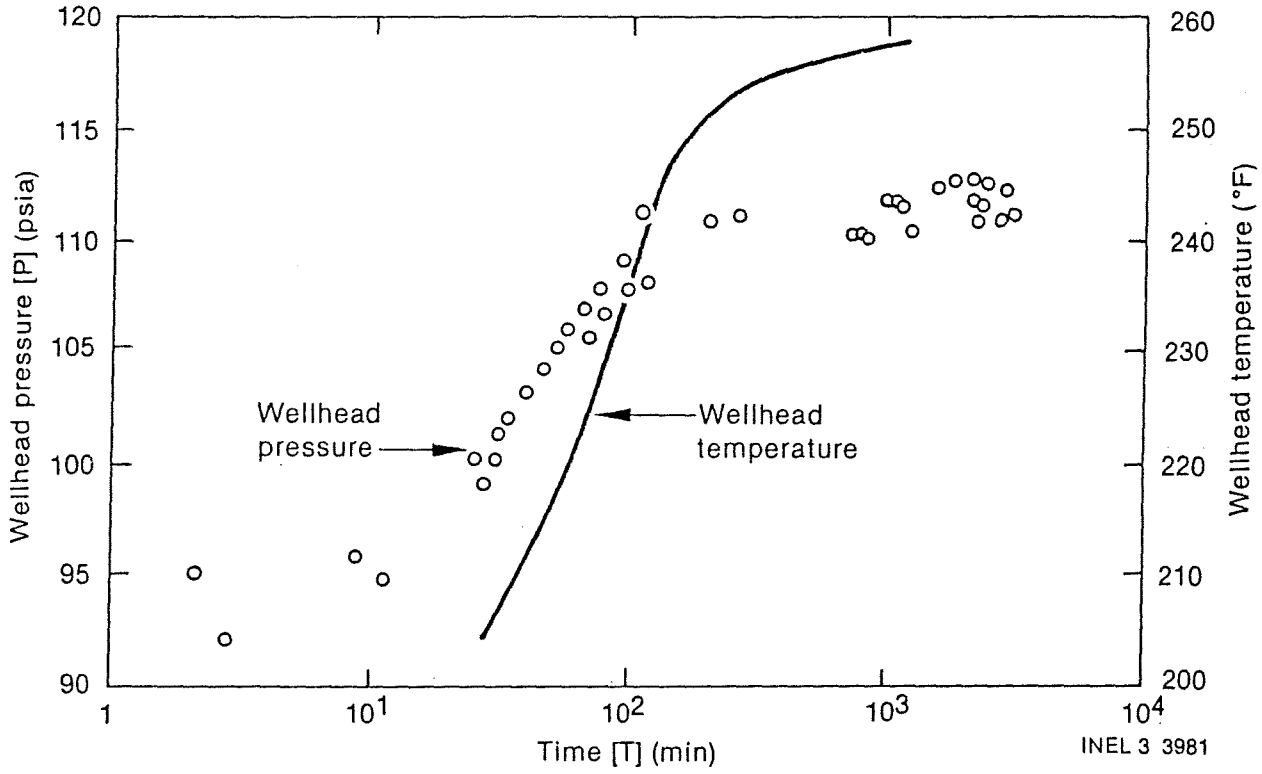

Figure 35. Test 4D backflow wellhead pressure and temperature for RRGP-5BF versus log time.

gradually increased to 111.3 psia at 250 min. After 250 min the pressure remained between 110.0 and 112.7 psia for the next 1000 min. At the end of backflow, the pressure was approximately 112.5 psia.

Sparse pressure recovery data were collected after well shutin. The wellhead pressure reached 134.9 psia approximately 180 min after well shutin. The temperature recorded at the end of backflow was in excess of 125°C (257.3°F).

3.2.1.2.8 Test 5--Long term injection Test No. 5 was conducted from 10-06-82 to 12-01-82. The injection continued for 22,560 min. The first 5 min of data are missing because of a Digitquartz printer problem. At 6 min the pressure was 135.4 psia and was decreasing slightly with increasing time. At 115 min the pressure declined to 102.9 psia after which the pressure increased until it reached 118.0 psia at 260 min. Between 260 min and the end of the test, the pressure fluctuated between 118 and 120 psia. The pressure increase between 120 min and 260 min was similar to the pressure increase recorded during Test 2C. The injected fluid temperature was approximately 223°F for 8 days and between 107°C and 108°C (225 and 226°F) for the last 8 days.

3.2.2 Pulse Tests

On December 1 several short duration pulse tests were conducted. The test discharge rates ranged from 4.7×10^{-3} to $2.1 \times 10^{-2} m^3/sec$ (75 to 325 gpm). The well was only capable of maintaining a $1.7 \times 10^{-2} m^3/sec$ (275 gpm) artesian discharge rate for steady-state conditions to develop with the valving system installed.

Seven pulse tests at constant discharge rates 4.7×10^{-3}, 7.9×10^{-3}, 1.1×10^{-2}, 1.4×10^{-2}, 1.7×10^{-2}, 2.1×10^{-2} and $1.9 \times 10^{-2} m^3/sec$ (75, 125, 175, 225, 276, 325, and 300 gpm) were conducted for periods ranging up to 33 min. The first pulse test at a discharge rate of 4.7×10^{-3} m^3/sec 75 gpm had a water hammer pressure effect for 40 sec (Figure 36). This figure is a semilogarithmic plot of wellhead pressure versus time since flow effectively began. A linear regression was

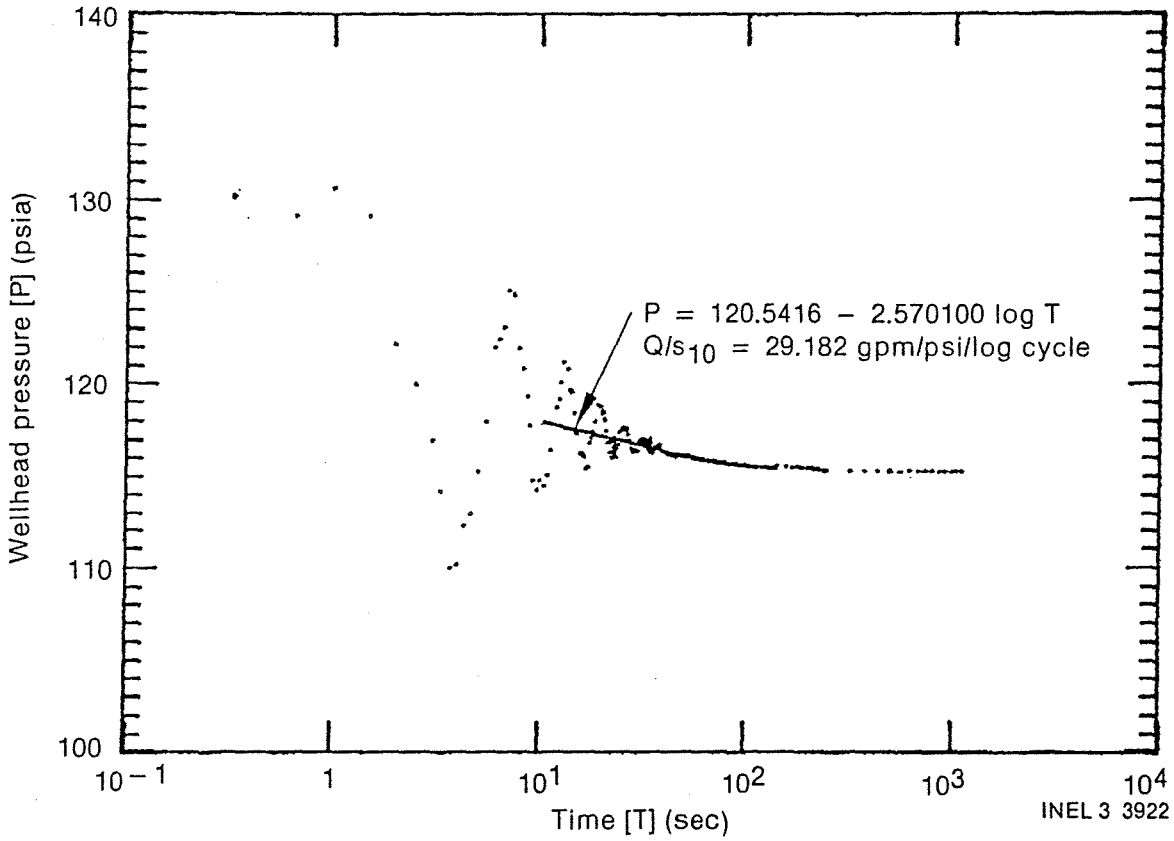

Semilogarithmic plot of wellhead pressure versus time for RRGP-5BF pulse test 1 (75 gpm) backflow.

fitted to the data between 10.7 and 61.0 sec after artesian flow effectively began at 4.7×10^{-3} m^3/sec (75 gpm) (Table 8). Later, the pressure essentially stopped declining and remained at 115.2 psia until flow was terminated at 1097 sec or approximately 18 min.

The 4.3×10^{-3} m^3/sec (75 gpm) pulse test was effectively shutin at 10:28:09 (Table 8). Figure 37 is a semilogarithmic plot of the wellhead pressure versus time since the wellhead discharge ceased. The linear regression was fitted to the data from 8.5 to 86.0 sec after shutin. The water hammer pressure surging effects are more evident for the recovery data than for the backflow data. The wellhead pressure surging during recovery is sufficiently large to render the linear regressions through the raw data somewhat less indicative of the actual pressure buildup. Occurring in the reservoir, the wellhead pressure essentially stabilized after 100 sec at 123.3 psia (Table 8). Recovery data were collected for 670 sec.

The second pulse flow test had a discharge rate of 125 gpm. A linear regression was fitted to the data collected between 6.0 and and 63.0 sec after the discharge was effectively initiated (Figure 38, Table 8). After 316 sec the wellhead pressure essentially stabilized at 106.3 psia. The wellhead was shutin after discharging for 950 sec or 15.8 min.

Recovery for the 7.9×10^{-3} m^3/sec (125 gpm) test began at 10:55:09, (Table 8). The water hammer effect was observed for approximately 2 min (Figure 39). A linear regression was fitted to the data between 9.7 and 80 sec after wellhead shutin. After 2 min the wellhead pressure stabilized at 123.2 psia and remained at this level during the 1161 sec or 19.4 min that the wellhead was shutin prior to the next test.

The discharge rate for the third pulse test was $1.1 \times 10^{-2} m^3$/sec (175 gpm) (Figure 40). The water hammer effect was observed for about 45 sec. A linear regression was fitted to the data between 6.7 and 64.0 sec after effectively initiating flow. The wellhead pressure

PULSE TEST DATA FOR RRGP-5BF ON 12-01-82 FOR SEMILOGARITHMIC PLOTS OF WELLHEAD PRESSURE VERSUS TIME

Test Number	Backflow Rate (Q) (gpm)	Recovery Rate (Q) (gpm)	Pressure Immediately Prior to Q Change (psia)	Time of Assumed Q Rate Change	Period Used for Regression From Time of Assumed Q Rate Change		First Order Regression Coefficient s_{10} (psi/log cycle)	Absolute Value Q/s_{10} (gpm/psi/log cycle)
					From (s)	To (s)		
1	75		123.3	10:09:52	10.7	61.0	-2.570100	29.182
1		75	115.2	10:28:09	8.5	86.0	2.238240	33.508
2	125		123.3	10:39:19	6.0	63.0	-7.348369	17.011
2		125	106.3	10:55:09	9.7	80.0	5.479123	22.814
3	175		123.2	11:14:30	6.7	64.0	-11.98500	14.602
3		175	95.0	11:37:38	15.3	57.7	10.00828	17.486
4	225		123.3	11:47:47	6.5	213.0	-15.46237	14.551
4		225	80.7	12:04:42	14.3	51.0	20.13567	11.174
5	276		122.3	14:02:41	1.5	100.0	-20.50485	13.460
5		276	71.8	14:35:31	11.5	52.3	24.79050	11.133
6	325		123.3	14:50:05	19.0	63.0	-26.25862	12.377
6		325	66.6	14:51:36	18.3	51.5	25.32394	12.834
7	300		123.3	14:58:26	16.0	35.0	-22.14030	13.550
7		300	65.5	15:01:13	18.0	51.0	30.03595	9.988

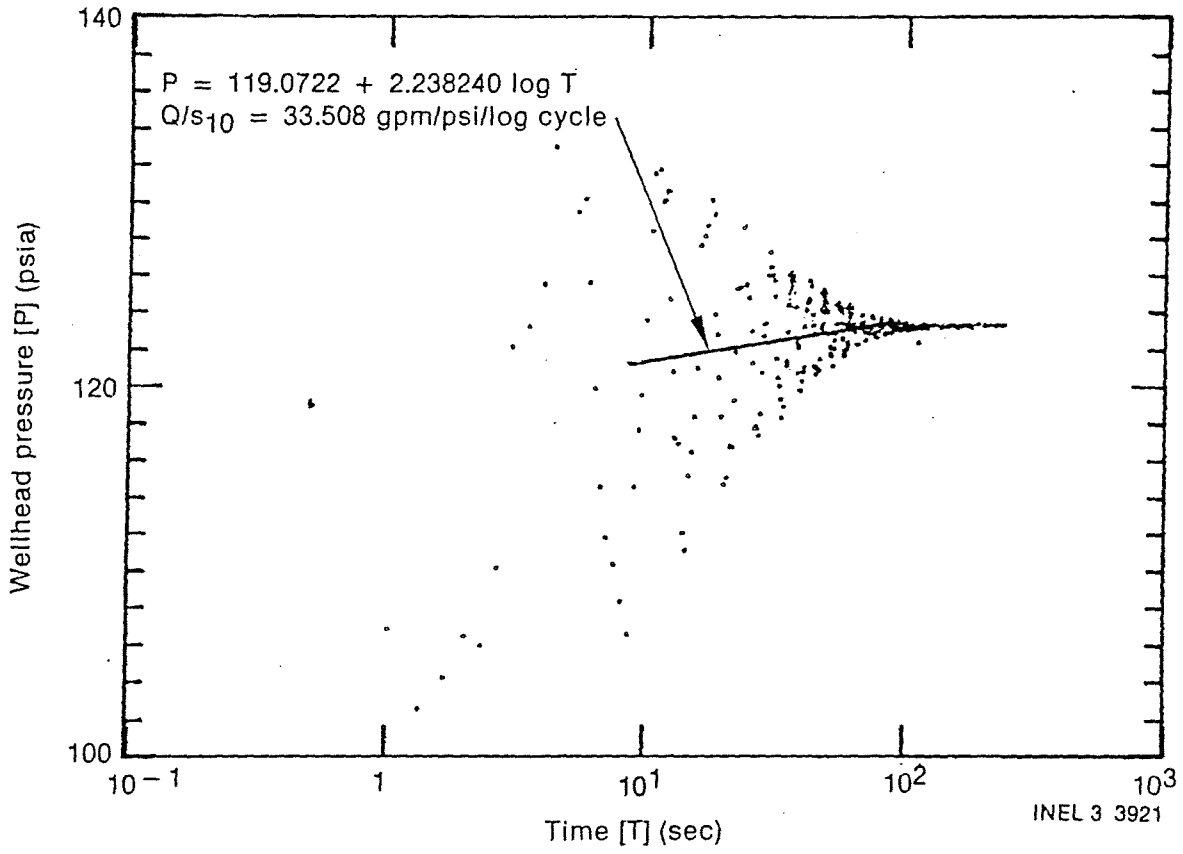

Figure 37. Semilogarithmic plot of wellhead pressure versus time for RRGP-5BF pulse Test 1 (75 gpm) recovery.

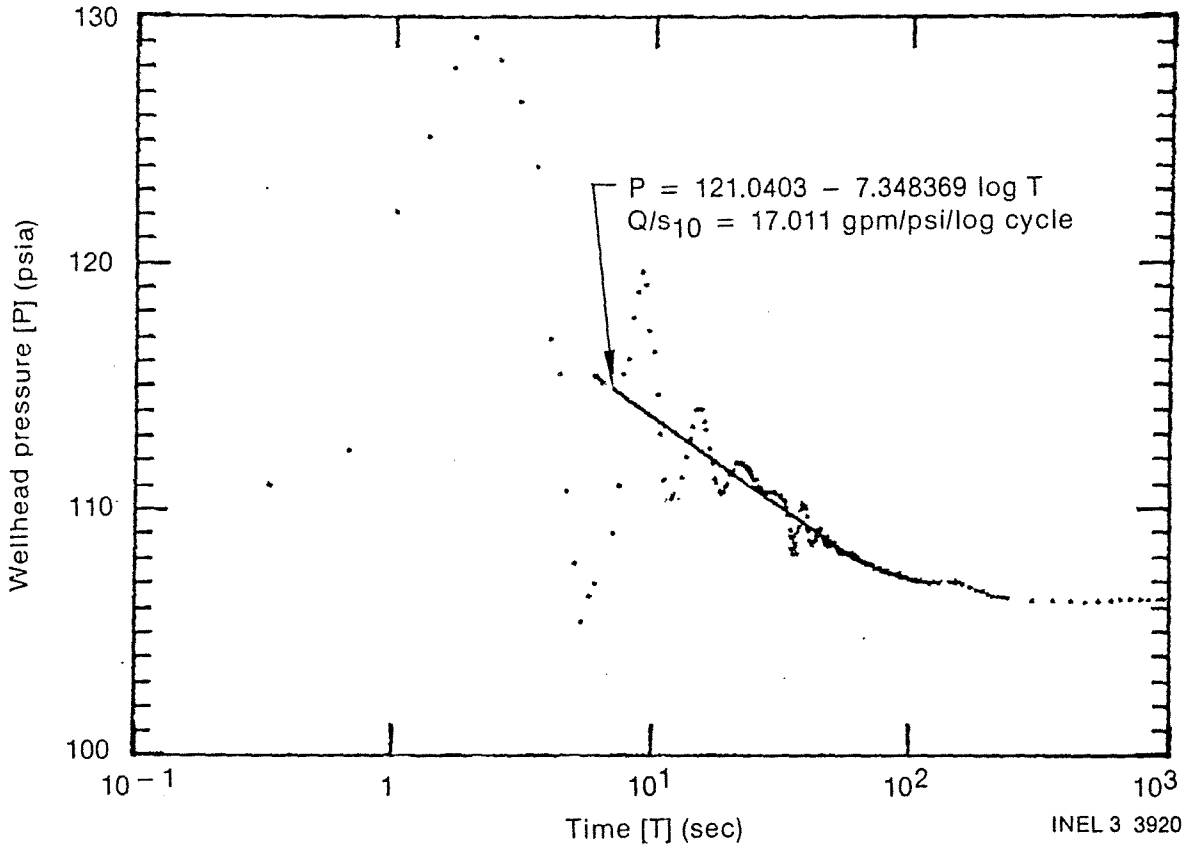

Figure 38. Semilogarithmic plot of wellhead pressure versus time for RRGP-5BF pulse Test 2 (125 gpm) backflow.

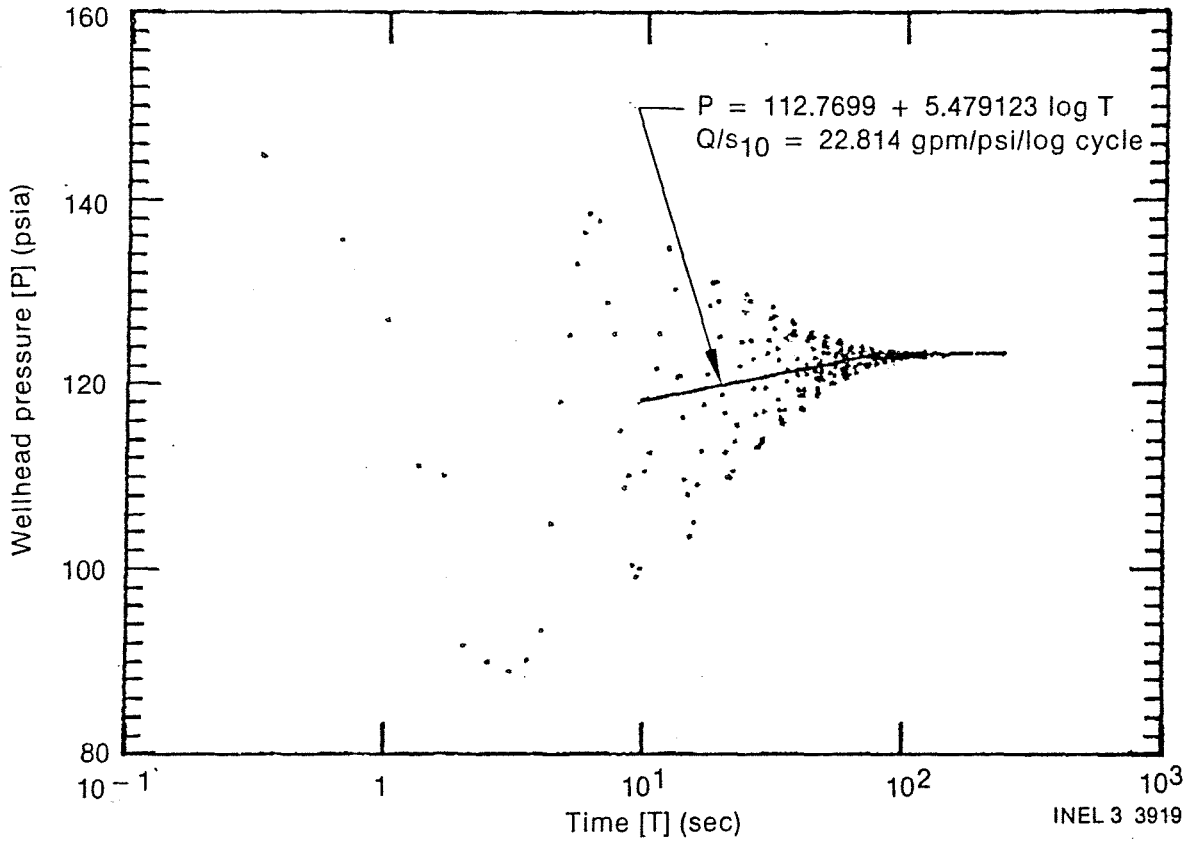

Figure 39. Semilogarithmic plot of wellhead pressure versus time for RRGP-5BF pulse Test 2 (125 gpm) recovery.

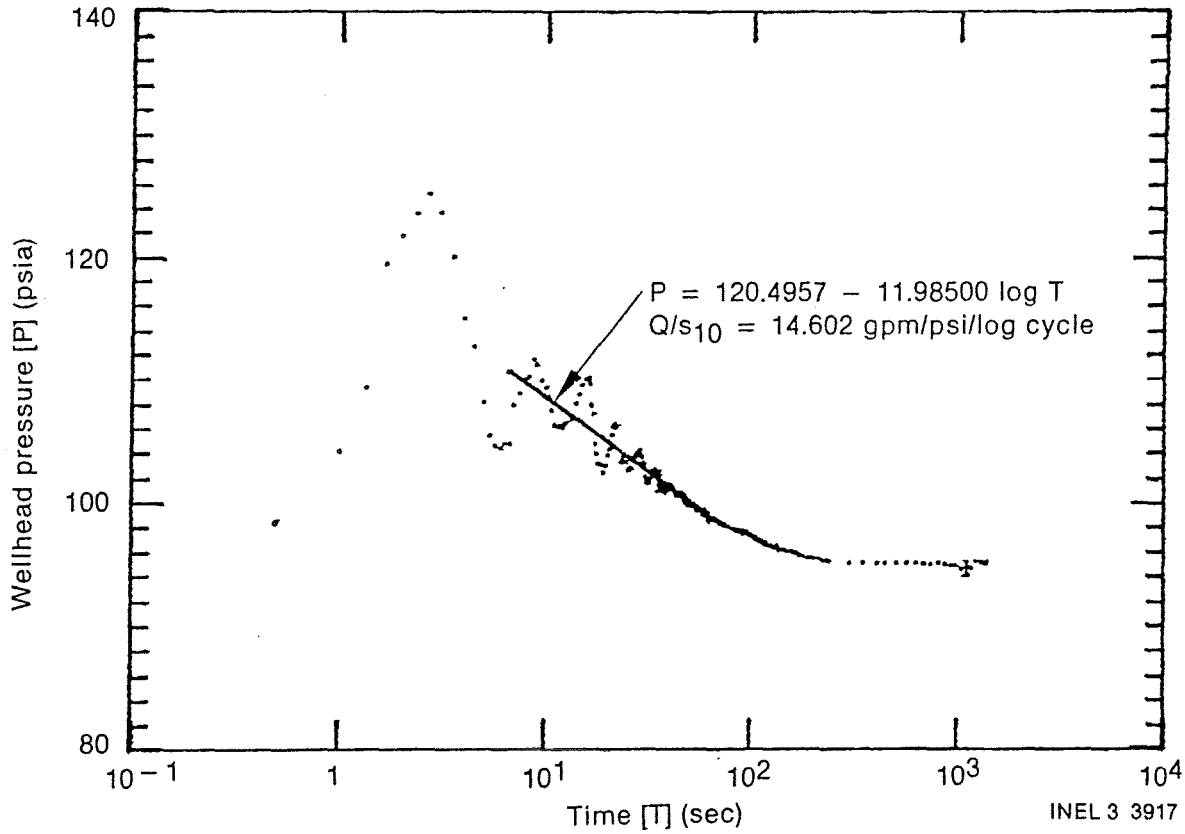

Figure 40. Semilogarithmic plot of wellhead pressure versus time for RRGP-5BF pulse Test 3 (175 gpm) backflow.

decreased to 95.1 psia after 300 sec (5 min). The pressure declined to 95.0 psia shortly before the test was terminated after 1388 sec (23.1 min) of flow.

The well was shutin at 11:37:38 for approximately 10 min. The pressure during recovery is plotted in Figure 41. A linear regression was fitted to the data between 15.3 and 57.7 sec (Table 8). The wellhead pressure recovered to 123.3 psia after approximately 100 sec.

The next pulse test discharge rate was $1.4 \times 10^{-2} m^3/sec$ (225 gpm). A linear regression was fitted through the data from 6.5 to 213 sec (Figure 42, Table 8). The pressure stabilized at 81.0 psia at approximately 175 sec, but, probably because of well development by flushing sand from the fractures and small discharge rate charges, was at 80.7 psia at the end of the test after discharging for 1015 sec (16.9 min).

The recovery for the $1.4 \times 10^{-2} m^3/sec$ (225 gpm) began at 12:04:42. A linear regression was fitted to the data collected between 14.3 and 51.0 sec after shutin (Figure 43, Table 8). The shutin pressure reached a maximum of 123.8 psia after 338 sec (5.6 min) but had essentially stabilized at 160 sec (2.7 min). Recovery continued for almost 2 hr while a larger sized orifice plate was installed. The decline in temperature of the wellbore fluid thus resulted in a wellhead pressure of only 122.3 psia at the beginning of the next test.

The fifth pulse test had a discharge rate of $1.7 \times 10^{-2} m^3/sec$ (276 gpm). Figure 44 suggests a linear trend between 1.5 and 100 sec to which a linear regression was fitted (Table 8). A quasi-steady-state pressure of 69.2 psia was reached after 232 sec (3.8 min). Well development by sand errosion from the fracture probably occurred during this test as addressed in subsequent data analysis. This and flow changes could account for the step-like increases observed in wellhead pressure. Wellbore fluid temperature increases that occurred would also result is an increasing wellhead pressure trend. At the end of the test after 1970 sec (32.8 min), the wellhead pressure had reached 71.8 psia.

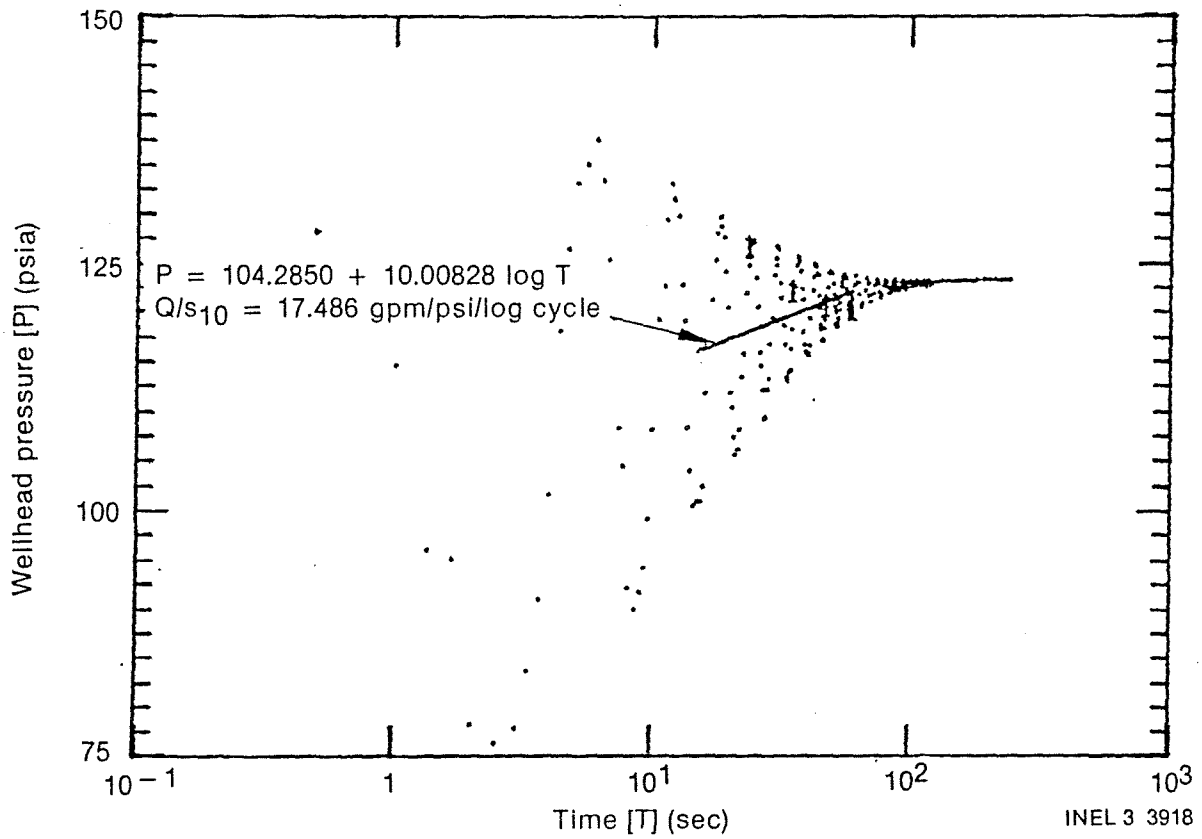

Figure 41. Semilogarithmic plot of wellhead pressure versus time for RRGP-5BF pulse Test 3 (175 gpm) recovery.

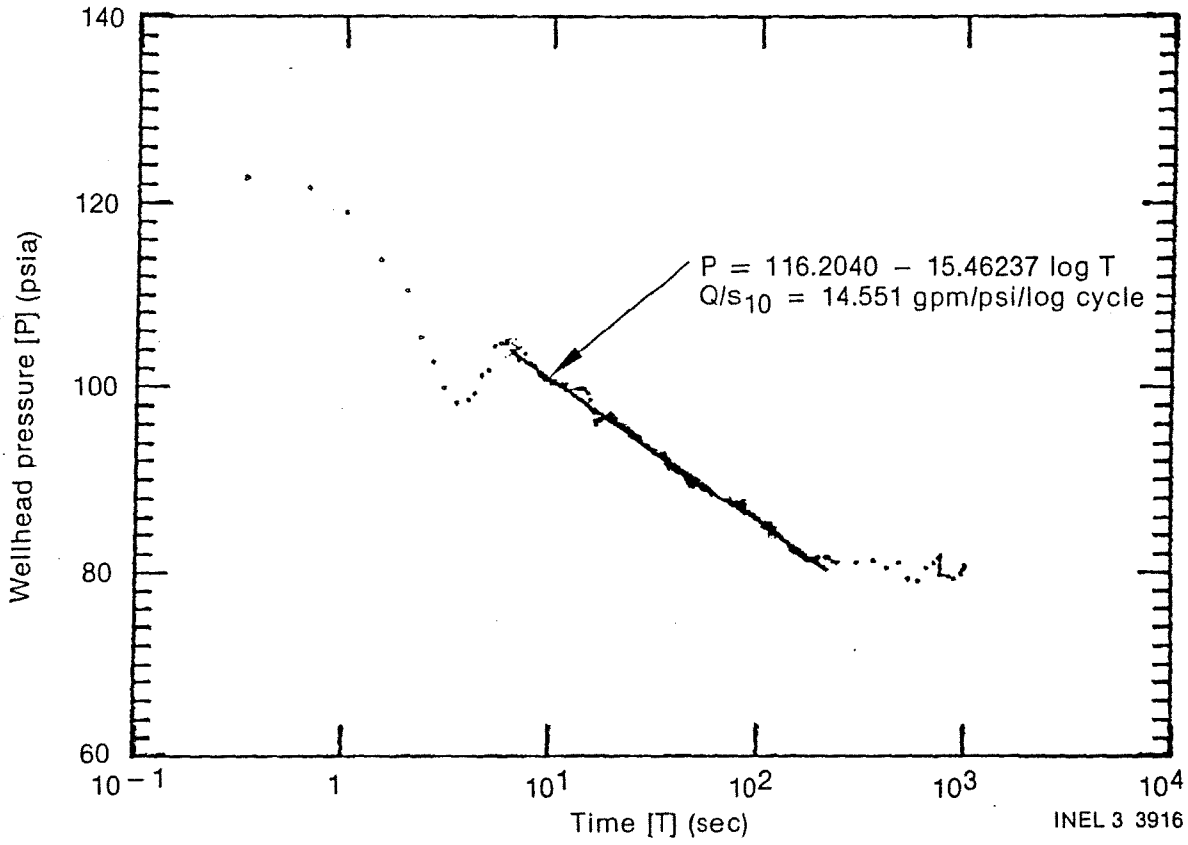

Semilogarithmic plot of wellhead pressure versus time for RRGP-5BF pulse Test 4 (225 gpm) backflow.

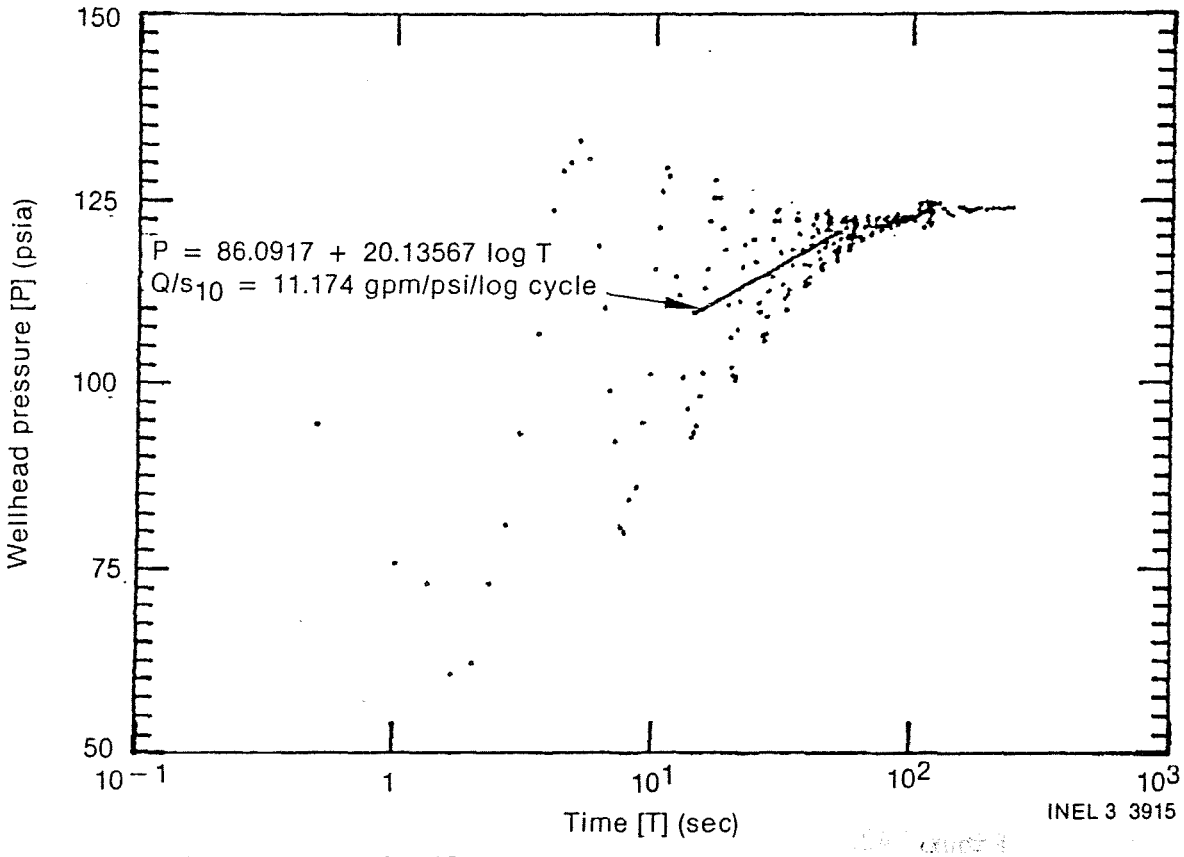

Semilogarithmic plot of wellhead pressure versus time for RRGP-5BF pulse Test 4 (225 gpm) recovery.

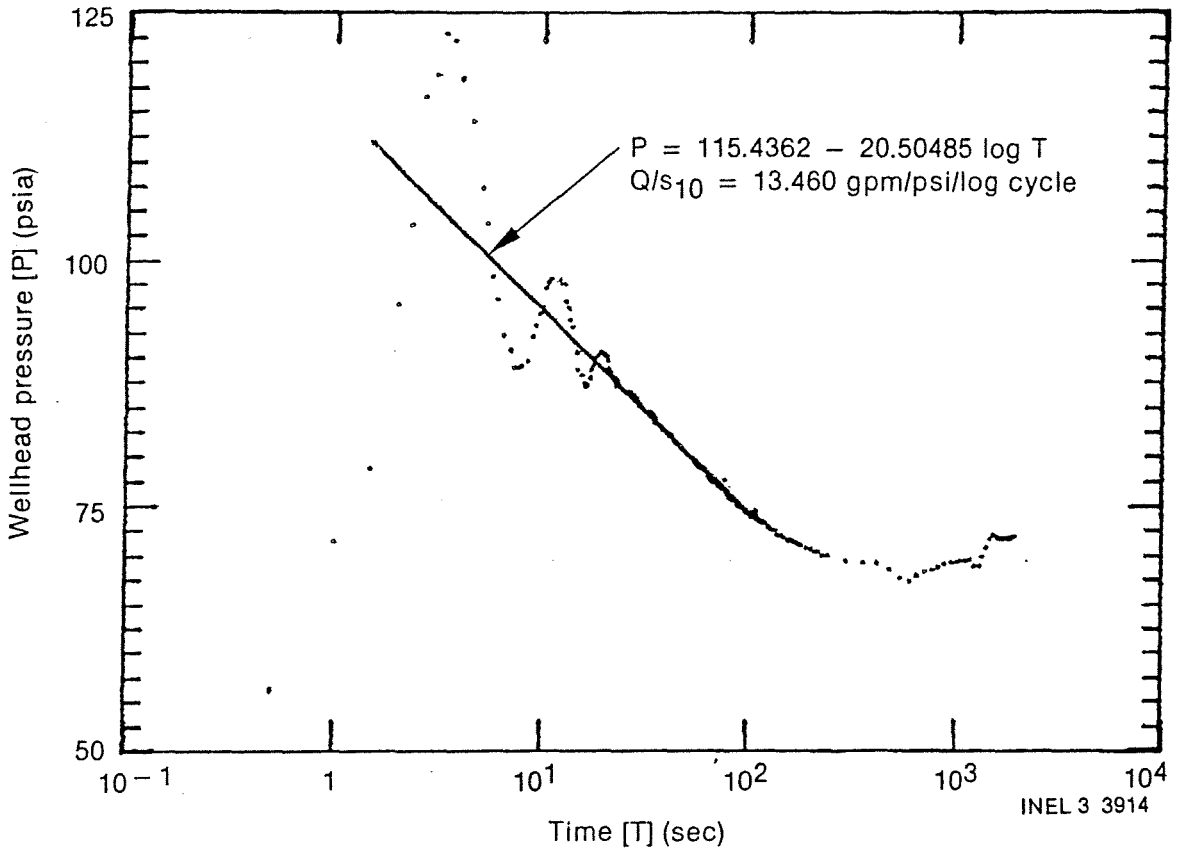

Figure 44. Semilogarithmic plot of wellhead pressure versus time for RRGP-5BF pulse Test 5 (276 gpm) backflow.

The recovery data for the 1.7 x $10^{-2}m^3$/sec (276 gpm) test are plotted in Figure 45. A linear regression was fitted to the data collected between 11.5 and 52.3 sec (Table 8). The pressure reached 123.3 psia after approximately 300 sec (5 min). Approximately 900 sec (15 min) of recovery data were collected.

The backflow at 2.1 x $10^{-2}m^3$/sec (325 gpm) effectively began at approximately 14:50:05, 10 sec after the valve was initially cracked. Since the valve required approximately 10 sec to go from the fully closed to open position, there is some doubt as to when the test effectively began from a hydraulic point-of-view because of the large valve opening required early in the test. The valve was fully opened at approximately 80 sec. The backflow pressure data are plotted in Figure 46. A linear regression was fitted to the data from 19.0 to 63.0 sec. The backflow continued for 91 sec with a wellhead pressure of 66.6 psia at the end of this period. Because of the flow control problem, there is some doubt regarding the accuracy of some data for the 2.1 x $10^{-2}m^3$/sec (325 gpm) test.

The shutin for the 2.1 x $10^{-2}m^3$/sec (325 gpm) tests is believed to have effectively begun at 14:51:36 (Table 8). Figure 47 is a plot of the recovery data with a linear regession fitted to the data between 18.3 and 51.5 sec. The wellhead pressure recovered to 123.2 psia after 180 sec (3 min). Recovery data were collected for 410 sec (6.8 min) with the wellhead pressure gradually recovering to 123.3 psia.

Pulse Test 7 was at a flow rate of 300 gpm. Figure 48 is a plot of the backflow data with a linear regression fitted through the data from 16.0 to 35.0 sec. The automatic flow control valve was fully opened after approximately 140 sec. Flow continued for 167 sec until the well was shutin. The wellhead pressure had declined to 65.5 psia at the end of the test. The backflow test data should be reasonably accurate except for the steady-state-pressure because the flow could be regulated for a relatively long period.

The recovery data for the 300 gpm pulse test are plotted in Figure 49 with the linear regression fitted to the data between 18.0 and 51.0 sec.

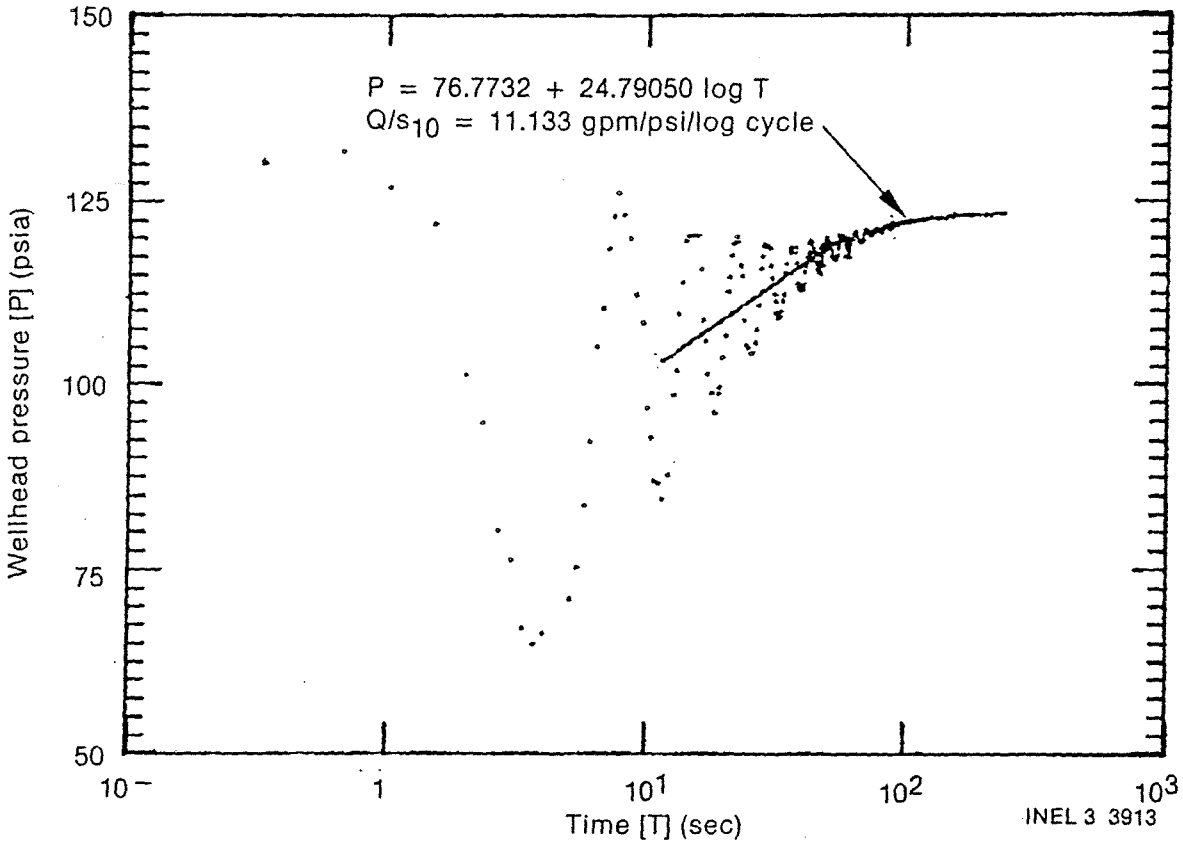

Figure 45. Semilogarithmic plot of wellhead pressure versus time for RRGP-5BF pulse Test 5 (276 gpm) recovery.

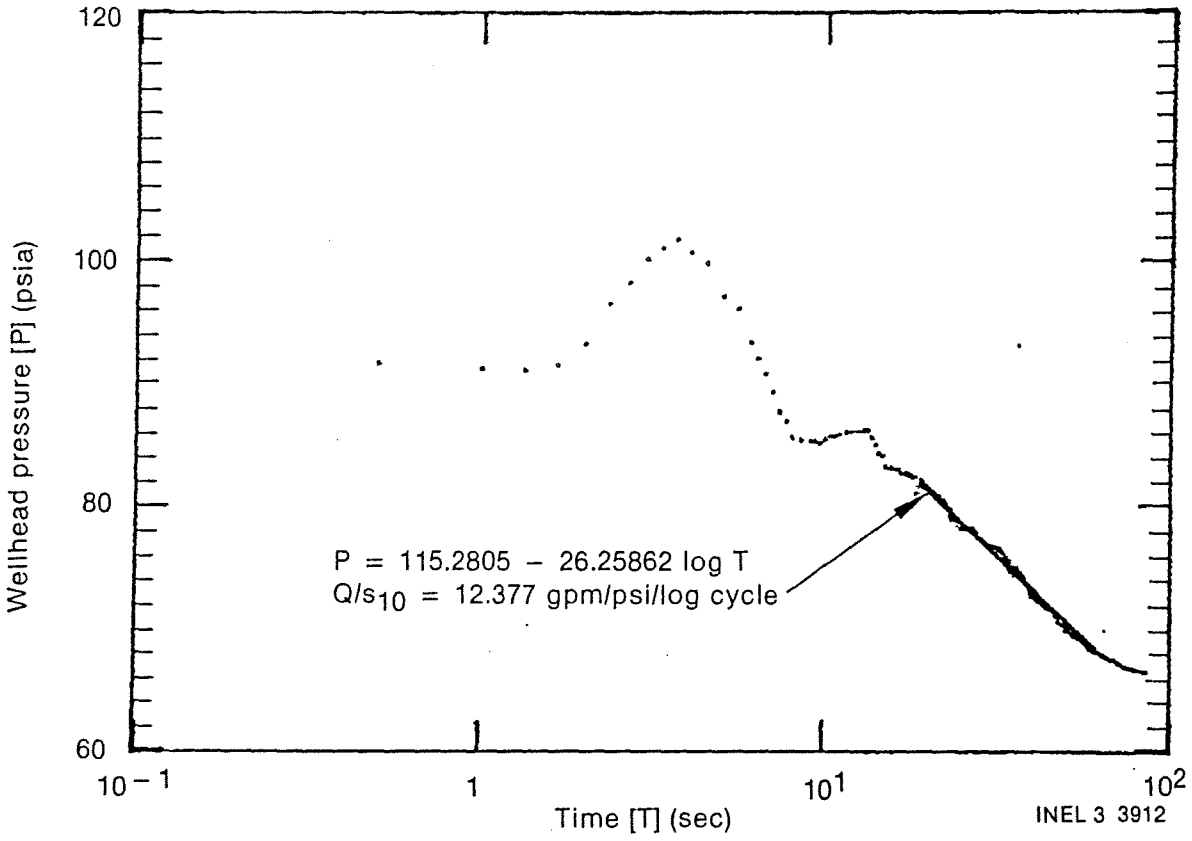

Figure 46. Semilogarithmic plot of wellhead pressure versus time for RRGP-5BF pulse Test 6 (325 gpm) backflow.

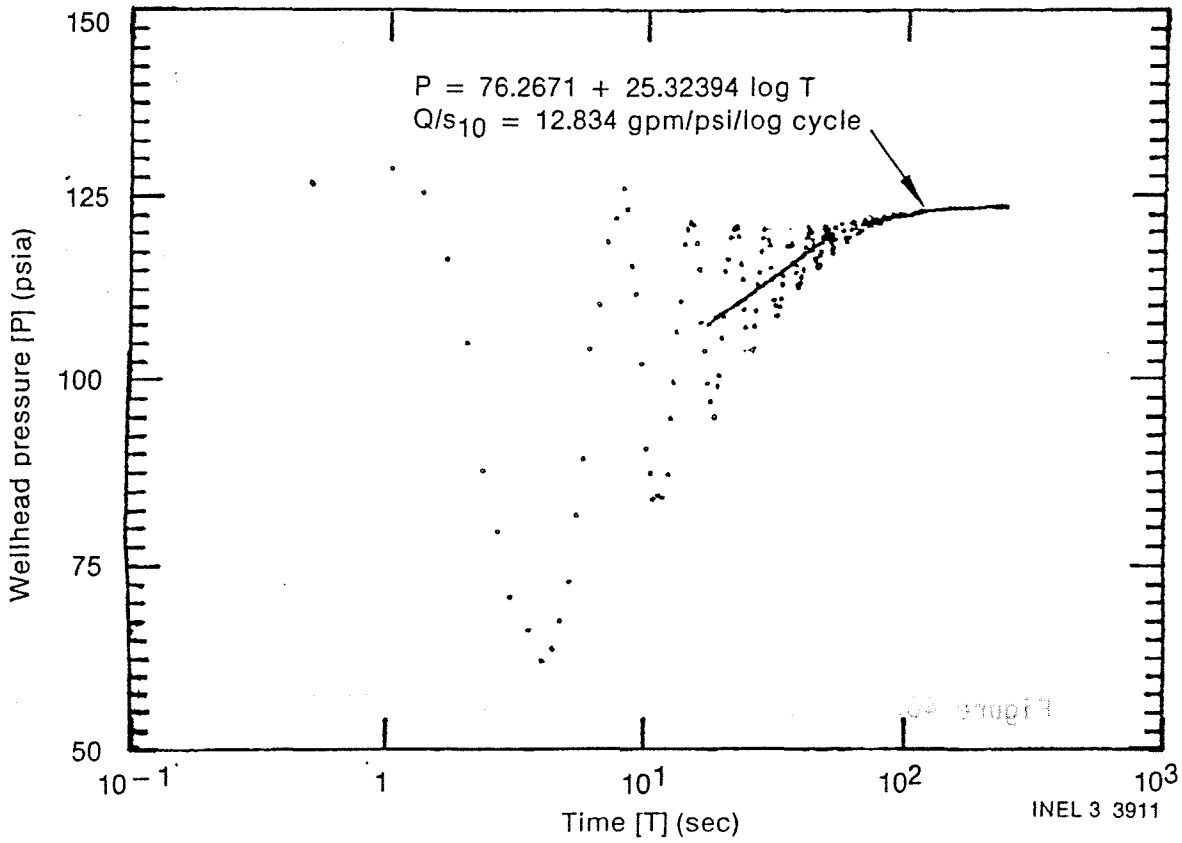

Figure 47. Semilogarithmic plot of wellhead pressure versus time for RRGP-5BF pulse Test 6 (325 gpm) recovery.

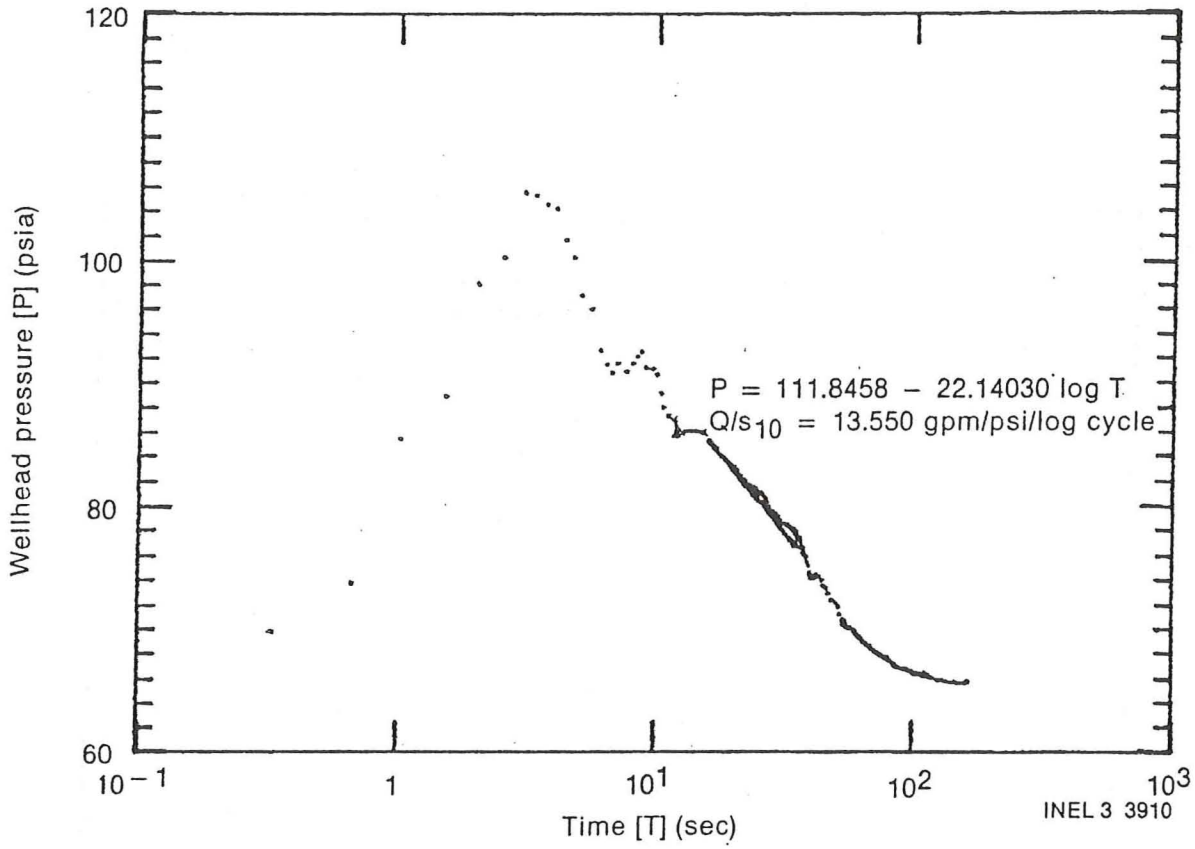

Semilogarithmic plot of wellhead pressure versus time for RRGP-5BF pulse Test 7 (300 gpm) backflow.

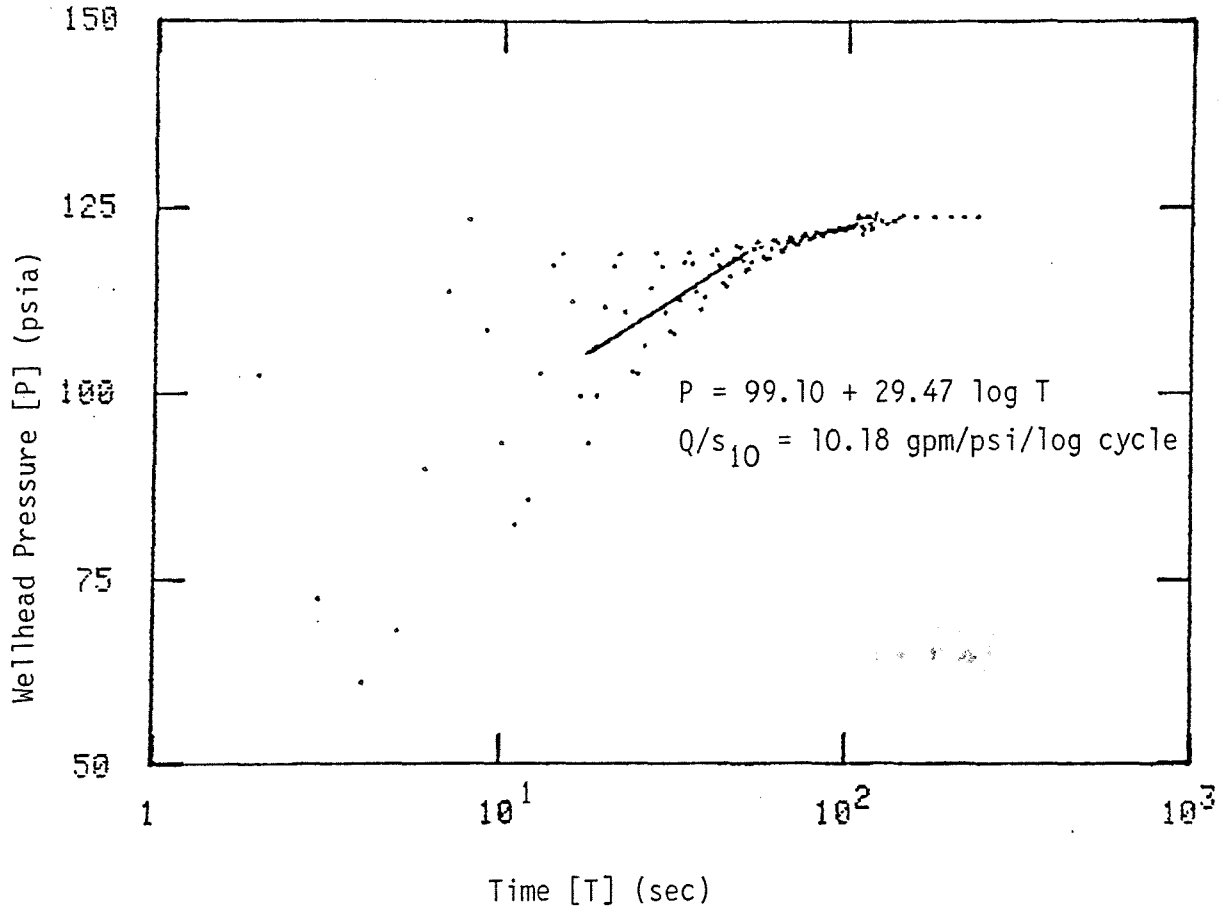

Semilogarithmic plot of wellhead pressure versus time for RRGP-5BF pulse Test & (300 gpm) recovery.

The wellhead pressure recovered to 123.6 psia after 160 sec of recovery time, with 237 sec (4 min) of recovery data plotted in Figure 49. These were the last test data collected for the pulse test series.

3.2.3 Evaluation of Hydraulic Responses for Late Post-Fracturing Tests

3.2.3.1 Q/s_{10}. The Q/s_{10} ratio is an important parameter for RRGP-5BF since it is indicative of the apparent transmissivity of the fractured zone between the wellbore and the essentially constant head boundary presumed to be the aquifer indicated on borehole geophysical logs to be between depths of 1364 and 1370 m (4475 and 4494 ft). The aquifer transmissivity as determined by a well with no well losses, fully penetrating a single, isotropic aquifer of infinite areal extent can be calculated using the following equation for semilogarithmic plots of pressure versus time:[13]

$$T = \frac{264 \times Q}{2.472 \times s_{10}}$$

where

T = transmissivity in gpd/ft at 270°F

Q = constant discharge rate in gpm

s_{10} = pressure difference for backflow/recovery per log cycle in psi

The factor 2.472 is the feet of water per psi at 270°F which is necessary to convert the conventional ground-water equation that is applicable to semilogarithmic plots of pressure in feet of water versus time. This technique for determining transmissivity is widely used in the ground water industry.

This equation is not valid, however, for the data for RRGP-5BF, as well as for RRGE-1 and RRGE-2 for several reasons, principally because

fracture flow is not necessarily laminar and because of the multiple aquifers in a single borehole. The equation is for a single aquifer in which flow is laminar. Ideally, the aquifer should have a transmissivity which is independent of the discharge rate. This is not true for RRGP-5BF as will be demonstrated. To circumvent these technical problems, the ratio Q/s_{10} is used to describe the characteristic of the completed well and its aquifers in comparison to the transmissivity exclusively of the aquifer.[14] For a given well with a constant aquifer temperature, the Q/s_{10} ratio is directly proportional to the aquifer transmissivity. Because RRGP-5BF is not like the ideal well used for the mathematical, the ratio Q/s_{10} is more applicable since the assumptions made for the ideal well aquifer model do not need to be fulfilled.

The values for s_{10} and Q/s_{10} for the pulse tests are listed in Table 8. These values are also indicated for the linear regressions in Figures 36 to 49 inclusive. Figure 50 is a graph of the absolute value of s_{10} for both backflow and recovery versus the discharge rate for the test. The recovery data for the $2.1 \times 10^{-2} m^3/sec$ (325 gpm) test are invalid because the drawdown did not stabilize and this resulted in the recovery data period being in the transition zone between the limited well entrance loss hydraulic regimen and the steady-state condition. For the first three tests, the backflow s_{10} values are greater than those for the recovery values; whereas this relationship is reversed for the tests 1.4×10^{-2}, 1.7×10^{-2} and $1.9 \times 10^{-2} m^3/sec$ (225, 276 and 300 gpm). The reason for this relationship change is not obvious, but the higher discharge rate data may be affected by the pressure surge due to the wellbore and reservoir fluid velocity decelleration when the wellhead is shutin. The water hammer effect at the wellhead indicates that significant inertial energy is stored in the wellbore fluid prior to shutin. The channelization within the 1.5 cm (0.6 in.) wide fracture will also probably result in significant inertial effects within the aquifer channels themselves. The conversion of pressure energy into inertial energy during backflow and the conversion of inertial energy into pressure during recovery could account for some of the differences that are observed between backflow and recovery pressures and pressure temporal trends.

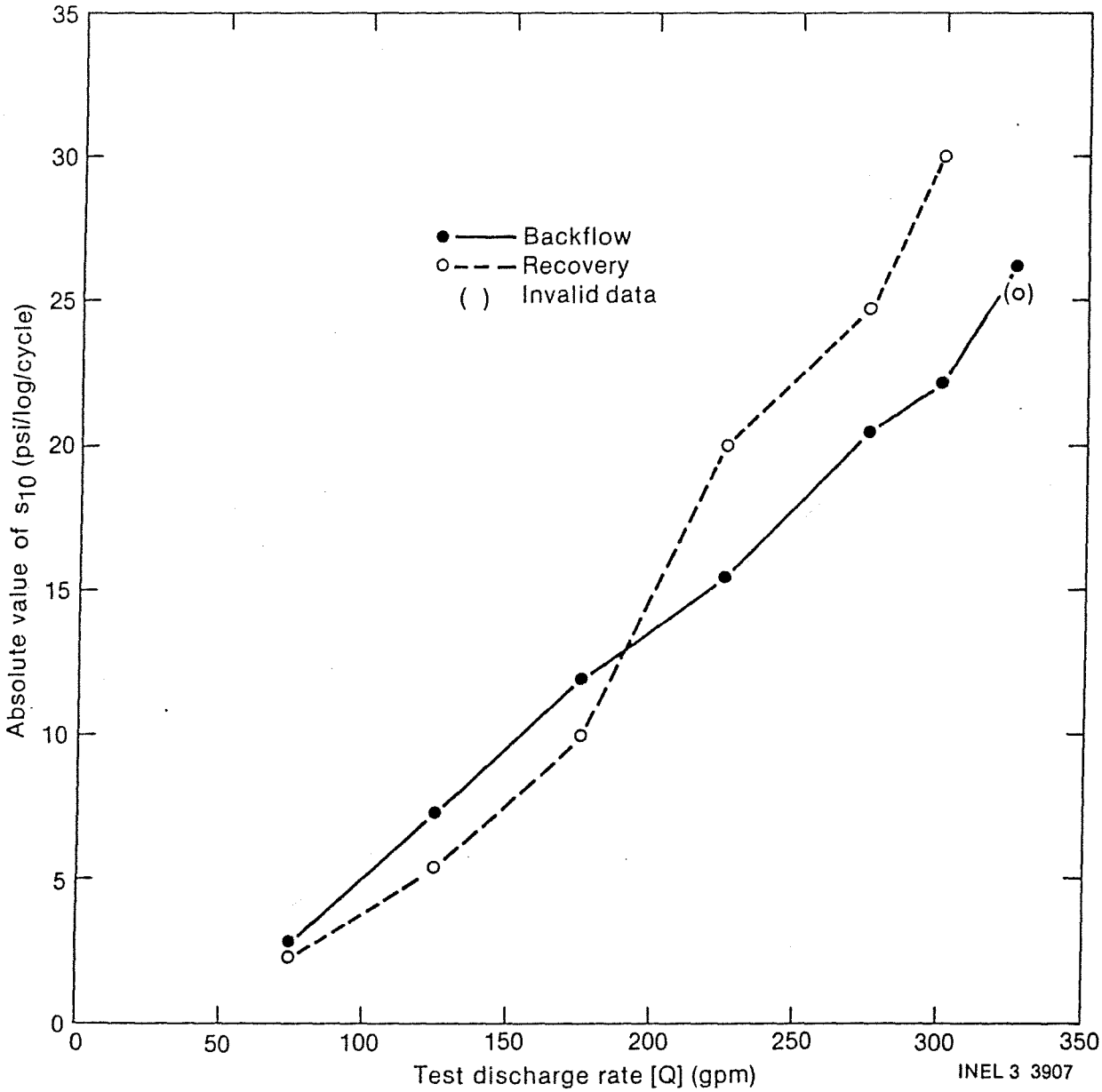

Figure 50. Absolute value for s_{10} versus Q for RRGP-5BF pulse tests.

The ratio of Q/s_{10} (Figure 51) is not a constant independent of the test discharge rate as is generally assumed for laminar flow conditions. The Q/s_{10} values indicate that the higher the discharge rate, the lower the value for Q/s_{10} for both the backflow and recovery data. This is analogous to the apparent transmissivity decreasing by 50% when the discharge rate increases from 4.7×10^{-3} m^3/sec to $1.1 \times 10^{-2} m^3$/sec (75 gpm to 175 gpm). Beyond approximately $1.3 \times 10^{-2} m^3$/sec (200 gpm), the rate of change of Q/s_{10} as a function of Q is much less than for data where Q < 200 gpm. If well development by erosion of the channels in the fracture were occurring at the higher flow rates, the Q/s_{10} as a function of Q would be affected by the unstable aquifer conditions. Whatever the reason(s), the Q/s_{10} values for early time data which are indicative that the flow regimen in the channelized fracture are not a constant. This condition is typical of the multiple aquifer fracture controlled production wells at the Raft River KGRA.

3.2.3.2 Wellhead Pressures at 1, 30, and 50 Seconds and at Steady State. Wellhead pressures using the linear regressions fitted through the early-time data in Figure 36 to 49 inclusive have been calculated for 1, 30, and 50 sec (Table 8) and plotted in Figure 52. The pressure at 1 sec is the regression intercept for the semilogarithmic plots in Figures 36 to 49 inclusive. The pressures were calculated for 50 sec since this is slightly less than the times at the ends of the periods of data to which the linear regressions were fitted (Table 8). In general, 50 sec is the end of the period for which the linear regressions are indicative of actual wellhead pressures. The 30-sec time was chosen as a convenient point between these two extremes. The wellhead pressures at steady-state conditions for backflow and recovery are also plotted as end reference pressures for the various tests. These calculated wellhead pressures have been used since water hammer effects and slight changes in flow rate during the tests prohibit the determination of actual temporal pressure.

The trends of the data in Figure 53 suggest that the pressure calculations at 1 sec have relatively large inconsistencies between tests and are thus likely to have relatively large errors. These errors are to be expected at this extremely early period of backflow and recovery since

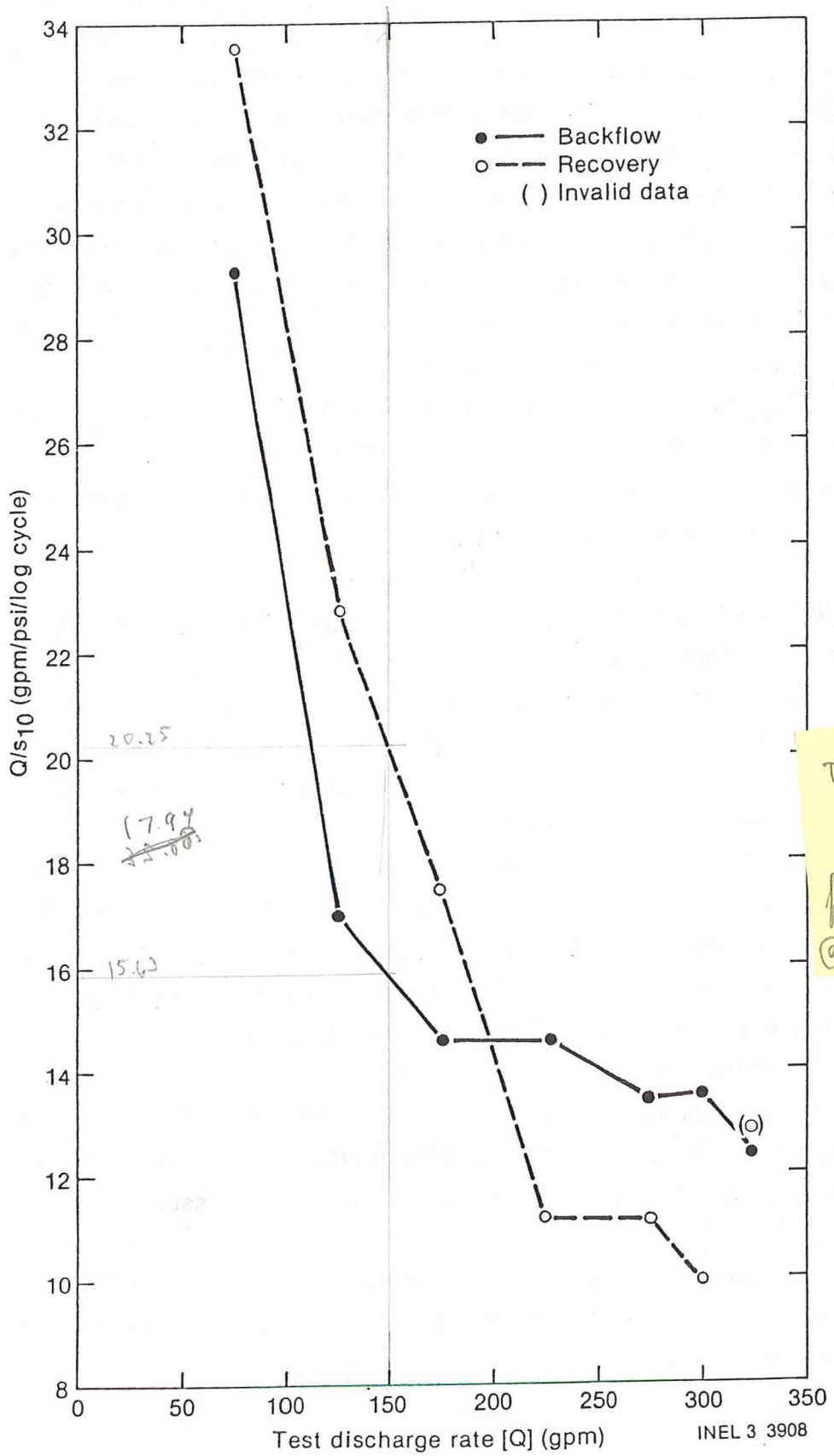

$T = \frac{264 \times 150}{17.94 \times 2.47}$

$= 893$ gpd/ft

for fracture only

@ 270°F

Ratio Q/s_{10} versus Q for RRGP-5BF pulse tests.

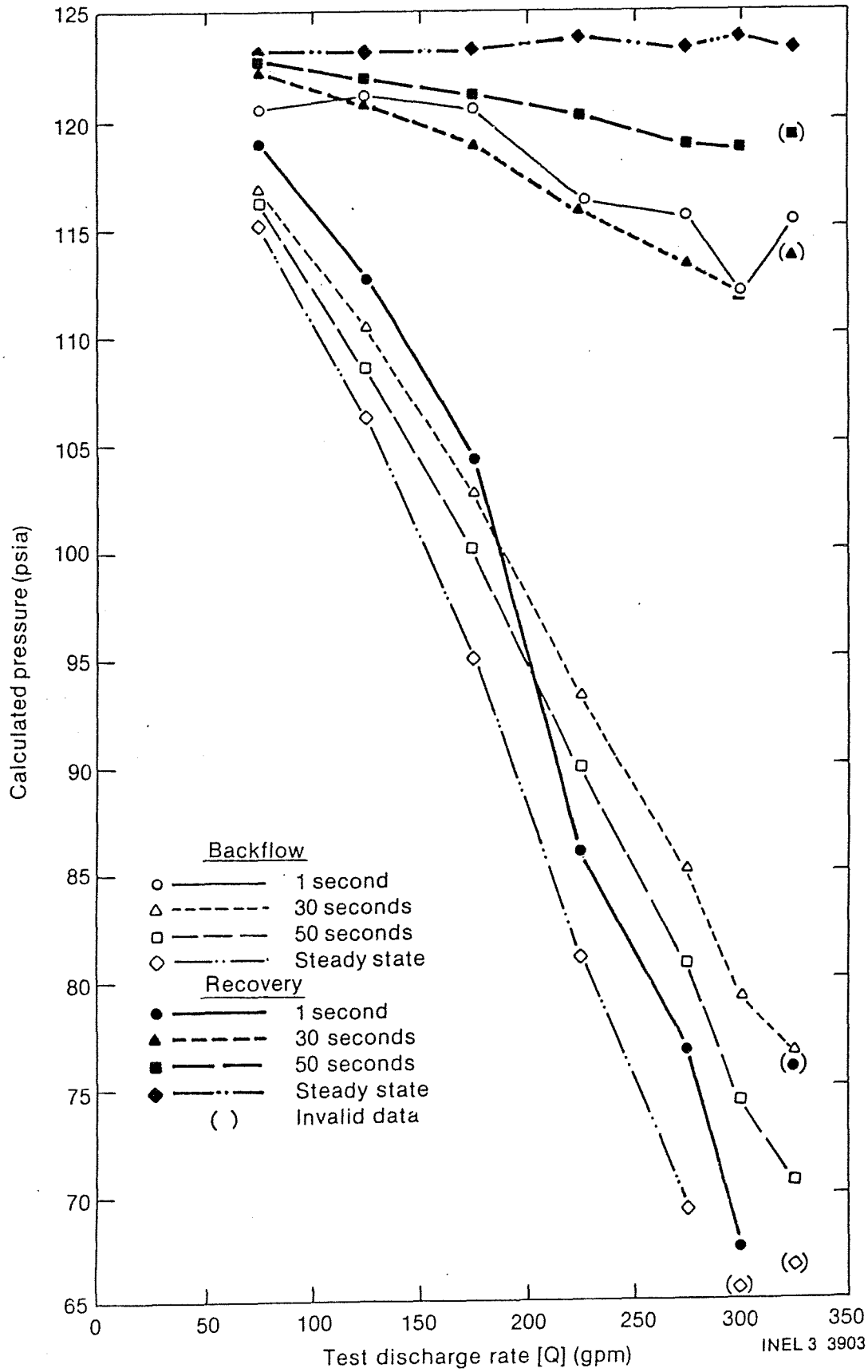

Figure 52. Calculated wellhead pressures at 1, 30, and 50 seconds as well as at steady state conditions for drawdown and recovery data

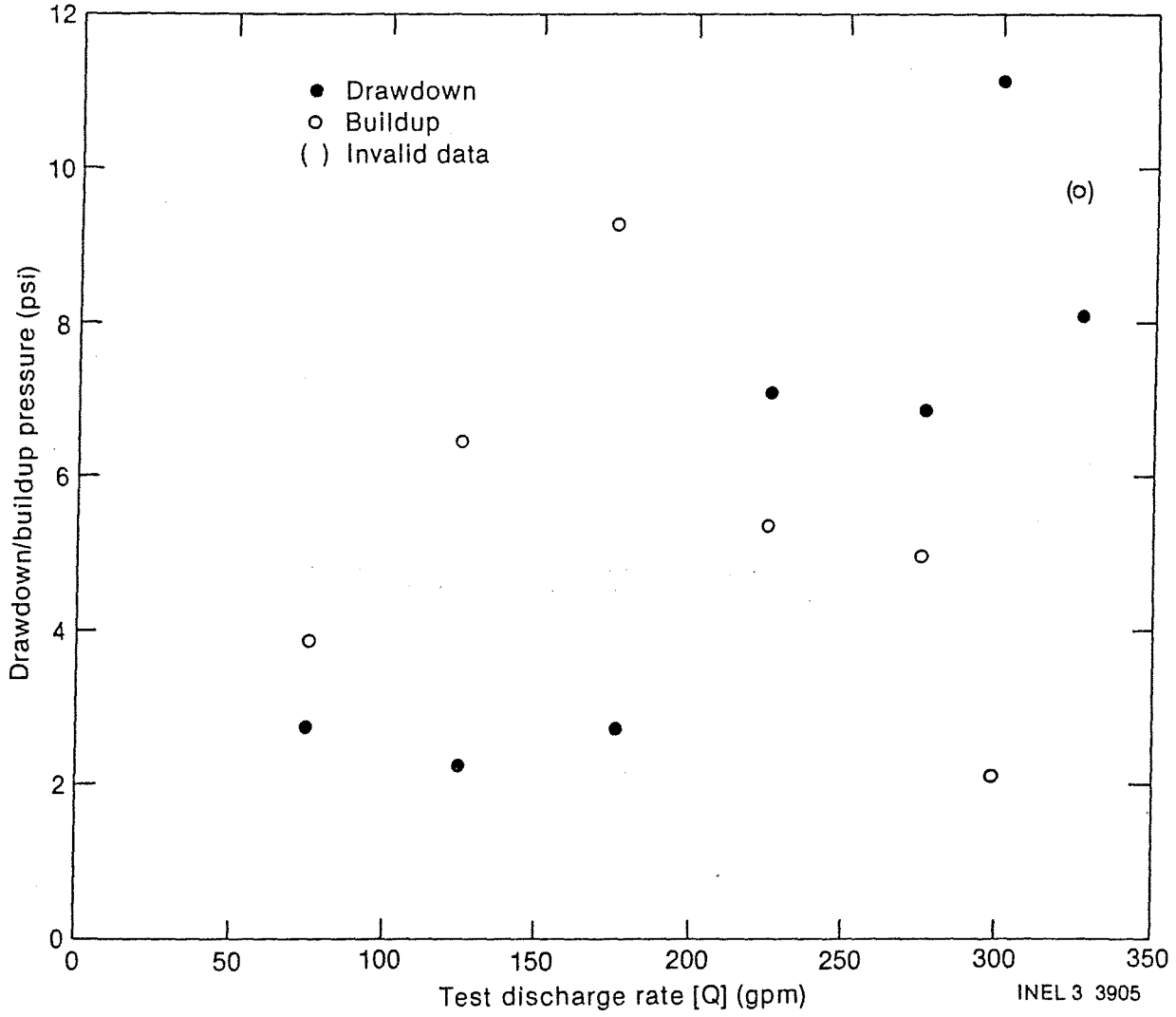

Figure 53. Calculated drawdown and buildup pressures one second after initiating/terminating discharge for RRGP-5BF versus Q.

several seconds were required to stabilize the discharge and shut in the wellhead. The zero time for the tests was usually fixed at 3 sec and after the control valve was adjusted to initiate or terminate flow. The exception of the backflow at 2.1 x $10^{-2}m^3$/sec (325 gpm) which was fixed at 10 sec because of the difficulty in quickly opening the valve (8 to 10 sec to fully open or close). The data trends at 30 and 50 sec are reasonably consistent. Some of the data (bracketed in Figure 52 and Table 8) for the 2.1 x $10^{-2}m^3$/sec (325 gpm) test had constant discharge control problems during backflow and did not attain a stabilized drawdown which invalidates the recovery analysis technique. This general consistency of the calculated wellhead pressures provides credance that the calculated regressions are reasonably consistent for the tests.

3.2.3.3 Drawdown/Buildup at 1, 30, and 50 Sec. The drawdowns and buildups have been calculated for 1, 30, and 50 sec (Figure 53, 54, 55, Table 8). The drawdowns were calculated by subtracting the observed wellhead pressure at the appropriate times from the shutin wellhead pressure immediately prior to initiating backflow. The buildups were calculated by subtracting the observed wellhead pressure at the appropriate times from the steady-state pressure which occurred after the restricted entry boundary effects were no longer causing a significant additional lowering of the wellhead pressure. The drawdown and buildup data have the advantage over the raw wellhead pressure data by facilitating comparisons between tests.

With the exception of the 1-sec data, the drawdowns and buildups exhibit consistent relationships between tests. The data for 1 sec (Figure 53) generally exhibit an increasing drawdown and buildup trend as the test discharge rate increases. The scatter of the data are due, in part, to the difficulty of accurately determining when the discharge rate was changed and the pronounced wellhead pressure surging during buildup. The drawdown and buildup trends, for the 30- and 50-sec data (Figures 54 and 55) are smooth functioned trends, especially for the drawdown data. The drawdown and buildup trends at 50 sec form relatively smoothly

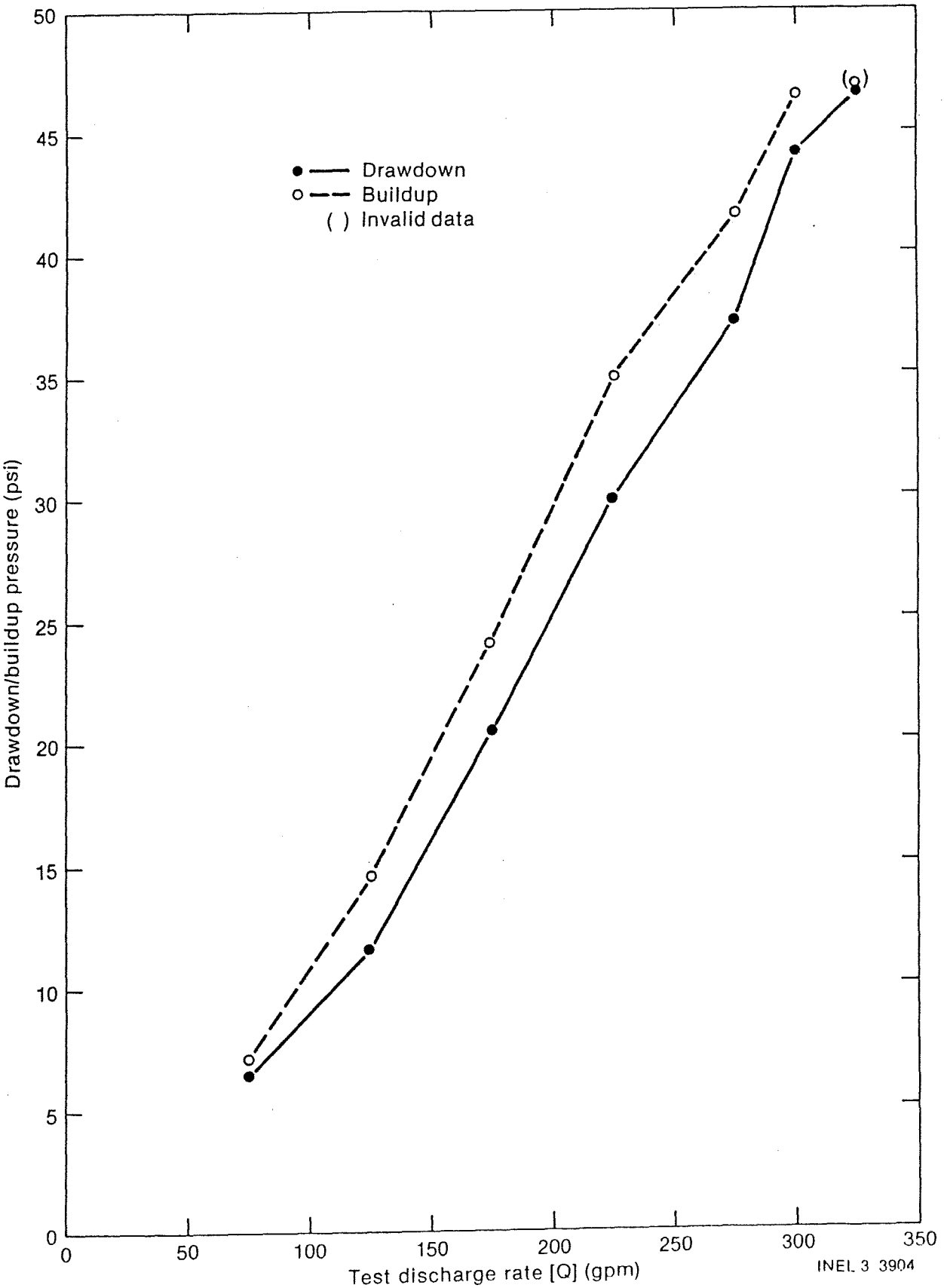

Figure 54. Calculated drawdown and buildup pressures 30 seconds after initiating/terminating discharge for RRGP-5BF versus Q.

Pulse Test Drawdown/Buildup Pressure vs Q for RRGP-5BF

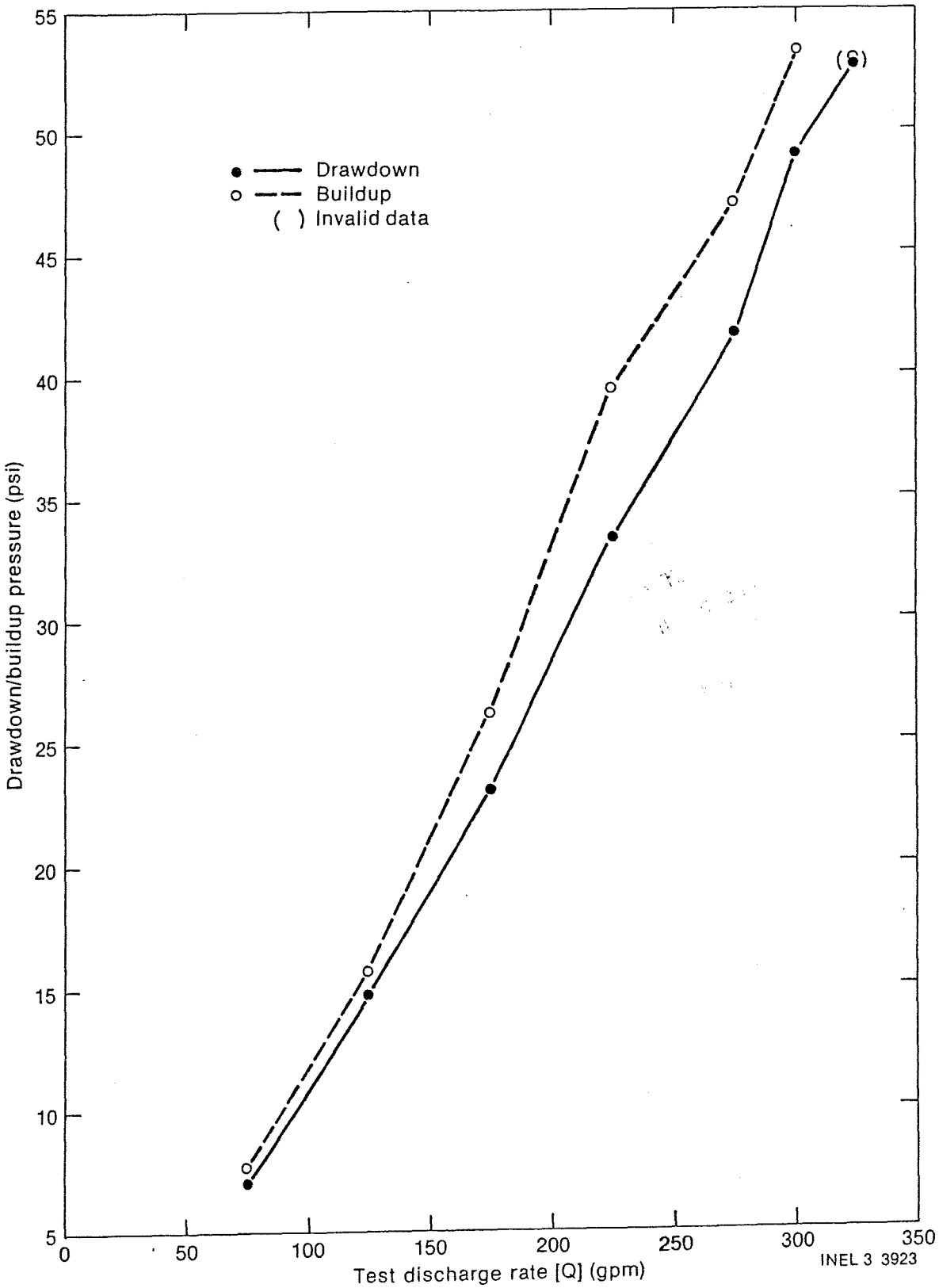

Calculated drawdown and buildup pressures 50 seconds after initiating/terminating discharge for RRGP-5BF versus Q.

functioned trends dependent on the test discharge rate; whereas the very early time, 1 sec, data do not exhibit a consistent relationship.

3.2.3.4 Well Losses. A simple but effective method to determine the well losses or the hydraulic head losses that are the result of nonlaminar flow near and in the wellbore is to compare the drawdown and buildup pressures. Drawdown results from the withdrawal of fluid from the wellbore. Hydraulic head losses result from the nonlaminar flow of water. However, when buildup results following backflow shutin, there is essentially no flow of water in the wellbore and, hence, no well losses for artesian flow. The differences between drawdowns and buildups as a function of discharge rate (Figure 56) exhibit an unusual relationship. In all tests in Figures 54 and 55, the buildup pressures are greater than the drawdowns. This is the opposite of what is normally expected for ideal porous media laminar flow; if there are no well losses the drawdown and pressure buildups should be equal for each test. However, if inertial effects are significant in the aquifers and in the wellbore, the drawdowns and buildups may not be equal. Computer modeling could provide some insight into the inertial effects. For nonlaminar flow in the channels of the fracture, the head losses that result could be dependent on flow direction, thereby giving differences between drawdown and buildup data. Commingling effects between the various producing/receiving zones in the reservoir could also result in differences between drawdown and recovery pressures. Well development by erosion of sand from the fracture is suspected to account for the trend changes in the buildup and drawdown data for discharge rates of the pulse tests. Additional field testing and data analysis would probably be necessary to ascertain the reason(s) for the buildup being greater than the drawdown for the 30- and 50-sec data and to ascertain if well development occurred at discharge rates greater than $1.4 \times 10^{-2} m^3/sec$ (225 gpm). Negative well losses are very unusual and are probably the result of inertial effects in the wellbore and reservoir.

3.2.3.5 Time for End of Limited Well Entrance Effects and Beginning of Constant-Head Boundary Effects. The time for the end of the limited well entrance effects and the beginning of the apparent constant head boundary effects can be calculated by extrapolating the linear regressions

of the backflow and recovery data (Figure 36 to 48 inclusive) to the steady state pressure that occurred after the restricted entry effects were overcome, Table 8. The times at which the extrapolated linear regression pressure trends had a value equal to the steady state pressures are listed in Table 8 and plotted as a function of the test discharge rate in Figure 57.

Ideally, for a laminar flow regimen, the apparent boundary effects should be independent of the test discharge rate and whether or not the calculation used backflow or recovery data. This is not the case for the backflow data. The general trend in Figure 57 is for the boundary time to increase as the discharge rate increases, at least up to 1.7 x $10^{-2}m^3$/sec (276 gpm). The boundary times calculated from the backflow data range from approximately 100 to 190 sec. In contrast with the backflow boundary times, the recovery times are essentially independent of the test discharge rate and average 76.6 sec. The reason(s) for the apparent differences is not known but could be related to commingling effects of the various aquifers as well as fluid inertial effects. The boundary time-discharge-backflow-recovery relationship is unusual and may be related to the unusual reservoir conditions in RRGP-5BF.

The well was shutin between 10-22-82 and 10-26-82 for approximately 6200 min. The pressure declined to 100.3 psia in 3.3 min and remained at near this level for 410 min. Data after 410 min are missing.

Backflow started on 11-26-82 and continued until 12-01-82 for a duration of 7100 min. The temperature during the initial 120 min reached 111°C (231°F) and increased to 119°C (246°F) during the remaining period of backflow. Pertinent early time backflow pressure data are missing because an instrument valve was essentially closed. Shortly before shutin this problem was rectified. The pressure immediately prior to shutin was 102.2 psia. The pressure recovered to 124.0 psia 2 min after shutin.

3.2.3.6 Specific Capacities. Specific capacity data for RRGP-5BF were obtained for tests conducted prior to and during injection-backflow during tests and for the pulse tests conducted on 12-01-82. The initial

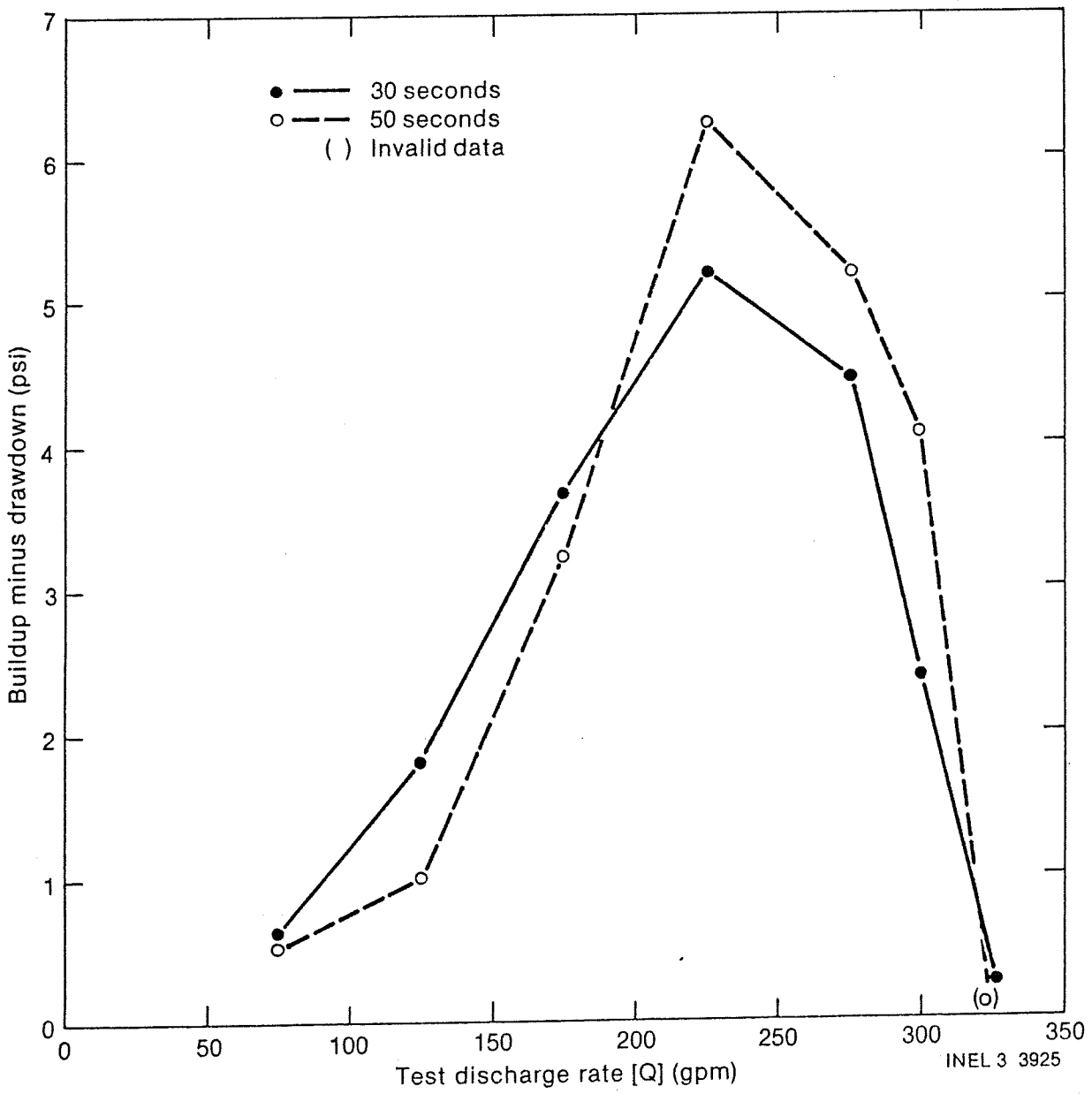

Figure 56. Calculated buildup minus drawdown at 30 and 50 seconds after initiating/terminating discharge at RRGP-5BF versus Q.

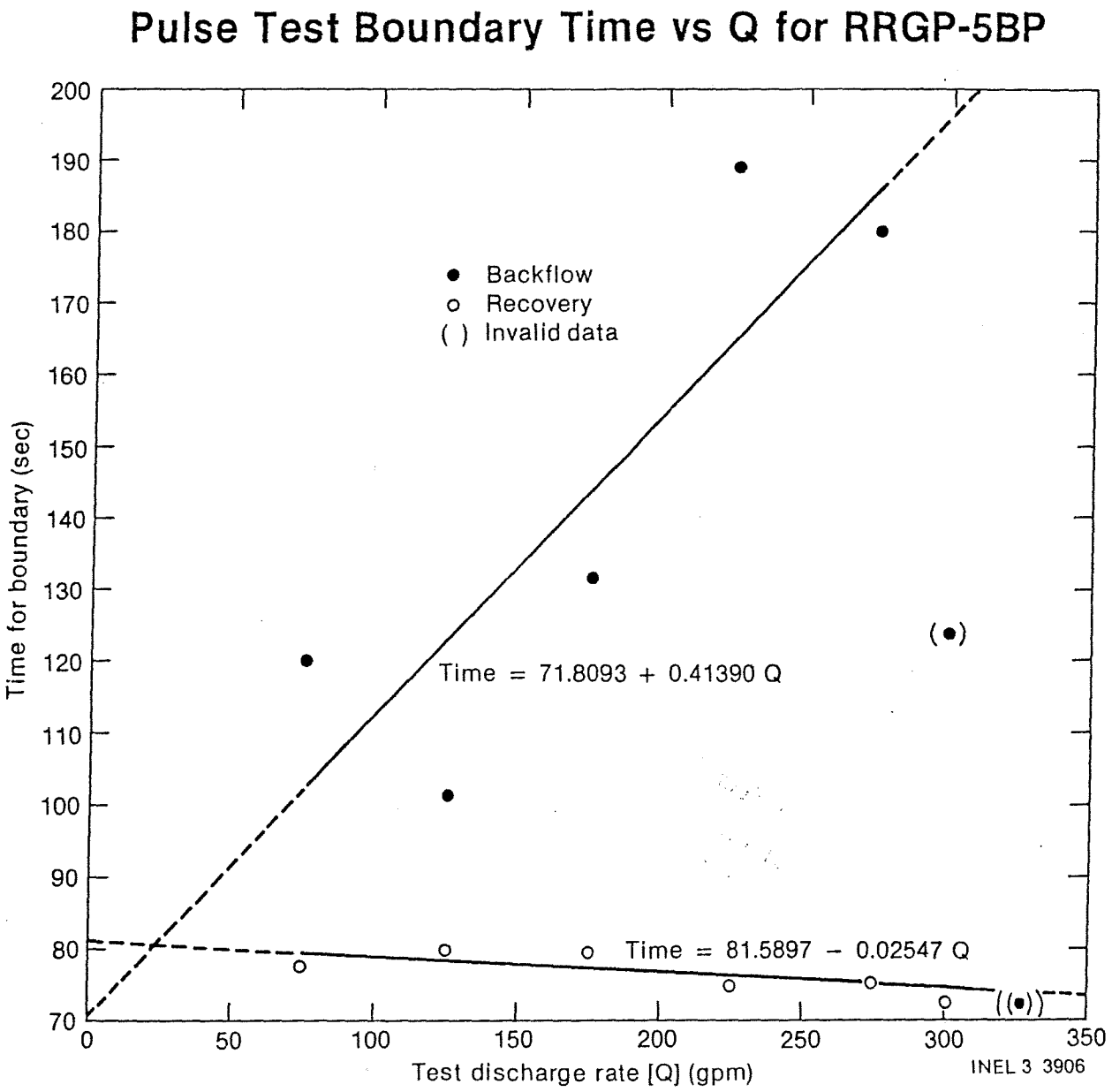

Time for end of additional limited well entrance effects and the beginning of constant head boundary effects for RRGP-5BF versus Q.

test on 11-25-79 was conducted 13 days after fracturing. The backflow of $1.3 \times 10^{-2} m^3$/sec (200 gpm) produced 100 psi of drawdown[3] for a specific capacity of $1.3 \times 10^{-4} m^3$/sec/psi (2 gpm/psi). The wellhead pressure exhibited a very rapid drawdown in the first minute due to the limited entry of fluid into the wellbore through the fracture. The pressure then stabilized with 100 psi of drawdown. The specific capacity for all the reported test data are for the stabilized portion of the drawdown or recovery which generally occurs between 2 and 5 min after initiating or terminating well discharge.

The specific capacity data are plotted as the logarithm of the flow rate in Figure 58. The 11-25-79 test data indicate a significantly lower specific capacity than the values for subsequent tests. Significant quantities of sand had been pumped from the fracture, thereby decreasing the hydraulic head losses in the sand propped fracture. The pumped sand gutted two pumps.[15] The channels presumably eroded in the fracture have decreased the magnitude of the limited entry losses in the fracture between the wellbore and the constant head aquifer.

A pump test and well cleaning test began 03-27-80 and lasted for 61.3 hrs[3]. This $4.1 \times 10^{-2} m^3$/sec (650 gpm) test resulted in a specific capacity of $1.3 \times 10^{-4} m^3$/sec/psi (2.05 gpm/psi) (Figure 58). A large quantity of sand was pumped from the well indicating that development was occurring during testing.

The next pump test began on 03-11-81. The well was pumped at $4.4 \times 10^{-2} m^3$/sec (697 gpm) for 64.8 h and then the discharge rate was reduced to $4.1 \times 10^{-2} m^3$/sec (648 gpm) for 27 h. After 0.5 h of pumping, the bubbler pressure had declined approximately 357 psi which gives a specific capacity of $1.2 \times 10^{-4} m^3$/sec/psi (1.95 gpm/psi) (Figure 58). After 64.8 h, the discharge of $4.1 \times 10^{-2} m^3$/sec (648 gpm) resulted in 333 psi of drawdown which resulted in a specific capacity of $1.2 \times 10^{-4} m^3$/sec/psi (1.95 gpm/psi) (Figure 58). The well was still producing sand but at a much lower rate than during the 3-27-80 test.

		Q	$\Delta\sigma_{10}$ psi/log cycle	G in cycle	
1/6 P-5A UNCRACKED	7-31-78	550	10.8	50.92	
5B	11-1-78	100 DD	3.02		
		~~100~~ REC	~~6.99~~	33.06	
		100 REC	6.99	14.35	
		~~140~~ DD	11.54	12.13	
		250 DD	21.46	11.65	
		~~140~~			
		250 REC	16.56	15.16	
		800 DD	24.40	12.30	3.46
		~~240~~			~~2.48~~
		300 REC	22.28	13.47	
				33.16	
5B	5-16-78	640	18.96	~~32.06~~	2.39
5BF		700	—	—	1.95
		650	—	—	1.95

at 40 min

	Date	Production Rate GPM	Specific Capacity GPM/PSI
P-5A	7/31/78	550	9.17
P-5B	11/1/78	40	2.30 [illegible] 29
	11/1/78	190	9.67
	11/1/78	530	2.81 9-74
P-5BF	11/21/78	200	1.92

999.52
1335.26

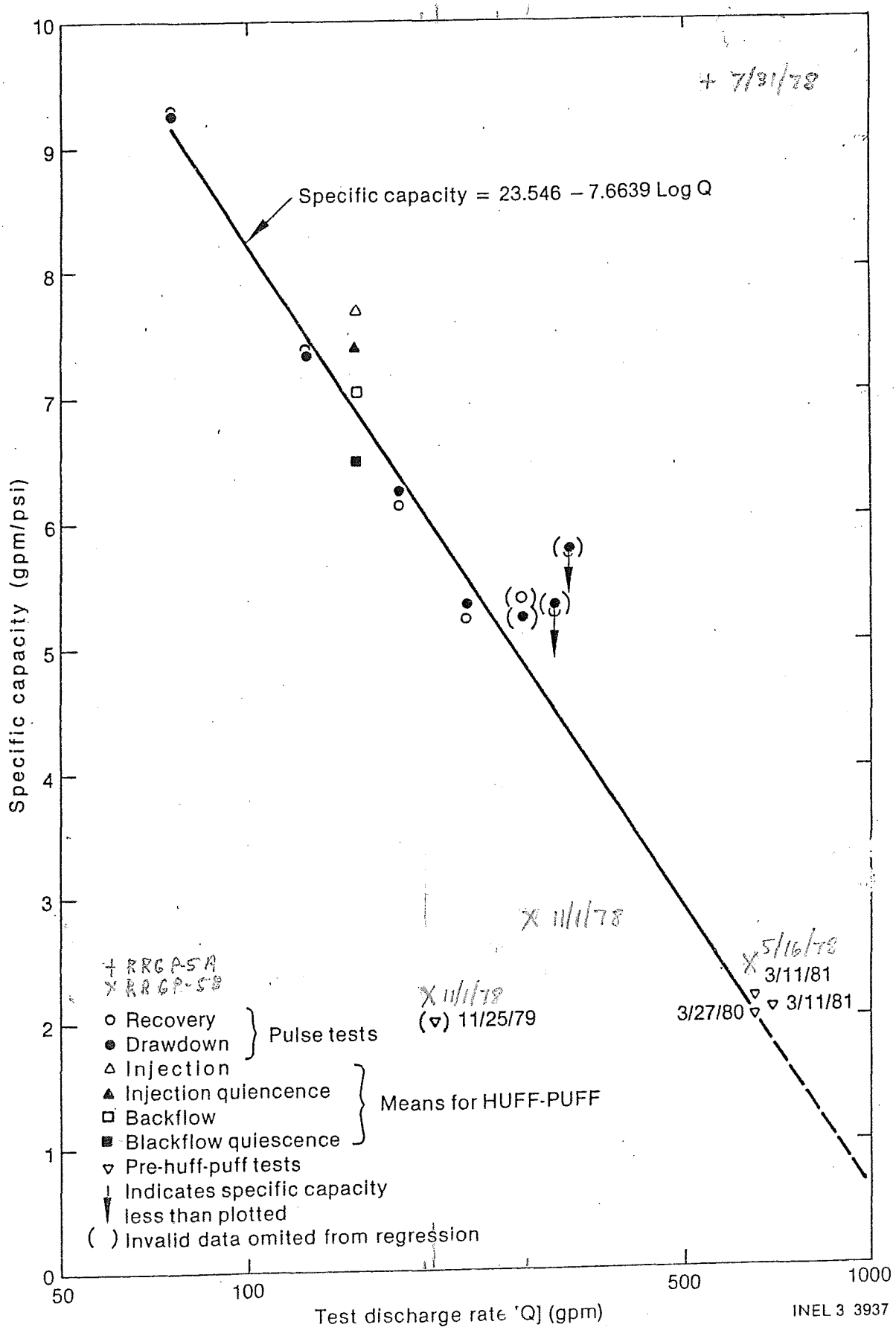

Semilogarithmic plot of specific capacity at early time apparent steady state conditions for selected tests on RRGP-5BF versus Q.

Thus, these specific capacity values have the potential to increase with additional proper well development.

Specific capacity data were also calculated for the 9.5 x 10^{-3}/sec (150 gpm) tests (Table 9). The specific capacities were calculated for each phase of these tests where sufficiently accurate data are available. For the injection phases of the tests, the specific capacities ranged from 7.41 to 8.07 with an arithmetic mean of 7.66 gpm/psi. For the quiescence following injection, the specific capacities ranged from 6.96 to 8.53 with a mean of 4.6 x $10^{-4}m^3$/sec/psi (7.36 gpm/psi). The backflow specific capacity values ranged from 4.0 x 10^{-4} to 4.9 x $10^{-4}m^3$/sec/psi (6.29 to 7.82) with a mean of 4.4 x $10^{-2}m^3$/sec/psi (7.03 gpm/psi). For the quiescent phase following backflow, the specific capacity values ranged from 3.8 x 10^{-4} to 4.3 x $10^{-4}m^3$/sec/psi (5.99 to 6.83 gpm/psi) with a mean of 4.1 x $10^{-4}m^3$/sec/psi (6.48 gpm/ psi). These means are plotted on Figure 58.

Although there are differences between the specific capacity means for the various phases, it is not known if they are significant. There could be slight differences in the indicated flow rates for the different orifice plates used for injection and backflow. Valve leaks could also affect the reported injection and backflow rate. Specific capacities would be expected to be less due to hydraulic well losses when there is actual flow occurring in the wellbore during injection and backflow. The data suggest the opposite is true with the injection and backflow nearly greater than the respective quiescence means, thus implying low well losses. Wellbore fluid density-induced wellhead pressure changes and formation fluid viscosity changes as the result of injection may also be affecting the specific capacities. A rigorous statistical treatment of the data may provide some insight into possible reasons for the apparent differences in specific capacities.

The specific capacities were also calculated for the pulse test data (Table 10). These data are plotted in Figure 58. There appears to be a break in the continuity of the data between the 1.4 x 10^{-2} and 1.7 x $10^{-2}m^3$/sec (225 and 276 gpm) tests. There are at least two potential

TABLE 9. HUFF-PUFF TEST SPECIFIC CAPACITIES

	Injection Phase						
Test Number	Pressure Immediately Prior to Injection (PSIA)	Steady-state Pressure During Injection[3] (PSIA)	Pressure Buildup (PSI)	Injection Rate When Steady-state Pressure[1] (GPM)	Injection Specific Capacity[2] (GPM/PSI)	Duration of Injection (Min)	Pressure at end of Injection (PSIA)
2A-2	133	(149.7)	(16.7)	146	--	242	102.5
2C	~116	(132.7)	(16.7)	146	--	2910	116.8
2D	130.3	150.5	(20.2)	151	7.48	5890	117.3
4A	129.0	--	--	variable	--	143	118.5
4B	134.1	152.2	18.1	146	8.07	141	126.6
4C	130.8	150.5	19.7	146	7.41	140	124.0
4D	(125)	144.0	(19.0)	151	--	144	118.5
5	115.7	135.4+	19.7	151	7.66	22560	118.0
Arithmetic Means					7.66		

1. Flow rate adjusted for 4 gpm diverted to chemical sampling between wellhead and orifice plates.

2. Specific capacities have been adjusted to 150 gpm.

3. Not density corrected.

( ) Bracked values invalid data.

TABLE 9. (Continued)

	Injection Quiescence Phase					
Test Number	Steady-state Pressure During Injection Quiescence (PSIA)	Pressure Falloff (PSI)	Injection Rate Prior to Quiescence[1] (GPM)	Injection Quiescence Specific Capacity[2] (GPM/PSI)	Duration of Injection Quiescence (Min.)	Pressure at end of Injection Quiescence (PSIA)
2A-2	82.2	20.3	146	7.19	--	84.0
2C	96.5	20.3	146	7.19	∿5.0	96.5
2D	97.5	19.8	148	7.47	<9.0	97.2
4A	--	--	146	--	1653	113.9
4B	105.8	20.8	146	7.02	130	111.0
4C	103.7	20.3	146	7.19	720	112.7
4D	96.8	21.7	151	6.96	2973	114.8
5	100.3	17.7	151	8.53	6200	--
Arithmetic Means				7.36		

TABLE 9. (Continued)

Test Number	Backflow Phase					
	Steady-state Pressure During Backflow[3] (PSIA)	Pressure Falloff (PSI)	Backflow Rate When Steady-state Pressure[1] (GPM)	Backflow Specific Capacity[2] (GPM/PSI)	Duration of Backflow (Min.)	Pressure at end of Backflow (PSIA)
2A-2	62.0	22.0	154	7.00	612	110.5
2C	72.0	24.5	154	6.29	6400	107.7
2D	74.2	23.0	152	6.61	14000	111.8
4A	89.3	19.7	154	7.82	960	109.0
4B	88.6	22.4	154	6.88	900	111.6
4C	91.9	20.8	154	7.40	520	111.6
4D	93.5	21.3	154	7.23	3660	112.5
5	--	--	149	--	7100	102.2
Arithmetic Means				7.03		

TABLE 9. (Continued)

Test Number	Backflow Quiescence Phase			
	Steady-state Pressure During Quiescence (PSIA)	Pressure Buildup (PSI)	Backflow Rate Prior to Quiescence[1] (GPM)	Backflow Quiescence Specific Capacity[2] (GPM/PSI)
2A-2	134.6	24.1	154	6.39
2C	131.7	24.0	159	6.63
2D	135.3	23.5	152	6.47
4A	134.7	25.7	154	5.99
4B	135.5	23.9	154	6.44
4C	135.0	23.4	154	6.58
4D	(134.9)	22.4	154	--
5	124.0	21.8	149	6.83
Arithmetic Means				6.48

TABLE 10. PULSE TEST SPECIFIC CAPACITIES

Pulse Test No.	Discharge Rate (GPM)	Drawdown	Recovery	Initial Wellhead Pressure (PSIA)	Steady-state Wellhead Pressure (PSIA)	Pressure Drawdown (PSI)	Pressure Recovery (PSI)	Specific Capacity (GPM/PSI)
1	75	x		123.3	115.2	8.1		9.26
1	75		x	115.2	123.3		8.1	9.26
2	125	x		123.3	106.3	17.0		7.35
2	125		x	106.3	123.2		16.9	7.40
3	175	x		123.2	95.1	28.1		6.23
3	175		x	95.0	123.3		28.3	6.18
4	225	x		123.3	81.0	42.3		5.32
4	225		x	80.7	123.8		43.1	5.22
5	276	x		122.3	69.2	53.1		5.20
5	276		x	71.8	123.3		51.5	5.36
6	325	x		123.3	(66.6-)	(56.7+)		(5.73-)
6	325		x	66.6	123.2		(56.6+)	(5.74-)
7	300	x		123.3	(65.5-)	(57.8+)		(5.19-)
7	300		x	65.5	123.6		(58.1+)	(5.16-)

( ) invalid data

explanations. One possible explanation is that the different orifice plate used for the tests with a discharge rate greater than $1.4 \times 10^{-2} m^3/sec$ (225 gpm) resulted in calculated discharge rates that were less compared to the calculated rates obtained from the orifice plate used for the other tests. Errors in discharge rates are possible with the change in orifice plates but are not likely of this magnitude. A more plausible explanation is that sand erosion in the reservoir began when the discharge rate equalled or $1.7 \times 10^{-2} m^3/sec$ (exceeded 276 gpm). Erosion in the reservoir would result in an increased specific capacity as is the case for the data plot in Figure 58. The discharge rates for the 1.9×10^{-2} and $2.1 \times 10^{-2} m^3/sec$ (300 and 325 gpm) pulse tests could not be maintained until steady-state conditions developed, thus the specific capacity values for these tests plot above the fitted regression curve as do the $1.7 \times 10^{-2} m^3/sec$ (276 gpm) test data. The pulse specific capacity data provide a valuable tool for defining some aspects of the drawdown characteristics for RRGP-5BF.

The specific capacity data calculated from the drawdown and recovery data for the first 5 min following a change in flow rate are a descriptive parameter for the hydraulic behavior of the limited fluid entrance nature of the well completion, i.e., fluid entrance is basically limited to channels in the fracture which is, at a maximum, 1.5 cm (0.6 in.) wide. The drawdown and recovery pressures for the aquifer which are presumably between depths of 1364 and 1370 m (4475 and 4494 ft) is essentially negligible. This is supported by the fact that even during the $4.4 \times 10^{-2} m^3/sec$ (697 gpm) test beginning 3/11/81, the potentrometric head only declined at 5.28 psi/log cycle of time after 35 min of pumping. For an ideal porous media aquifer, the steady-state specific capacity should be a constant if one assumes the presence of a constant head hydraulic boundary. The constant head boundary is a reasonable approximation, which suggests that flow in the fracture is not dominated by laminar flow as would occur in a porous media. The 3.7 to 13.7 m^3 (4 to 15 yd^3) of sand eroded from the fracture, as well as the spinner, temperature, and fluid specific conductance log data suggest the possibility of channel type flow of a non-laminar nature is possible. Commingling effects of the

various aquifers in the fracture could also account for deviation of the specific capacity data from the theoretical response of a single aquifer. The logarithmic relationship between specific capacity and the flow rate suggests a non-laminar component to the flow regimen in RRGP-5BF fracture. The commingling effects of the multiple aquifer completion could also account for the unusual specific capacity-discharge rate relationship.

3.3 Hydraulic Interference Effects of RRGP-5 On RRGE-1

Hydraulic interference data are available for RRGE-1 for a 21-day test beginning 05-16-79 at a pumping rate from RRGP-5B of 640 gpm. Figure 59 is a semilogarithmic plot of the wellhead pressure at RRGE-1 during the 30,248-min pump test at RRGP-5B. It appears that the keep-warm discharge from RRGE-1 decreased at approximately 20,000 min which resulted in an abnormally low wellhead pressure from 20,000 min until the end of the test. This decreased keep-warm flow is presumed to result in a maximum recovery pressure of only 147 psi at 50,000 min for RRGE-1; whereas it should have recovered to approximately 155 psi. The estimated interference effects of RRGP-5B was 12.8 psia after 30,000 min, with a s_{10} of 10.6 psi/log cycle. This would result in an estimated drawdown in RRGE-1 of 26.1 psi after 1 yr of pumping RRGP-5B at 4.0×10^{-2} m^3/sec (640 gpm). These data indicate that interference effects occurred between RRGP-5B and RRGE-1 prior to hydraulic fracturing. This is contrary to that reported by Republic Geothermal Inc.[3] Because of the hydraulic interference effects of RRGP-5B on RRGE-1 and other hydrogeologic and water quality data, RRGE-1 was judged to be a suitable monitor well in which breakthrough of tracer injected into RRGP-5BF could be possible.

Hydraulic interference effects also resulted in RRGE-1 during the hydraulic fracturing of RRGP-5BF. The only hydraulic interference data between RRGP-5BF and RRGE-1 available are those data collected during the hydraulic fracturing process on 11-12-79. Figure 60 is a plot of the RRGE-1 wellhead pressure during this period. The wellhead was shut in at approximately 03:47 on 11-12-79. The wellhead pressure continued to recover until approximately 06:10 when the wellbore fluid density effects on pressure resulted in a declining wellhead pressure which continued until

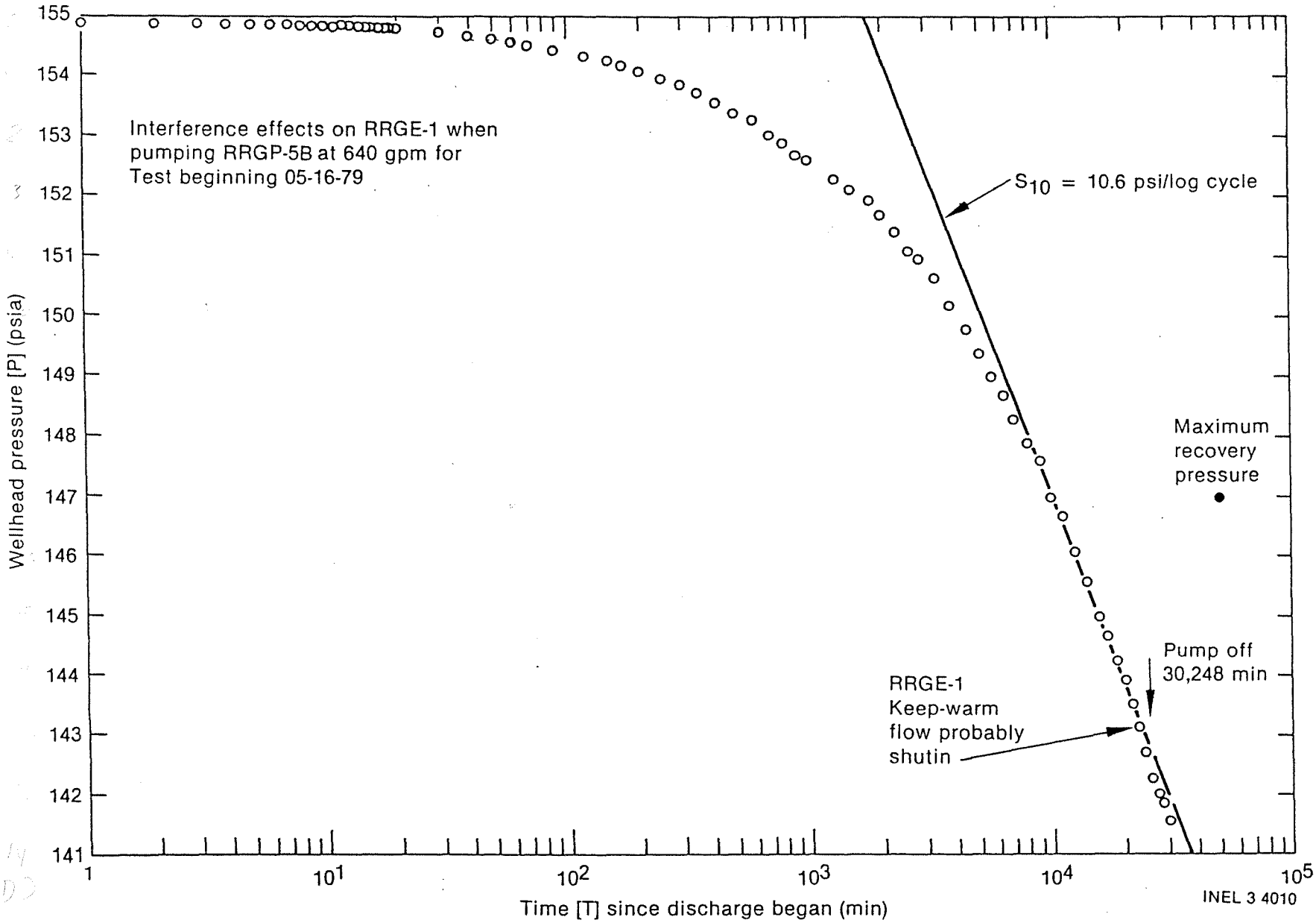

Figure 59. Interference effects on RRGE-1 when pumping RRGP-5BF at 640 gpm for test beginning 05-16-79.

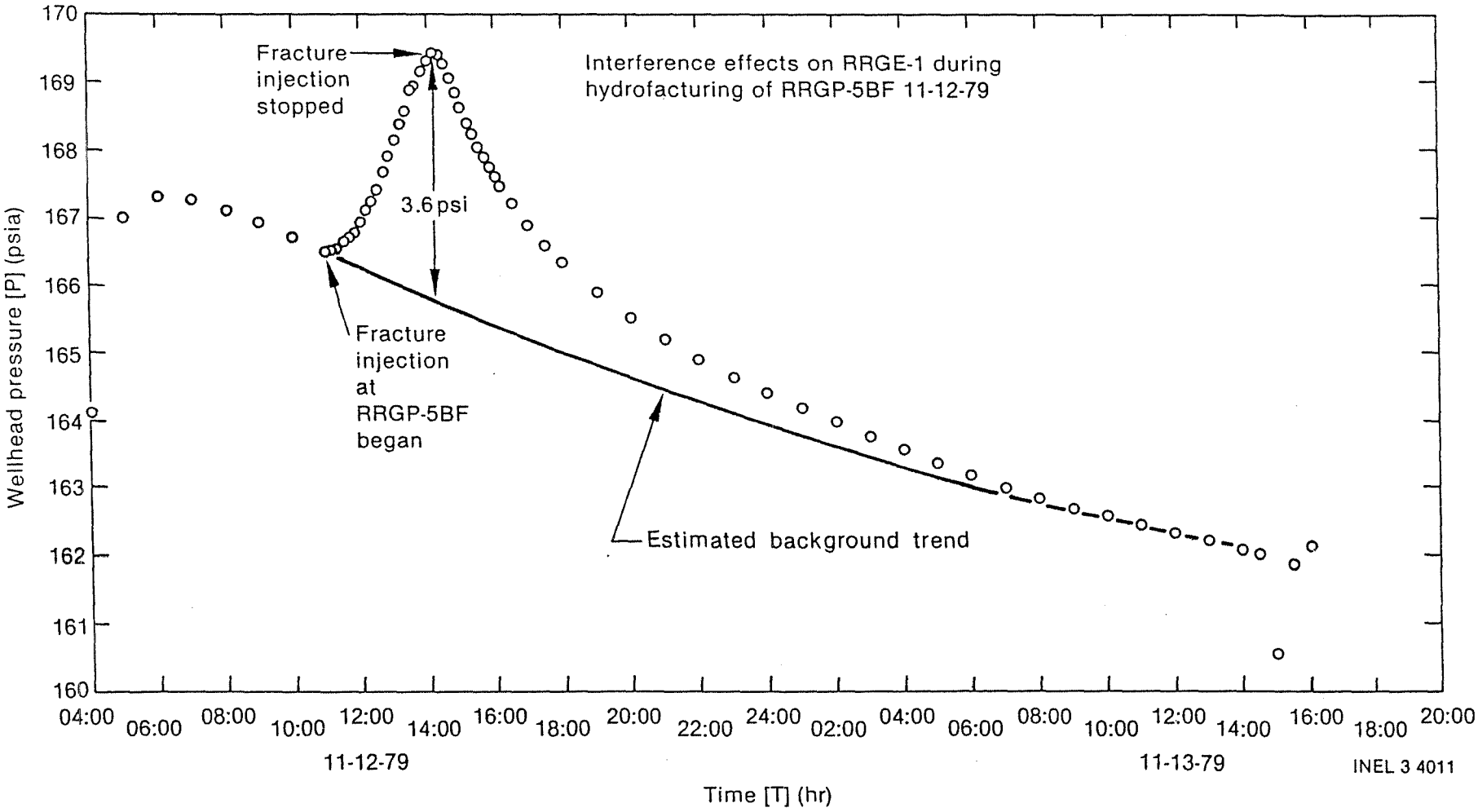

Figure 60. Interference effects on RRGE-1 during hydrofracturing of RRGP-5BF on 11-12-79.

15:00 on 11-13-79 when the discharge rate was increased. By subtracting the maximum observed pressure 169.4 psia, during fracturing, from the extrapolated wellhead pressure 165.8 psia, had injection not occurred, it is estimated that the maximum wellhead pressure buildup due to injection at RRGP-5BF was 3.6 psi at the end of injection. The injection rate was approximately 1.4 x $10^{-1}m^3$/sec (2142 gpm) and continued for 192 min. Wellhead pressure data indicate a 3.6 psi pressure buildup at RRGE-1 during the hydrofracturing of RRGP-5BF.

The wellhead pressure buildup at RRGP-5BF during hydrofracturing (Figure 60) was greater than that expected from the 4.0 x $10^{-2}m^3$/sec (640 gpm) pump test (Figure 59). At 192 min of pumping (Figure 59), the drawdown was 0.75 psi. For a pumping rate of 1.4 x $10^{-1}m^3$/sec (2142 gpm), a pressure buildup of 2.5 psi would be expected for a laminar flow aquifer. Thus, the observed pressure buildup in RRGE-1 during hydrofracturing RRGP-5BF was 1.1 psi or 44% greater than expected based on a pump test for RRGP-5B.

Several explanations for this observed result are possible. One possible explanation is that laminar flow did not occur to the same extent during hydrofracturing when wellhead pressures in excess of 1800 psig occurred. Pressure buildup would thus not necessarily be directly proportional to the flow rate at RRGP-5B and RRGP-5BF. Heterogeneities in the reservoir and the presence of a multiporosity fractured reservoir could likewise result in unexpected pressure interference effects. The hydraulic fracturing at RRGP-5BF has also undoubtedly modified the hydraulic interconnection between the aquifers in the Schist of the Upper Narrows. This hydraulic modification of the reservoir could result in a different pressure response at RRGE-1. It is likely that a combination of the above explanations and possibly others resulted in the excessive pressure response at RRGE-1. However, it may only be possible to ascertain if hydraulic fracturing has increased the pressure response at RRGE-1 by repeating a 4.0 x $10^{-2}m^3$/sec (640 gpm) pump test at RRGP-5BF and comparing the results to the 4.0 x $10^{-2}m^3$/sec (640 gpm) pump test on RRGP-5B.

3.4 Injection Test Tracer Responses

One of the major objectives of this program was to determine whether the shape of tracer recovery curves could be used to gain information about the physical characteristics of a fracture dominated geothermal reservoir. In order for materials to be useful as tracers it must meet the following criteria:

1. The material should be absent or occur in very low concentrations in the fluids of the test reservoir.

2. The material should not react with the dissolved species in the geothermal fluid to form a precipitate.

3. The material should not react with the rocks and minerals which make up the reservoir.

4. The material should have a very small environmental impact in the event of an accidental spill (i.e., nontoxic, nonteratogenic, nonmutagenic).

5. Analysis of low concentrations of the material should be relatively easy and capable of being carried out at the test site.

6. Because orders of magnitude of dilution can usually be expected, high concentrations of the material must be injected into the reservoir over relatively long periods of time, so the material must be relatively inexpensive or detectable at extremely low concentrations.

3.4.1 Tracer Evaluation

As stated in a previous section of this report, the concentrations of dissolved species in the injectant fluid from RRGP-3 were considerably higher than those of the fluids native to RRGP-5 (Table 1). These higher

concentration, higher conductivity fluids served as their own primary tracer. The added or exotic tracers were of two types, chemical and dye.

The chemical species which we expected to meet criteria outlined above were iodide, I^-; bromide, Br^-; thiocyanide, SCN^-; magnesium, Mg^{2+}; and boron, B^{3+}. Use of these tracers in various tests demonstrated that problems were encountered with several of them. Bromide and thiocyanide are usually analyzed with selective ion electrodes. The chloride concentrations in these geothermal brines, 2260 mg/kg, effectively blocked some sites on the ion sensitive membranes and caused a large amount of scatter in these data. Iodide had the problem to a lesser extent and a standard additions method was finally used to give internally consistent data sets. The relatively strong electrolyte solutions from the RRGP-3 reservoir also caused a problem with the colorimetric determination of boron concentrations and these data were later replaced with the results of inductively coupled plasma emission spectrographic (ICP) analyses. Magnesium analysis by atomic absorption spectroscopy (AAS) presented fewer problems. Magnesium, however, reacted with the reservoir materials and proved to be a non-conservative tracer.

Both of the dyes we tried, fluorescein and rhodamine B, are complex heterocyclic organics with several functional groups attached to the rings. These functional groups attach themselves to almost any site that has an electrostatic charge. These dyes, therefore, adsorb onto nearly everything and cannot be considered conservative tracers; however do have their uses. Fluorescein, for example, is detectable with the human eye at concentrations in excess of 30 µg/kg and will act as a signal that the injected fluid is returning which allows one to modify their solution sampling scheme to monitor maximum rates of change in the concentrations of more conservative tracers.

While each of the tracers tested had some problems associated with it, iodide and boron did in fact prove to be conservative. Another conservative tracer proved to be the moderately high concentrations of NaCl found naturally in these geothermal fluids. The Raft River reservoir

fluids can be characterized as a (Na, K, Ca) Cl solution. Because the solubilities of the chloride minerals are orders of magnitude higher than the concentrations found in the Raft River reservoir, there is no potential for loss due to precipitation. The presence of these strong electrolytes made the geothermal fluids very conductive and the contrast in solution conductivities between the test well (RRGP-5, μ = 2700 μmho/cm; and the injectant supply well, RRGP-3, μ = 8000 μmho/cm) provided a means of estimating the amount of injectant fluid present in the backflow stream. During the short term tests the amount of mixing was calculated from either the conductivities or the conservative tracer data. For the long-term tests, the chloride ion concentrations were used for the mixing calculations.

A second concern is the change in background concentrations of the RRGP-5 reservoir as a function of time. Each test left some of the injectant fluid in the reservoir. A plot of the chloride concentration at the termination of each test, Figure 61, indicates that the longer-term injection tests, 2C and 2D, left about 100 mg/kg of Cl^- in the reservoir and that background values were never reached after the initiation of testing. There is not a regular trend of increasing concentration with time. The longer term injection tests increase the Cl^- concentration and the shorter term tests decrease Cl^-. In our data analysis the Cl^- concentration determined before the onset of testing was considered actual baseline and not the concentration of the last sample from the previous test. There are two reasons for this decision. The first is that some of the short term tests actually brought the chloride concentration below that present at the beginning of the test which would lead to negative dilution factors. The second reason is that the injected fluids were always at least 1500 mg/kg more concentrated than the fluids left in the formation. All of the tests were terminated before background values were reached because of time considerations. The actual extrapolation to background concentration can be handled mathematically.

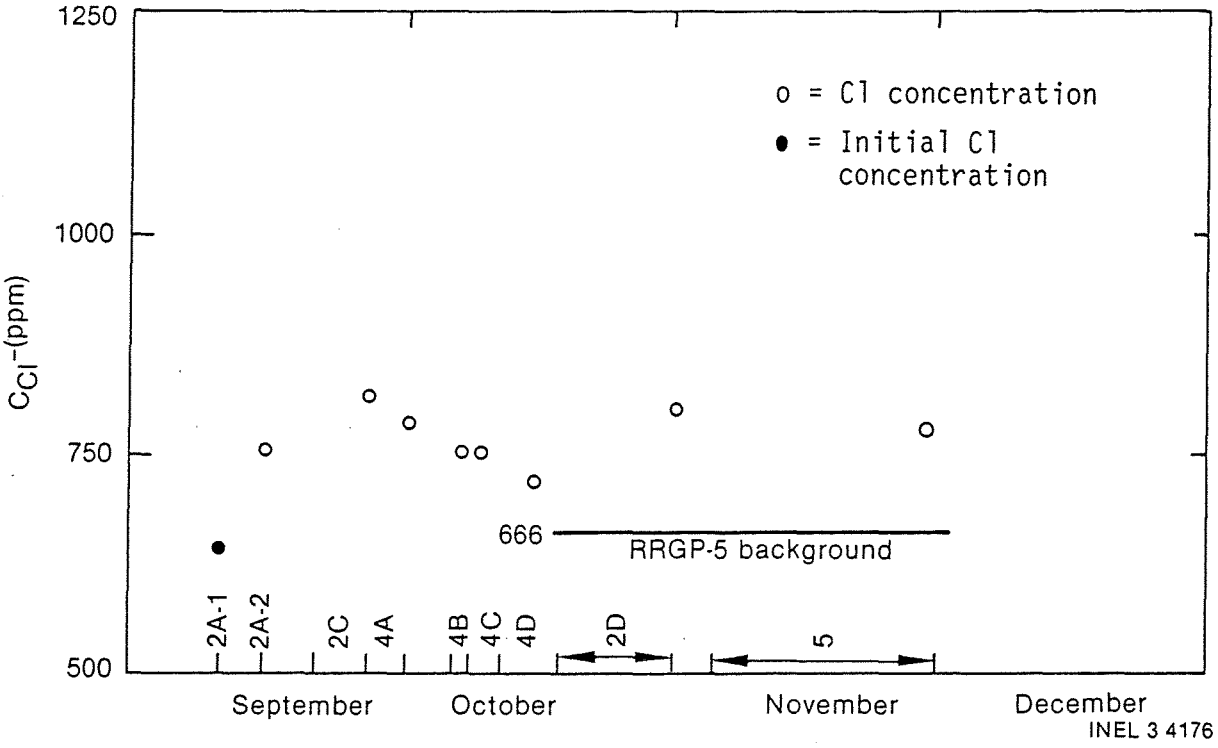

Figure 61. Final chloride concentration at the termination of each test.

3.4.2 Tracer Response

A plot of the tracer concentration during backflow as a function of time yields a smoothly decreasing curve. The slopes and the rate of change of these slopes are significantly different depending on the conservatism of the tracer and the injection scheme used (slug or continuous injection). Figure 62 is a comparison of the conservative tracer responses for tests 2A-2, 2C and 2D. Time "zero" is the initiation of backflow. Negative times are for injection and positive times indicate backflow. The ordinate is in terms of reduced concentration which is the ratio of the concentration at any given time to the concentration of the injected fluid. As expected, the reservoir was perturbed more and required more time to recover with the longer injection times. When the test times are converted to volumes and normalized by dividing by the injection volume (Figure 63), the backflow curves all lie on top of one another. This indicates that the reservoir behaves homogeneously throughout the entire volume explored. The processes causing the decrease in tracer concentration are the same at all volumes that were explored, and there are no detectable changes in the reservoir characteristics within those volumes.

During the injection phase of Test 2D, tracers were injected as high concentration slugs. At the initiation of injection, a slug of NaI was injected. Twenty-four hours later a borax slug was injected and to test for reproducibility of continuous injection, $MgCl_2$ was added during the last six hours of injection (Figure 64). Fluorescein dye was added along with the other tracers, but, due to the fact that it is non-conservative, no attempt was made to interpret the results of these analyses. The total injection time into the formation was 96.33 h. The tracer slugs, iodide and boron, respectively, were injected, therefore, 98 and 72 h before the initiation of backflow. The boron concentration was above background when the first fluids arrived from the reservoir (Figure 65). This concentration continued to increase for the next 39 h where it reached a plateau at 2.9 mg/kg. The boron concentration remained constant for the next 28 h and then started a steady decline toward background values. The iodide concentration started to increase within 1.5 h after the first

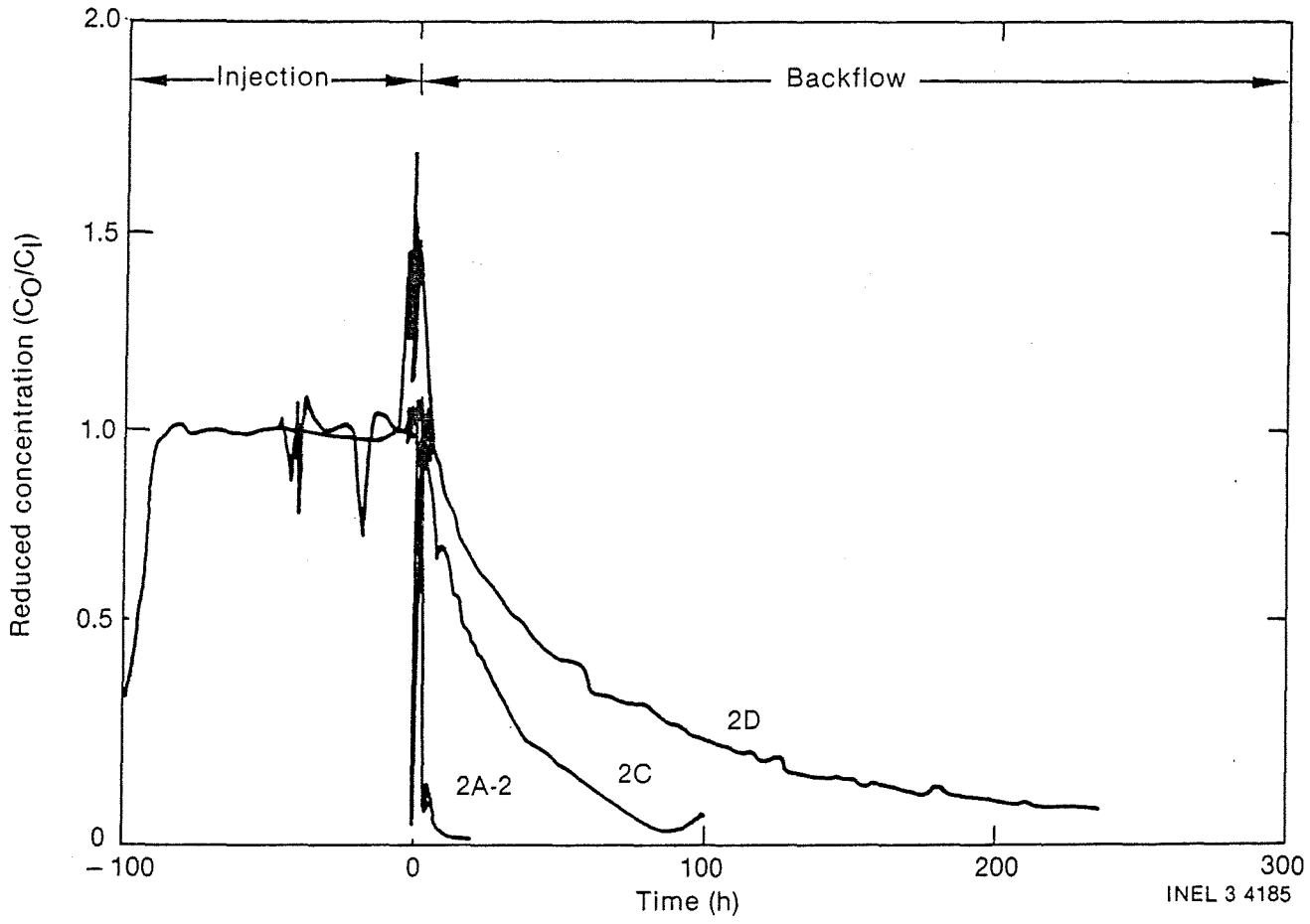

Figure 62. Comparison of conservative tracer responses for Test 2 experiments.

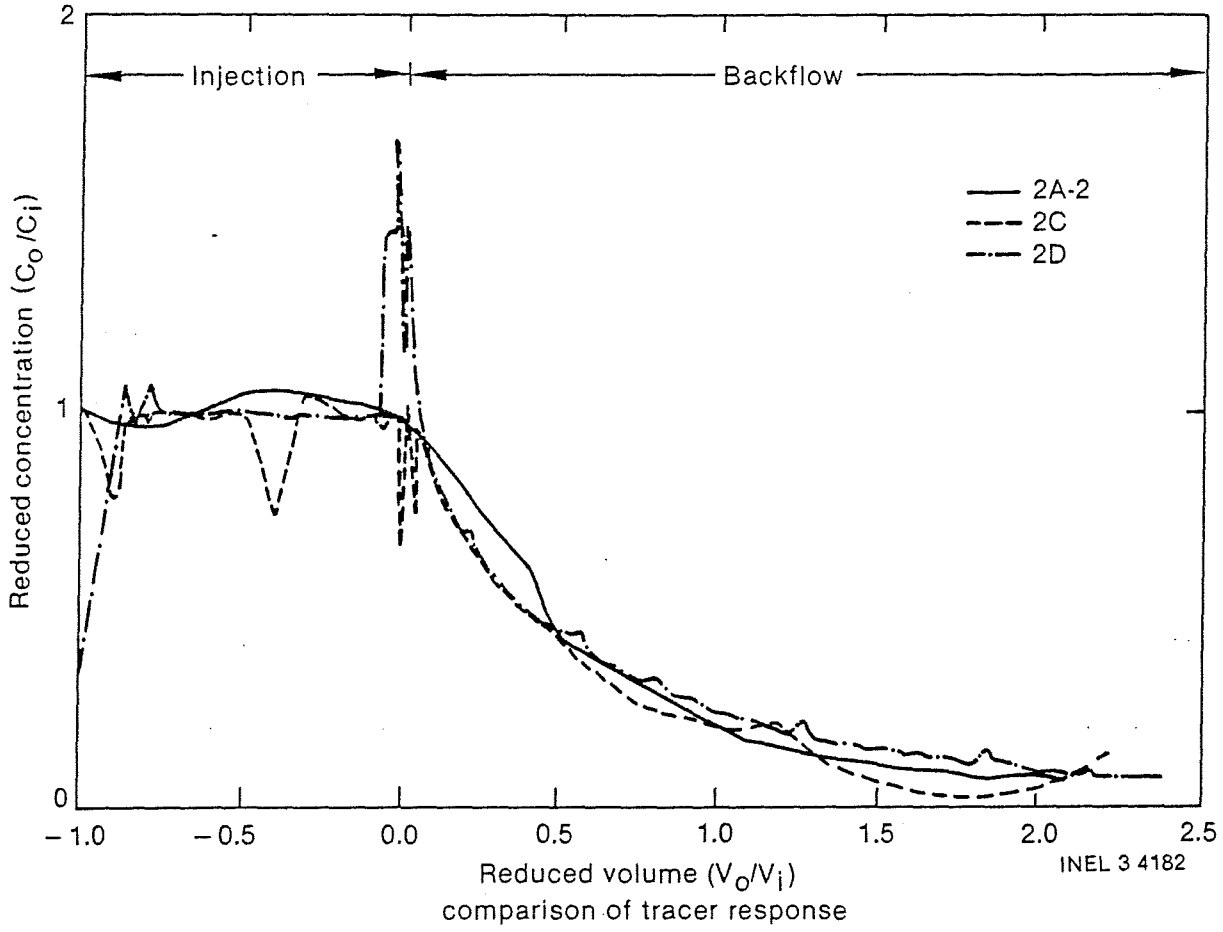

Figure 63. Comparison of normalized conservative tracer responses for Test 2 experiments.

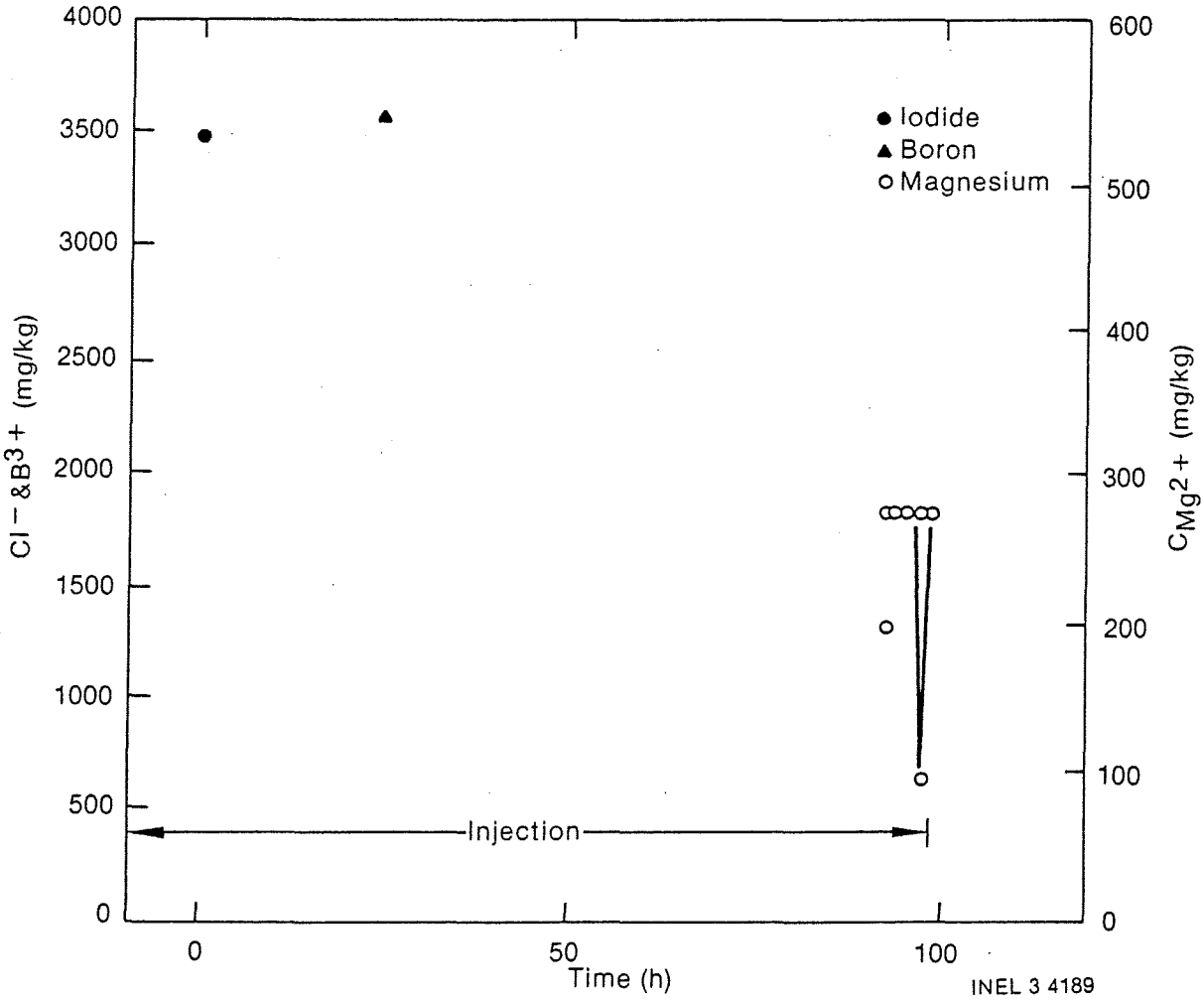

Figure 64. Test 2D tracer injection as a function of time.

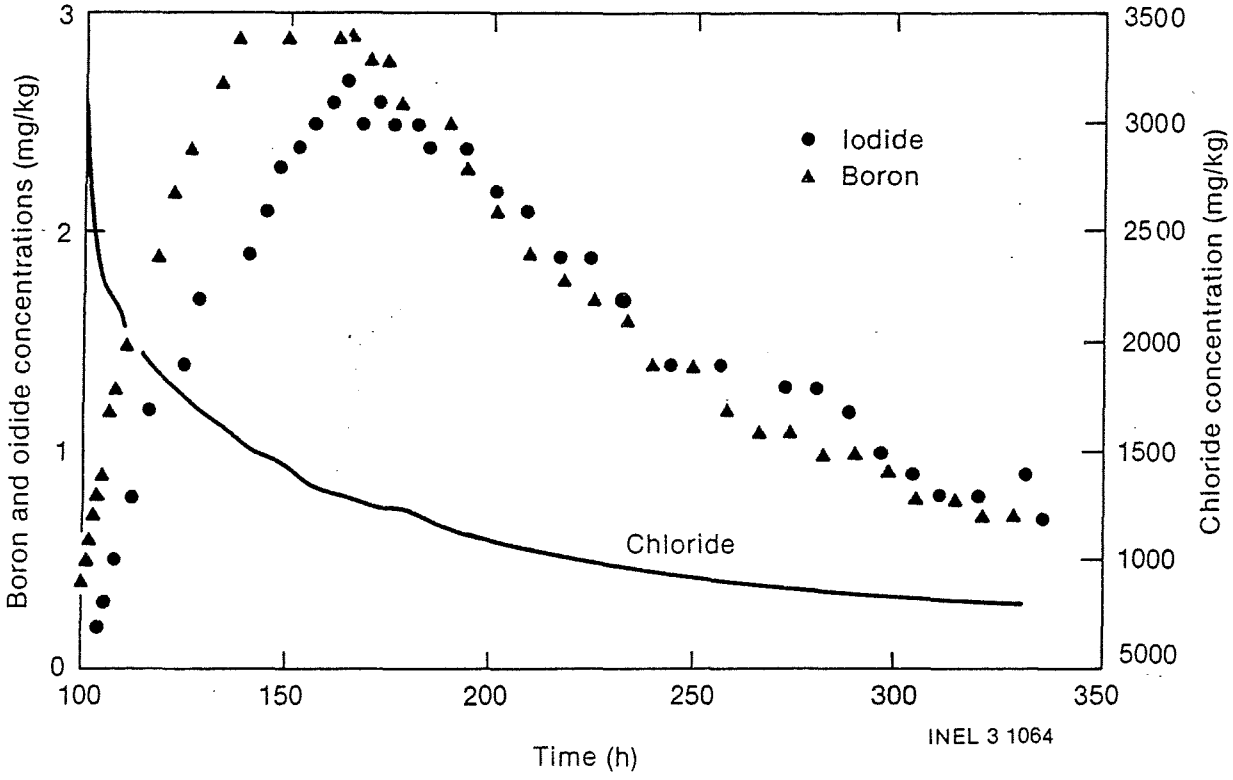

Figure 65. Test 2D tracer concentration as a function of time during backflow.

fluids arrived at the wellhead from the reservoir and increased at a slower rate for the next 63 h. A maximum concentration of 2.8 mg/kg was maintained for about 11 h and then the iodide values decreased at the same rate as the boron data. Also plotted in Figure 65 are the Cl^- concentrations which have been used as an indication of mixing. There is no correlation between the mixing of injectant fluids and native reservoir fluids and the return of the tracer slugs.

The maxima for the two tracers are attained approximately 24 h apart, the same separation as for injection. The dilution of the two species is about the same, 1:1000. Once these maxima have been attained, the declines in concentration are identical. If the chloride concentration for test times greater than 160 h--the point at which the B^{3+} and I^- curves converge--is arbitrarily limited to the same vertical scale, all three curves are the same (Figure 66). This data reduction was accomplished by subtracting the RRGP-5 background chloride concentration of 666 mg/kg and dividing the result by 200. The factor 200 was determined as necessary to bring the B^{3+} and Cl^- data at 160 h into coincidence. This manipulation was used to show that the shape of the tracer curves after they have reached their maximum concentrations are determined not by physical dispersion but by mixing with the fluids native to the RRGP-5 reservoir. This mixing effect overpowers the dispersion effect and causes a "smearing" of the dispersion controlled tracer peaks.

The very rapid return of the tracer slugs suggests that the mass of the tracer did not travel very far from the well and that this reservoir is large and relatively open.

3.4.3 Natural Flow in Reservoir

The Test 4 series was designed with the object of determining whether a uniform flow field exists in the RRGP-5 reservoir. Unfortunately, it proved to be impossible to completely stop flow from the well during the quiescent period. The amount of leakage can be determined by the time it takes to empty the high conductivity injectant fluid from the well bore.

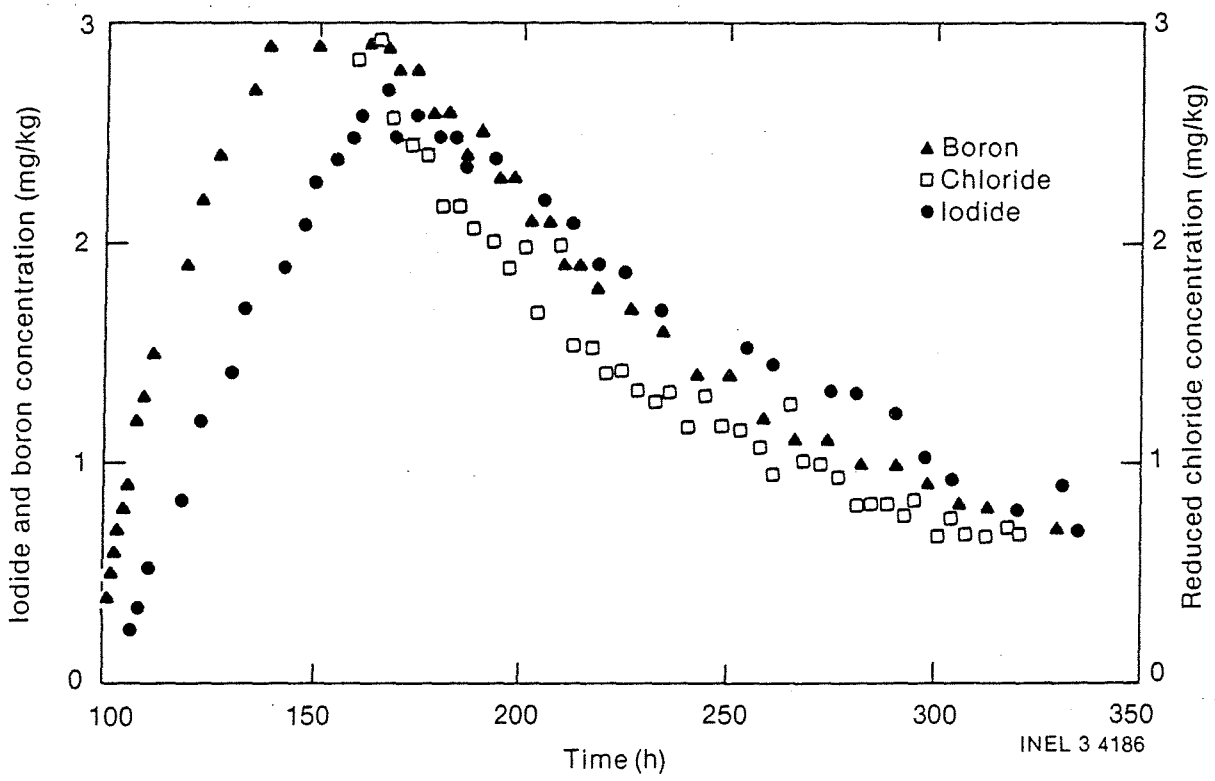

Figure 66. Test 2D tracer concentration as a function of time (Cl^- concentration reduced to the same scale).

The leakage rates were usually on the order of 0.2 to 0.3 x 10^{-3} m^3/sec (3 to 5 gpm). When the quiescent times were on the order of 24 to 48 h, this small leakage rate became significant. Because of this leakage, it is impossible to establish exactly how long a particular sample of fluid was in residence in the reservoir. It normally takes 1.83 h to empty the injectant fluid from the RRGP-5 bore. If one ignores the actual time necessary to clear the bore and plots fluid conductivity as a function of time a "shoulder" is evident in the conductivity data which become more pronounced with ostensibly longer quiescent time tests (Figures 67 and 68). This "shoulder" develops into an isolated peak in the tests with longer quiescent times (Figures 69 and 70). The time interval between the breakin slope which indicates clearing of the well bore and the mid-point of the shoulder or peak increases directly as a function of the quiescent or, in this case, reduced flow time (Figure 71). It cannot be over emphasized that we did not have a true quiescent time in these experiments. We are, however, able to conclude that there was a movement of high conductivity fluid away from the bottom of the well bore. The linear relationship shown in Figure 71 could be used to calculate a mass flow past the bottom of the well if RRGP-5 had truly been shut in during the quiescent time. No attempt was made at these calculations because at the time that backflow was initiated, both the injectant-native fluid interface and the slug of higher conductivity fluid which defined the shoulder or peak were up in the well bore. The existence or length of an actual quiescent time is unknown.

3.4.4 Heat Transfer to Backflowing Solutions

The final data sets that provide insight into the characteristics of the reservoir are those for temperature and chloride. By the time the fluid from the supply well, RRGP-3, had traveled the 3.6 km to RRGP-5, its temperature had decreased from 149°C (300°F) to 106°C (223°F) which was 18°C (32°F) cooler than the reservoir which was at 124°C (255°F). Because a cooler fluid was being injected into a warm reservoir, the injectant picked up some heat from the rock mass. The energy contained within the backflowing fluid, therefore, had three components: the energy of the

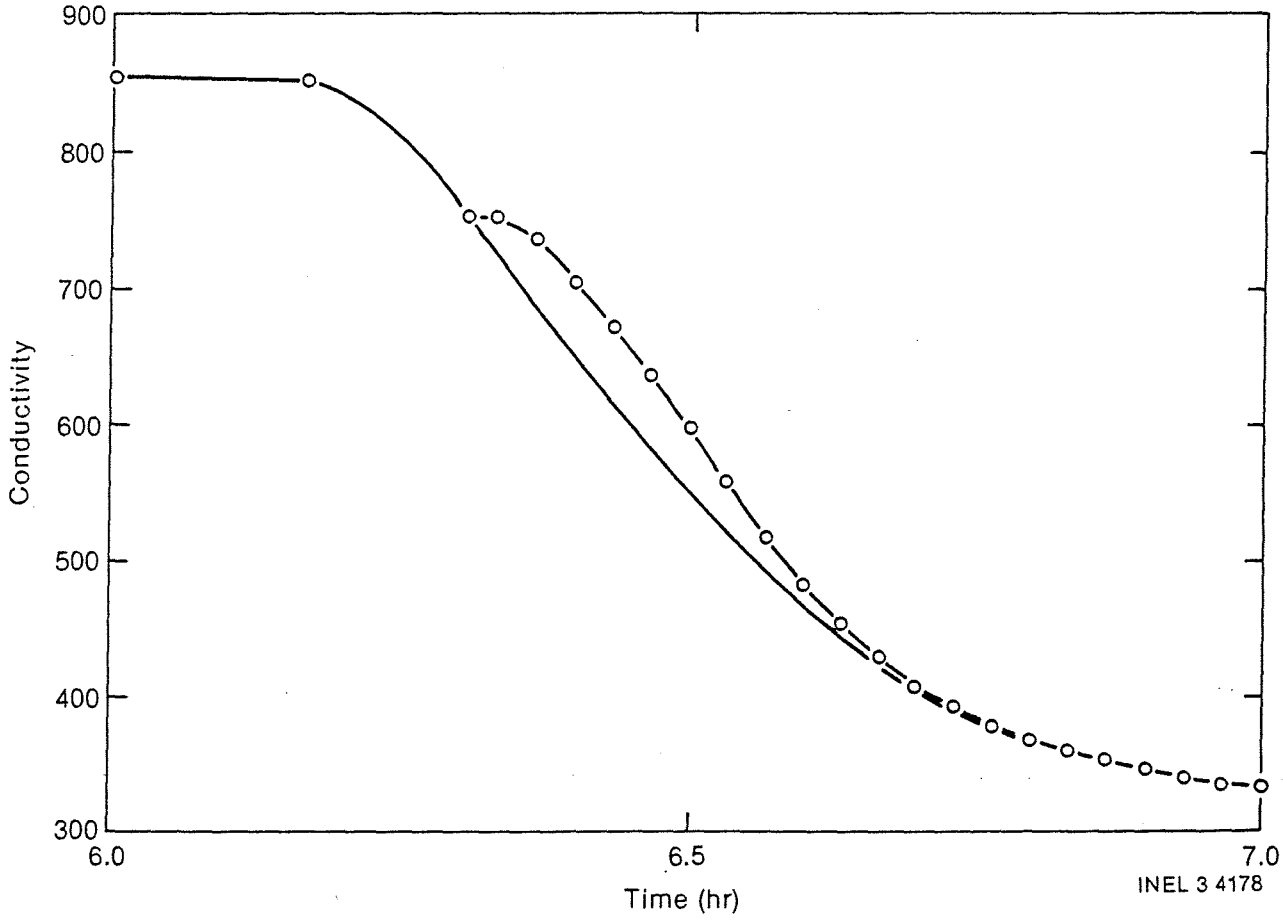

Figure 67. Test 4B conductivity response as a function of time.

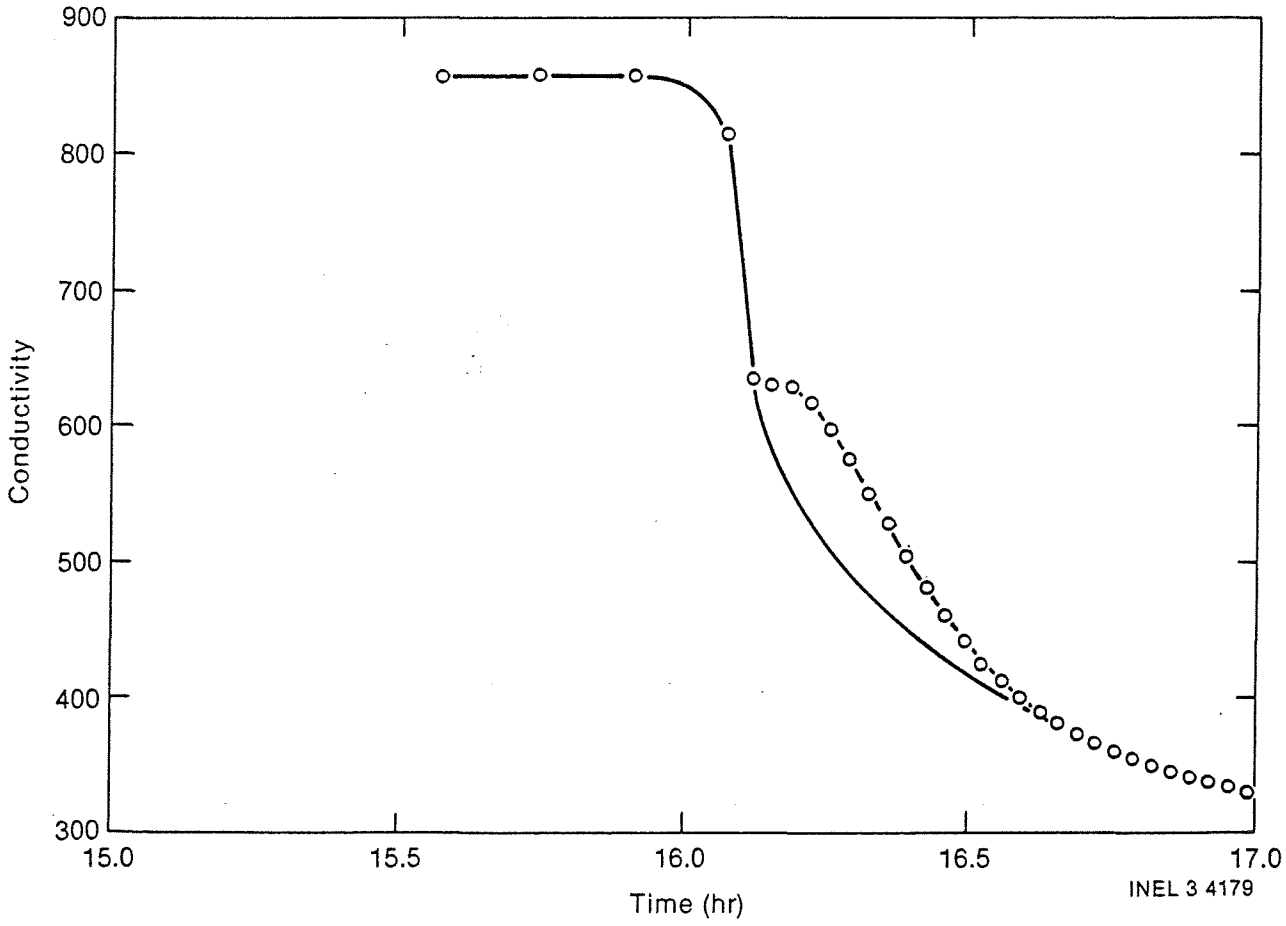

Figure 68. Test 4C conductivity response as a function of time.

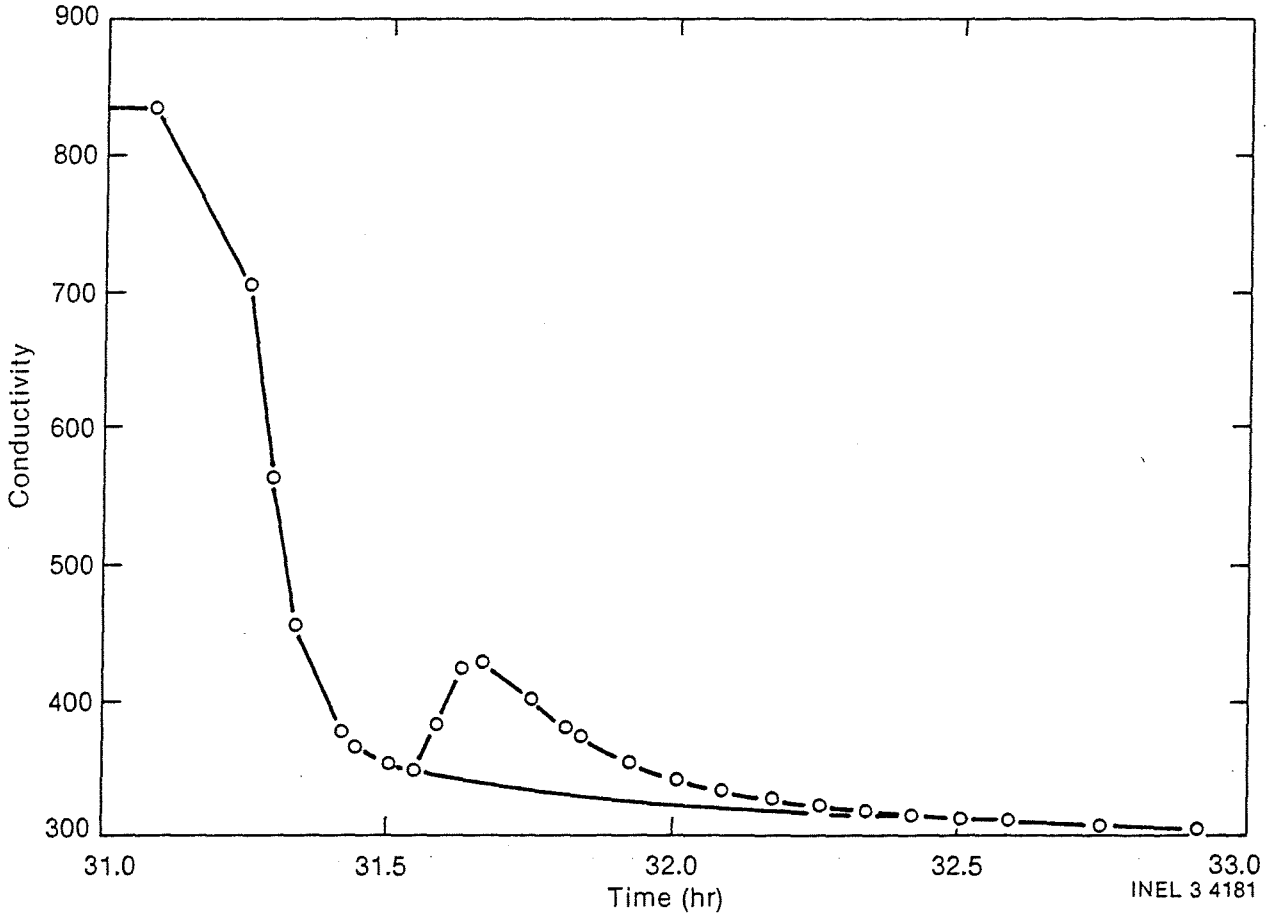

Figure 69. Test 4A conductivity response as a function of time.

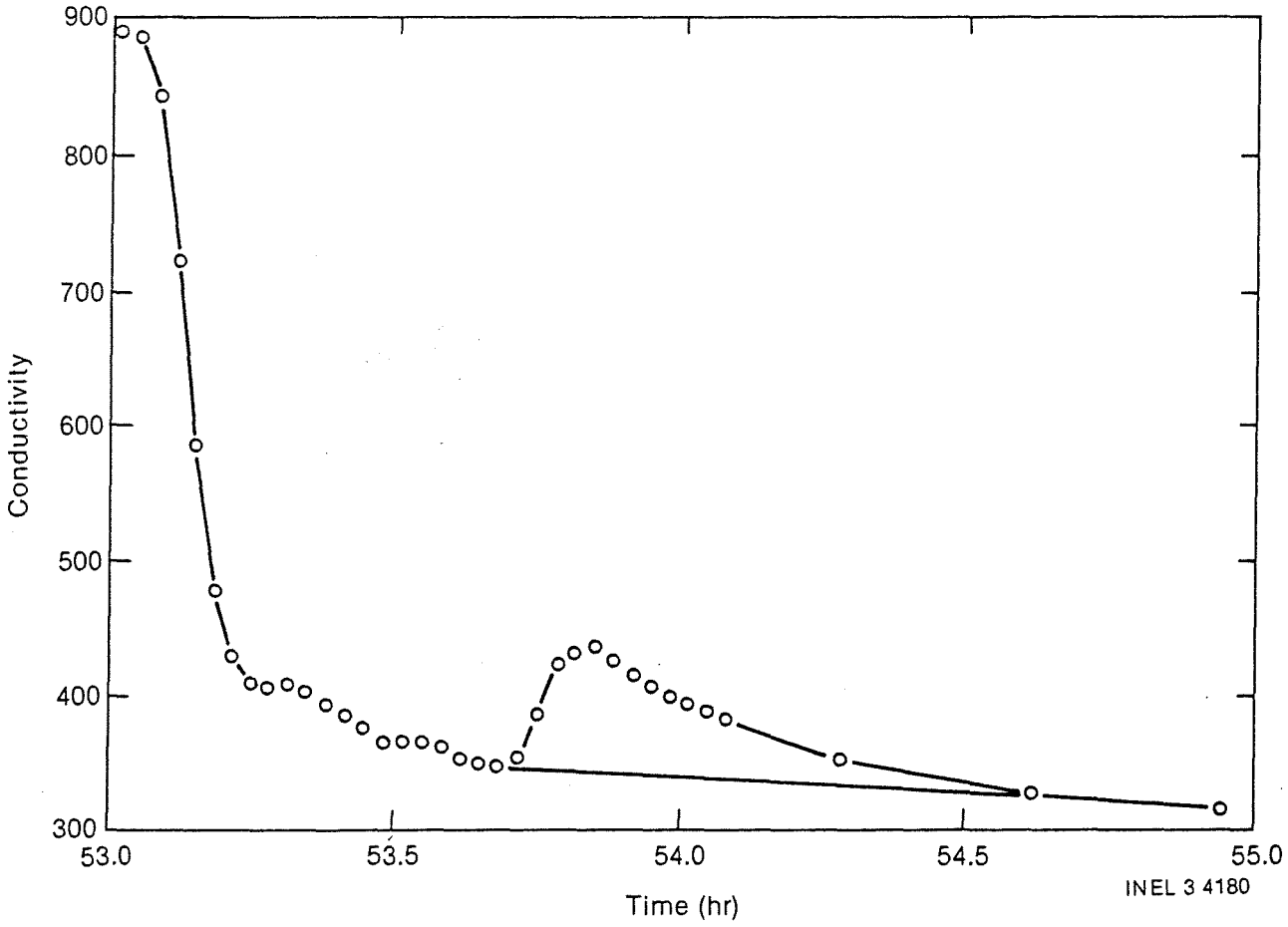

Figure 70. Test 4D conductivity response as a function of time.

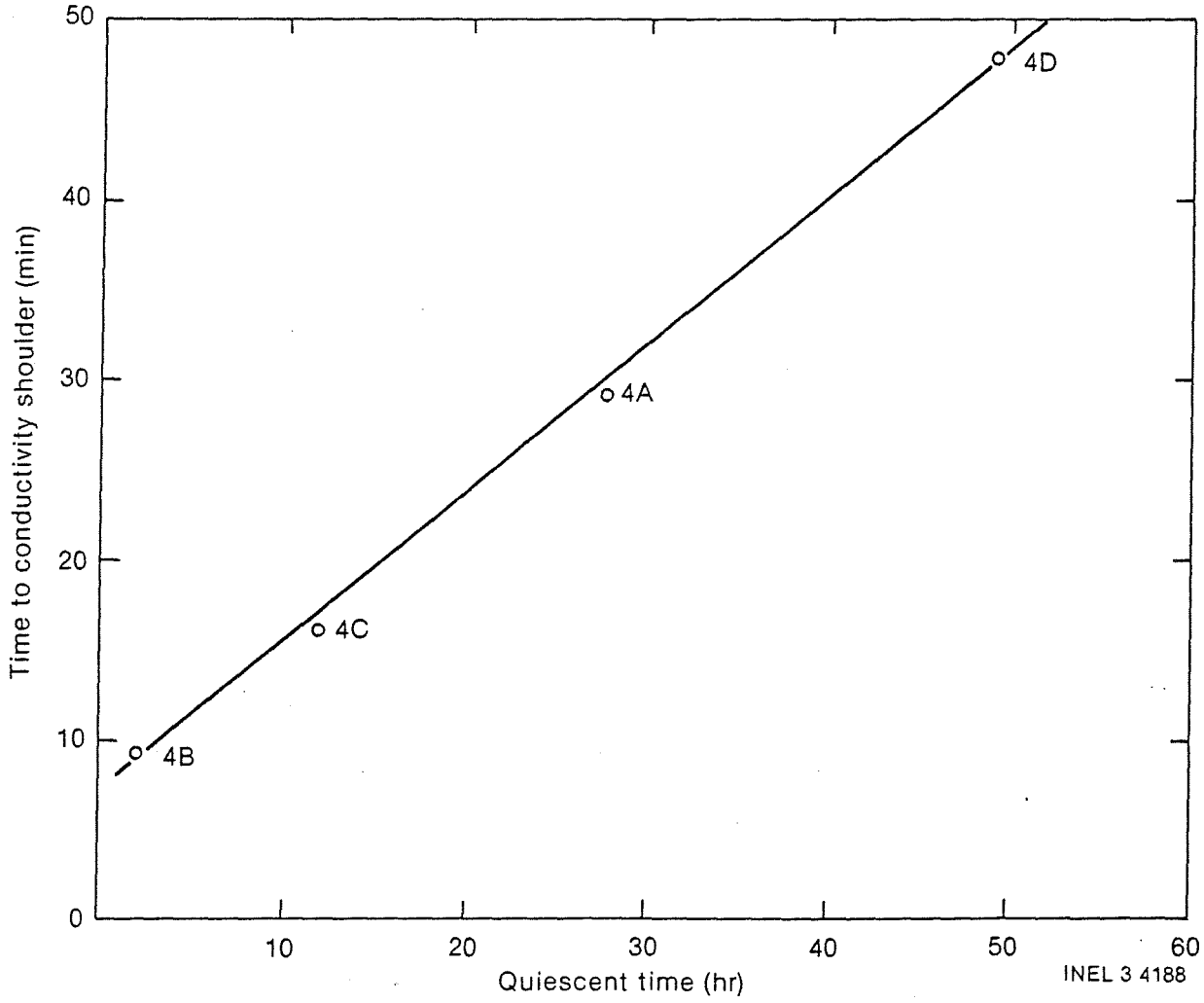

Figure 71. The time to the conductivity shoulder or peak as a function of quiescent time.

injectant fluid, the energy of the reservoir fluid, and the energy added to the injectant fluid by the reservoir.

$$U_{BF} = U_{IF} + U_{RF} + \Delta U_{IF}$$

In terms of specific heat and temperature,

$$C_{BF}\, m_{BF} T_{BF} = C_{IF} m_{IF} T_{IF} + C_{RF} m_{RF} T_{RF} + C_{IF} m_{IF} \Delta T_{IF}$$

where

C = specific heat

M = mass of solution

T = temperature

BF = backflowing fluid parameters

IF = injectant fluid parameters

RF = reservoir fluid parameters.

Figure 72 is a plot of the temperature and chloride concentrations for the backflowing fluid from Test 2C. The chloride concentrations provide a measure of the masses of the injected and native fluids and an expected temperature response curve can be calculated using these masses and the measured injection and reservoir temperatures. The difference between the expected and actual temperature responses gives one an estimate of the heat added to the injectant fluid by the reservoir. The transfer of heat across an interface per unit time:

dQ = KAdT

K = heat transfer coefficient

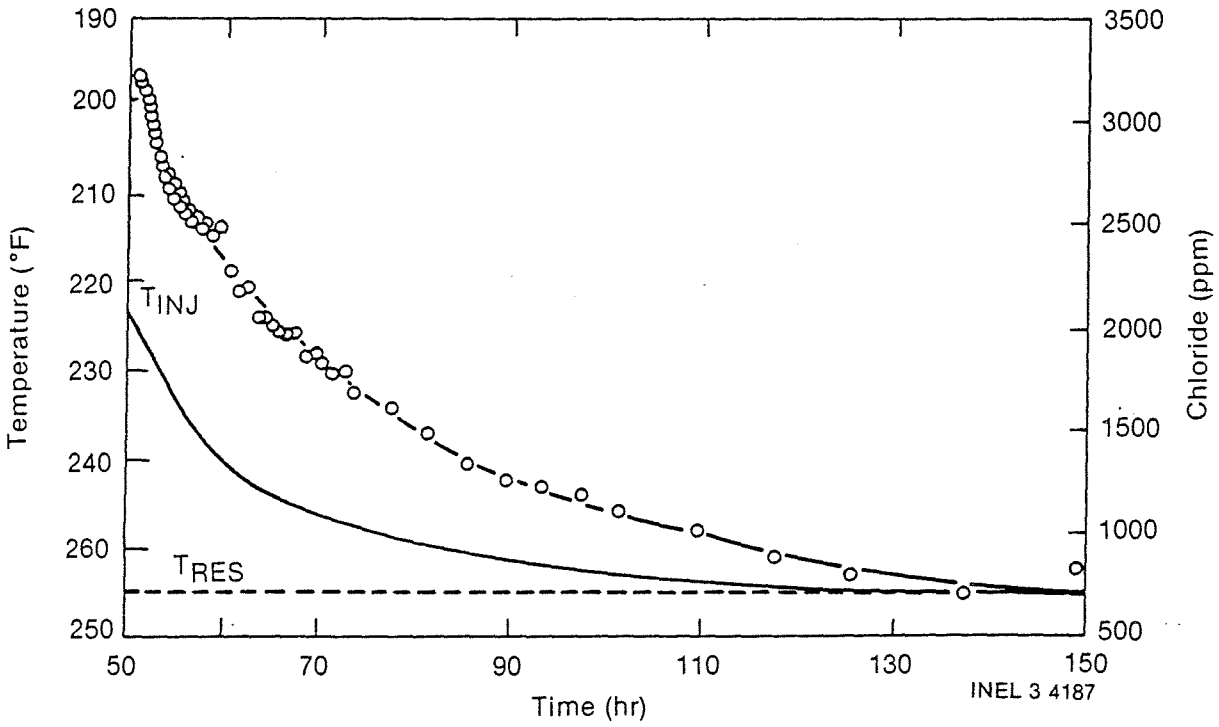

Figure 72. Test 2C: Temperature and chloride concentrations plotted as a function of time.

A = contact surface area

dT = temperature contrast between fluid and reservoir.

The change in heat, dQ can be calculated, the temperature contrast, dT, is measured and an attempt is being made to estimate the heat transfer coefficient, K. This should allow us to calculate a contact surface areas, A, per unit volume. Figure 73 is a plot of the temperature responses for our Test 4 series. Each of the curves represents the heat added to the same amount of fluid in contact with the same amount of rock with a different residence time. At this time, we are attempting to estimate a heat transfer coefficient, K, from these data.

The ultimate objective of this exercise is to try to determine a contact surface area, A, per unit volume, V, of injectant solution. This should allow us to make estimates of the configuration of the reservoir and perhaps an effective porosity. The logical extremes of A/V ratios can be many orders of magnitude. A minimum would be represented by a cylindrical pipe and a maximum would be represented by a porous media composed of spherical particles. In between there are numerous configurations such as narrow planar cracks and fracture networks of different densities. The best we can hope for is "order-of-magnitude" estimates that may allow us to place limits on the realistic configurations for any given reservoir.

The last data analysis is an attempt to evaluate heat transfer from the formation to the colder injected fluid. The formation temperature is approximately 135°C (275°F) at the producing zones while the injected fluid temperature was approximately 106°C (223°F) at the wellhead.

The analysis is based on a comparison of wellhead temperature during withdrawal with that found by mixing injected and formation fluids in the ratio derived from conductivity measurements. An excess of measured temperature over that due solely to mixing would be due to heat transferred from the formation. Unfortunately, the data were dominated by transient heat transfer in the wellbore since the estimated formation exit

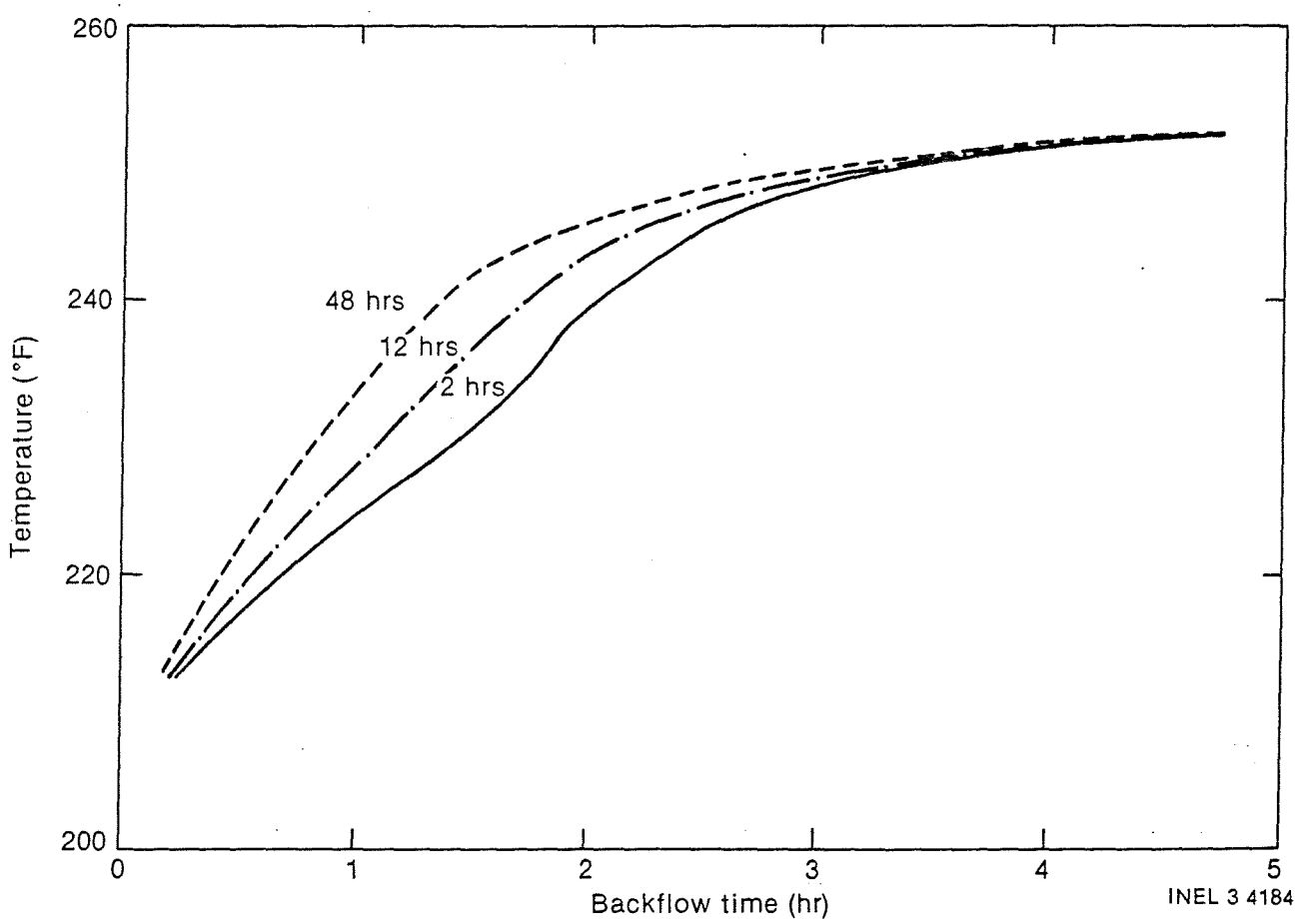

Figure 73. Test 4: Backflow fluid temperature as a function of residence time in well.

temperature had to be corrected to the wellhead. Steady state values of temperature rises over the depth of the well at 150 gpm were found from the temperature logs to be 4°C (7°F) for injection and 11°C (20°F) for withdrawal.

Figures 74 through 76 show temperature, conductivity, and chloride concentration at the wellhead during the withdrawal phase of Tests 2C and 2D. Time zero is at the beginning of pumping.

Since the chloride is known to be a conservative tracer, it would give the best indication in injectant-native mixing. However, the curves shown in Figure 76 are rough. The conductivity curves shown in Figure 75 were used because of their smoothness and because they retain the shape of the concentration curves, rather than being distorted by non-conservative elements.

The 110°C (230°F) bottom-of-well injectant was mixed with the 135°C (275°F) formation fluid in the proportions derived from these conductivity curves. Figure 77 shows the excess of this temperature over that measured at the wellhead. The time scale is measured from the beginning of withdrawal and is normalized with respect to the injection time of 48 h for Test 2C or 96 h for Test 2D.

This temperature excess must be corrected by subtracting the drop incurred in rising from the formation to the wellhead. The result is mixed temperature, corrected to wellhead, less measured wellhead temperature. Formation heating would then show up as a negative value.

The final uncorrected temperature differential of 10.6°C (19°F) approaches the steady state wellbore drop. The temperature drop in rising to the wellhead must be lower earlier in the withdrawal since the rising fluid is colder and, therefore, closer to the casing temperature. Consider the fluid which reached the bottom of the well at the instant injection was terminated. It originated at the wellhead at 106°C (223°F) and was heated to 110°C (230°F) during its descent. Since there was no quiescent time, it

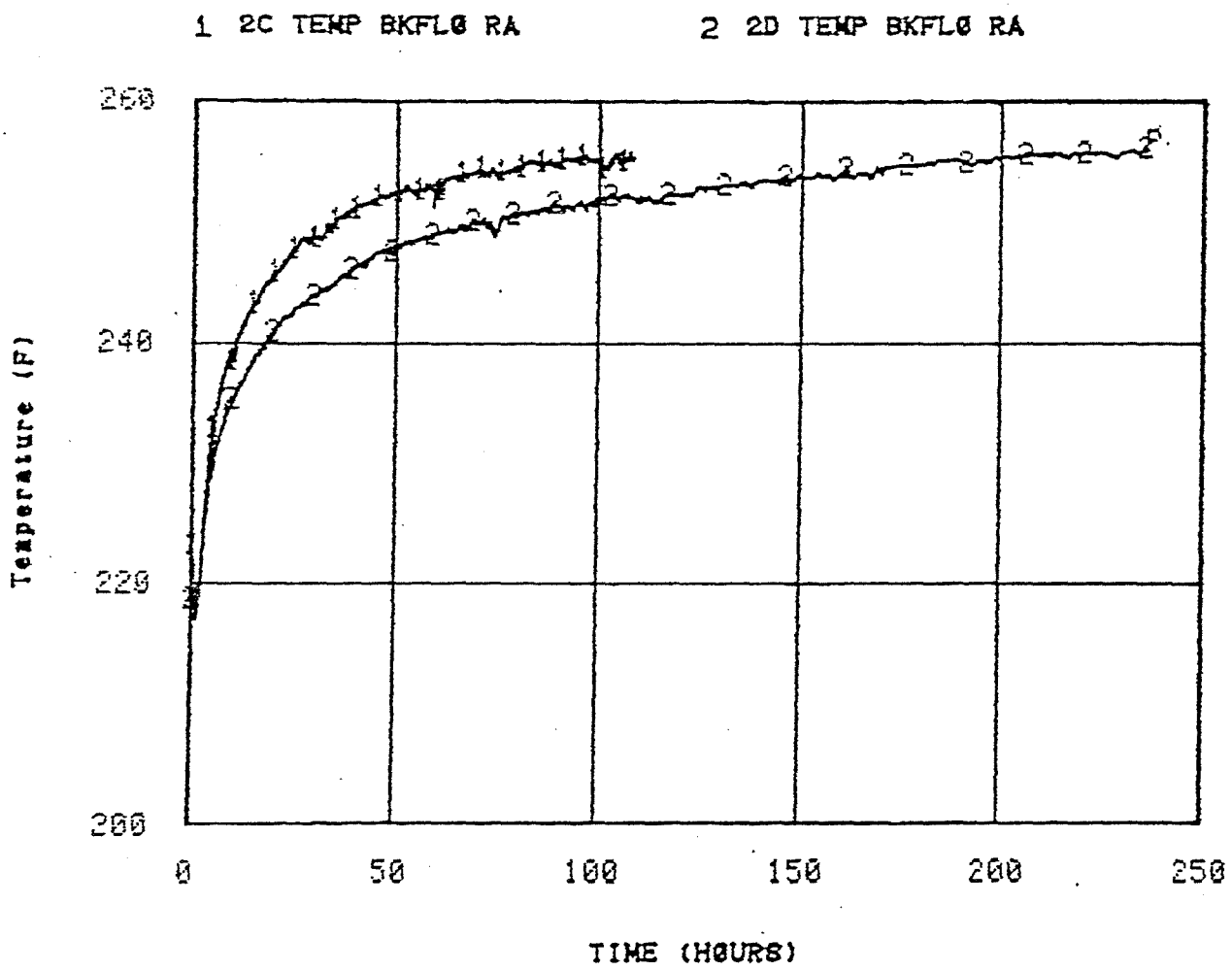

Figure 74. Wellhead Temperature vs. Withdrawal Time, Tests 2C and 2D

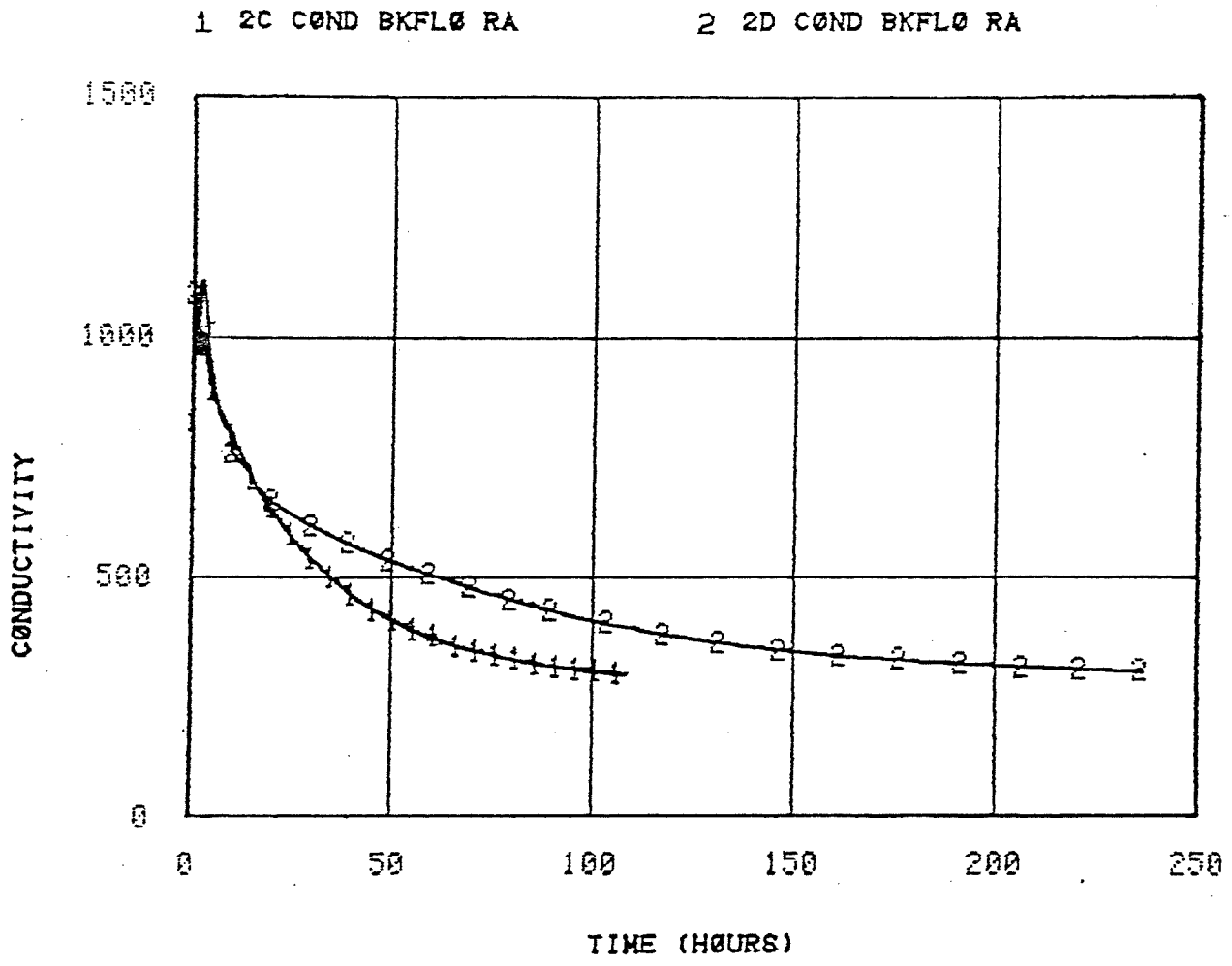

Figure 75. Wellhead Conductivity (mv) vs. Withdrawal Time, Tests 2C and 2D

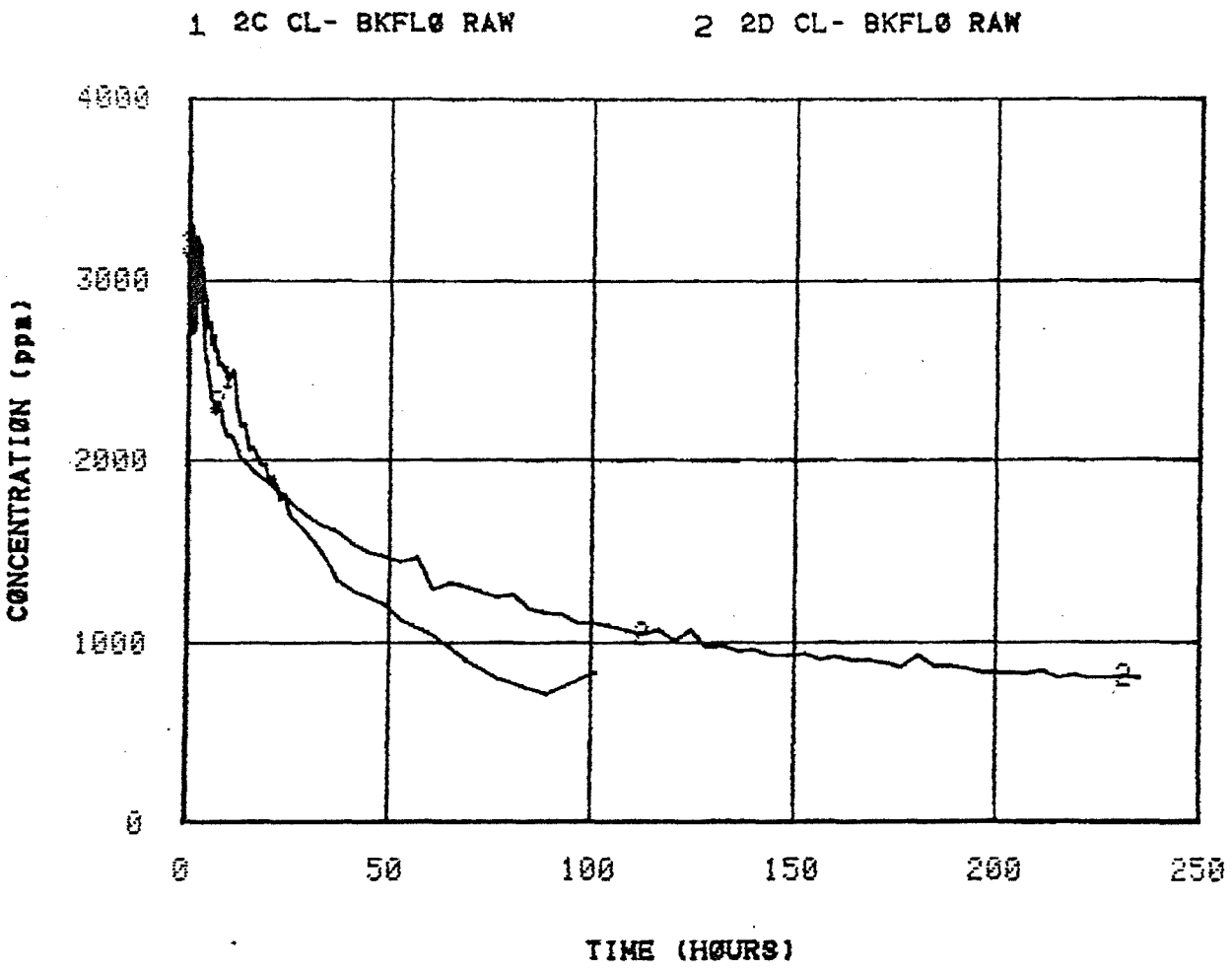

Figure 76. Chloride Concentration vs. Withdrawal Time, Tests 2C and 2D

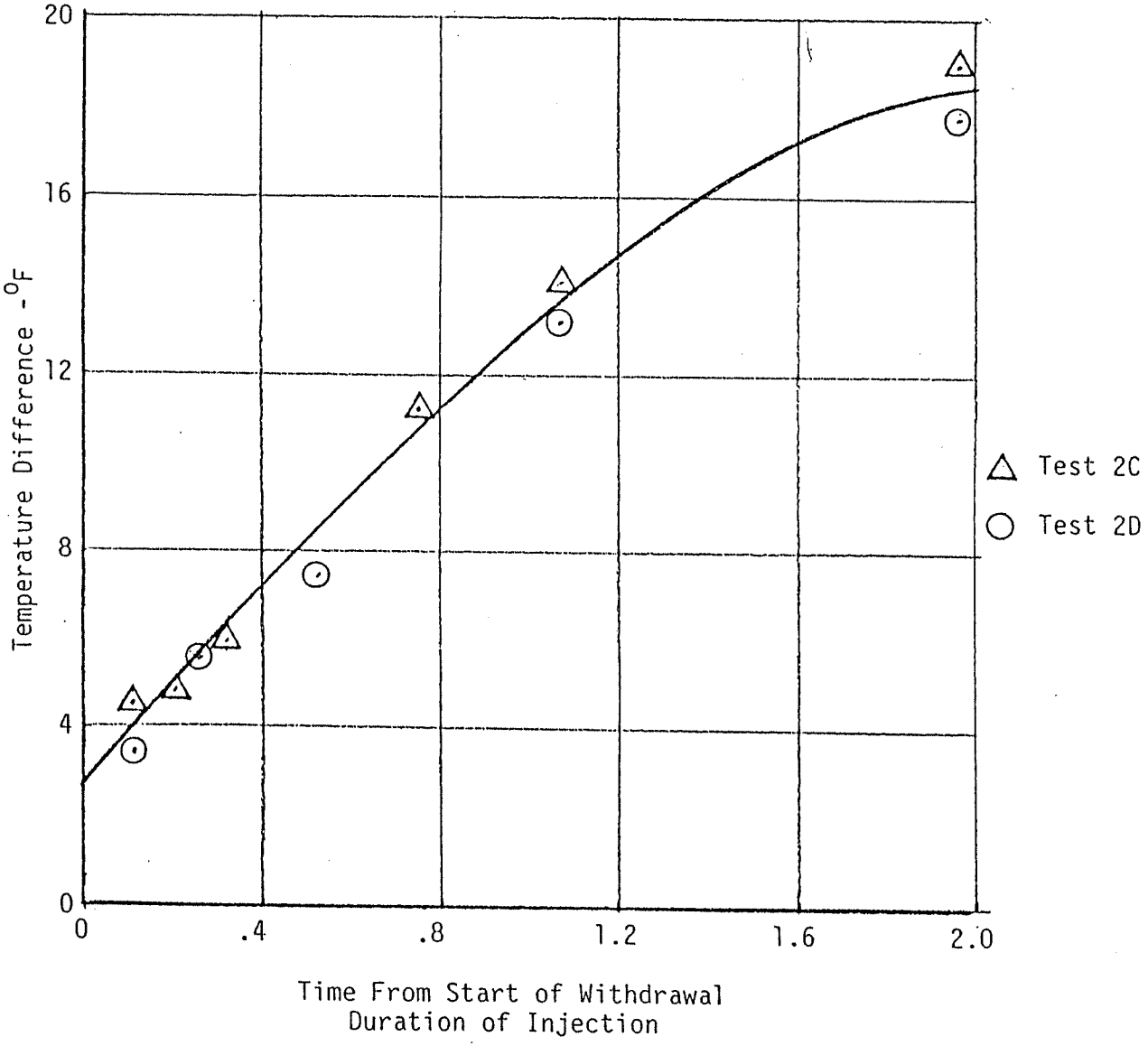

Figure 77. Mixed Bottom-Hole Temperature Minus Measured Wellhead Temperature

immediately began its return trip. Assuming that the casing temperature had not changed, this fluid must be heated by less than 7°F in rising to the wellhead since the average casing to fluid temperature differential is now smaller. Figure 77 shows an excess of mixed (bottom hole) temperature over measured wellhead temperature of 2.2°C (4°F) for very early times. It is, therefore, concluded that the temperature excess shown in the Figure is approximately due to the wellbore heat transfer and that formation heat transfer, if any, cannot exceed a few degrees centrigrade. Bottom hole temperature and conductivity measurements would be necessary to define this level of formation heat transfer.

4. NUMERICAL MODELING

4.1 Technical Approach

A fractured reservoir consists of a rock matrix with interspersed and interconnected water spaces. These spaces range from major faults and secondary cracks, which constitute the global flow system, to dead-ended microcracks, which provide the majority of the fluid volume for water storage and the surface area for heat transfer and sorption.

The reservoir flow calculation in this study is based on a single continual approach whereby water may flow between two points through specifically described major fractures or through the rock matrix (actually the myriad of small-to-microscale cracks).

The dispersion calculation then follows since the global movement of tracer is, of course, due to advection in the major-fracture system. In the standard approach to transport in fractures, this dispersion is calculated using a porous media type longitudinal dispersivity. This dispersion is actually the net effect of variations of velocity across the fracture, variations in fracture cross-section, and flow disturbances at fracture intersections. In this study these fundamental mechanisms are addressed specifically. Dispersion characteristics are determined for certain discrete fracture geometries by the use of an elementary fluid dynamics code. This code solves the Navier-Stokes equations for two-dimensional laminar flow. Dispersion characteristics are determined by monitoring the paths of imaginary marker particles as they move with the calculated velocity vectors. These characteristics are verified by physical model tests, as described subsequently, and are input to a separate reservoir simulation code.

The discrete element characteristics are integrated into a meaningful reservoir model on the basis of a study of fracture geometry (and hydraulics) from the literature. Fracture systems are generically characterized in terms of number of sets of nominally parallel fractures, spacing, lateral and longitudinal extent, thickness, contour, etc. This

parametric description is the basis for extrapolating limited bore-hole data to a reservoir system model. Some studies have already been collected and considerable expansion is expected on the basis of the soon-to-be published stripa data.

Local dispersion within the matrix itself is based on a classical porous media approach. These reservoir dispersion characteristics are also evaluated using imaginary marker particles.

The complete RRGP-5 simulation is accomplished by integrating borehole fracture geometry, generic fracture system geometry from the literature and the conceptual hydrogeologic model. Reservoir physical parameters are varied within these constraints to match measured hydraulic and dispersion characteristics.

As detailed in the following discussion, the work accomplished to date consists of selecting isothermal element end reservoir codes, revising or extending these codes to provide the desired capabilities and a limited amount of verification and demonstration.

A number of capabilities required for a complete fractured media simulation are deferred to FY-84 and beyond. The following listing is in rough order of priority:

1. Numerical studies to develop facility with and confidence in the codes as developed

2. Fracture geometry characterization from the literature

3. Calculation and verification of a library of fracture element dispersion characteristics

4. Well-bore flow and dispersion

5. Flow and dispersion at the intersection of the well-bore with the initial fractures

6. Molecular diffusion

7. Integration of and correlation with Raft River flow and dispersion data

8. 3D fracture element simulations

9. Discrete-based numerical and physical studies of dispersion at the dead-ended fractures which couple the global flow system and the matrix

10. Well-bore heat transfer

11. Heat transfer and sorption in the matrix, based on microscale fracture geometry

12. Inertia and buoyancy terms in the reservoir flow calculation

13. 3-D reservoir simulation (if found necessary).

4.2 Code Selection Requirements

In view of the number of available fluid dynamics and reservoir codes, the approach taken was to select the best of these codes and add modifications or extensions as required.

In addition to the specific capabilities discussed subsequently, each of the codes selected must have acceptable validity and operational use factors. These attributes include credibility of the code and the author, verification, validation, availability of the author or knowledgeable current users, quality of documentation, user friendliness, consistency of nomenclature and logic conventions, level of commenting, suitability or adaptability to a Cyber system, program length, modular character, absence of overlays, etc.

Barring the availability of an unbiased user, these factors can only be evaluated on the basis of the user's manual, technical background papers

and code listing. Actual performance and, most important of all, the cost effectiveness of the code can only be determined after the code installation and learning phase.

4.3 Fracture Element Simulation

4.3.1 Code Selection

The code must be capable of simulating very low speed isothermal flow and dispersion of water in complex geometries. While two dimensional geometry is adequate for initial studies, the third dimension may be required later.

The codes considered for this application include APACHE,[16] SOLA,[17] SOLA-VOF,[18] and SALE.[19] All were written at Los Alamos within the last five years; all are installed in the INEL CYBER system, and none have been used at INEL.

4.3.1.1 APACHE. APACHE is a two-dimensional finite difference code which solves multi-component and/or chemically reactive fluid flow problems in combustion, chemical lasers, and chemical reactors.

The code provides for convective flow, molecular diffusion, chemical reaction, and conservation of species, mass, momentum, and energy within an isothermal two dimensional boundary.

According to the second author, John K. Dukowicz, the code has not been used at LASL for quite a while. It is being used in its original chemical laser application at the Weapons Lab at Kirtland AFB.

The code is apparently not well suited to the proposed application since a major change would be required to incorporate water as the flowing medium. In addition, the code is best suited to higher Mach numbers. The option for pressure iteration for incompressible flow is the weak point of the code. They found poor computational efficiency in a single attempt at a low Mach number combustion problem and did not pursue the problem.

4.3.1.2 SOLA/SOLA-VOF. SOLA and SOLA-VOF were briefly considered and not explored in any great depth since they were less applicable than SALE and APACHE. The VOF (volume of fluid) feature of SOLA-VOF was considered as an adjunct to the selected code as described subsequently.

4.3.1.3 SALE. SALE (Simplified Arbitrary Lagrangian-Eulerian) is a simplified numerical fluid dynamics computing technique for calculating two-dimensional fluid flows at all speeds. The speed versatility is attributed to the use of an implicit treatment of the pressure calculation. The computing mesh may move with the fluid in a typical Lagrangian fashion, be held fixed in a Eulerian manner, or move in some arbitrary specified way to provide a continuous rezoning capability. "The program was written in modular form with extensive annotation and input options that provide a wide range of capabilities to facilitate its use by persons with modest experience in numerical fluid dynamics."[19] A 3-D version of this code[20] has become available recently.

The user's manual provides a mathematical approach, code summary, five sample calculations, one sample output, and a listing. The code contains approximately 2400 lines. The sample problem has been run at INEL and the output modified to provide curve plotting using the IGS software.

Mr. Hans M. Ruppel is the second author and the hydrodynamics expert on the project. He stated that the code is in current use at LASL and elsewhere, but declined to provide a list for use in comparing notes on applications, etc.

Applicability for the elementary fracture simulations was discussed in some depth. The low speed condition is handled by using the implicit pressure iteration. Specific data to be used were discussed. Flags or modified "do" loops could be used to drop out the inactive cells in a fracture junction simulation. While SALE does not incorporate a dispersion calculation, this capability, as subsequently discussed, has been added without major effort.

4.3.1.4 Selected Code. The SALE code was selected on the basis of its capability for incompressible low speed flow, its current usage at LASL and elsewhere, the existence of a 3-D version, its being operational with curve plotting on the Cyber system, acceptable structure, length and documentation and specific recommendations by its author for its intended application.

4.3.2 Dispersion Calculation

The code is required to monitor the spreading of the interface between the native and tracer fluids as it moves through a specific geometry with the prevailing flow. Spreading due to molecular diffusion is not initially required since the advection driven dispersion will be substantially larger in most cases.

An initial attempt was made to define the interface by monitoring the concentration of the tracer in each of the 100 cells in the standard pipe-flow problem discussed subsequently. The calculation, based on a similar capability in the predecessor to SALE, was unsuccessful because of a phenomenon termed numerical diffusion. The small amount of tracer crossing into a downstream cell in a given time step is evenly distributed throughout the entire cell. A smaller amount of tracer enters the next (downstream) cell during the next time step, and so on. The initially sharp boundary is rapidly smeared through the active network, contrary to physical behavior.

The volume-of-fluid (VOF) technique is used in SOLA-VOF to confine the entering fluid to the appropriate portion of the cell. The geometry is complex even in the two-dimensional rectangular cells in SOLA-VOF. Since SALE will be used with more complex, and ultimately 3-D geometry, the technique was not considered further.

A marker particle approach was selected because of its simplicity. These imaginary particles travel downstream under the influence of the local velocity field and therefore mark the position of the boundary

between the two fluids. This capability was coded, integrated with SALE, and demonstrated as described below.

4.3.3 Standard Problem Solution

A simplified flow problem with a known analytic solution was simulated in order to develop confidence in code usage. The problem involves imposing a step change in axial pressure differential on water initially at rest in a horizontal pipe. A velocity profile is established across the cross section as the flow is accelerated. As given in Reference 21, the analytic solution provides velocity profiles at the steady state condition (the Poiseuille curve) and at intermediate times.

The problem was simulated in cylindrical coordinates with a 1-ft pipe length, 0.1-ft pipe radius and a 0.01-psi axial pressure differential applied at time zero. The radius was divided into ten equal increments. The length was divided into eight equal increments of 0.125 ft with additional boundary increments of 0.01 ft at each end. The problem was simulated out to 97 sec which corresponds to 40% of the steady state velocity. As shown in Figure 78, the SALE velocity is 12% lower than the analytic solution at the centerline but agrees well over the remainder of the cross section.

The marker particles inserted along a sharp front at the inlet to the pipe at the beginning of the transient moved down the pipe to properly conform to a curve matching the velocity profile.

The SALE run required 405 CP sec at a cost of $29. Fracture element simulations could be substantially less expensive because of shorter run times and lower velocities, assuming no greater noding detail is required.

Step change in pressure gradient on water initially at rest in a horizontal pipe.

pipe length	1.0 ft
pipe radius	.1 ft
pressure at left end	.01 lb/ft^2 after t=0 sec
pressure at right end	0. lb/ft^2
water temperature	70°F
number of axial cells	8 at .125 ft plus 1 at .0125 at each end
numer of radial cells	10 at .01 (cylindrical coordinates)
SALE calculation	fully incompressible, Eulerian
transient duration	97 sec
CPU time	405 sec
run cost	$31 (PI)
reference	Transport Phenomena, Bird, Stewart and Lightfoot

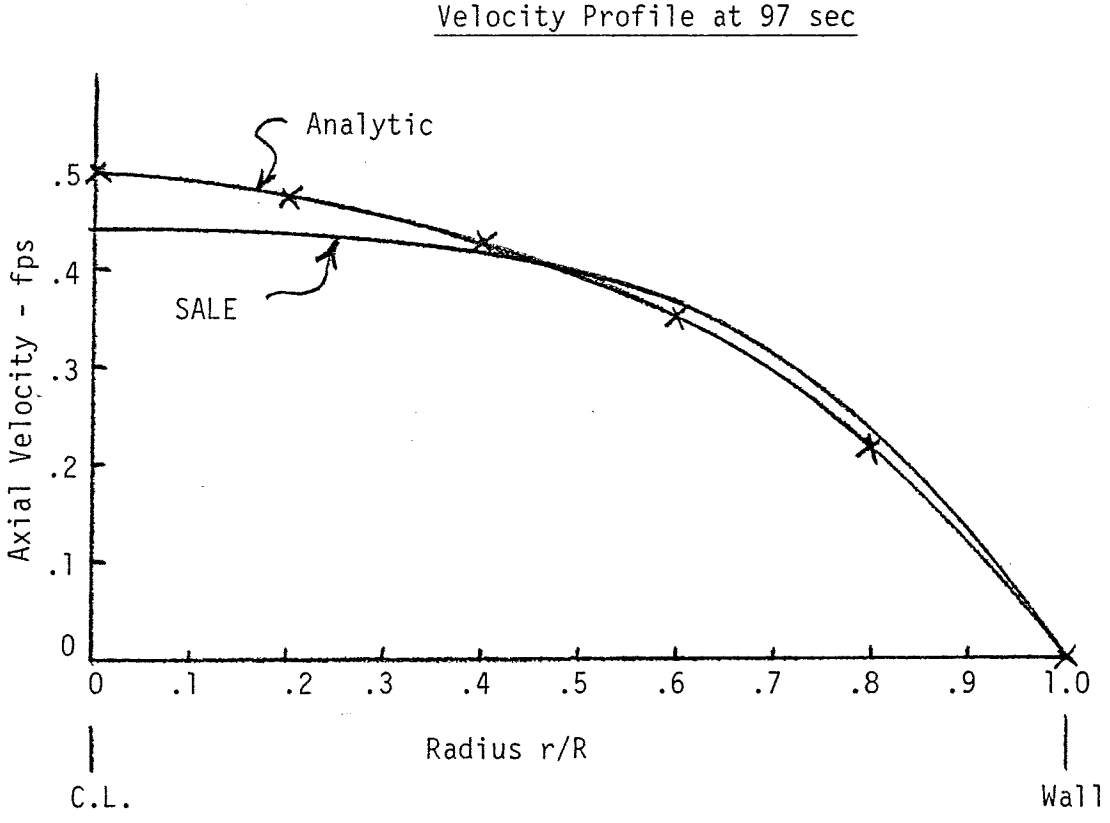

Figure 78. SALE Standard Problem

4.4 Reservoir Simulation

4.4.1 Code Selection

The region of interest in both the Raft River RRGP-5 injection-backflow tests and the physical model tests is the "near field," i.e., the well and a limited number of fractures and associated matrix "close" to the well which are known to some degree or can be specified in terms of a repeated or regular pattern. Test data are essentially limited to flow, temperature, pressure, and tracer concentration characteristics. The model may be limited to an isothermal two-dimensional vertical section of uniform depth since the additional freedom of depth variation and buoyancy driven circulation is not necessary to correlate observed behavior or justified in terms of known near-field properties.

The reservoir code will be partially verified by comparison to the multiple fracture physical model which is isothermal and is two-dimensional to the extent that the fractures are sufficiently deep relative to their width that end effects from the top and bottom surfaces may be ignored.

A mathematical model consistent with this discrete (known) fracture characterization should provide for flow and storage in the well, turbulent or laminar flow in the initial fractures, flow in the remaining fractures based on the cubic law, and a Darcy flow field in the rock matrix. Transport due to advection, molecular diffusion, and hydrodynamic dispersion occur throughout the matrix; and advection, dispersion, and diffusion occur in the fractures. Each of the known features is assigned a unique set of properties.

A fracture is commonly simulated as an element of the overall matrix. Very large differences in hydraulic properties and in thickness may result in extremely fine noding or a very wide range of eigenvalues, usually with substantial penalty in computing cost. A modern approach implemented in three of the codes discussed subsequently treats a fracture as a line element with special numerics for computational efficiency.

Future studies of complete reservoirs would require heat transport and possibly three-dimensional models as part of a far-field analysis capability.

4.4.1.1 FTRANS. FTRANS (Fracture Flow and Transport of RAdioactive NuclideS) is a two-dimensional finite element program which simulates isothermal flow and transport of radionuclides in a fractured, porous, confined aquifer.[22] It was written by Peter Huyakorn of GeoTrans under DOE funding (Battelle Office of Nuclear Waste Isolation) for analysis of deep geologic isolation of nuclear waste. Dr. S. R. Gupta is the Battelle project manager. The final version of the user's manual is now being printed.

The FTRANS Code provides the best treatment of discrete fractures of any of the codes surveyed. The porous matrix continuum is described in a rectangular finite element mesh of uniform, geometrically changing or irregular spacing in the x-y plane with uniform thickness in the z direction. Each of the 225 (current maximum) elements is assigned one of five sets of properties. Coupled flow and transport codes define the Darcy flow field and the transport of up to three species.

Superimposed on the continuum is a set of up to 100 (current maximum) fractures. Each fracture is described by a starting and ending node which must be on the same matrix cell, an effective aperture width and one of five different sets of values of longitudinal dispersivity, porosity and hydraulic conductivity.

FTRANS also incorporates a dual porosity model. In the FTRANS version, a two-dimensional fracture is bounded by a porous matrix of one layer of rectangular blocks of specified thickness or of spheres of specified diameter and packing. The matrix exchanges mass and solute with the plane fracture by one-dimensional diffusion. Other shapes could be programmed without significant difficulty.

Both Dr. Huyakorn and Dr. Gupta are recognized authorities in the reservoir modeling area. The FTRANS user's manual includes six verification problems. Excellent agreement was shown for the three problems for which analytic solutions exist.

The manual is extensively detailed. The code consists of approximately 2000 lines, is fairly well commented, and seems to have acceptable nomenclature and consistent use of positive logic. Diagramming is limited to one page. A number of contradictions and omissions were found in the manual and brought to the attention of the custodian (ONWI).

4.4.1.2 Noorishad. Noorishad[23] describes a similar discrete fracture approach in a two dimensional model for flow and transport. He references work by Huyakorn on the upstream weighted finite element scheme and describes the one-dimensional line element representation of a fracture which ". . . not only facilitates this mesh generation and numbering of the elements but greatly enhances the computation efficiency while reducing the requirement of the computer storage capacity." This code was not publicly available.

4.4.1.3 MAGNUM/CHAINT. A similar line element model of a discrete fracture is incorporated in the 2-D flow and heat transport code MAGNUM and the compatible solute transport code CHAINT, both developed[24] at Rockwell-Hanford.

These codes are not considered further since validation for NRC review is in progress and the codes will not be documented and released for approximately one year.

4.4.1.4 LBL Codes. The dual porosity simulation is given in considerably more flexible fashion in some of the LBL integrated finite difference codes. GMINC[25] is a geometry preprocessor for inputting a regular, irregular, or stochastic geometry to SHAFT79.[26] This combination would provide a dual porosity calculation of two-phase flow and heat transport in two or three dimensions. SHAFT79 is widely used and verified.

A solute transport calculation with a matching grid could conceivably be performed with TRUMP.[27] This code is widely used, is the source of the integrated finite difference approach used in the LBL codes, and has been used[28] for transport in dual porosity media. This latter study describes a disadvantage in the TRUMP model in that the iterative solution of the set of simultaneous equations (after temporal finite differencing) is rather slow when time constants vary widely over the flow region. Work was in progress on a direct solver technique.

Karsten Pruess of LBL has commented on the computational problem discussed earlier: the very small volume elements necessary to represent a discrete fracture as a grid element can slow computations by several orders of magnitude. The LBL codes may, therefore, present liabilities in integration and numerics in those areas of interest in this program. The additional capabilities in 3-D and two phase, while potentially useful for other work, may complicate and slow calculations in the simpler case.

4.4.1.5 PORFLO. The PORFLO-R Code,[20] according to its author quoting Rockwell-Hanford experience, is relatively effective in modeling fractures as grid elements with sharply different dimensions and properties. "Fractures aligned with the X or Y dimensions are acceptable. Rectangular grid elements with aspect ratio of 1000 have been used. Fractures can be incorporated as discrete grid elements with 100:1 ratio in thickness to adjacent elements without too much problem with numerics. Bob Baca (Rockwell-Hanford) has used hydraulic properties differing by 10^5 in adjacent elements." A heat transport capability is included and the code apparently has a high level of "user-friendliness."

This code is funded through Rockwell-Hanford. An NRC review is in progress and the code is not available to the general public. The code is in use at Rockwell-Hanford, the Canadian AEC and, in an earlier version without source capability, at British Nuclear Fuels.

A dual porosity version of PORFLO is in development. A discrete fracture version which handles flow in multiple fractures or heat and mass

transport in a single fracture is in developmental status. A manual has not been prepared as yet. This code is very expensive for multiple fractures and odd geometry.

PORFLO-R would be an attractive candidate except that its fracture numerics apparently can be improved.

4.4.1.6 SWIFT. The SWIFT (Sandia Waste Isolation Flow and Transport) code[30] is a very powerful, very long (over 10,000 lines), and very complicated finite difference code with many capabilities. In its current form it provides (a) 2D or 3D, (b) flow, (c) heat, brine and radionuclide transport, (d) confined, semi-confined or unconfined aquifers, (e) heat loss to over and underburdens, (f) radiation boundary conditions, and (g) a well-bore model.

This code has a very long development history. It originated as a two-phase proprietary petroleum code named INTERCOMP. One phase was removed to make it non-proprietary and it was issued as SWIP by the USGS. Radionuclide transport was added and from 1977 to its release by NRC in 1981 it was under continuous development by Mark Reeves in INTERA. Current users of this code are given as Golder Associates, NRC, GTC (an INTERA subsidiary in Ottawa), and the Technical University of Berlin. A fracture capability has been added by Reeves. Draft documentation was requested on March 18, has not been received, and has not been pursued further.

Difficulties in operation can be expected due to its complexity, its length, the use of dynamic storage and awkward Fortran nomenclature.

4.4.1.7 Other Codes. A number of other codes were considered in the course of this study. The GeoTrans survey[31] for NRC presented an in-depth review of 31 codes useful for the complete range of problems in repository siting analysis. The categories and codes of interest for the injection program are listed below:

Saturated Flow	Cooley FE3DGW USGS2D and USGS3D VTT V3 (Prickett and Lonnquist)
Heat Transport	CCC SHAFT 79 MAGNUM2D
Solute and Heat Transport	SHALT SWIFT
Solute Transport (Saturated Flow)	CHAINT MMT NWFT/DVM GETOUT DPCT NUTRAN AT123D KONBRED (USGS Method of Characteristics) PATHS

The saturated regime codes proposed by GeoTrans for the subsequent benchmarking study are:

USGS3D
CCC
NWFT/DVM or NUTRAN
CHAINT or FTRANS
SWIFT

Several earlier surveys were also reviewed for content.

The Prickett and Lonnquist Code,[32] presents the "random-walk" approach to dispersion as a normal distribution of particle velocities. This approach, as subsequently discussed, was incorporated in the marker particle addition to the reservoir code.

4.4.1.8 Selected Code. The FTRANS Code was selected on the basis of its efficient fracture treatment and because it provides the majority of the required capabilities and meets the basic validity and use requirements.

4.4.2 Code Evaluation

An evaluation of the FTRANS Code was conducted over a period of several months with disappointing results.

The documentation proved to be incomplete in that the input instructions were inconsistent with the Fortran coding. While a revised input summary was constructed for the discrete fracture case, the input for the "dual porosity" calculation used in one of the author's sample problems could not be corrected in a reasonable time. Significant coding errors were also found and corrected. Discussions with the ONWI project manager and the author of the code did not result in any commitments toward properly finishing the code.

Numerical evaluation was accomplished by simulating flow in a porous matrix with a superimposed fracture. An initial case was run with a single fracture along the extent of the bottom of the aquifer. Drawdown curves for the latter case were given in the user's manual and shown to agree with theory. It was found, however, that the corresponding matrix velocities were oscillatory in time. In addition, the grid layout was very poor--92% of the horizontal and vertical dimensions occurred in two of the total of nine increments.

A mass balance calculation was added to the code to verify continuity of flow. A more complex case was run with a second fracture orthogonal to the first at its midpoint. Substantial errors were found, particularly at discontinuities such as the upper end of the second fracture. Attempts to force the head calculation to a second pass, as partially implemented in the original coding, were unsuccessful.

Calculations made with the FTRANS transport code showed the same type of numerical diffusion as discussed earlier for the SALE code.

4.4.3 Rework and Extension

A decision was made at this point to replace the FTRANS head and transport calculations and to implement the code using the Advanced Continuous Simulation Language (ACSL) problem solver.[33] The ACSL problem solver was chosen because of the writer's experience in using it to implement a number of fluid systems models. The resultant code is named FRACSL.

The mass balance calculation previously programmed was modified to yield the derivative, with respect to time, of the heads at each of the various nodes. The equation and the geometric scheme for associating matrix volume with the appropriate nodes are given in Figure 79. The resulting set of first order differential equations is integrated using one of the five algorithms available in the ACSL software: Adams-Moulton, Gears Stiff System and Runge-Kutta first, second or fourth order. The first two are variable step-variable order schemes which satisfy a specified accuracy tolerance. The Runge-Kutta algorithms use a specified step size.

Rather than simply appending one of these integration algorithms, the problem was modified to use the entire ACSL code. The problem solver approach is essentially the digital computer equivalent of an analog computer in that the user formulates his problem in a set of algebraic and first order differential equations, function and data. The system performs all those functions common to every problem: interpolation, integration, input/output, etc. The ACSL problem solver also provides the capability for direct steady state calculation without resorting to integration. Use of this capability is discussed subsequently. In addition, ACSL provides for debugging and for line printer plots. The code is widely distributed throughout the world and is supported by a users' group and by telephone consultation with the author. The writer has used ACSL for major transient simulations of a geothermal pipeline and well system, a recuperator system and major portions of a Gas Cooled Fast Reactor (GCFR). An earlier problem solver with similar capabilities has been used by the writer to simulate a nuclear rocket engine, various nuclear test facilities, a turbopump system, an air-cushion vehicle, and a geothermal-electric plant.

Initial transient simulations of the two-fracture system were oscillatory in time and space. The matrix velocity calculations were then modified from a scheme using the heads at the corners of a cell to define the velocities at the cell centers to one which uses pairs of heads to define velocities co-linear with the cell edges. The latter scheme is illustrated in Figure 79. This scheme was similarly oscillatory. The

The derivative of head with respect to time is given by

$$\frac{dH}{dt} = \frac{Q}{A \cdot T \cdot S_s}$$

where

H	=	head in feet
t	=	time in days
ΣQ	=	net volumetric inflow (from wells, matrix and fractures) in ft^3/day
A	=	reservoir area - ft^2
T	=	1. reservoir thickness - ft
S_s	=	specific storage = ft^3 of water released from a ft^3 of water per unit drop in head
V_{yi}	=	matrix flow velocity, node i
V_{xi}	=	matrix flow velocity, node i
V_F	=	fracture flow velocity.

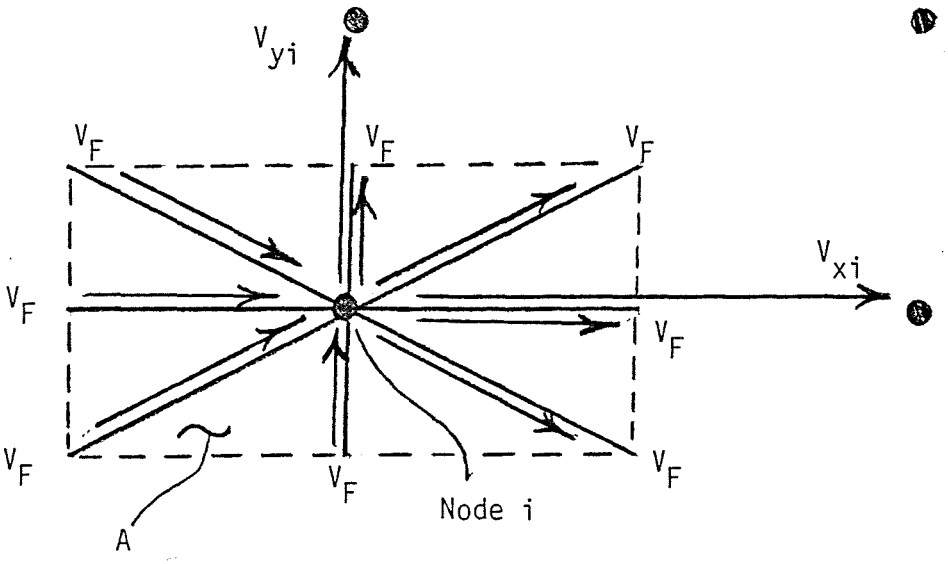

Figure 79. FRACSL head-flow model.

addition of inertia to the matrix and fracture flows did not stabilize the system until the inertias were artificially increased to very high levels. This oscillation is similar to that described in the SALE code as the justification for the use of Alternate Node Coupling (ANC) to artificially restrain repeated geometric distortions.

A solution was found by using the ASCL direct steady-state capability. The derivatives of the system state variables (the heads) are found by linearizing the system and using a Newton-Raphson iteration to find trial values of the state variables which will ultimately reduce the derivatives to near zero. The mathematics are detailed in Figure 80. It should be noted that this steady-state flow simulation capability is equivalent to that of the typical reservoir code since transient flow conditions are not usually of interest.

Figure 81 shows a complex fracture system solved for a steady-state injection (huff) condition and for a steady-state withdrawal (puff) condition. The computation required 84 CP sec at a cost of $11.

These steady-state flow conditions are maintained for the appropriate period while the transport calculations are performed. Marker particles are used, as for the SALE code, to define the motion of a tracer through the system.

The marker particle capability developed for this project is summarized below. The discussion presents the sequence of major calculations for each time step and is followed by a review and critique of each step. Figure 82 illustrates some of the concepts presented.

A dynamic system linearized over a small interval may be expressed[1] as:

$$\dot{\bar{H}} = [A]\,\bar{H}$$

where $\bar{H}$ is the vector of system states, in this case the heads at the grid nodes.

$\dot{\bar{H}}$ is the vector of state derivatives with respect to time.

[A] is the Jacobian matrix

$$[A] = \begin{bmatrix} \frac{\partial \dot{H}_1}{\partial H_1} & \frac{\partial \dot{H}_1}{\partial H_2} & \text{-----} \\ \frac{\partial \dot{H}_2}{\partial H_1} & & \\ \text{-----} & \text{------} & \frac{\partial \dot{H}_n}{\partial H_n} \end{bmatrix}$$

The Jacobian is evaluated by perturbing each of the heads, in turn, by a small amount and finding the resultant change in each of the head derivatives, e.g.:

$$\frac{\partial \dot{H}_1}{\partial H_7} = \frac{(\dot{H}_1 \text{ at } H_7 + \Delta H_7) - (\dot{H}_1 \text{ at } H_7)}{\Delta H_7}$$

Figure 80. ACSL Steady State Solution Algorithm

If the first equation is interpreted as relating the derivative and the deviation of the head from its steady state value, the deviation may be found as:

$$\overline{\delta H} = [A]^{-1} \dot{\overline{H}}$$

where $[A]^{-1}$ is the inverse of the Jacobian.

A trial value of the state vector, therefore, yields a derivative vector $\dot{\overline{H}}$ and a state vector error $\overline{\delta H}$. Iteration using the Newton-Raphson algorithm then yields the next trial value of the state vector and ultimately the state vector which drives the derivative vector below a specified tolerance.

[1]Digital Control of Dynamic Systems, G. F. Franklin and J. D. Powell, Addison-Wesley Publishing Co., 1980.

FIGURE 80. (Cont'd)

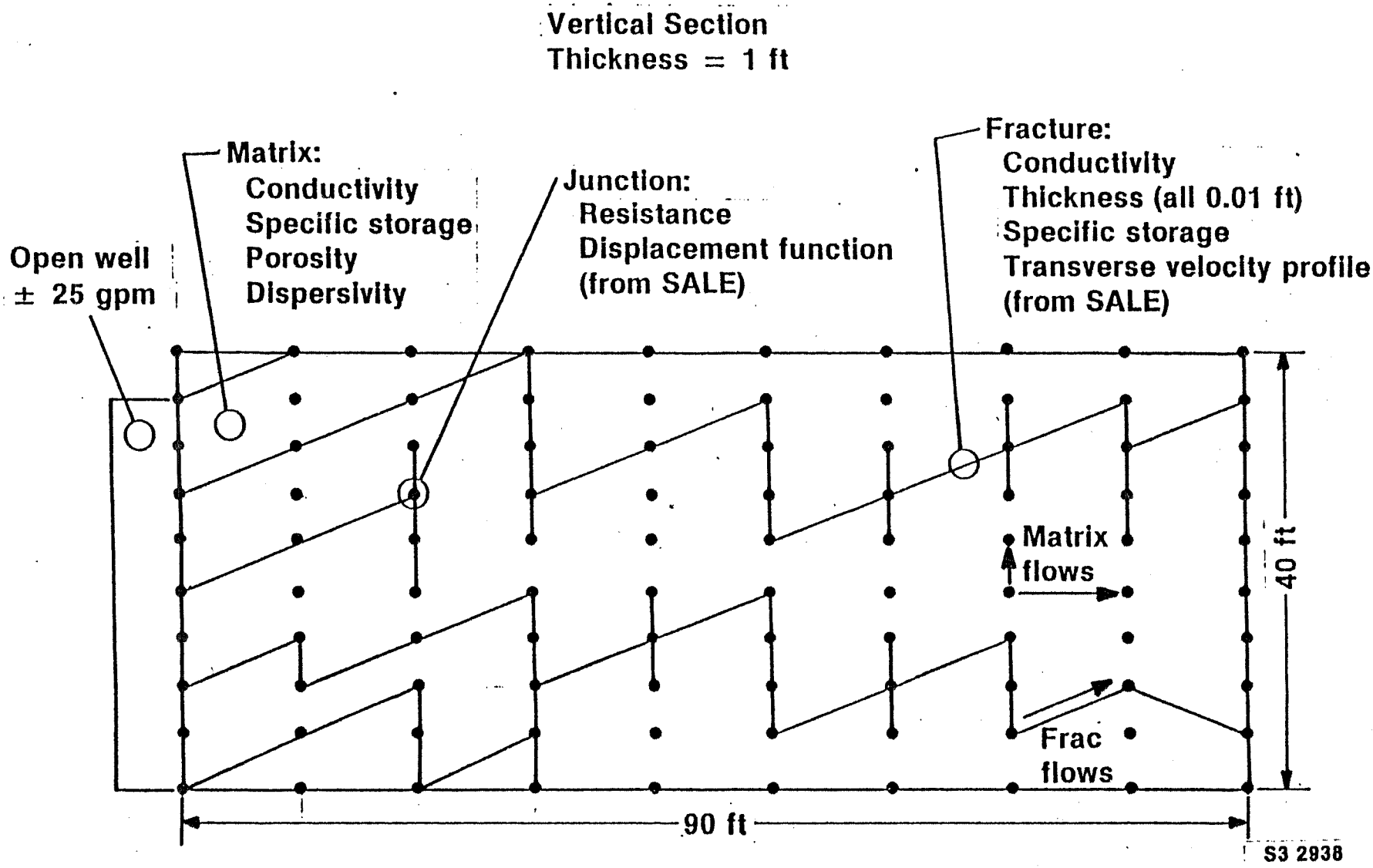

Figure 81. Typical injection-backflow reservoir simulation.

Marker Particle Calculations

- Direct calculation of cell concentration is inaccurate
- Single fracture (SALE code)

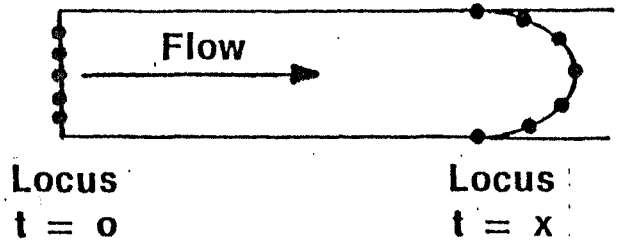

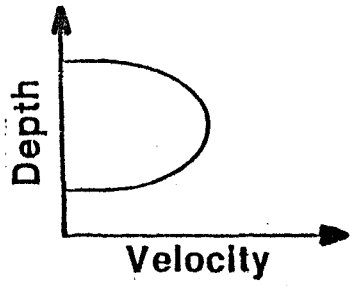

- Fracture junction (SALE code)

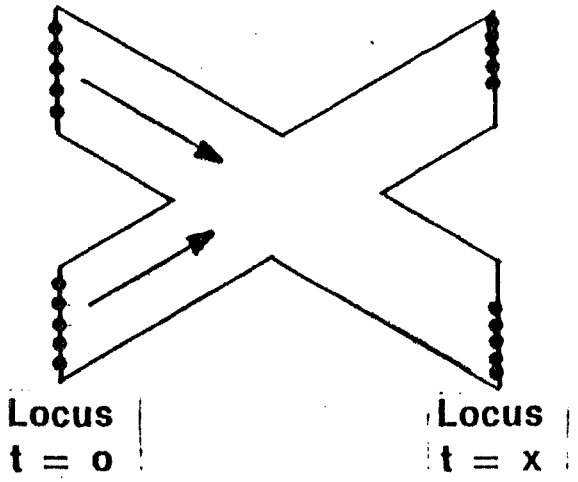

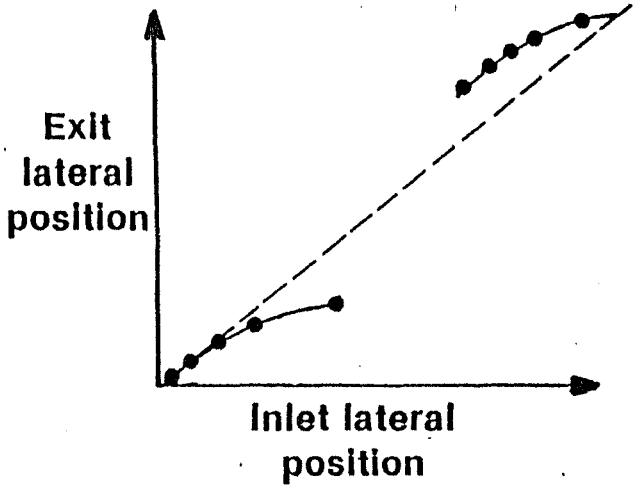

S3 2921

Figure 82. Marker particle calculations.

Marker Particle Calculations (cont'd)

- Reservoir (FRACSL code)

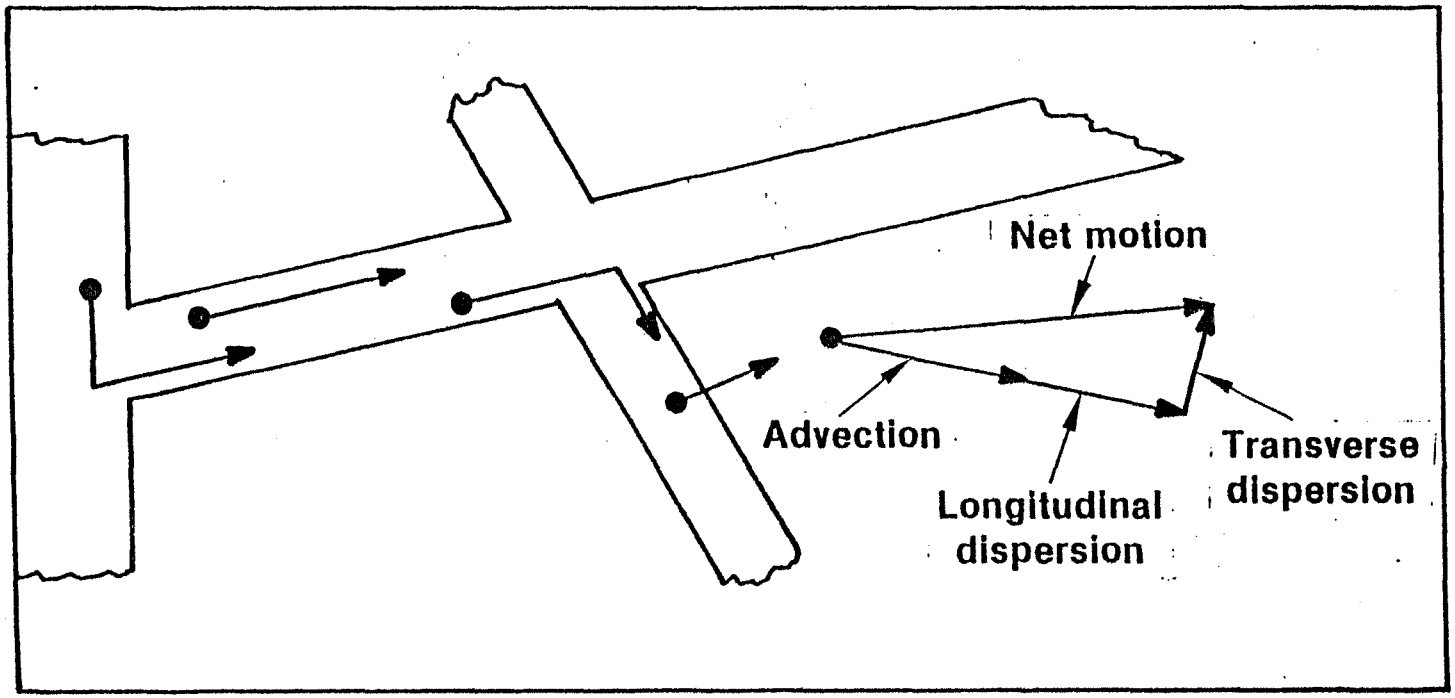

S3 2922

Figure 82. (Cont'd)

1. A set of particles is released at specified times in the injection phase. These particles are distributed evenly across the entrances to each of the fractures intersecting the injection well.

2. A particle moves down the fracture with the local velocity consistent with the mean velocity computed earlier between nodes and the Poiseuille velocity variation across the fracture.

3. A particle reaching a junction with another fracture completes the time interval in the new fracture at the lateral position given by a displacement function. The displacement function is determined by the SALE code for the appropriate geometry and flow conditions.

4. A particle reaching a well leaves the system.

5. As shown in Figure 79, the mass balance for a given node includes the quarter sections of the matrix in the adjoining cells and the half fractures (8 maximum) which terminate at the node. The excess of flow entering the area in fractures and from wells over that leaving the node in fractures, must enter the matrix. Each fracture ending or starting at the node loses a fraction of its fluid volume depending on its flow-times-length product relative to the total for that node.

6. Any element of fluid in that fracture, regardless of axial or lateral position, is equally likely to enter the matrix. Any marker particles in the fluid entering the matrix also enter the matrix.

7. The transfer from fracture to matrix occurs at the end of the time step and is essentially a change in status, not position.

8. A particle in the matrix moves with the local velocity as determined by vertical two-point interpolation for the horizontal component and horizontal two-point interpolation for the vertical component.

9. This advection motion drives a longitudinal dispersion motion in the same (or reverse) direction and a transverse dispersion motion in an orthogonal direction. These dispersion motions are elements of normal distributions.

10. A matrix motion is the sum of the three components, each determined for the velocities at the initial position.

11. A particle reaching the boundary of the reservoir leaves the system.

12. During the withdrawal phase, the net movement of fluid is from matrix to fracture. The excess of matrix outflow over inflow enters the half fractures at that node. Each fracture receives a portion of this fraction according to its fraction of the flow-length product for all fractures at that node. The water entering each fracture is taken from an adjacent strip of matrix of the appropriate area. Any particles in that strip also enter the fracture.

13. The particle entering the fracture moves normal to the fracture and is assigned a lateral position in the fracture which is drawn from a random distribution.

14. This transfer also occurs at the end of the time increment.

15. Particles are monitored as they leave the fractures at the withdrawal well.

The stepwise rationale and critique are given as follows:

1. Injection is actually at the well-head. Significant dispersion will occur in the well and the well-fracture junctions. These elements require further study.

2. Real fractures vary in thickness in the longitudinal and transverse directions. Dispersion will increase as a result. Three-dimensional effects should be studied using SALE 3D.

3. Current displacement functions are arbitrary. A library should be developed to cover the range of fracture geometries anticipated.

4. See Critique 1.

5. An additional cancelling transfer between matrix and fracture may occur and increase the dispersion. See next critique.

6. The random depth feature should be explored numerically and with physical models, based on generic fracture geometry data.

7. Approximation suitable for reasonable time steps.

8. Approximation.

9. This is a classic porous media approach as given in Prickett and Lonnquist.[32]

10. Approximation suitable for small time steps.

11. Since the boundary is assumed impermeable, particle transfer out of a matrix boundary should not occur.

12. See Critique 5.

13. See Critique 6.

14. Approximation suitable for reasonable time steps.

15. See Critique 1.

The marker particle calculation has been programmed and is in numerical debug.

In addition to the specific improvements just discussed, the work planned for FY-84 and beyond also includes other areas as given in Section 4.1, "Technical Approach."

5. PHYSICAL MODELING

5.1 Introduction

Tracer tests can provide the researcher with an increased understanding of the reservoir, in particular to the degree of fracturing. The interpretation of tracer tests is commonly based on the analysis of flow through porous media. But, in geothermal reservoirs the principal permeability is through fractures. A complete understanding of the transport mechanisms through fractures is required for the proper analysis of breakthrough curves. Dispersion theories developed for porous media are generally inadequate for fracture networks. It is the intent of our research efforts to identify and evaluate these differences.

Physical model development and experimentation is coordinated toward the common goal of developing a reasonable picture of the Raft River reservoir. This shall be accomplished by examining the effects of flow field velocities and injection rates, volumes, and quiescence times on the dispersion of solutes in fracture networks. By simulating the Raft River injection-backflow field testing we hope to provide information to aid in the interpretation of the tracer breakthrough data. The physical modeling efforts will interface with computer simulations, by providing input data to the selected codes.

Actual dispersion parameters calculated from laboratory experiments would not be directly applicable to field situations due to disparity in scale. Dispersion coefficients measured in the laboratory are on the order of centimeters or less[34,35] and actual values used to model aquifers are on the order of 30 to 100 m.[36,37] However, general concepts concerning the properties of fracture networks controlling dispersion would be determined and these concepts would be transferable to field situations.

5.1.1 Dispersion Phenomenon

Dispersion is the spreading-out of solutes due to the many alternate flow paths and ranges of flow velocities. This mixing process results in a modification of the solute concentration in the aquifer.

In porous media, dispersion depends on the distance traveled by the front, the average linear velocity, and the flow direction. In fractured media, dispersion is governed by the same processes as in porous media. However, the effects of dispersion in fractured media can be quite different from those of porous media. For instance, individual fracture velocities may be significantly different from the average linear velocity. In fractures, velocity profile effects are important in determining the convective transport and dispersion of the solutes. Mixing of fluids travelling along different channels are limited to a few fracture junctions rather than in many pore spaces, as is the case in porous media. Also, in fracture networks, the flow direction often departs from the hydraulic gradient for much longer distances than in porous media. This is of concern because dispersion increases with distance travelled. The classical concept of flow through porous media is inadequate to describe flow and dispersion through fracture networks.

5.1.2 Literature Review

The theories and analysis techniques describing dispersion in porous media are well established.[38-42] It has only been within the past 10-15 years that studies have been published dealing with solute transport in fractured media. Recent studies of dispersion in fractured media have led to a deparature from classical dispersion theory.

Classical dispersion theory is based on the one-dimensional form of the governing flow equation describing advective and dispersive transport (see Table 11 for list of symbols):

$$\frac{\partial C}{\partial t} = D_L \frac{\partial^2 C}{\partial x^2} - \bar{v} \frac{\partial C}{\partial x} \qquad (5\text{-}1)$$

TABLE 11. SYMBOLS OF HYDROLOGIC PARAMETERS

SYMBOLS	
A	cross sectional area
b	fracture width
C	concentration
D_L	longitudinal dispersion
D_m	molecular diffusion
f	number of fractures
K	hydraulic conductivity
P	Peclet number
Q	discharge
R_e	Reynolds number
T	temperature
t	time
$\bar{v}$	average linear velocity
X	length of model
w	width of model
Z	fracture height
Δ	fracture spacing
ρ	mass density
μ	dynamic viscosity
γ	specific weight

Ogata and Banks[43] present an analytical solution to Equation 5-1 for steady-state, uniform flow conditions under the following boundary conditions:

$$C = 0 \text{ for } x \geq 0,\ t = 0$$

$$C = C_o \text{ for } x = 0,\ t > 0$$

$$C = 0 \text{ for } x = \infty,\ t \geq 0$$

The equation is:

$$C(x,t) = \frac{C_o}{2} \operatorname{erfc} \frac{\bar{x}-vt}{2\ D_L t} + \exp \frac{x\bar{v}}{D_L} \operatorname{erfc} \frac{x + \bar{v}t}{2\ D_L t} \qquad (5\text{-}2)$$

For values of $D_L/\bar{v}x < 0.002$, the product of the exponential and complementary error function terms becomes negligible.[43,44] Equation 5-2 then reduces to:

$$C(x,t) = \frac{C_o}{2} \operatorname{erfc} \frac{x - \bar{v}t}{2\ D_L t} \qquad (5\text{-}3)$$

Equation 5-3 forms the basis for data reduction to determine the longitudinal dispersion and dispersivity coefficients. However, the analysis techniques for determining the input parameter, longitudinal dispersion, often vary. For example, Bear[39] defines the functional relation between longitudinal dispersion and velocity as:

$$D_L = \alpha\ \bar{v}\ P^n \qquad (5\text{-}4)$$

Replacing the Peclet number by its definition gives:

$$D_L = \alpha\ \bar{v}^{\,1+n} \left(\frac{d}{D_m}\right)^n = \alpha'\ \bar{v}^{\,1+n} \qquad (5\text{-}5)$$

where α' is defined as an apparent dispersivity coefficient equal to:

$$\alpha' = \alpha \left(\frac{d}{D_m}\right)^n \tag{5-6}$$

α' can be experimentally determined and will have units of (length $^{1-n}$ time^n).

Alternative methods for dealing with longitudinal dispersion in fractured rocks have been proposed by many investigators.[45-50] Horne and Rodriguez[46] and Fossum and Horne[45] use the classic advection-dispersion equation, but with a dispersion coefficient that is related to fracture width. The form is the same as the classic dispersion coefficient (Equation 5-5) with n = 1.0

$$D_L = \frac{2b}{105} \bar{v} \left(\frac{\bar{v}b}{D_m}\right) \tag{5-7}$$

The departure from classic dispersion theory is that this equation is derived from the parabolic velocity distribution equation for flow between parallel plates and includes lateral diffusion between stream lines. The importance of the velocity profile in controlling dispersion will depend on the relative time scales for transverse diffusion within a single fracture and the migration of a tracer front between fracture junctions. Figure 83 shows a plot of Equation 5-3 where D_L is calculated from Equation 5-7 and fracture parameters as given in the figure. Equation 5-7 is only valid when sufficient time is available for transverse diffusion to homogenize the tracer concentration across the width of the fracture. This condition is met when $D_m t/b^2 < 0.5$. Using the parameters given in Figure 83 and $D_m = 1.5 \times 10^{-5}$ cm^2/sec gives a critical time of 213 sec. At a flow rate of 0.413 cm/sec, Equation 5-7 is valid when fracture spacing is on the order of one meter.

An alternative approach is to look at dispersion based on the parabolic velocity profile without transverse diffusion. An analytical

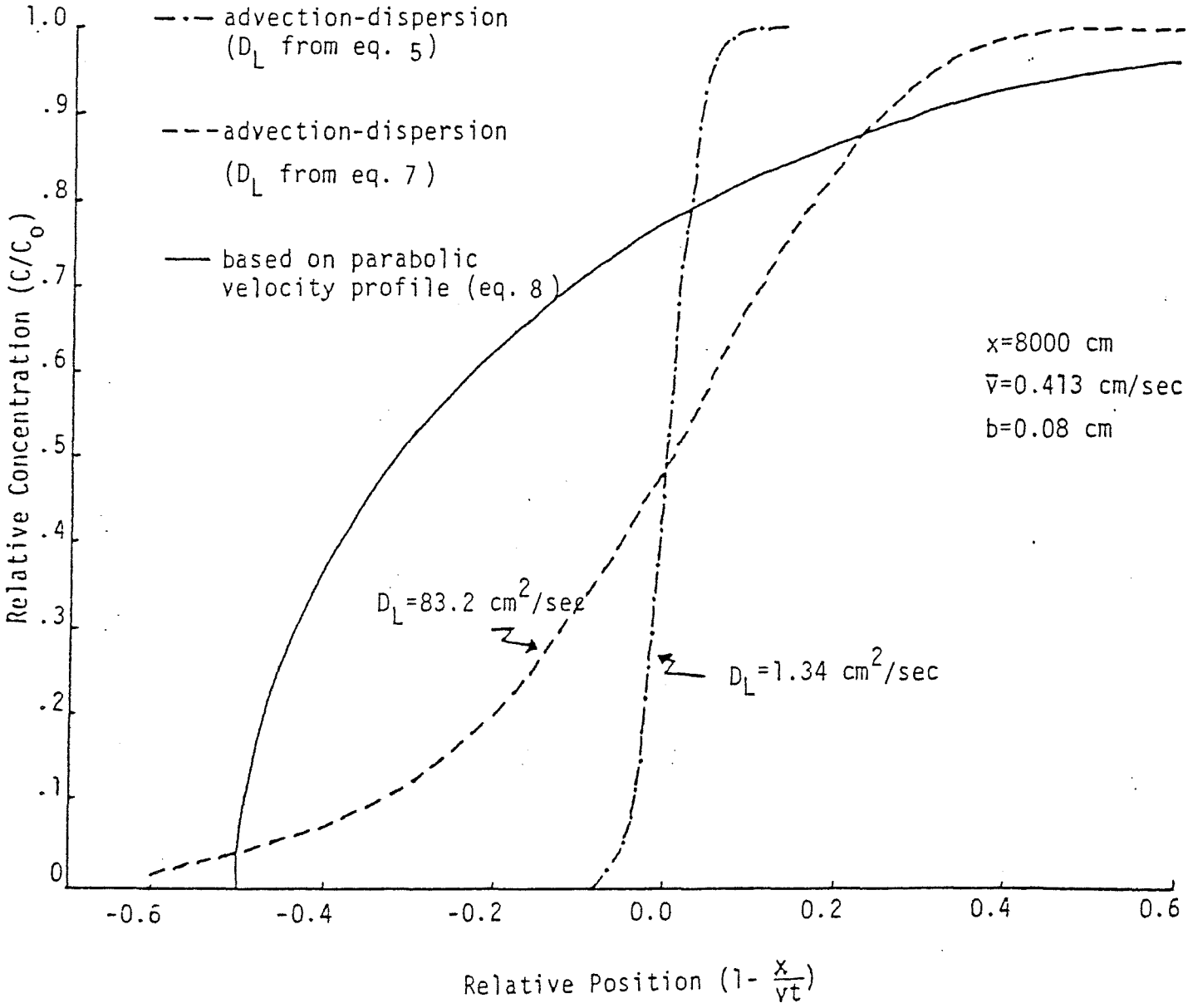

Figure 83. Comparison of breakthrough curves calculated from the advection-dispersion equation and based on a parabolic velocity profile.

solution describing tracer breakthrough in a single fracture can be derived based on a parabolic velocity profile. The derivation follows that of Bear[39] for flow in a capillary with the proper geometry changes. For an infinite fracture of width 2b, the tracer breakthrough is given by

$$C(x,t) = \frac{C_o}{2} (4 - 3\xi^2 - \xi^3)^{1/2} \qquad (5\text{-}8)$$

where

$$\xi = \frac{2x}{3\bar{v}t}$$

Figure 83 shows comparative breakthrough curves for Equation 5-8 and the traditional advection-dispersion equation (Equation 5-3). Equation 5-8 does not match experimental results obtained by Neretnieks et al.,[50] which show a much less abrupt rise as breakthrough begins. Equation 5-8 does produce, however, long drawnout tails to breakthrough curves, resulting from extremely slow velocities along fracture walls. Equations 5-7 and 5-8 represent two different cases describing dispersion in fractures based on the velocity profile concept. An intermediate case with some transverse diffusion is the more likely candidate to fit measured data. It is apparent that dispersion is a much more significant process in fractures than in porous media.

Krizek et al.[47] developed a numerical model for solute transport in a fracture network. In order to evaluate the validity of the theoretical model, experimental tests were run on single fracture junctions. Dispersion was found to be a direct result of the velocity profile of the fluid moving through individual fractures. Solute breakthrough curves generated by their model are similar in form to breakthrough curves based on the velocity profile concept.

Neretnieks and coworkers[48-51] have taken the approach that channeling within a fracture produces dispersion. Their model is based on an idealization of a fracture as a set of parallel channels of differing

width. The channel population has a log normal frequency distribution of fracture apertures and each channel has an average velocity proportional to the square of the aperture. Solute breakthrough measurements are made on mixtures of water from all channels, producing a gradual breakthrough curve. Application of this model to solute breakthrough curves measured in a laboratory fracture in granite required matrix diffusion to produce a good match to measured data.

Work at the INEL has been directed at measuring the transport of solutes in laboratory scale fracture networks.[52,53] The fracture network consisted of a radial (quarter circle) flow configuration composed of two sets of orthogonal fractures (Figure 84). Radial flow injection tracer tests allowed for data to be collected for a variety of flow orientations to the major fracture axis with a single test. Injection tracer tests were conducted at three different flow rates (30, 60, 90 cm^3/min). Calculated dispersivity coefficients increased with increasing flow rates. Dispersion in the fracture network was not linearly related to velocity, but related to velocity raised to a power of 1.4. Complete mixing of the two fluids was not observed at fracture intersections. Instead a distinct streamlining of the fluids was observed.

5.2. Model Design

The model design is directed towards quantifying the effects of flow field velocities and injection rates, volumes, and quiescence times on the dispersion of solutes in fracture networks. Further knowledge of the effects of these parameters on the shape of breakthrough curves will aid in the interpretation of the Raft River injection-backflow field testing.

5.2.1 Description of Model

The fracture network was built by cutting orthogonal fractures 0.32 cm wide and 1.91 cm deep into a sheet of plexiglass. Plexiglass was chosen as the material for model construction due to several inherent properties.

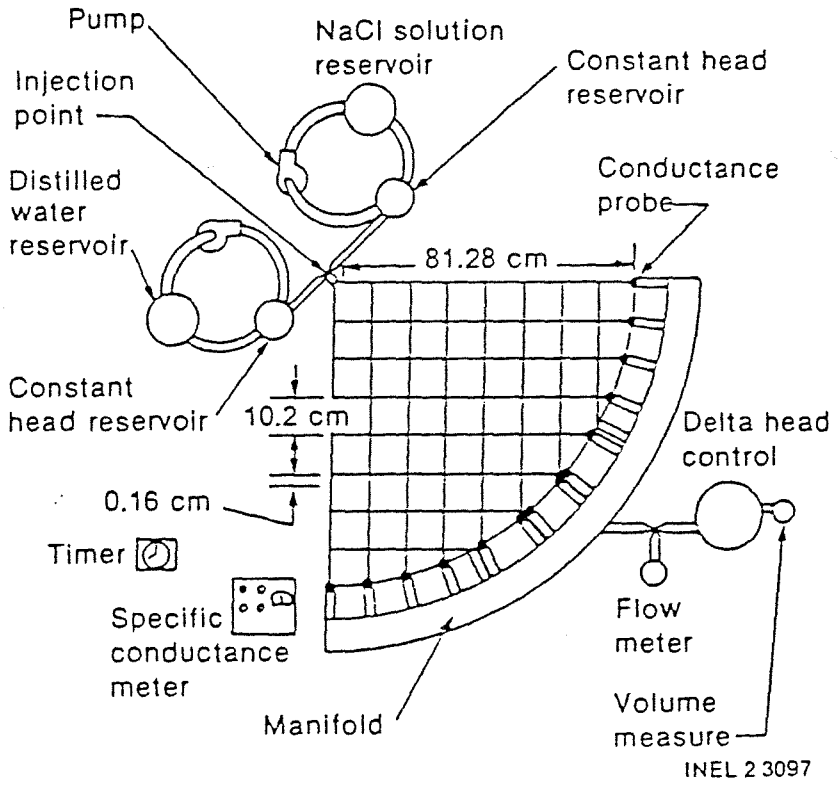

Figure 84. Schematic of physical model and support equipment for conducting radial flow dispersion tests.

First, plexiglass allows for visual observation of the tracer front; second, adsorption of solute particles onto fracture walls would not take place; and third, the fracture walls would be impermeable.

The fracture network consists of fractures at right angles to one another with a fracture spacing of 10.16 cm (Figure 85). The network is enclosed by rectangular boundaries 0.57 m by 1.72 m. Fractures intersect the boundaries at 45 degrees. All fractures have uniform openings, roughness, and spacing.

A constant head reservoir supplies the model with distilled water, with a conductance of about 10 μS. A syringe pump controls the injection of a dilute sodium chloride solution, with a conductance of 100 μS. Withdrawal is controlled by a flow meter and a constant head reservoir. Due to the low tracer concentration, density effects are considered minor. Both solutions are dyed with food coloring, enabling visual observation of the tracer front. Head drop across the model is controlled by a third constant head reservoir. Several piezometers are installed to monitor the pressure within the model. A flow meter, at the network outlet, measures the volumetric flow rate passing through the model (Figure 86).

Conductance electrodes embedded in the fractures measure the breakthrough curves for the injected sodium chloride solution. A computerized data acquisition system allows point measurements of conductance to be made within a few seconds of each other. Data are recorded on a Hewlett-Packard 1000 computer and stored on magnetic tapes that can be transferred to the Cyber 176 computer for analysis.

5.2.2 Model Calculations

The designed experimental study examines the dispersion of solutes under steady-state flow conditions. To accomplish this, the model must meet the following hydraulic criteria: (a) laminar flow, (b) advection

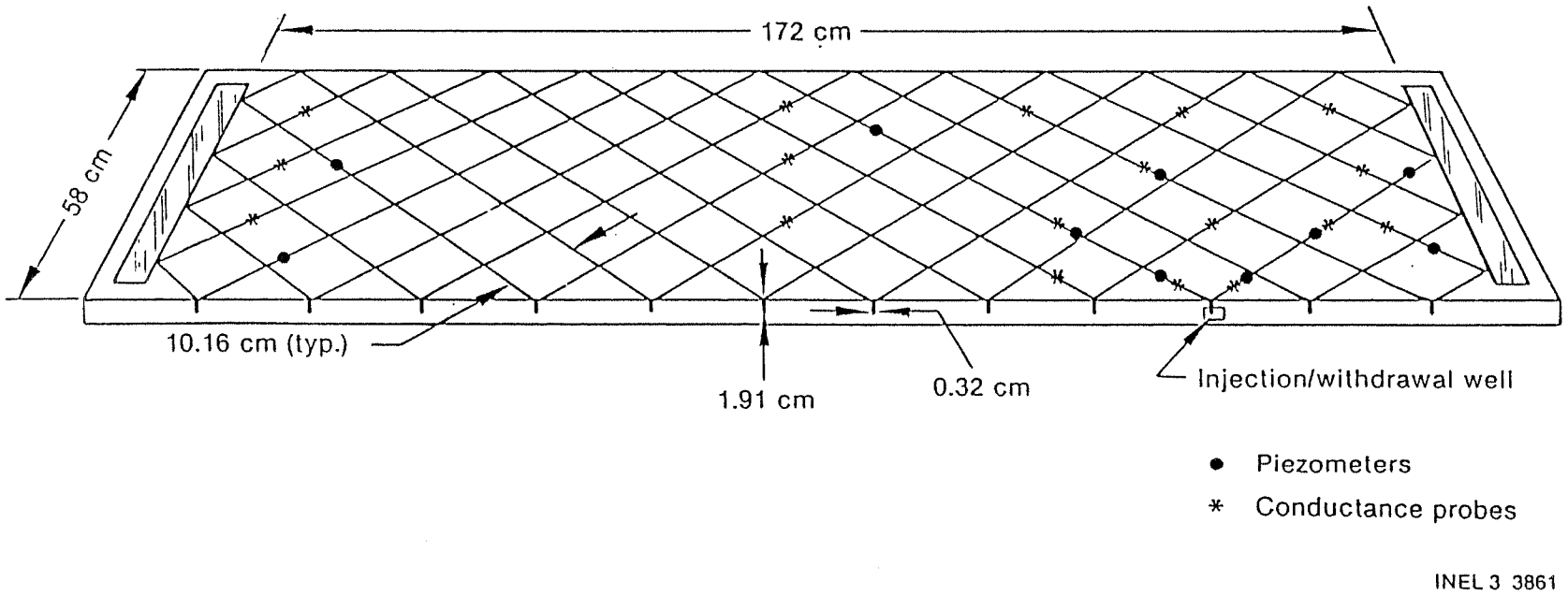

Figure 85. Design of Fracture Network.

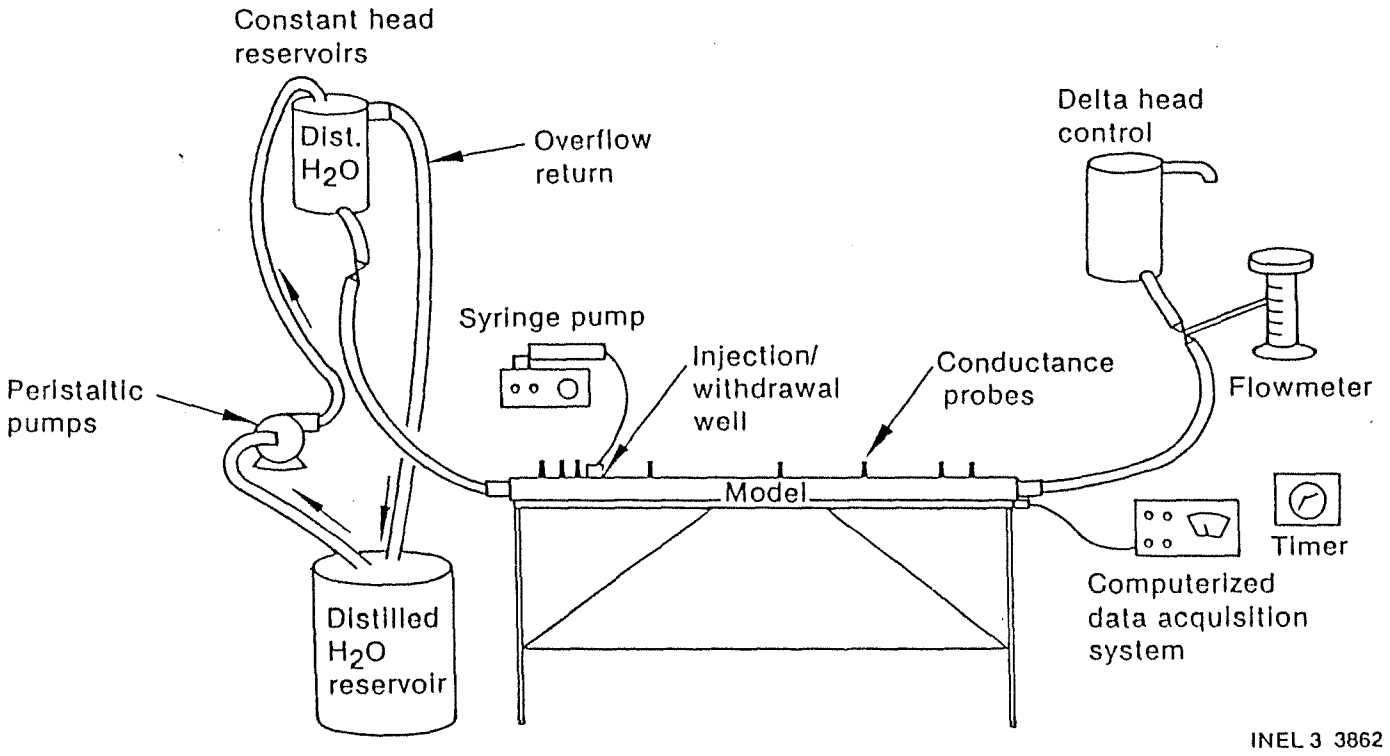

Figure 86. Physical model and support equipment.

dominant over diffusion, and (c) a small head loss across the model. Several model calculations must be made to see if the model meets the above hydraulic criteria. The following model parameters are assumed:

$w = 57.47$ cm

$Q = 0.33$ cc/s, 0.50 cc/s, 0.83 cc/s, 1.67 cc/s

$Z = 1.91$ cm

$\Delta = 10.16$ cm

$b = 0.32$ cm

$T = 25°C$

$X = 172.24$ cm

Darcy's law, an approximation of the general Navier-Stokes equation for momentum conservation, is used to describe the fluid motion. Darcy's law for fluid flow is described by the following equation:

$$Q = -KA\frac{dh}{dx} \tag{5-9}$$

When the specific discharge q is replaced in the above equation, the resultant equation is:

$$q = -K\frac{dh}{dx} \tag{5-10}$$

where $q = Q/A$.

The first hydraulic criteria is to maintain laminar flow; therefore the Reynolds number, a dimensionless parameter defined by the ratio of the

forces of inertia to the forces of viscosity within the fluid, must be low. The Reynolds number is calculated by the following equation:

$$R_e = \frac{\rho q b}{\mu} \qquad (5\text{-}11)$$

Darcy's law is valid only in cases where the Reynolds number is less than one.[54] Using the following flow rates 0.33, 0.50, 0.83, and 1.67 cc/s, the Reynolds number is calculated to be 0.11, 0.17, 0.28, and 0.56, respectively. Since, the Reynolds number is below one for all flow situations, Darcy's law is valid and laminar flow exists.

The second hydraulic criteria is advection dominant over longitudinal diffusion; therefore the Peclet number, a dimensionless parameter defined by the advection to diffusion ratio, must be high. The Peclet number is calculated by the following equation:

$$P = \frac{qb}{D_m} \qquad (5\text{-}12)$$

For diffusion in an open fracture, a free-water diffusion coefficient of $1 \cdot 10^{-5}$ cm^2/s is used.[42] For the indicated flow rates, a Peclet number of 97, 145, 242, and 483, respectively, is calculated. This is in the range where advection will exceed diffusion to the extent that longitudinal diffusion can be ignored in the model.

The final hydraulic criteria is for a reasonable head loss across the model. The head loss is determined using Darcy's law:

$$q = -K\frac{dh}{dx} \qquad (5\text{-}10)$$

For an idealized fracture network Freeze and Cherry define the hydraulic conductivity (K) by the following equation:[42]

$$K = \frac{\gamma}{\mu} \frac{Nb^3}{12} \qquad (5\text{-}11)$$

where $N = 1/\Delta = 0.098$ cm.

The hydraulic conductivity (K) is calculated to be 28.60 cm/s. Using this K, the specific discharge, and the length of the model, the change in head is calculated by the following equation:

$$dh = \frac{q}{-K} X \qquad (5\text{-}12)$$

For the following flow rates: 0.33, 0.50, 0.83, and 1.67 cc/s, the head loss across the model is -0.02, -0.03, -0.05, and -0.10 cm, respectively. These calculations indicate the head loss across the model will be small.

5.3 Analysis

The physical model of the fracture network was designed to enhance the interpretation of the Raft River injection-backflow field testing. Two sets of tests were run: quiescence and volume testing (Table 12). Quiescence testing was designed to examine the effects a flow field has on tracer recovery and the shape of the recovery curve. Volume testing allows for different volumes of the reservoir, around the wellbore, to be examined.

Observation of tracer migration during tests showed that velocity profile effects result in a large concentration gradient across fractures. The tracer fluid moves down the center of the fracture in a sharp point, that widens gradually behind the front (Figure 87). Even quite some time after the tracer front has passed, remnants of the native reservoir fluid can be seen along the fracture walls. At fracture junctions, the pointed tracer fronts move through the junction without mixing. Fronts will sometimes split, depending on the direction of the hydraulic gradient, but retain their coherance.

Variable volume injection-backflow tests, with no flow field, were conducted in the physical model fracture network to determine the effects of injecting fluid various distances into a fractured reservoir. The raw data from these four tests is plotted in Figure 88. The injection period has

TABLE 12. SUMMARY OF QUIESCENCE AND VOLUME MODEL TESTING

Injected Volume (cc)		Flow Field (cc/min)	Quiescence (min)	Backflow (cc/min)
Quiescence Testing	120	20	0, 1, 3, 5	20
	120	5.3	0, 1, 7, 15, 19	20
	120	10	0, 3, 6, 10, 14	20
	120	30	0, 1, 3, 3 1/3, 5	20
Volume Testing	60	none	none	20
	120	none	none	20
	180	none	none	20
	240	none	none	20

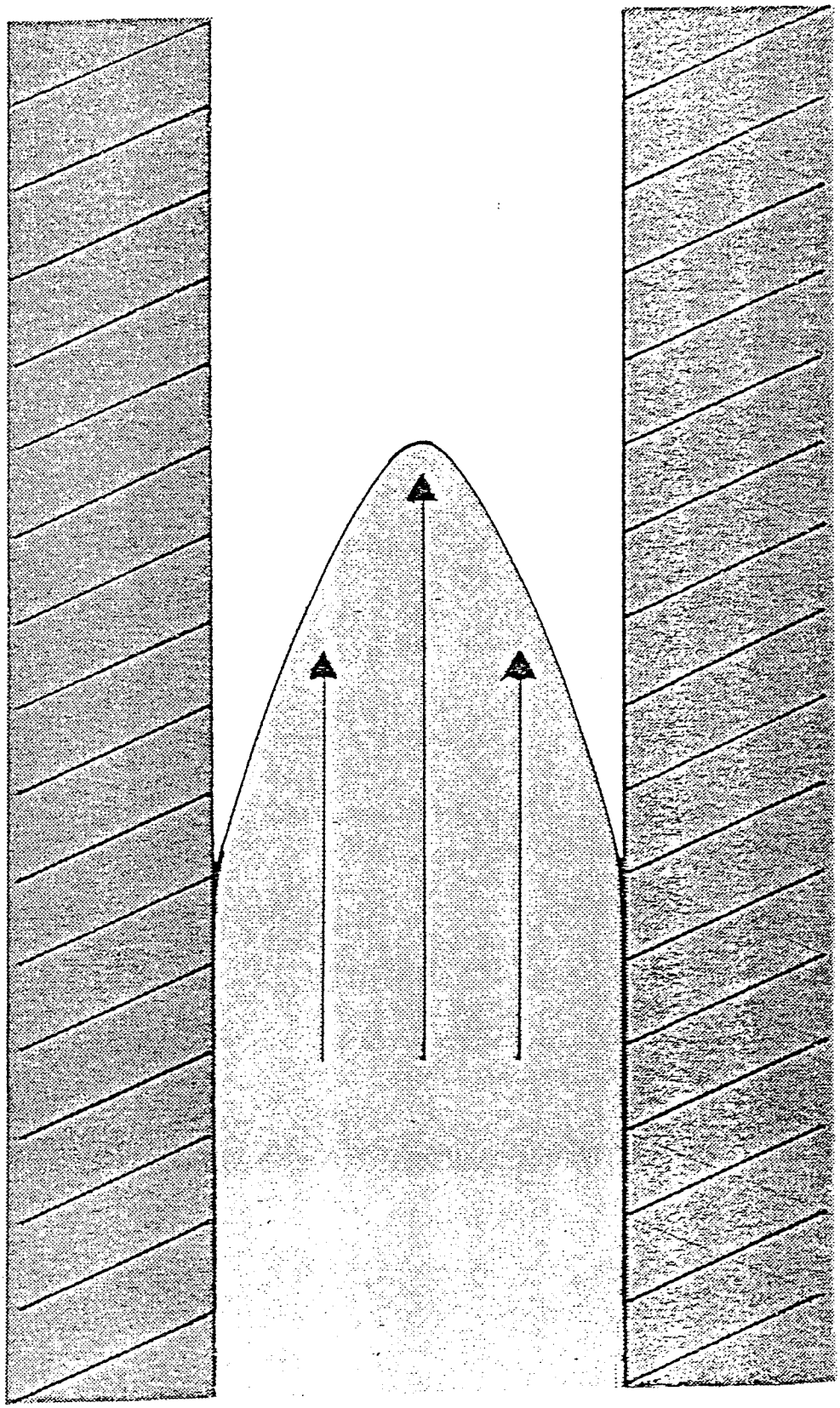

Figure 87. Schematic of velocity profile in fracture.

Physical Model Test

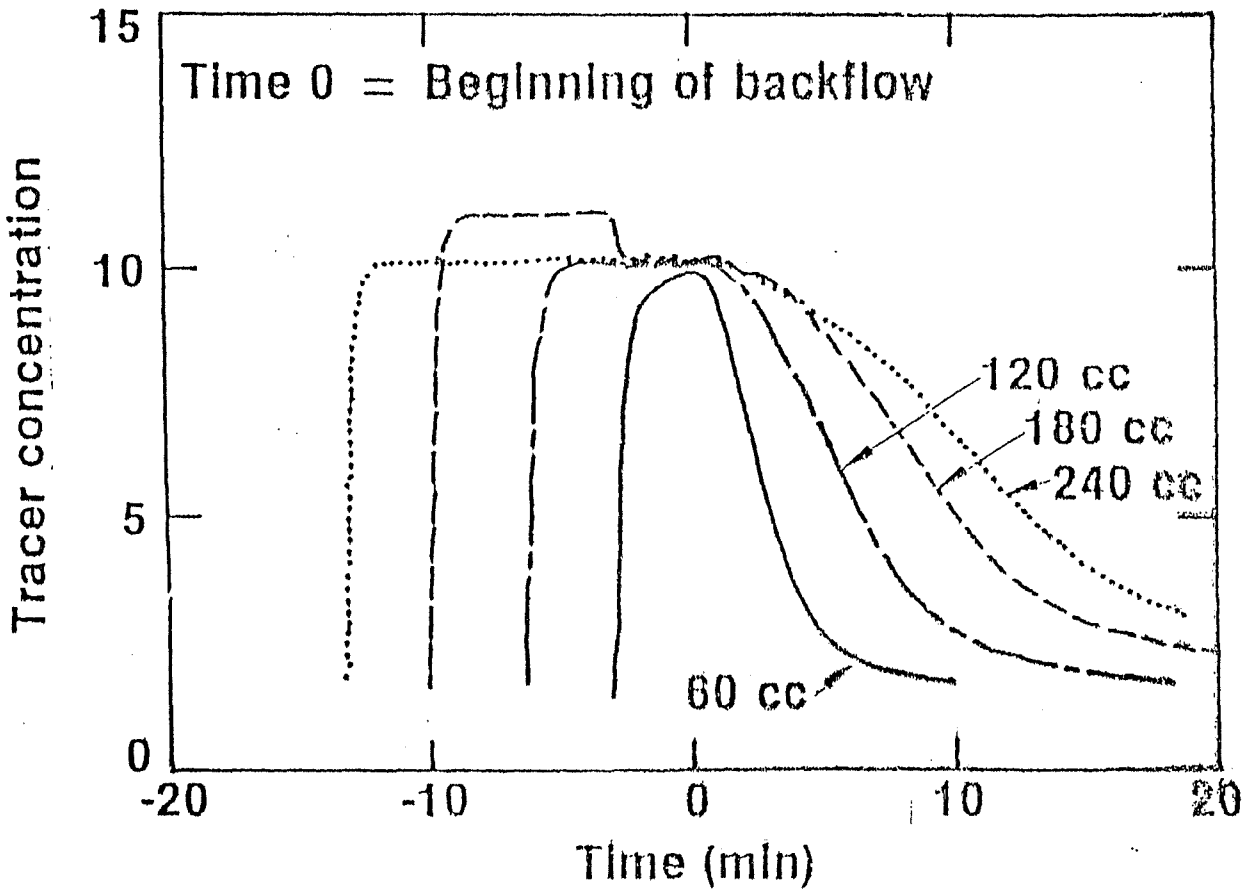

Figure 88. Variable volume injection/backflow tests with reservoir flow field.

83 2847

been subtracted from the time axis, so that backflow begins at time equals zero. The greater the injection volume, the further the front has traveled and the greater the dispersion. However, reducing the data to a relative volume scale by dividing the backflow volume by the injection volume, the effects of increasing dispersion with distance can be removed. The four curves are now coincident, indicating a constant dispersivity for the reservoir (Figure 88). This is as expected for the physical model which was designed to be homogeneous.

The final phase of testing involved injecting into the fracture network when a background flow field was present. This set of tests replicated the format of the Test 4 series conducted at Raft River. With increasing quiessance times, the drop off in the tracer recovery curves became more abrupt (Figure 89). When the quiessance time was long enough for reservoir flow volume to be on the order of the injected volume (14-min curve, Figure 90), tracer recovery dropped to very low values. Another variable to be considered is the relative rate of backflow to reservoir background flow. When flow in the reservoir is large relative to the backflow rate, tracer recover is further reduced. The tracer recovery can be related to reservoir flow rate for the relatively simple geometry of our laboratory model. Tracer recovery is a linear function of quiessance time. Experiments have only been conducted for one injection-backflow rate. Additional experiments need to be conducted over a range of injection-backflow rates. Equations will be arranged so that the ratio of injection-backflow rate to reservoir flow rate can be calculated from tracer recovery and quiessance time. The techniques will require field testing to determine if laboratory parameters are meaningful for field situations.

5.4 Future Applications

Data from our physical modeling efforts will be used to verify numerical models that explicitly simulate solute transport in fracture networks. The ability to reliably predict the migration of solutes through fractured rocks could enhance the design of a reinjection program. The theories and concepts developed would be used to aid in the proper interpretation of field observations.

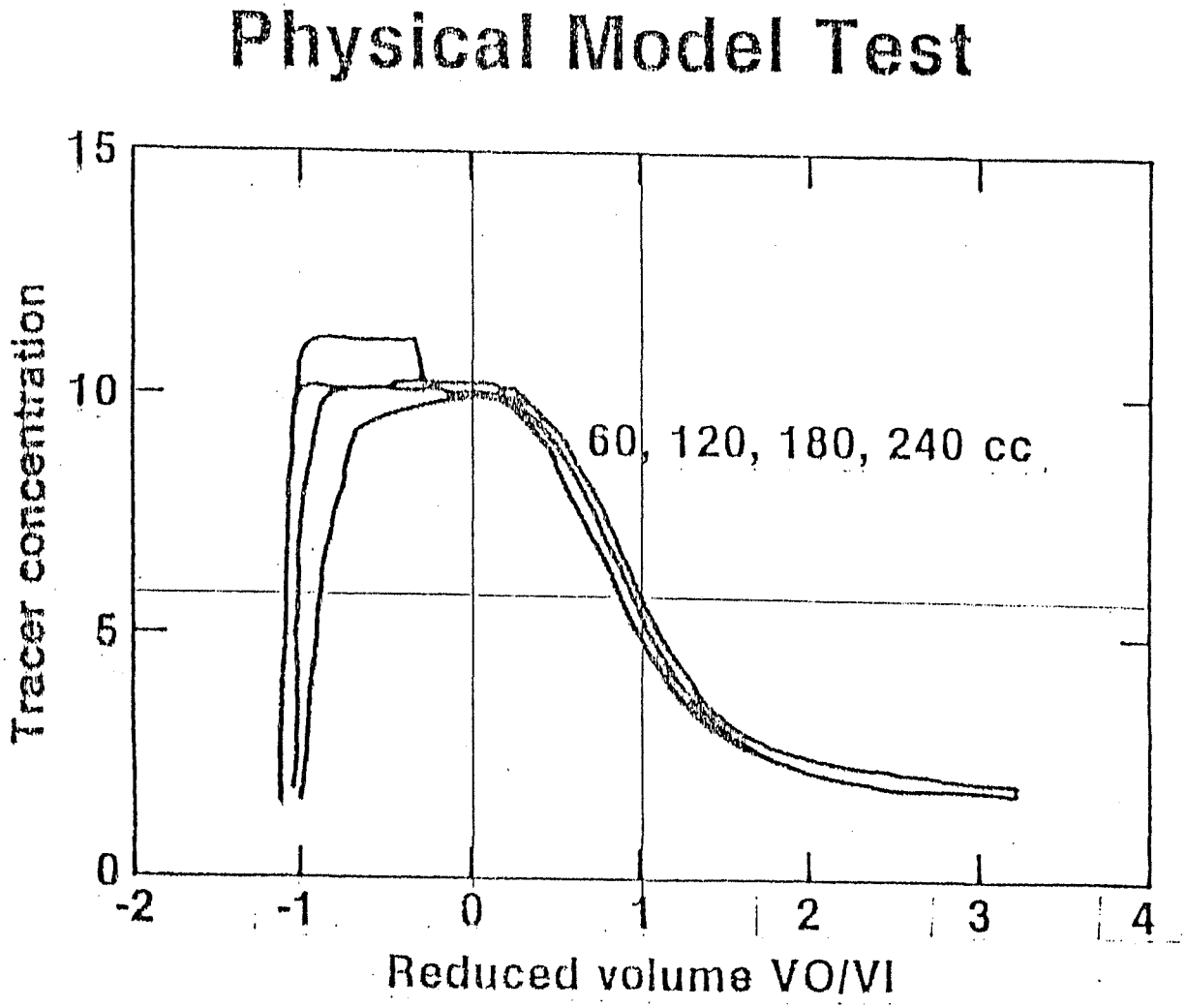

Figure 89. Normalized variable volume injection/ backflow tests with reservoir flow field.

S3 2944

Physical Model Test

Flow Field - 10.8 cc/min

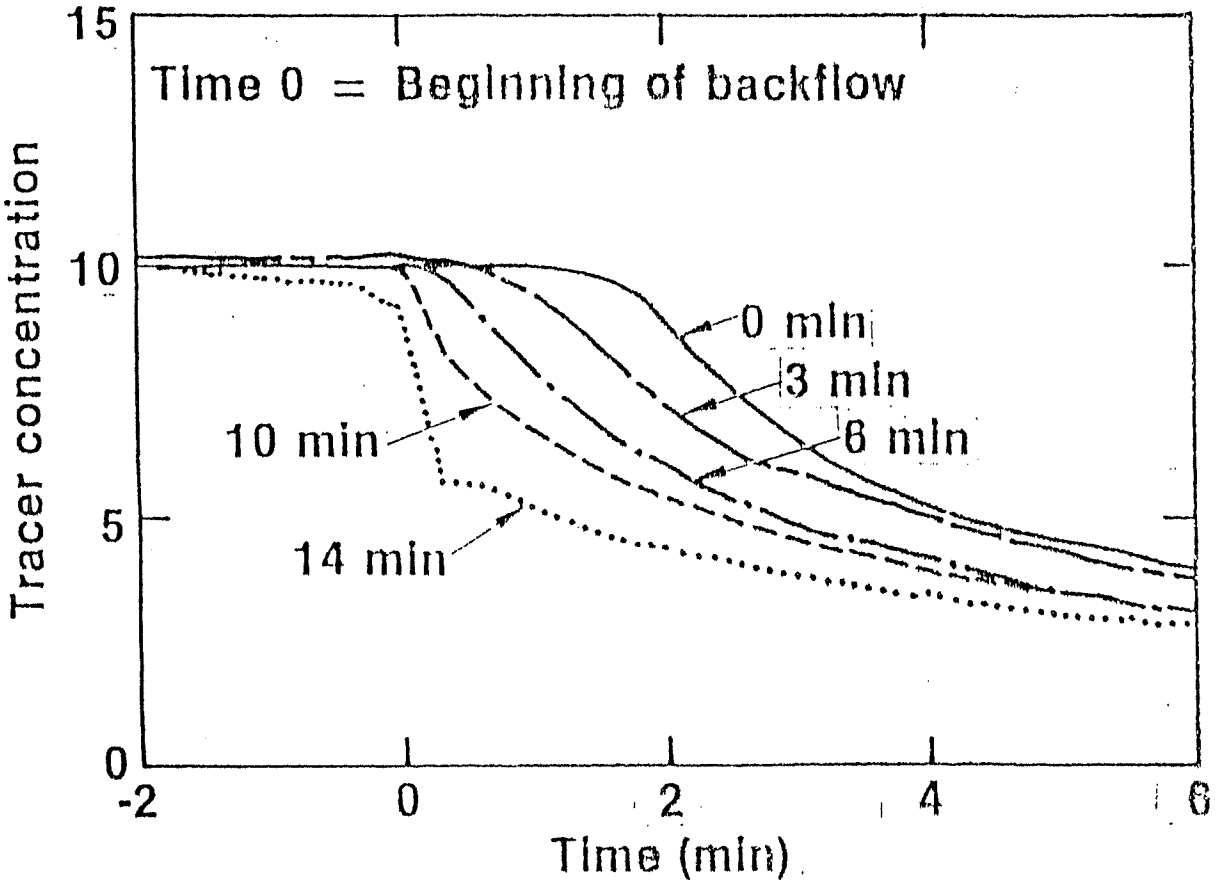

Figure 90. Tracer recovery curves for variable quiescence with reservoir flow field.

REFERENCES

1. L. G. Miller and S. M. Prestwich, Completion Report: Raft River Geothermal Production Well Five (RRGP-5), IDO-10082.

2. M. R. Dolenc et al., Raft River Geoscience Case Study, 1, EGG-2125, pp. 79-83.

3. Republic Geothermal Inc., Maurer Engineering Inc. and Vetter Research, Raft River Well Stimulation Experiments, DOE/AL/10563-T7.

4. R. M. Large, Hydrothermal Injection Program Phase I Test Data, EGG-PB-015-83.

5. Schlumberger, Fullbore Spinner, RRGP-5, 07-08-78, unpublished.

6. Gearhart-Owen Wireline Services, X-Y Caliper, RRGP-5, 07-06-78, unpublished.

7. Rocky Mountain Geo-Engineering Company, Driller's Log, RRGP-5, 06-22-78, unpublished.

8. W. S. Keys, Acoustic Televiewer Logs for RRGP-5B, United States Geological Survey, unpublished.

9. D. W. Allman, J. A. Tullis, M. R. Dolenc, T. L. Thurow, P. A. Skiba, Raft River Monitor Well Potentiometric Head Responses and Water Quality as Related to the Conceptual Ground-Water Flow System, II, EGG-2215, September 1982.

10. H. R. Covington, Deep Drilling Data, Raft River Geothermal Area, Idaho--Raft River Geothermal Exploration Well No. 5, United States Geological Survey Open-File Report 79-382, 1979.

11. H. R. Covington, Deep Drilling Data, Raft River Geothermal Area, Idaho--Raft River Geothermal Exploration Well, No. 1, United States Geological Survey Open-File Report 77-226, 1977.

12. Reynolds Electrical & Engineering Co., Inc., Completion Report--Raft Geothermal Exploratory Hole No. 1 (RRGE-1), IDO-10062, (NVO-410-80), October 1975.,

13. W. C. Walton, Groundwater Resource Evaluation, McGraw-Hill Book Co., 1970.

14. S. W. Lohman et al., Definitions of Selected Ground-Water Terms, Revisions and Conceptual Refinements, U.S. Department of the Interior, Geological Survey, Open-File Report, August 1970.

15. C. J. Bliem and L. F. Walrath, Raft River Binary-Cycle Geothermal Pilot Power Plant Final Report, EGG-2208, EG&G Idaho, April 1983.

16. J. D. Ramshaw and J. K. Dukowicz, APACHE: A Generalized Mesh Eulerian Computer Code for Multicomponent Chemically Reactive Fluid Flow, LASL Report LA-7427, January 1979.

17. K. M. Peery, Description and Use of the SOLA and the SOLA-SURF Fluid Dynamic Computer Codes, EG&G RE&C, Report RE-A-77-047, June 1977.

18. B. D. Nichols, C. W. Hirt, R. S. Hotchkiss, SOLA-VOF: A Solution Algorithm for Transient Fluid Flow with Multiple Free Boundaries, Los Alamos Report LA-8355, August 1980.

19. A. A. Amsden, H. M. Ruppel, C. W. Hirt, SALE: A Simplified ALE Computer Program for Fluid Flow at All Speeds, Los Alamos Report LA-8095 UC-32, June 1980.

20. A. A. Amsden et al., SALE 3-D, Los Alamos Report LA 8905, 1983.

21. R. B. Bird et al., Transport Phenomena, John Wiley & Sons, 1960.

22. GeoTrans, Inc. for INTERA Environmental Consultants, Inc., FTRANS-A Two-Dimensional Code for Simulating Fluid Flow and Transport of Radioactive Nuclides in Fractured Rock for Repository Performance Assessment, Documentation and User's Manual, Final Draft ONWI/E512-02900/CD-17 410-02G-01A, September 1982.

23. J. Noorishad and M. Mehran, "An Upstream Finite Element Method for Solution of Transient Transport Equation in Fractured Porous Media," Water Resources Research, 18, 3, June 1982, pp. 588-596.

24. R. G. Baca and R. C. Arnett, "Analysis of Fracture Flow and Transport in the Near-Field of a Nuclear Waste Repository," Proceedings of the Symposium on Uncertainties Associated with the Regulation of the Geologic Disposal of High-Level Radioactive Waste, Gatlinburg, TN, March 9-13, 1981, NUREG/CP-0022, CONF-810372, pp. 469-479.

25. K. Pruess, GMINC-A Mesn Generator for Flow Simulations in Fractured Reservoirs, Lawrence Berkeley Laboratory Report LBL-15227 (draft), March 1983.

26. K. Pruess and R. C. Schroeder, SHAFT79--User's Manual, Report LBL-10861, UC-66a, March 1980.

27. A. L. Edwards, TRUMP: A Computer Program for Transient- and Steady-State Temperature Distributions in Multidimensional Systems, LBL Report UCRL-14754, Rev. 3, September 1, 1972.

28. A. Rasmuson, T. N. Narasimhan, I. Neretnieks, "Chemical Transport in a Fissured Rock: Verification of a Numerical Model," Water Resources Research, 18, 5, October 1982, pp. 1479-1492.

29. A. Runchal, PORFLOW-R: A Mathematical Model for Coupled Ground Water Flow, Heat Transfer, and Radionuclide Transport in Porous Media, Analytic and Computational Research, Inc., Draft Report REP-014, July 22, 1982.

30. M. Reeves and R. M. Cranwell, User's Manual for the Sandia Waste-Isolation Flow and Transport Model (SWIFT), Release 4.81, NUREG/CR-2324, November 1981.

31. S. D. Thomas, G. Ross, J. W. Mercer, A Summary of Repository Siting Models, NUREG/CR-2782, July 1982.

32. T. A. Prickett et al., A "Random-Walk" Solute Transport Model for Selected Groundwater Quality Evaluation, Illinois State Water Supply, ISWS/BUL-65/81, 1981.

33. Advanced Continuous Simulation Language User Guide/Reference Manual, Mitchell and Gauthier, Assoc. Inc., 1981.

34. J. Bear, "Some Experiments in Dispersion," Journal of Geophysical Research, 66, 8, August 1961.

35. J. F. Pickens, et al., "Measurement of Distribution Coefficients Using a Radial Injection Dual-Tracer," Water Resources Research, 17, 3, June 1981.

36. J. B. Robertson, Digital Modeling of Radioactive and Chemical Waste Transport in the Snake River Plain Aquifer at the National Reactor Testing Station, Idaho USGS, Open-File Report, IDO-22054, May 1974.

37. L. A. Swain, "Predicted Water-Level and Water-Quality Effects of Artificial Recharge in the Upper Coachella Valley, California, Using a Finite Element Model," USGS Water Resources Investigations, April 1978.

38. J. J. Fried and M. A. Combarnous, "Dispersion in Porous Media," Advances in Hydroscience, 7, New York: Academic Press, 1971.

39. J. Bear, Dynamics of Fluids in Porous Media, New York: American Elsevier Publishing Co., Inc., 1972.

40. J. J. Fried, Groundwater Pollution, New York: Elsevier Scientific Publishing Co., 1975.

41. G. Sposito, V. K. Gupta, R. N. Bhattacharya, "Foundation Theories of Solute Transport in Porous Media: A Critical Review," Advances in Water Resources, 2 1979.

42. R. A. Freeze and J. A. Cherry, Groundwater, Englewood Cliffs, NJ: Prentice-Hall, Inc., 1979.

43. A. Ogata and R. B. Banks, A Solution of the Differential Equation of Longitudinal Dispersion in Porous Media, U.S. Geological Survey Professional Paper 411-A, 1961, pp. A1-47.

44. J. A. Hoopes and D. R. F. Harleman, "Dispersion in Radial Flow from a Recharge Well," Journal of Geophysical Research, 72, 1967, pp. 3595-3607.

45. M. P. Fossum and R. N. Horne, Interpretation of Tracer Return Profiles at Wairakei Geothermal Field Using Fracture Analysis, 6, Geothermal Resources Council Transactions, 1982.

46. R. N. Horne and F. Rodriguez, "Dispersion in Tracer Flow in Fractured Geothermal Systems," Seventh Stanford Geothermal Reservoir Engineering Conference, Stanford University, CA., 1981.

47. R. J. Krizek and G. M. Karadi, Symposium on Percolation Through Fissured Rock, Stuttgart, Germany.

48. I. Neretnieks, "Analysis of Some Tracer Runs in Granite Rock Using a Fissure Model," Scientific Basis for Nuclear Waste Management, 1, New York: Plenum Press, 1979.

49. I. Neretnieks, "Some Difficulties in Interpreting In Situ Tracer Tests," Scientific Basis for Nuclear Waste Management, 3, New York: Plenum Press, 1981, pp. 473-482.

50. I. Neretnieks, T. Eriksen, P. Tahtinen, "Tracer Movement in a Single Fissure in Granitic Rock: Some Experimental Results and Their Interpretation," Water Resources Research, 18, 1982, pp. 349-858.

51. H. Abelin, J. Gidlund, I. Neretnieks, "Migration in a Single Fracture," Scientific Basis for Nuclear Waste Management, V, 11, New York: Elsevier Science Publishing Co., Inc., 1982, pp. 529-538.

52. K. N. Koslow and L. C. Hull, Design of a Model to Study Dispersion in Fracture Networks, EGG-ELS-5718, EG&G Idaho, Inc., Idaho Falls, ID, 1982.

53. L. C. Hull and K. N. Koslow, "Dispersion in Fracture Networks," Proceedings of the Eight Annual Geothermal Reservoir Engineering Conference, Stanford University, Stanford, CA., 1982.

54. W. Viessman, Jr., J. W. Knapp, G. L. Lewis, T. E. Harbaugh, Introduction to Hydrology, New York: Harper and Row, 1977.

APPENDIX C

ANALYTICAL METHODS FOR TRACER CONCENTRATION DETERMINATIONS IN THE FIELD

TABLE OF CONTENTS

A-1: IODIDE, I^-, BY THE SPECIFIC ION ELECTRODE METHOD

A. Principle:

Specific ion electrodes are constructed to measure ion activities for a particular ion. The electrode develops an electrical potential proportional to the logarithm of the concentration of the measured ion. For iodide ions a solid state electrode with AgI/Ag_2S membrane is used in conjunction with single junction Ag/AgCl reference electrode. When the electrodes are placed in a solution containing iodide ion and leads from these electrodes are connected across a high impedance meter, the electrical potential can be read. Most specific ion meters manufactured at present read directly as concentration of iodide ions.

B. Apparatus:

(1) 150-mL beakers with stirring bars
(2) Specific ion meter, (Orion Model 901) (Orion 94-53), and reference probe (Orion 90-01).
(3) Magnetic stirrer
(4) Eppendorf pipet, 1.0 mL
(5) Polishing strips (Orion at No. 94-82-01)

C. Reagents:

(1) ionic strength adjustor (ISA), to keep a constant background ionic strength. Prepare 5 M $NaNO_3$ by dissolving 425 g of reagent grade sodium nitrate in 1 L of distilled water. Two mL of this solution is added to a 100 mL of standard or sample solutions.

(2) Standard solution. Dissolve 1.18 g of reagent grade sodium iodide to 500 mL of distilled water in a one liter volumetric flask. Swirl until dissolved. Add distilled water to the flask until it reaches the one-liter mark. Also, Orion Cat. No. 94-53-06 is a 0.1 molar (12,700 ppm) iodide solution which can be diluted with distilled water to an appropriate standard concentration.

(3) Reference electrode filling solution, for iodide measurements the reference probe, Orion model 90-01, single junction electrode is used. The filling solution is Orion Cat. No. 90-00-01.

D. Procedure (Direct Measurement):

(1) Prepare two standard solutions with concentrations higher and lower than the expected concentration of the sample. The standard solutions should have a ten-fold difference in their concentrations. For example, if the sample concentration is ∿75 ppm, then the two standard solutions should have concentrations of 50 ppm and 500 ppm.

(2) Place 100 mL of the sample in a 150-mL beaker. Add 2.0 mL of ISA solution. Repeat this for each standard solution. Place a stirring bar in each beaker.

(3) Place the low concentration standard solution on a magnetic stirrer. Stir with a minimum solution vertex.

(4) Set the Orion model 901 ion analyzer mode switch to CONC and place the electrodes in the above standard solution.

(5) Set the STD valve switches to the concentration of the standard solution. Set the SLOPE switches to ∿57.00. Press CLEAR/READ MV. When the instrument reading stabilizes (∿/min.), press SET CONCN button. The instrument will read out the concentration set on the STD VALUE switches.

(6) Remove the low concentration standard solution and replace with the high concentration standard solution. Wash the electrodes with distilled water, wipe with a lintless towel, and place in the high concentration standard solution.

(7) Adjust the SLOPE switches until the instrument readout is the same as the concentration of the high standard solution. The slope should be between 53-59.

(8) Remove the standard solution and replace with the sample solution. The electrodes should be cleaned and placed in the sample solution. The instrument will read out concentration of the sample.

(9) The calibration procedure must be repeated every 2-4 samples when the samples are highly saline. Also, if the instrument becomes difficult to calibrate, the iodide probe should be cleaned as follows:

(a) Cut off 1 in. of the polishing strip furnished with the probe.

(b) Hold the electrode with the membrane facing upward.

(c) Place the frosted side of the polishing strip on the membrane using light finger pressure. Rotate probe ∿30 sec.

(f) Rinse probe and soak in a 1-ppm standard solution for about 5 min before using.

E. Interferences:

Although it requires concentrations of bromide and chloride greater than 3160 ppm and 280,000 ppm, respectively, to directly interfere with the specific ion measurement of iodide, high salinity waters (∿3000 ppm chloride) cause the probe to be more unstable and require increased membrane cleaning.

Sulfide concentrations of less than 1.0 ppm can interfere significantly. Sulfide ion can be removed by adding nickel (+2) to the sample solution.

The specific ion electrode is sensitive to temperature changes. Care should be taken to have the sample solutions and the standard solutions at the same temperature. This can be accomplished by allowing the temperatures of the sample solutions to reach room temperature. The sample and standard solutions could be placed in a constant water bath until both reach the bath temperature.

A-2: Boron, B^{3+}, by the carmine colorimetric method

A. Principle:

When carmine is dissolved in concentrated sulfuric acid and reacted with boron, the solution color changes from a bright red to bluish-red or blue. The color change is relative to the boron concentration. Absorbance at 605 nm results in detection limits of ~20 µg of boron.

B. Apparatus:

(1) Colorimetric equipment

(a) Hach DREL/4 spectrophotometer

(b) Perkin Elmer spectrophotometer Model 550 with 12 m x 25 mm cell for 1-cm light path.

(2) 125-mL plastic erlenmeyer flasks

(3) Volumetric pipettes, 50 mL and 1 mL size, Class A

(4) Hach 25-mL sample cells or disposable 12 mm x 25 mm cuvetes

(5) 500-mL plastic graduate cylinder.

C. Reagents:

(1) Standard boron solution, Hach Cat. #1963-11, 4.0 mg/L as B.

(2) Concentrated hydrochloric acid, Caution: Hydrochloric acid is very corrosive. Handle with Care.

(3) Concentrated sulfuric acid, Caution: sulfuric acid is very corrosive. Handle with care.

(4) Carmine reagent. Hach Boro Ver III pillows Cat. #14170-99, 69 mg of carmine.

(5) Carminic acid, preparation: measure 375 mL of sulfuric acid in a 500-mL plastic graduate cylinder. Pour carefully into a 1000-mL plastic beaker. Caution: sulfuric acid is very corrosive. Carefully add 345 mg of carmine reagent (5 Boro Ver III pillows) to the sulfuric acid in the 1000-mL plastic beaker. Caution: hydrochloric acid fumes will be given off in the reaction. The procedure should be conducted in a fume hood. Also the reaction mixture will froth vigorously.

The frothing will diminish when the reaction is complete. The reagent is stable up to 48 h.

D. Procedure:

(1) Using a Class A volumetric piet, piet 2 mL of distilled water into a clean, completely dry 0.125-mL plastic erlenmeyer flask. Repeat this step using the 4.0-mg/L Boron standard solution and the water sample to be analyzed.

(2) Using a 50-mL graduate cylinder, measure 35 mL of the carminic acid solution prepared as shown in Section C-5. Caution: The carmimc acid solution is very corrosive. Carefully add the 35 mL of carminic acid reagent to the 2 mL of distilled water in the 125-mL erlenmyer flask; repeat this step for the 4.0-mg/L B standard and the sample to be analyzed. Swirl each to mix.

(3) Allow 20 min but not more than 30 min for the color to develop. Pour 25 mL of each flask into a Hach sample cell or the plastic curvette.

(4) Place the sample cell containing the distilled water sample into the sample compartment of the Hach spectrophotometer. Set the wavelength dial to 605 nm. Insert the boron meter scale into the meter of the Hach instrument. Adjust the light control so the meter reading is zero mg/L. Check the instrument by replacing the distilled water sample with the 4.0-mg/L B sample, if the Varian Spectrophometer is used, calibrate using the 4.0 mg/L B standard.

(5) Remove the standard solution from the sample compartment and replace it with the sample cell containing the water sample and read the meter in mg/L. For the Perkin Elmer instrument the concentration is read from the LED readout (Note 1).

E. Interferences:

Generally there are no interfering ions in natural waters. However, if glassware is used, it should be completely dry as the presence of water causes a low reading. The carminic acid reagent should not be stored in pyrex or kimax bottles. These are borosilicate glasses and the reagent can leach boron from them. Use plastic bottles for storage.

Note(1). When disposing of the prepared samples, pour carefully into a larger volume of water ~500 mL before disposing of it.
Caution: When pouring the reagent into water, there is vigorous reaction and could cause hot droplets of water and acid to be splashed into the eyes. Wear safety glasses and protective clothing when performing this task.

A-3: Fluroescein by the UV-VIS Spectrophotometric Method

A. Principle:

Any fluoresent molecule in a given environment has two characteristic spectra: The excitation spectrum and the emission spectrum. The shape of the excitation spectrum is the absorbance curve of the molecule. The excitation wavelength for fluorescein for maximum absorbance is 490 nm. However, for analysis purposes, the absorption wavelength at 451.2 nm was more responsive. The amplitude of the absorption wavelength of fluorescein is pH dependent. As the pH increases from ∿4.0 to ∿10, the amplitude of the absorption at the selected wavelength increases. However, the fluorescein samples were buffered at 4.6. At this pH there was adequate sensitivity and buffer preparation is much simpler. UV-VIS spectra photometric measurements when using a cell with a 1-cm light path are sensitive to 10 µg/L fluorescein ion. The calibration curve for the Perkin Elmer UV-Vis spectro photometer model 55 was linear between 10-µg/mL and 1000-mg/L fluorescein ion.

B. Apparatus:

(1) Perkin Elmer Model 550 spectrophotometer with 12 m x 25 mm curvettes

(2) 1-mL Eppendorf pipette and disposable tips

(3) 10-mL + 50 mL Class A pipettes

(4) 100-mL and 1000-mL volumeteric flasks

(5) 100-mL beakers or flasks.